f-Block and *d*,*f*-Block Phosphonate Cages: Synthesis, Structure and Magnetic Properties

Karzan H. Zangana

A thesis submitted to the University of Manchester for the degree of
Doctor of Philosophy
in the Faculty of Engineering and Physical Sciences

2015

School of Chemistry
The University of Manchester

Table of Contents

List of Figures

List of abbreviations

tertiary butyl	^{t}Bu
iso-propyl	^{i}Pr
methyl	Me
n-propyl	*n*Pr
phenyl	Ph
Pyridyl	py
ethyl	Et
super-conducting quantum interference device	SQUID
zero-field splitting	ZFS
Direct current	d.c.
Alternating current	a.c.
Frequency	f
Hamiltonian operator	$\hat{H}$
In-phase susceptibility	χ'
Out-of-phase susceptibility	χ''
Isotropic exchange constant	J
Magnetic Field	H
Molar magnetic susceptibility	χ_M
Saturation magnetisation	M_{sat}
Anisotropy barrier	U_{eff}
Temperature	T
Electronic Bohr magneton	B
Spin angular momentum	S
Single-molecule magnets	SMMs
Electron paramagnetic resonance spectroscopy	EPR

Magnetisation	M
Magnetocaloric effect	MCE
Zero-field splitting parameter	D
One, two and three-dimensional	1-D, 2- D and 3-D
Zero-dimensional	0-D

Dedication

To my beloved parents, the reason of what I become today.

To my wife, her hours of work in loving our children Vali and Sidra, enabled the hours of research, contemplation, and writing necessary to complete this thesis.

To all those who touched my life.

Abstract

'*f*-Block and *d*,*f*-Block Phosphonate Cages: Synthesis, Structure and Magnetic Properties' is a thesis submitted to The University of Manchester for the degree of Doctor of Philosophy in the Faculty of Engineering and Physical Sciences.

Research into molecular magnetism has undergone a revival over the past two decades following the discovery of Single Molecule Magnetism (SMM). Compounds which show this property have the potential to increase the storage capacity of magnetic media by many orders of magnitude compared to current generation devices. Developments in the field have come from synthesis involving mainly simple bridging ligands such as carboxylates, alkoxides, pyridonates and heterocyclic ligands.

The use of phosphonic acid ligands in the synthesis of 4f–phosphonate or 3d–4f phosphonate clusters has recently begun to be explored, primarily for interest into their magnetic properties. The present work builds on studies which show that the reaction of oxo–centred metal triangles with phosphonate ligands can generate larger clusters retaining some motifs of the starting material. There are only few examples on the use of lanthanide carboxylates, such as $[Ln_2(O_2C^tBu)_6(HO_2C^tBu)_6]$ (Ln = Dy, Gd, Tb, Ho or Er) and/or a preformed cluster $[Cr(III)_3(\mu_3\text{-}O)(O_2C^tBu)_6(H_2O)_3][O_2C^tBu]$ in combination with phosphonate ligands. This work investigates the use of bi-metallic lanthanide and tri-metallic transition metal starting materials in conjunction with the flexible tertiary-butylphosphonic acid ligand, to yield novel 4f–phosphonate and 3d–4f cages.

Several Cr–4f phosphonate cages have been obtained, where each structure contains two oxo-centred $\{Cr_3\}$ triangles, bridged by phosphonates and lanthanides. Additionally, new 4f–phosphonate clusters have been synthesised by treating tertiary-butylphosphonic acid ligand with lanthanide nitrate salts or preformed lanthanide dimers. A number of 4f–phosphonate cages reported in the thesis show interesting structural or magnetic properties, for example, $\{Ln_{10}P_6\}$ is the largest 4f–phosphonate odd number metal ring centred by a tenth metal site, the $\{Gd_8P_6\}$ cluster demonstrates interesting MCE properties, and the $\{Dy_4P_2\}$ complex is shown to be an SMM.

Karzan H. Zangana
August 2015

Declaration

No portion of the work credited to the author in this thesis has been submitted in support of an application for another degree or qualification of this or any other university or other institute of learning.

Copyright Statement

Acknowledgements

Primarily I would like to thank my supervisors, Professor Richard Winpenny and Eric McInnes for their constant support and encouragement throughout this work, and also Professor David Collison and Dr. Grigore Timco, for their additional help and guidance for which I am exceptionally grateful.

Many thanks to all those who have provided useful suggestions and have contributed to my work. In particular, Dr. Eufemio M. Pineda has been a great mentor, lab colleague, friend and brother to me. Many thanks to the past and present members of the Molecular Magnetism Group and inorganic section Asad, James, Nick, Joseph, Sam, Rob, Maria, Simon, Antonio and Jesus for their support, and for helping me get through the ups and downs of life as a PhD student.

I would like to thank the KRG-Scholarship program in "Human Capacity Development (HCDP)" scholarship program for their financial support during my studies. The author would also like to deliver thanks to the Faculty for laboratory facilities such as elemental microanalysis, X-ray facilities, mass spectrometry, etc.

The author wishes to express his gratitude to his beloved family members for their support and endless love through the duration of his studies, particularly my mother and father. Finally and especially, all my love and appreciations to my wife for always being by my side and for understanding.

A journey of a thousand miles begins with a single step.

Laozi

Chapter 1

Introduction

1.1 Rationale for submitting this thesis in the alternative format

The alternative format thesis is feasible for this thesis as it concerns a number of well defined, though closely related sections. The high impact nature of the results obtained for the author of this thesis has resulted in five publications in peer-reviewed journals. Postponing publication would significantly diminish the impact of this work, as further advances are made in a quickly expanding field, such as molecular magnetism. Also, for all those contributing publication is thus desirable, especially for those facilities whose only exposure is by their work in journals, such as the National EPR Facility utilised in Chapter Nine. It has therefore been crucial and desirable to publish during the course of the author's PhD studies. The published papers cover all aspects of the work undertaken and so are deemed suitable for submission as part of this thesis. As the thesis author's work is exemplified by the publications presented here, the alternative format is deemed appropriate.

1.2 Organisation of this thesis

Chapter Two is a general introduction to the field of magnetism, paramagnetic metal co-ordination complexes and single-molecule magnetism, this chapter sets out the

aims of this project with particular emphasis on 3d, 4f and 3d–4f phosphonate cages. Chapter Three presents a comprehensive review of all discrete 4f–phosphonate cages reported to date. Chapter Eight is a full review of all 3d–4f phosphonate cages reported thus far. Chapters Four, Five, Six, Seven and Nine are published original research articles. Chapter Ten contains some conclusions based on the work undertaken, and some suggestions for future work.

1.3 Contributing Authors

Chapter 4, Paper 1, "Octametallic 4f–phosphonate horseshoes" is an original research communication written by the author of the thesis and his supervisor, Professor Richard E. P. Winpenny. Synthesis and single crystal X-ray data collection were performed by the thesis author. Dr. Eufemio M. Pineda and the author of the thesis jointly performed SQUID measurements and processing of the data, Professor Jürgen Schnack modelled the magnetic data for the $\{Gd_8P_6\}$ cage.

Chapter 5, Paper 2, "Centred nine-metal rings of lanthanides" is an original research communication written by the thesis author and his supervisors, Professors Richard E. P. Winpenny and Eric J. L. McInnes. The author of the thesis performed the synthesis and X-ray crystallography. The author of the thesis and Dr. Eufemio M. Pineda together performed SQUID measurements and processing of the data, Professor Jürgen Schnack (University of Bielefeld) modelled the magnetic data for the $\{Gd_{10}P_6\}$ cage.

Chapter 6, Paper 3, "Tetrametallic lanthanide(III) phosphonate cages: synthetic, structural and magnetic studies" is an original research full paper written by the author of the thesis and his supervisor, Professor Richard E. P. Winpenny. Synthesis and X-ray crystallography were completed by the thesis author. Dr. Eufemio M. Pineda and the author of the thesis jointly performed SQUID measurements and processing of the data, Dr. Eufemio M. Pineda modelled the magnetic data for the $\{Gd_4P_4\}$ cage.

Chapter 7, Paper 4, "Single Molecule Magnet behaviour in a Lanthanide-Phosphonate Octahedron" is an original research communication written by the thesis author and his supervisor, Professor Richard E. P. Winpenny. Synthesis and X-ray crystallography were performed by the thesis author. Dr. Eufemio M. Pineda and the author of the thesis jointly performed SQUID measurements and processing of the data, Dr. Eufemio M. Pineda modelled the magnetic data for the cages.

Chapter 9, Paper 5, "Linking Cr_3 triangles through phosphonates and lanthanides: synthetic, structural, magnetic and EPR studies" is an original research full paper written by the author of the thesis and his supervisors, Professors Richard E. P. Winpenny and Eric J. L. McInnes. Synthesis and X-ray crystallography were performed by the author of the thesis. Dr. Eufemio M. Pineda and the author of the thesis jointly performed SQUID measurements and processing of the data, Dr. Eufemio M. Pineda modelled the magnetic data for the cages. The author of the

thesis and Dr. Eufemio M. Pineda cooperatively performed EPR data collection. Dr. Eufemio M. Pineda carried out simulation of the EPR data.

Chapter 2

2.1 The interest in paramagnetic metal co-ordination complexes

Paramagnetic metal co-ordination complexes are molecular compounds with at least one metal ion bonded to ligands with at least one of these parts possessing an unpaired electron. Relying on their structural dimensionality, they can be classified in four different types: zero-dimensional (0-D) molecules,[1] infinite 1-D chains,[2] 2-D layers,[3] and 3-D networks[4] (Figure 2.1(a—d)).

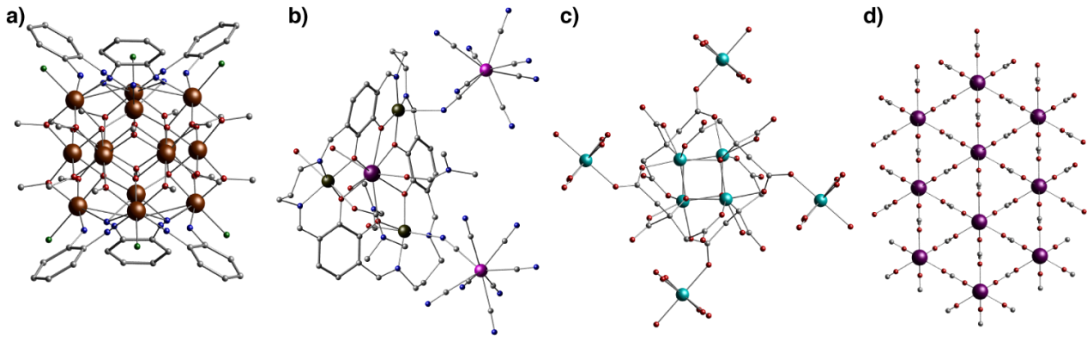

Figure 2.1: From left to right 0→3D compounds: (a)$[Fe_{14}(bta)_6O_6(OMe)_{18}Cl_6]$, where bta is benzotriazolate; (b) $\{[Cu_3Tb(LPr)W(CN)_8(DMF)_4]\bullet(DMF)\}_n$ chain; (c) $[\mu-\{Co(ethylene\ glycol)(H_2O)_2\}_2\{Co_4(citrate)_4\}]_n$ layer, and (d) $[Sm(HCOO)_3]_n$ network. Colour codes: O, red; C, grey; Co, cyan; N, blue; Ln, purple; W, Pink; Cu, olive green. Hydrogens omitted for clarity.

These materials have a wide range of potential applications and have been extensively studied as: quantum bits in powerful new types of computers,[5] luminescent light sources,[6] high density memory in storage devices using single-molecule magnets (SMMs),[7] and low temperature refrigerants (MCE).[8] SMMs are the most active research topic in the area of Molecular Magnetism.[9] Moreover, these systems are a

milestone for physicists and chemists for the understanding of physical phenomena occurring at the pure molecular level.[10]

2.1.1 Magnetocaloric Effect (MCE)

The magnetocaloric effect (MCE) was first discovered in iron by the German physicist, Emil Gabriel Warburg in 1881.[11] In simple terms, the MCE is the response of a magnetic solid to a changing magnetic field which is observed as a change in its temperature. The basic understanding of MCE lies in the thermodynamic relationships that relate the magnetic entropy change (ΔS_m), the magnetisation of a system (M_β) and the temperature (T). The MCE can be demonstrated with reference to (Figure 2.2). Take a magnetic material in a state A(T_i, H_i), at initial temperature T_i and initial field H_i, where H_i is zero or very near to zero, and then raise the magnetic field isothermally, thus the temperature of the system remains constant to H_f. This can be achieved experimentally by connecting the sample to the helium bath, the helium bath absorbs the heat generated by the sample as its entropy decreases, keeping its temperature constant. The magnetic entropy of the sample S_m, will fall as the field rises, transporting the system to a state B(T_i, H_f) with the magnetic entropy change (eq. 2.1).

$$\Delta S_m(T)_{\Delta H} = \left(S(T)_{H_f} - S(T)_{H_i}\right)_T \tag{2.1}$$

By isolating the material from surroundings (*i.e* removing of the helium bath), and the field gradually and reversibly dropped from H_f to H_i, the total magnetic entropy of the material must stay constant and since the unpaired electrons want to become randomised again, the energy for this must be absorbed from the sample itself, therefore the temperature of the sample decreases by the temperature change (eq. 2.2).

$$\Delta T_{ad}(T)_{\Delta H} = \left(T(S)_{H_f} - T(S)_{H_i}\right)_S \tag{2.2}$$

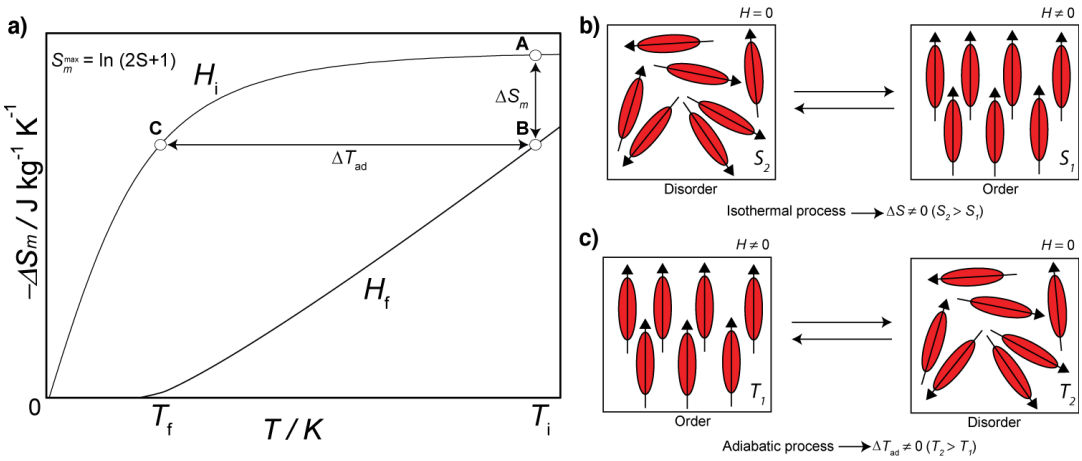

Figure 2.2: Diagram displaying processes of the MCE while a magnetic field is applied or removed within a magnetic system: (a) Molar magnetic entropy of a of super-paramagnet with spin S per formula unit, for magnetic field H_i and $H_f > H_i$. A→B process: isothermal magnetisation providing ΔS_m. B→C process: adiabatic magnetisation process providing ΔT_{ad}; (b) the isothermal process; (c) the adiabatic process.

$\Delta T_{ad}(T)_{\Delta H}$ is called as the adiabatic temperature change, the term adiabatic indicates that the total entropy of the sample remains constant during the magnetic field change. The mathematical relationship between the magnetic field H, the

magnetisation of a material and the temperature and the MCE-related values, $\Delta T_{ad}(T)_{\Delta H}$ and $\Delta S_m(T)_{\Delta H}$ is defined by the Maxwell relations.[12, 13]

$$\left(\frac{\partial S(T,H)}{\partial H}\right)_T = \left(\frac{\partial M(T,H)}{\partial T}\right)_H \tag{2.3}$$

Which for an isothermal and isobaric process give rise to:

$$\Delta S_m(T,\Delta H) = \int_{H_i}^{H_f} \left(\frac{\partial M(T,H)}{\partial T}\right)_H dH \tag{2.4}$$

The equation (2.4) shows that the magnetic entropy variation is proportional to both the derivative of magnetisation with respect to temperature at constant field and to the field change.

2.1.2 Single Molecule Magnetism

This field came about with the discovery molecular systems can remember magnetisation at the pure molecular level at zero applied magnetic field.[14-16] The first single molecule magnet (SMM) was observed in 1991 in a manganese complex, $[Mn^{III}_8Mn^{IV}_4O_{12}(O_2CMe)_{16}(H_2O)_4]$ (known as "Mn12")[17, 18] (Figure 2.3a), since then the magnetic properties of polymetallic transition metal clusters have become of particular interest. The manganese cage, can be described as an internal tetrahedron of Mn^{IV} and an external octagon of Mn^{III}, with overall S_4 symmetry bridged by (μ_3–O) ions and by carboxylate bridges from acetate anions.

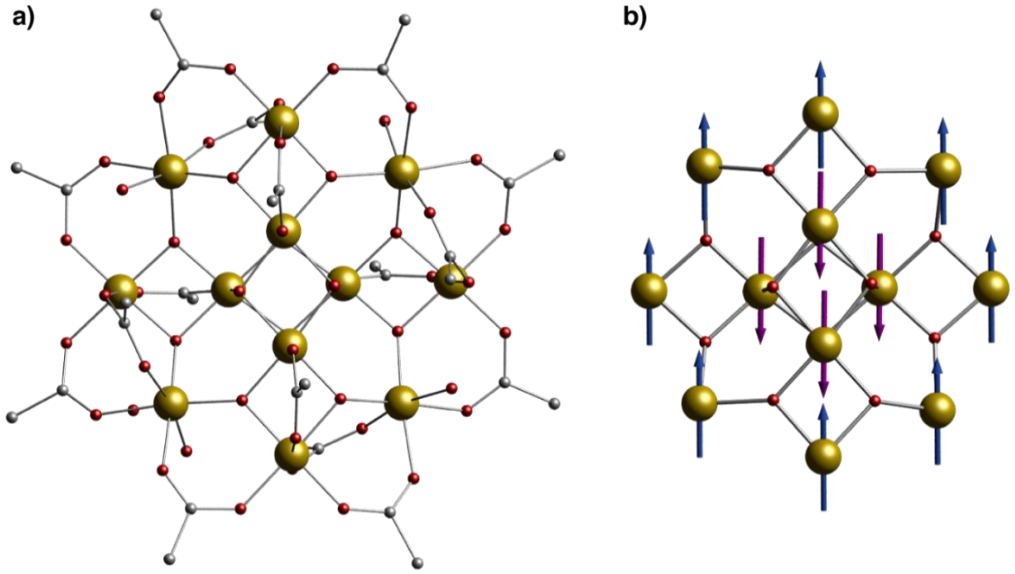

Figure 2.3: (a) Molecular structure of $[Mn_{12}O_{12}(OAc)_{16}(H_2O)_4]$ viewed down the tetragonal C_4 axis (z); (b) Demonstration of relative orientations of Mn^{III} (S = 2) and Mn^{IV} (S = 3/2) spins in the ground state. Colour code: O, red; C, grey, Mn, gold. Hydrogen atoms omitted for clarity.

This cluster has an energy barrier to the relaxation of magnetisation, which results in magnetisation *vs.* applied field hysteresis below a blocking temperature, and these SMMs are characterised by combination of a high ground state spin (S, resulting from magnetic exchange interactions between paramagnetic ion centres), and a large negative zero-field splitting (D) in the ground state, this leads to a significant barrier to relaxation of magnetisation = $|D|S^2$. The spin ground state of $\{Mn_{12}\}$ can be described by the Mn^{IV} ions aligning parallel due to a ferromagnetic interaction. In the complex, each of the four Mn^{III} spins is aligned in opposite spin direction to the Mn^{IV} ions, resulting in a total spin-ground state of S = 10 (Figure 2.3b).[19,20,21] The energy barrier originating from the zero-field splitting causes the m_s levels to split in energy ranging from $m_s = \pm 10$ at lowest energy to $m_s = 0$ at high energy (Figure 2.4). In zero-field the ±10 states are equal in energy and can be described as the "up" and "down"

states of the system. Application of the field removes the degeneracy of the ±10 states and results in one of these levels being lowered in energy and this level is preferentially populated. On removal of the field the m_s = ±10 states become degenerate in energy again, and in order for the system to return to equilibrium, the system must be able to pass from m_s = +10, through m_s = 0 and then down again to occupy the m_s = −10 level. Slow relaxation times are a direct result of this energy barrier.

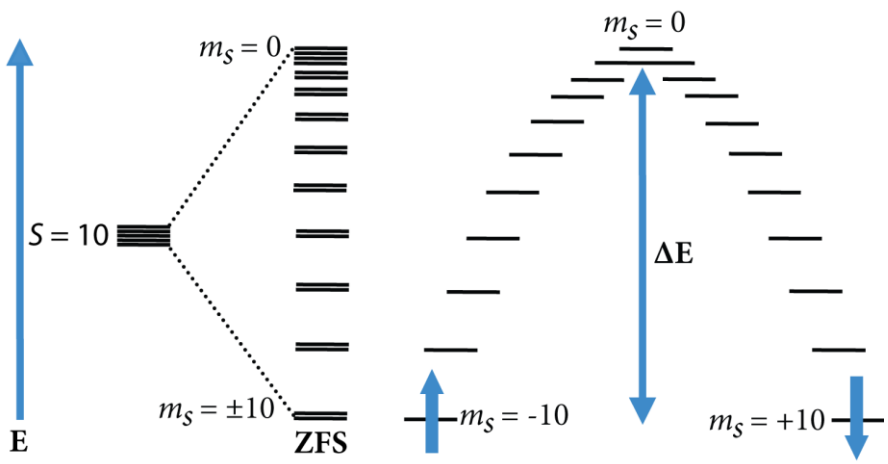

Figure 2.4: Diagram presenting the zero-field spliting of an S = 10 ground state with negative D. The energy barrier between the ms = +10 and −10 is indicated by ΔE.

There are many examples of manganese molecules that show these magnetic properties, for example $[Mn(III)_6O_2(sao)_6(O_2CH)_2(MeOH)_4]$ (where sao^{2-} is the dianion of salicylaldoxime or 2-hydroxybenzaldehyde oxime) and $[Mn_{30}O_{24}(OH)_8(O_2CCH_2{}^tBu)_{32}(H_2O)_2(MeNO_2)_4]$.[22, 23] SMM behaviours are also detected in other 3d metal cages with different nuclearity such as, Fe_4, Fe_8, Fe_{10}, Co_4, V_4 and Ni_{21}. [24-27] Though, none of these examples show SMM memory effects over 4

K. The lack of geometric control has resulted in some complexes with extremely large spin values that do not behave as SMMs due to the absence of uni-axial magnetic anisotropy.[28,29]

For 4f spin carriers, the large total angular moment (*J*) and significant single ion anisotropy make them the excellent spin carriers for SMMs, there is the disadvantage of only a very weak exchange interaction due to internal nature of 4f orbitals.[30,31] The interest in SMMs based on 4f ions was advanced by the report of Ishikawa *et al.* in 2003.[32] The report considered the first observation of single molecule magnet behaviour in complexes with a single metal ion entity comprising Tb(III) or Dy(III). The compound comprised a lanthanide sandwiched between two phthalocyanines, giving a series of double-decker compounds of formula $[Ln(III)Pc_2]\bullet TBA^+$ (Pc = phthalocyanine dianion; $TBA^+ = N(C_4H_9)^+$). Four N donors atoms of the phthalocyaninate ligand bind the central metal ion, which are staggered above and below (Figure 2.5).

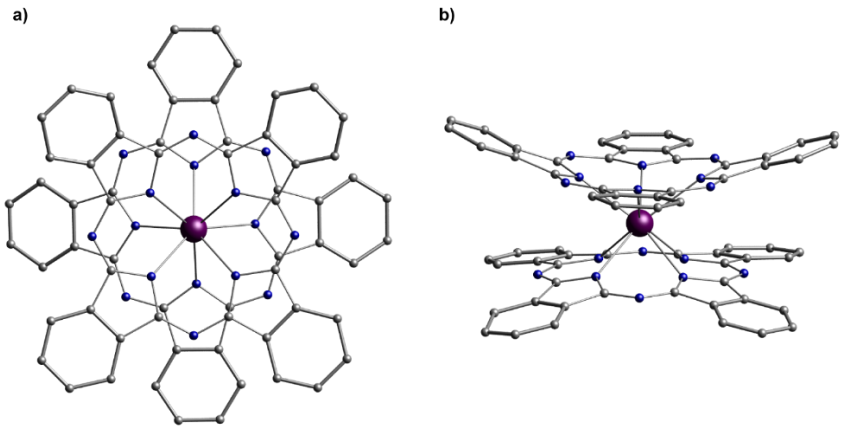

Figure 2.5: (a) To view of $[LnPc_2]^-$; (b) Side view of $[LnPc_2]^-$, where Ln = Tb(III) or Dy(III). Colour code: C, grey; Ln, purple, N, blue. Hydrogens omitted for clarity.

Studies of the magnetic interactions involving transition metal and lanthanide ions were pioneered by Gatteschi and co-workers (Figure 2.6),[33] they observed that when Cu(II) and Gd(III) were bridged together, the coupling between the ions was ferromagnetic.[34] Many other Cu-Ln mixed-metal systems have since been explored, displaying ferromagnetic interactions for most of them.[35-37] At first most of the effort was toward the transition metal systems and the isotropic lanthanide, Gd(III), and several complexes have been reported toward this trend.[38,39] Merging of the 3d and 4f spin carriers together with appropriate bridging ligands into a singular material with the benefits of ; i) 3d metal ions can transmit strong exchange interactions;[40] ii) the strong spin orbit coupling substantial to lanthanide systems can give better SMM properties (when Ln = Tb(III), Dy(III), Ho(III) and Er(III)), whereas Ln = Gd(III), higher magnetic entropy can be reached.[20,40,41]

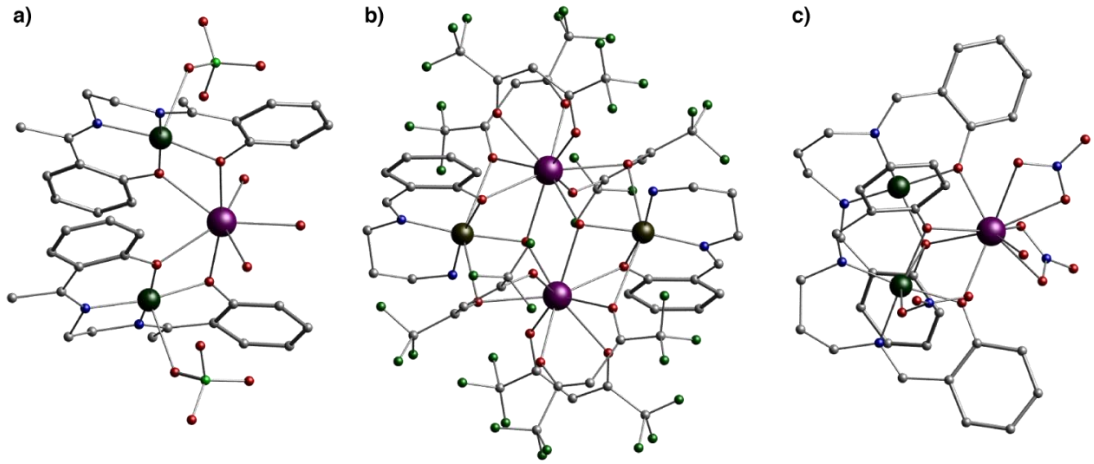

Figure 2.6: View of crystal structures of CuGd molecules: (a) $[CuHAPen)_2Gd(H_2O)_3](ClO_4)_3 \bullet 2CuHAPen$; (b) $[Dy(hfac)_3CuSatnOH]_2$; (c) $[CuSALtn)_2Gd(H_2O)(NO_3) \bullet 2EtNO_2]$. Where; CuHAPen = N'-ethylenebis(o-hydroxyacetophenoniminato)]copper(II); CuSatnOH = [N-(3-aminopropyl)salicylaldiminato]hydroxocopper(II), and CuSALtn = [N,N'- 1,3-propylenebis(salicylaldiminato)]copper(II). Colour code: C, grey; Ln, purple, N, blue; Cu, olive green; F, dark green; Cl, light green; O, red. Hydrogens and solvent molecules were omitted for clarity.

2.2 Synthetic Strategies

There are two strategies employed in the synthesis of multi-metallic clusters. The first is 'designed assembly', and relies on the use of a rigid ligand in which the geometry of the resultant cluster is largely predictable given that the ligand can adopt few bridging modes, for example, cyanide. The second, called 'Serendipitous Assembly', uses flexible ligands that impose little or no geometry and which may display a multitude of bridging modes, for example phosphonates.[42]

From a synthetic standpoint, methods must be found to combine 3d and 4f ions within a coordination compound. Practise has exposed that simply mixing the components does not lead to the self- assembly of the desired mixed compounds, but frequently to pure 3d compounds. This results from the specific chemical nature of 3d and 4f ions and in a complicated heterometallic reaction systems, may be the ligand field stabilisation for 3d compounds driving force leading to 3d complexes.[43] According to hard and soft acids and bases (HSAB),[44] lanthanide ions prefer to bind to hard donor atoms such as oxygen, while transition metal ions prefer to bind to softer donor atoms such as nitrogen. This recognition of donor atoms by metal ions offers a potential approach to the synthesis of 3d–4f coordination complexes, from the point of thermodynamics, potential energy in reaction system is a key factor for the creation of the final products,[45] the relative energy level of each potential complex (pure 3d, pure 4f and 3d–4f complex) is expected qualitatively according to HSAB.

2.2.1 Solvothermal Synthesis

Solvothermal chemistry involves conducting experiments with superheated solvents (*i.e.*, solvents that are heated under pressure beyond their atmospheric boiling points).[46,47] These experiments are performed in a Teflon-lined autoclave in an oven, under autogenous pressure, commonly in temperatures up to 250 °C. Superheated solvents have several benefits. First of all, superheated solvents can exhibit very different solubilising properties than at ambient pressures and temperatures. This

difference in solubility can lead to otherwise insoluble products being solubilised under solvothermal environments, and this can also be exploited to tackle the solubility differences between metal salts and ligands. Secondly, a reduced viscosity of the solvent aids diffusion of chemical species, leading to better crystal growth from the reaction solution, this improves crystal quality necessary when single crystal X-ray diffraction is required for complex characterisation. Furthermore, the temperature regime used in solvothermal techniques is intermediate between those used in low temperature 'conventional' solution chemistry and high temperature solid state routes. The controlled heating and cooling of the oven allows the reactions to be cooled very slowly, regularly enabling crystallisation of the products directly from the autoclave, this method of crystal growth provides the solvothermal route an excessive benefit over 'conventional' methods.

Lately, solvothermal techniques have been employed by coordination chemists to synthesise a variety of molecular cages, including magnetic materials (See Chapter 3). But in spite of all the above profits (especially the ability to crystallise products from the reaction solution - cluster chemistry is completely dependent on single crystal X-ray crystallography, given the complexity and the unpredictability of the cages formed), there are limited literatures on the syntheses of discrete molecular clusters by solvothermal methods.[48]

2.3 Phosphonate Chemistry

One way to make a cluster with increasing number of paramagnetic metal ions is choosing the ligands which have flexible arms and affinity towards the metals after activation by base. There are diversity of flexible ligands reported for example; triethanolamine ($teaH_3$), 1,2-bis(4-pyridyl)ethane (bpe), biphenylethene-4,4'-dicarboxylic acid (bpea), hydroxypyridine (hp), 6-methyl-2-hydroxypyridine (mhp) and 1,1,1-tris(hydroxymethyl)ethane. In this work, we proposed to explore the coordination chemistry of phosphonate ligands with 4f and mixed 3d–4f metals.

Organophosphonates $[RP(O)_2OH]^-$ and $[RPO_3]^{2-}$, obtained from the deprotonation of $RP(O)(OH)_2$ (where R is an organic functional group), have been used in synthetic inorganic chemistry for many years to synthesise coordination networks.[49] The charge of phosphonate ligands varied according to the nature of R group, for example, a carboxylic acid can add another negative charge to the anion, another phosphonic acid will add two further negative charges, whilst a protonated amine will reduce the negative charge on the anion. The pH of the reaction medium can further change the extent of protonation/deprotonation of these groups, and this must also be considered. The R groups can be varied almost infinitely, and materials have been reported containing simple moieties such as alkyl chains and phenyl groups, carboxylic acids, alcohols, amines, as well as more complex organic functional groups such as such as crown ethers (See Chapter 3).

In principal, a phosphonate ligand can bond through the nine lone pairs of the three oxygen donor atoms to a total of nine metal ions, practically, this theoretical maximum coordination mode has not been seen, the highest coordination mode seen is a μ_8 coordination polymer.[50] Some common coordination modes of phosphonate ligands are shown in (Scheme 2.1). Several bonding modes displayed by the phosphonate ligands can be expressed in Harris notation. Harris notation[51] describes the binding mode as $[X.\ Y_1Y_2\ldots Y_n]$ where X is represents the overall number of metals bound by the whole ligand, and each value of Y refers to the number of metal atoms attached to the different oxygen atoms.

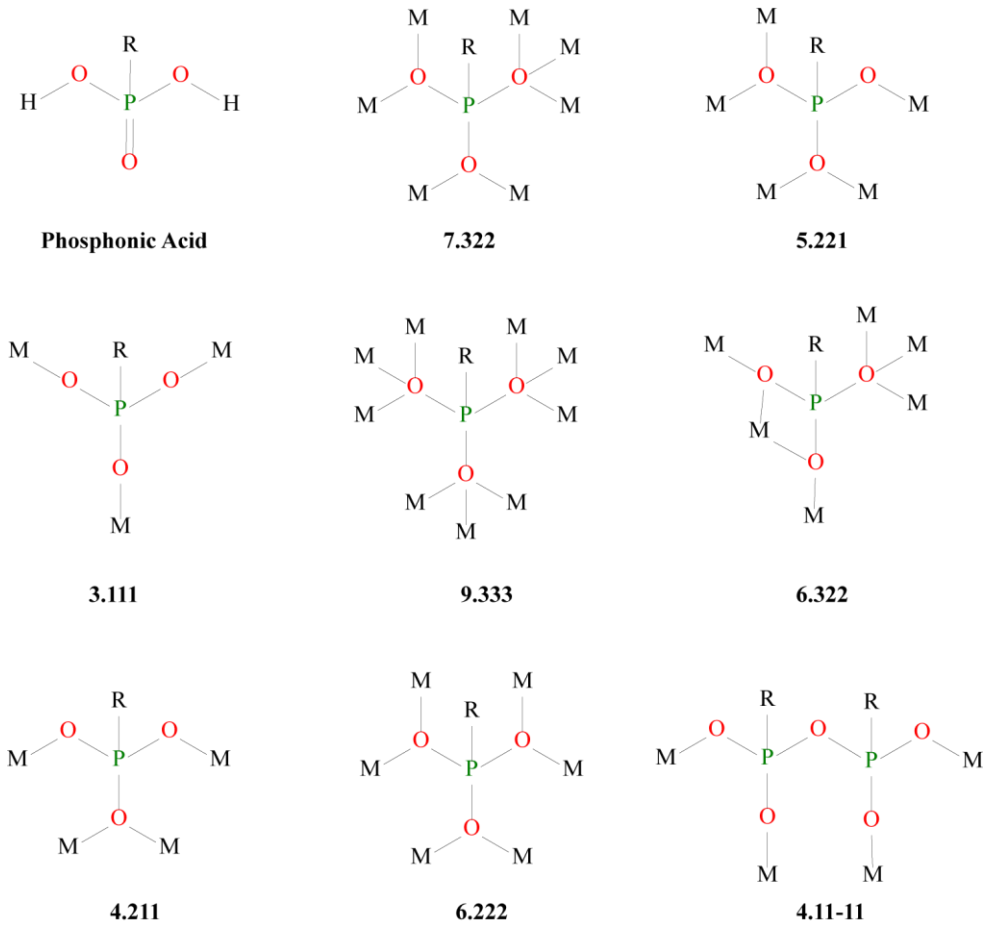

Scheme 2.1: Common coordination modes for phosphonate ligands, including Harris notation.

Because of the affinity to coordinate in a diversity of ways with metal centres it is usually impossible to predict the resultant product obtained from the reaction. Hence, for our research we are completely dependent on X-ray diffraction to expose the structure of the complexes, which is essential to study their electronic and magnetic properties. In contrast to designed assembly, we have been following an approach named 'serendipitous' assembly, where we can see several kinds of coordination geometry around the metal centres due to the unpredictable nature of the coordination ability of the elastic phosphonate ligand. The chemical reactivity of the phosphonates can be significantly modified by substituting different functional groups, as a result various products can be obtained with various chemical and physical properties.

Hence, phosphonate chemistry generates unpredictable results. This affects the choice of phosphonic acid ligands, it is very important to mention, firstly, ligands that need huge synthetic effort should be avoided, as it cannot be predicted whether they will be useful. Secondly, as slight differences in the ligands may affect structure ideally a series of related ligands should be explored. Finally, as a range of solvents will need to be inspected for crystallisation of the cage complex, it is valuable if the ligand has solubility in as many solvents as possible. One disappointingly common result is the formation of perfect, colourless crystals of ligand grown from coloured solutions of complex.

The main difficulty associated with the phosphonates is the insolubility of the resultant product, which eventually forced many synthetic chemists to search for a different synthetic strategy. The first synthetic strategy that utilises excess of co-ligand alongside the phosphonate arises from Chandrasekhar and Kingsley.[52] The co-ligand occupies a certain number of coordination sites on the metal ion as a result of which the number of coordination sites that are accessible for the phosphonate ligands decrease and the resultant cage stays in the solution itself rather than forming an insoluble powder, this methodology has been used to synthesise molecular cages containing manganese,[53] nickel,[54] cobalt,[55] vanadium,[56] iron[57] and copper.[58] Another synthetic strategy to tackle the solubility problem is to react the ligand with a preformed metal carboxylate cage such as $[M_3(O)(RCO_2)_6(py)_3]^{0/+}$ (where M = Mn,[59] Cr,[60] Co,[61] Fe[62]) or metal dimers such as $[Ln_2(O_2C^tBu)_6(HO_2C^tBu)_6]$ (Ln= Gd, Tb, Dy, Ho or Er) rather than metal salts, as precursors to obtain large cages (See Chapter 3). In this thesis we have followed both strategies and the obtained results are discussed.

2.3.1 Extended Networks

The synthetic methods used in the production of metal phosphonates can be diverse, depending upon the nature of the organic group in the phosphonate anion and the metal being used. Moreover, it has been shown that an enormous diversity of extended networks can be synthesised with metal centres and phosphonic acid

ligands by changing reaction conditions such as reaction stoichiometry whilst using the same reagents (See Chapter 3).

Metal phosphonates *(d*-block*)* were first reported in 1978 by Giulio Alberti *et al.*[63] The zirconium containing compounds reported by Alberti was layered in nature but no structures were upcoming because of their very low soluble nature. It was not until 1993 that the structure of the phenylphosphonate $Zr(O_3PC_6H_5)_2$ was solved by Poojary *et al.* (Figure 2.7),[64] and since then hundreds of papers have been published on layered phosphonate materials. The structure of these materials can be simply described as containing layers of metal cations coordinated by the oxygen atoms of the $[PO_3]^{2-}$ group of the phosphonate anions. The R group is then suspended in the interlayer region of the material, but can bond to metal ions in the next inorganic layer if there is a suitable donor atom accessible.[65] The capability of the phosphonate ligand to form chain, layered and 3-D complexes could be different by varying the metal centre used, the bulk of organic substituent, by the use of bis-, tris- or tetrakis-phosphonates and the use of multifunctional phosphonate ligands, for example using phosphonates functionalised with crown-ethers.

The first lanthanide phosphonates were synthesised in 1990 by Mallouk and co-workers.[66] They prepared lanthanide phenylphosphonates with formula $Ln(O_3PC_6H_5)(HO_3PC_6H_5)$ (Ln = La and Ce), and a series of alkylphosphonates such as $Ln(O_3PMe)(HO_3PMe)$. From the unit cell parameters they assumed that the

structures of these lanthanide phosphonates were most likely associated to those of $Zr(O_3PR)_2$ and $Ca(HO_3PR)_2$ (R=Me, C_6H_5–) both having a layered structure. Two years later, Clearfield and co-workers[65] reported the layered structure of $La(O_3PC_6H_5)(HO_3PC_6H_5)$ (Figure 2.7). The La(III) ion is 8-coordinate with eight phosphonate oxygen atoms to complete the coordination spheres for the La(III) metal ion.

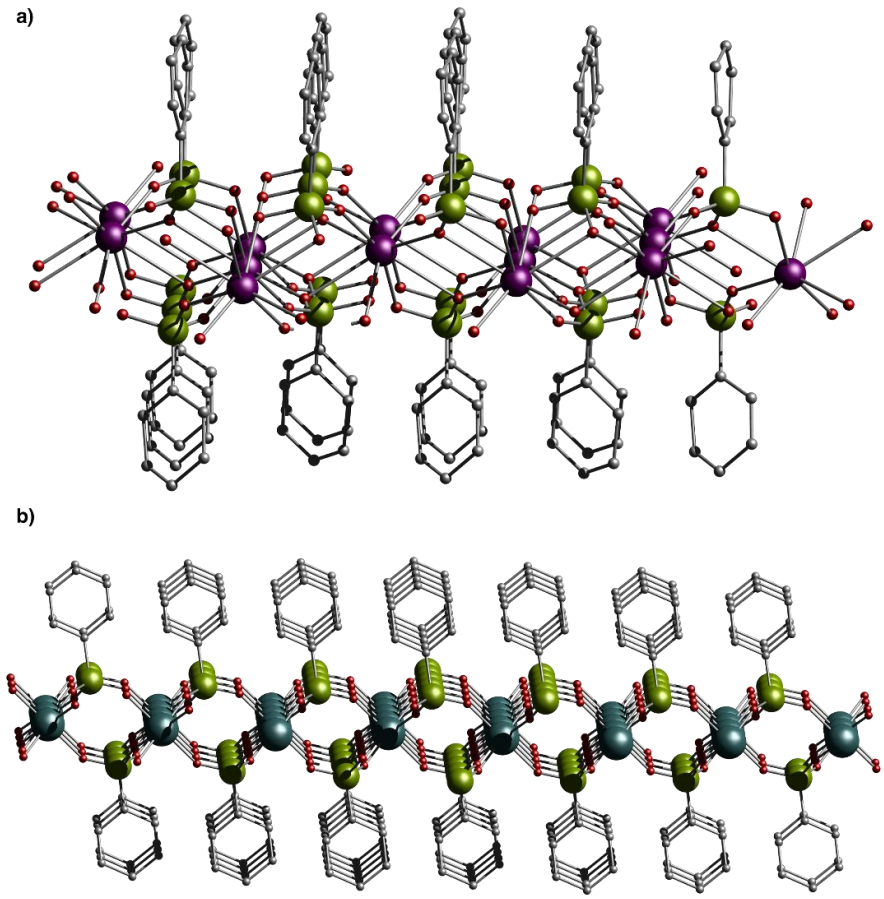

Figure 2.7: Structures of $Zr(O_3PC_6H_5)_2$ (a) and $La(O_3PC_6H_5)(HO_3PC_6H_5)$ (b), showing the layers formed by the metal ions, P and O atoms. Colour code: C, grey; La, purple; Zr, teal; O, red. Hydrogens omitted for clarity.

Recently, intense effort has been focused on the design and synthesis of heterometallic 3d–4f phosphonate clusters, and a variety of structures has been reported in this field. These compounds have been studied extensively because of their applications in magnetochemistry and coordination chemistry (See Chapter 8). In contrast to the transition metal phosphonates, compounds containing mixed 3d–4f or only 4f metals are unusual, the first 3d–4f phosphonate with SMM behaviour, $[Cu_{24}Dy_8(Ph_3C–PO_3)_6(Ph_3C–PO_3H)_6(MeCO_2)_{12}(MeCO_2H)_6(OH)_{42}(NO_3)(OH_2)_6][H_3O]$ was reported by Baskar *et al.* in 2010 (See Chapter 3). The compound contains eight Dy(III) centres arranged at the vertexes of a cube with twelve coppers inside and twelve copper outside the cube, the twelve inner coppers are organised in the form of a cuboctahedron (Figure 2.8).

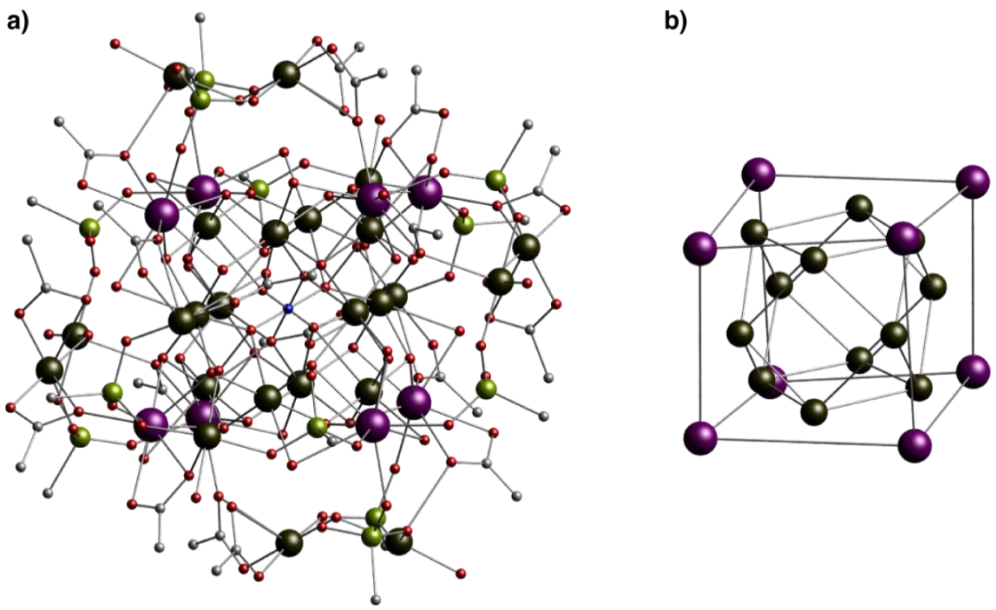

Figure 2.8: (a) Crystal structure of the $\{Cu_{24}Dy_8P_{12}\}$ cluster; (b) View of the Dy_8 cube encapsulating a Cu_{12} cuboctahedron. Colour codes: O, red; C, grey; Dy, purple; Cu, olive green; P, lime; N, blue. Hydrogens and phenyl groups were omitted for clarity.

2.4 References

1. R. Shaw, R. H. Laye, L. F. Jones, D. M. Low, C. Talbot-Eeckelaers, Q. Wei, C. J. Milios, S. Teat, M. Helliwell, J. Raftery, M. Evangelisti, M. Affronte, D. Collison, E. K. Brechin and E. J. L. McInnes, *Inorg. Chem.*, 2007, **46**, 4968.
2. S. Dhers, H. L. C. Feltham, R. Clérac and S. Brooker, *Inorg. Chem.*, 2013, **52**, 13685.
3. E. Burzurí, J. Campo, L. R. Falvello, E. Forcén.-Vázquez, F. Luis, I. Mayoral, F. Palacio, C. S. de Pipaón and M. Tomás, *Chem. Eur. J.*, 2011, **17**, 2818.
4. Y. Xu, S. H. Ding, G. P. Zhou and Y. G. Liu, *Acta Crystallogr. Sect. E: Struct. Rep. Online*, 2006, **62**, M1749.
5. F. Meier, J. Levy and D. Loss, *Physical Review B*, 2003, **68**, 15, 134417.
6. F. Ruibiao, H. Shengmin and X. Wu, *Cryst. Growth Des.*, 2014, **14**, 6197.
7. E. Coronado and D. Gatteschi, *J. Mater. Chem.*, 2006, **16**, 2513.
8. E. M. Pineda, F. Tuna, Y.-Z. Zheng and R. E. P. Winpenny, *Inorg. Chem.*, 2013, **52**, 13702.
9. O. Kahn, O. Cador, J. Larionova, C. Mathoniere, J. P. Sutter and L. Ouahab, *Molecular Crystals and Liquid Crystals Science and Technology Section a-Molecular Crystals and Liquid Crystals*, 1997, **305**, 1.
10. R. H. Laye and E. J. L. McInnes, *Eur. J. Inorg. Chem.*, 2004, **14**, 2811.
11. E. Warburg, *Ann. Phys. Chem.*, 1881, **13**, 141.

12. A. H. Morrish., *'The Physical Principles of Magnetism'*, Wiley, New York, 1965.

13. M. Evangelisti and E. K. Brechin, *Dalton Trans.*, 2010, **39**, 4672.

14. R. L. Carlin, *Magnetochemistry*, Springer-Verlag, Berlin, 1986.

15. O. Kahn, *Molecular Magnetism*, VCH, New York, 1993.

16. D. Gatteschi, R. Sessoli and J. Villain, *Molecular nanomagnets*, Oxford University Press, Oxford, 2006.

17. R. Sessoli, H.-L. Tsai, A. R. Schake, S. Wang, J. B. Vincent, K. Folting, D. Gatteschi, G. Christou and D. N. Hendrickson, *J. Am. Chem. Soc.*, 1993, **115**, 1804.

18. R. Sessoli, D. Gatteschi, A. Caneschi and M. A. Novak, *Nature*, 1993, **365**, 141.

19. Y.-Z. Zheng, E. M. Pineda, M. Helliwell and R. E. P. Winpenny, *Chem. Eur. J.*, 2012, **18**, 4161.

20. J. W. Sharples and D. Collison, *Polyhedron*, 2013, **54**, 91.

21. A. M. Tichin and Y. I. Spichkin, *The Magnetocaloric Effect and its Applications*, Institute of Physics Publishing, Bristol and Philadelphia, 2003.

22. C. J. Milios, R. Inglis, A. Vinslava, R. Bagai, W. Wernsdorfer, S. Parsons, S. P. Perlepes, G. Christou and E. K. Brechin, *J. Chem Soc.*, 2007, **41**, 12505.

23. M. Soler, W. Wernsdorfer, K. Folting, M. Pink and G. Christou, *J. Am. Chem. Soc.*, 2004, **7**, 2156.

24. C. Sangregorio, T. Ohm, C. Paulsen, R. Sessoli and D. Gatteschi, *Phys. Rev. Lett.*, 1997, **24**, 4645.

25. M. Murrie, S. J. Teat, H. Stoeckli-Evans and H.-U. Güdel, *Angew. Chem. Int. Ed.*, 2003, **38**, 4653.

26. S. L. Castro, Z. Sun, C. M. Grant, J. C. Bollinger, D. N. Hendrickson and G. Christou, *J. Am. Chem. Soc.*,1998, **10**, 2365.

27. S. T. Ochsenbein, M. Murrie, E. Rusanov, H. Stoeckli-Evans, C. Sekine and H.-U. Güdel, *Inorg. Chem.*, 2002, **41**, 5133.

28. D. M. Low, L. F. Jones, A. Bell, E. K. Brechin, T. Mallah, E. Riviére, S. J. Teat and E. J. L. McInnes, *Angew. Chem. Int. Ed.*, 2003, **42**, 3781.

29. A. M. Ako, I. J. Hewitt, V. Mereacre, R. Clérac, W. Wernsdorfer, C. E. Anson and A. K. Powell, *Angew. Chem. Int. Ed.*, 2006, **45**, 4926.

30. C. Benelli and D. Gatteschi, *Chem. Rev.*, 2002, **102**, 2369.

31. S. Fahrendorf, N. Atodiresei, C. Besson, V. Caciuc, F. Matthes, S. Blügel, P. Kögerler, D. E. Bürgler and Claus M. Schneider, *Nature Communications*, 2013, **4**, 3425.

32. N. Ishikawa, M. Sugita, T. Ishikawa, S. Koshihara and Y. Kaizu, *J. Am. Chem. Soc.*, 2003, **125**, 8694.

33. C. Bencini, C. Benelli, A. Caneschi, R. L. Carlin, A. Dei and D. Gatteschi, *J. Am. Chem. Soc.*, 1985, **107**, 8128.

34. Y. Pei, Y. Journaux, O. Kahn, A. Dei and D. Gatteschi, *J. Chem. Soc., Chem. Commun.*, 1986, **16**, 1300.

35. V. Gadet, T. Mallah, I. Castro and M. Verdaguer, *J. Am. Chem. Soc.*, 1992, **114**, 9213.

36. S. Ferlay, T. Mallah, R. Ouahès, P. Veillet and M. Verdaguer, *Nature*, 1995, **378**, 701.

37. T. Mallah, S. Thiébaut, M. Verdaguer and P. Veillet, *Science*, 1993, **262**, 1554.

38. A. Bencini, C. Benelli, A. Caneschi, A. Dei and D. Gatteschi, *Inorg. Chem.*, 1986, **25**, 572.

39. C. Benelli, A. Caneschi, D. Gatteschi O. Guillou and L. Pardi, *Inorg. Chem.*, 1990, **29**, 1750.

40. R. E. P. Winpenny, *Chem. Soc. Rev.*, 1998, **27**, 447.

41. R. Sessoli, *Angew. Chem. Int. Ed.*, 2012, **51**, 43.

42. R. E. P. Winpenny, *Dalton Trans.*, 2002, **1**, 1.

43. R. Sessoli and A. K. Powell, *Coord. Chem. Rev.*, 2009, **253**, 2328.

44. R. G. Pearson, *J. Am. Chem. Soc.*, 1962, **85**, 3533.

45. D. T. Richens, *Chem. Rev.*, 2005, **105**, 1961.

46. A. Rabenau, *Angew. Chem. Int. Ed.*, 1985, **24**, 1026.

47. G. Demazeau, *J. Mater. Chem.*, 1999, **9**, 15.

48. R. H. Laye and E. J. L. McInnes, *Eur. J. Inorg. Chem.*, 2004, **14**, 2811.

49. J. Goura, P. Bag, V. Mereacre, A. K. Powell and V. Chandrasekhar, *Inorg. Chem.*, 2014, **53**, 8147.

50. R. B. Fu, S. M. Hu, H. S. Zhang, L. S. Wang, Y. M. Li, X. H. Huang and X. T. Wu, *Chinese J. Struct. Chem.*, 2005, **24**, 1231.

51. Harris notation describes the binding mode as [*XY1Y2...Yn*] where *X* is the overall number of metal bound to the whole ligand, and each value of *Y* refers to the number of metal atoms attached to the different donor atoms. See: R. A. Coxall, S. G. Harris, D. K. Henderson, S. Parsons, P. A. Tasker and R. E. P. Winpenny, *Dalton Trans.*, 2000, **14**, 2349.

52. V. Chandrasekhar and S. Kingsley, *Angew. Chem., Int. Ed.*, 2000, **39**, 2320.

53. (a) M. Shanmugam, G. Chastanet, T. Mallah, R. Sessoli, S. J. Teat, G. A. Timco and R. E. P. Winpenny, *Chem.–Eur. J.*, 2006, 12, 8777; (b) S. Maheswaran, G. Chastanet, S. J. Teat, T. Mallah, R. Sessoli, W. Wernsdorfer and R. E. P. Winpenny, *Angew. Chem., Int. Ed.*, 2005, **44**, 5044.

54. (a) S. K. Langley, M. Helliwell, S. J. Teat and R. E. P. Winpenny, *Inorg. Chem.*, 2014, **53**, 1128; (b) B. A. Breeze, M. Shanmugam, F. Tuna and R. E. P. Winpenny, *Chem. Commun.*, 2007, **12**, 5185.

55. (a) S. K. Langley, M. Helliwell, S. J. Teat and R. E. P. Winpenny, *Dalton Trans.*, 2012, **41**, 12807; (b) S. Langley, M. Helliwell, R. Sessoli, S. J. Teat and R. E. P. Winpenny, *Inorg. Chem.*, 2008, **47**, 497.

56. (a) S. Khanra, R. Shaw, M. Helliwell, F. Tuna, C. A. Muryn, E. J. L. McInnes and R. E. P. Winpenny, *Materials*, 2010, **3**, 232; (b) S. Khanra, M. Kloth, H. Mansaray, C. A. Muryn, F. Tuna, E. C. Sañudo, M. Helliwell, E. J. L. McInnes and R. E. P. Winpenny, *Angew. Chem., Int. Ed.*, 2007, **46**, 5568.

57. (a) S. Konar and A. Clearfield, *Inorg. Chem.*, 2008, **47**, 3492; (b) E. I. Tolis, M. Helliwell, S. Langley, J. Raftery and R. E. P. Winpenny, *Angew. Chem., Int. Ed.*, 2003, **42**, 3804.

58. (a) V. Chandrasekhar, L. Nagarajan, R. Clérac, S. Ghosh, T. Senapati and S. Verma, *Inorg. Chem.*, 2008, **47**, 5347; (b) V. Chandrasekhar, L. Nagarajan, K. Gopal, V. Baskar and P. Kögerler, *Dalton Trans.*, 2005, **43**, 3143.

59. R. Wu, M. Poyraz, F. E. Sowrey, C. E. Anson, S. Wocadlo, A. K. Powell, U. A. Jayasooriya, R. D. Cannon, T. Nakamoto, M. Katada and H. Sano, *Inorg. Chem.*, 1998, **37**, 1913.

60. B. N. Figgis and G. B. Robertson, *Nature (London)*, 1965, **205**, 649.

61. G. Aromi, A. S. Batsanov, P. Christian, M. Helliwell, A. Parkin, S. Parsons, A. A. Smith, G. A. Timco and R. E. P. Winpenny, *Chem. Eur. J.*, 2003, **9**, 5142.

62. Y.-Z. Zheng and R. E. P. Winpenny, *Sci. China Chem.*, 2012, **55**, 910.

63. G. Alberti, U. Costantino, S. Allulli and N. Tomassini, *J. Inorg. Nucl. Chem.*, 1978, **40**, 1113.

64. D. M. Poojary, H. L. Hu, F. L. Campbell III and A. Clearfield, *Acta Cryst. B*, 1993, **49**, 996.

65. A. Clearfield and K. Demadis, '*Metal Phosphonate Chemistry: From Synthesis to Applications*', Royal Society of Chemistry, Cambridge, UK, 2012.

66. G. Cao, V. M. Lynch, J. S. Swinnea and T. E. Mallouk, *Inorg. Chem.*, 1990, **29**, 2112.

Chapter 3

3.1 A review of discrete 4f–phosphonate cages

Phosphonate complexes with Ln(III) ions have been extensively investigated with regard to their structures and their various practical applications such as: biological applications,[1] luminescent properties,[2,3] applications in solvent extraction[4] and more recently for their magnetic properties (See Chapters 4–7). In particular, lanthanides have become important components for contrast enhancement media used in nuclear medicine, for magnetic resonance imaging, and as optical probes.[5] However, the varied coordination requirements of the lanthanide ions make them difficult to design, compared with the predictability of the coordination geometry of the transition metals.[6]

This section reviews the structural chemistry of discrete 4f–phosphonate cages, including those containing additional functional groups or second metal linkers. The structures and abbreviations for some of the phosphonic acids used are shown in (Scheme 3.1). In the following sections, all reported 4f–phosphonate complexes will be classified as; mono-, bis-, tris- and tetrakis-metal phosphonate complexes.

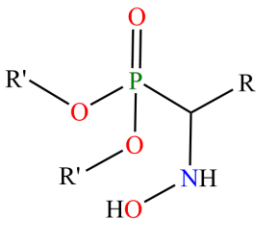

L[1]

	R	R'
L[1']	Et	Et
L[1'']	Et	^{i}Pr

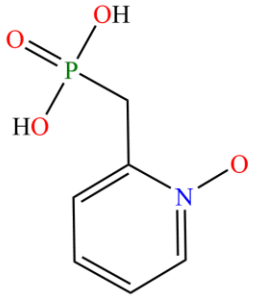

H_2L^2

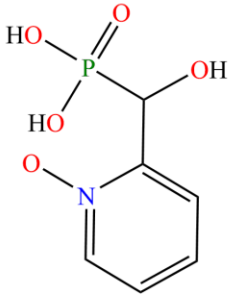

H_3L^3

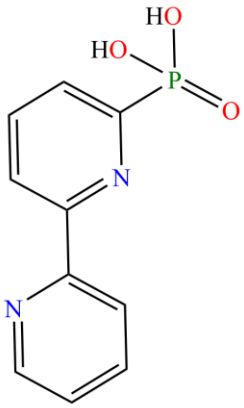

H_2L^4

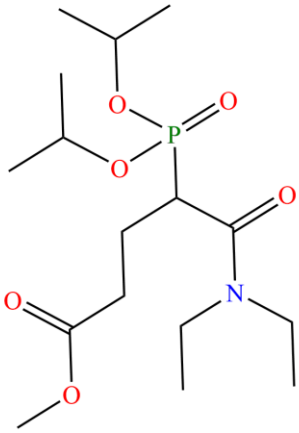

L^5

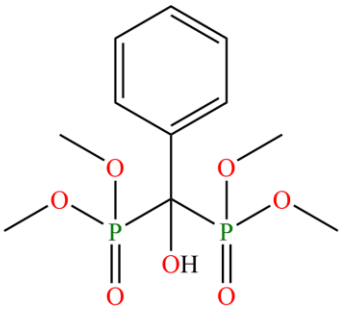

L^6

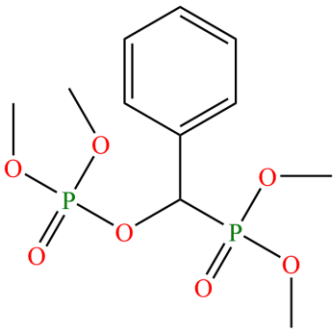

L^7

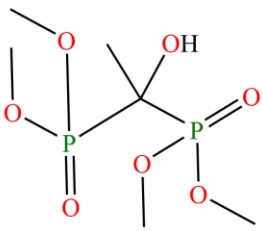

L^8

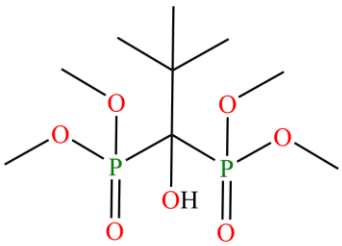

L^9

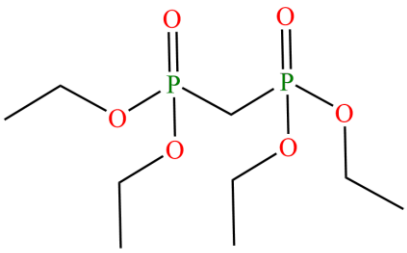

L^{10}

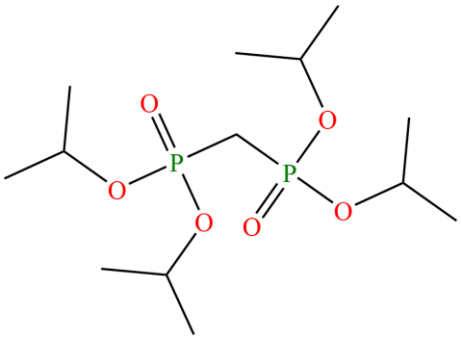

L^{11}

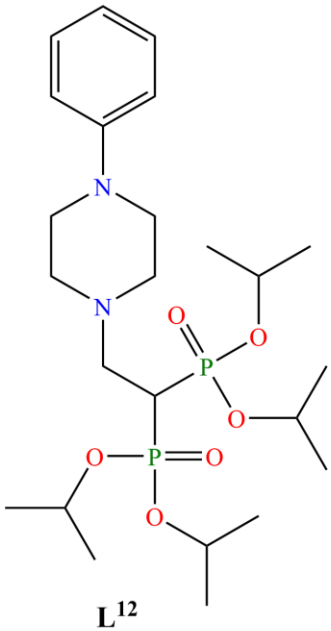

L^{12}

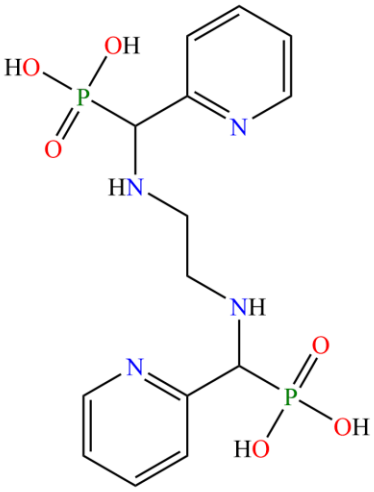

L^{13}

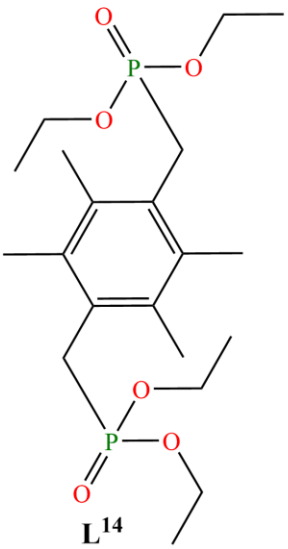

L^{14}

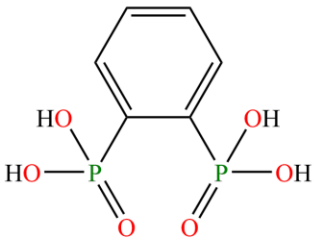

H$_4$L^{15}

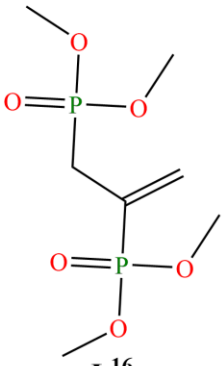

L^{16}

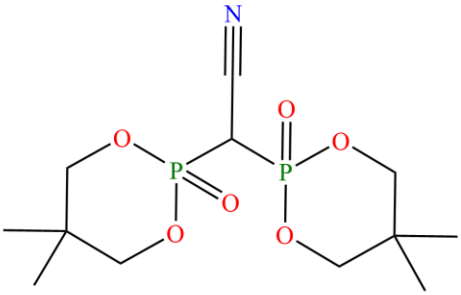

L^{17}

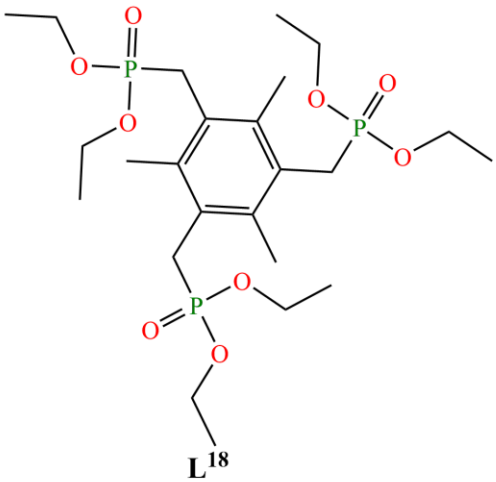

L^{18}

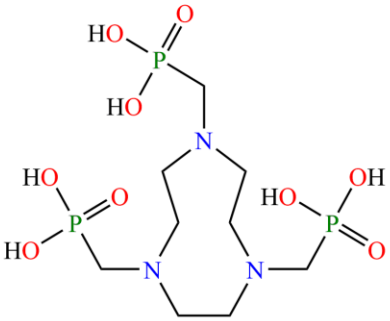

notpH$_6$

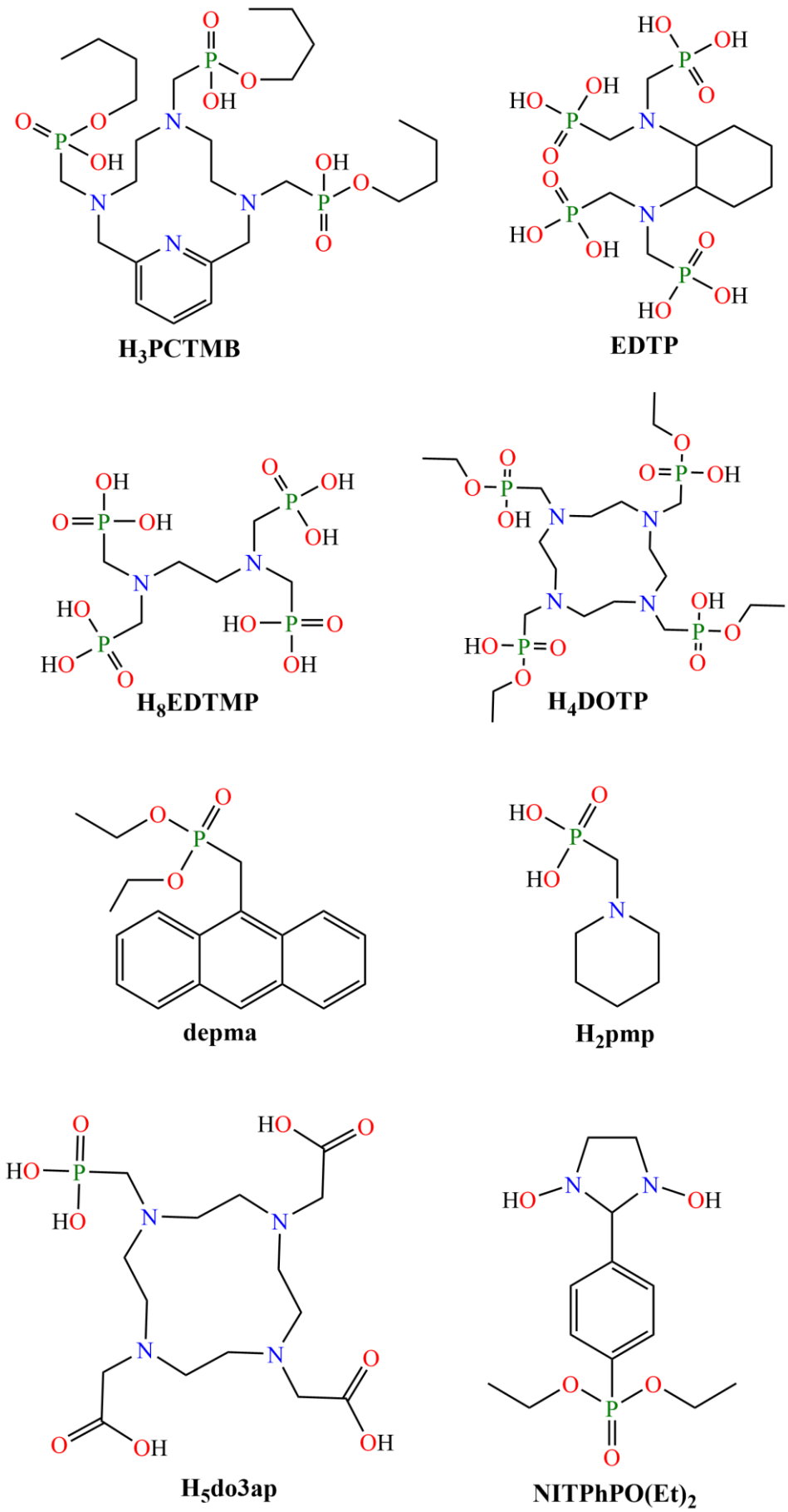

Scheme 3.1: Phosphonic acids in some lanthanide compounds.

3.1.1 Lanthanide complexes with mono- phosphonates

Bligh and co-workers[7] synthesised phosphonic acids of dialky α-hydroxyiminophosphonates RC=N(OH)P(O)(OR')$_2$ (L^1), with different bulky substituents (R = Et, R'= Et ($L^{1'}$); R = Et, R'= ^{i}Pr ($L^{1''}$)). These have been used to make neutral metal complexes with lanthanides(III) metal ions of La and Pr, In each compound the charge being balanced by anionic chloride ligands. The reaction was performed by adding hydrated $LnCl_3$ (Ln = La, Pr) to a methanolic solution of the dialkyl α-hydroxyiminophosphonate. After mixing the solution was left to stand and after several days the resulting solid was filtered off, washed with cold methanol and air-dried. In both complexes [La($L^{1'}$)$_3$Cl$_3$] (Figure 3.1a) and [Pr($L^{1''}$)$_3$Cl$_3$] (Figure 3.1b), the ligand coordinates *via* the oxime nitrogen and the phosphoryl oxygen, it is in an asymmetric bidentate coordination mode. The compound [Pr($L^{1''}$)$_3$Cl$_3$] has C_3 symmetry and [La($HL^{'}$)$_3$Cl$_3$] has a structure close to C_3 symmetry. Both complexes have identical nine-coordinate geometry at the Ln(III) metal ion, the structure can be imagined as a tricapped-trigonal prism. Imine nitrogen atoms occupied the three capping sites, the La–N and Pr–N bond length are about 2.851(9) and 2.798(7) Å, respectively. One end of the trigonal prism formed by oxygen donors, while the three chloro ligands form the other end, the La–O, Pr–O, La–Cl and Pr–Cl bond length are about 2.512(9), 2.461(9), 2.860(5) and 2.784(4) Å, respectively.

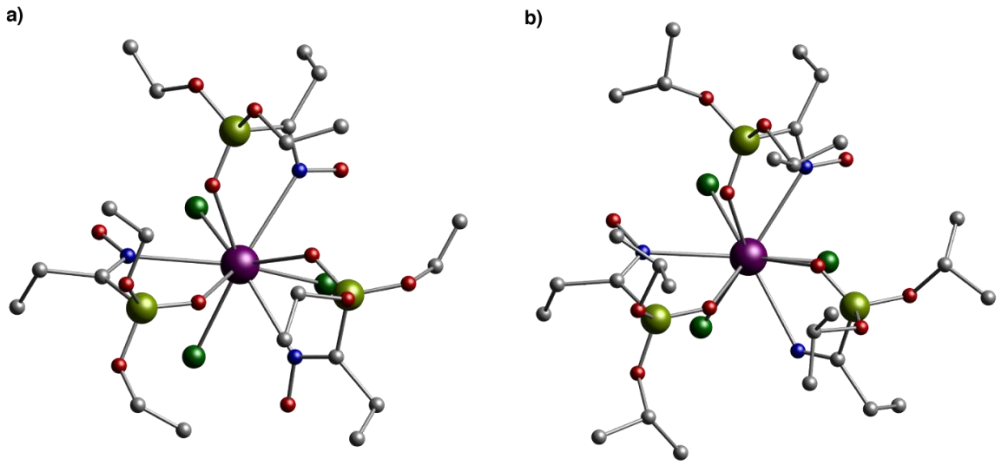

Figure 3.1: (a) The tricapped-prismatic co-ordination geometry in the complex $[La(L^{1'})_3Cl_3]$, displaying the asymmetric bidentate coordination mode of L^1; (b) The structure of $[Pr(L^{1''})_3Cl_3]$, it is very similar to $[La(L^{1'})_3Cl_3]$ but has crystallographic C_3 symmetry. Colour code: O, red; C, grey; Cl, green; Ln, purple; P, lime; N, blue. Hydrogens omitted for clarity.

Paine *et al.* reported two phosphonic acids based on 2-pyridyl N-oxide, 2-(pyridyl N-oxide) methylphosphonic acid (H_2L^2) and 2-(pyridyl N-oxide) hydroxymethylphosphonic acid (H_3L^3).[8] Reaction of 4 equiv of these ligands with 1 equiv of freshly prepared erbium hydroxide give rise to two isostructural compounds, namely, $Er(L^2)_3(H_2L^2)\bullet 8H_2O$ (Figure 3.2a) and $Er(L^3)_3(H_2L^3)\bullet 8H_2O$ (Figure 3.2b). Each compound has a 2-fold axis passing through the Er(III) metal atom and the asymmetric unit contains one-half Er(III) ion, two phosphonate ligands and four water molecules. All ligands are linked to the Er(III) ion with a bidentate coordination mode through the N-oxide and phosphoryl oxygen atoms, these eight oxygen atoms produce a square antiprismatic internal sphere coordination polyhedron. Each phosphonate ligand in the compound forms a seven-member chelating ring with an Er(III) ion with one phosphonate oxygen and one oxygen atom from the N-oxide group.

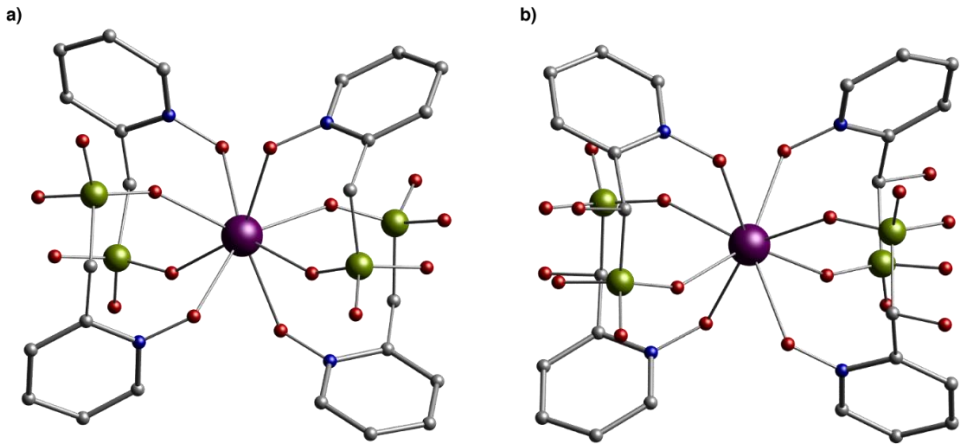

Figure 3.2: (a) The molecular structure of the complex $Er(L^2)_3(H_2L^2)\bullet 8H_2O$; (b) Crystal structure of $Er(L^3)_3(H_2L^3)\bullet 8H_2O$. Colour code: O, red; C, grey; Ln, purple; P, lime; N, blue. Hydrogens omitted for clarity.

Lukeš and co-workers synthesised a sequence of lanthanide compounds with 1,4,7,10-tetraazacyclodecane-1,4,7-triacetic-10-methylphosphonic acid (H_5do3ap), M[Ln(Hdo3ap)]•$x$$H_2O$ (M= H (Figure 3.3a) or Li (Figure 3.3b), and Ln=Nd, Tb, Dy, Er, Lu and Y).[9] The complexes were obtained by mixing H_5do3ap and corresponding metal chlorides in water, the pH was slowly adjusted to ~8 with a dilute solution of LiOH, and the solutions were fleetingly heated. After being allowed to stand overnight, the solutions were filtered, and the pH was dropped to ~4 with dilute hydrochloric acid. Crystals of the complexes were grown from aqueous solutions by the slow vapour diffusion of ethanol at room temperature within several weeks. The lanthanide(III) metal ions in all these complexes form a $\{Ln(Hdo3ap)\}^-$ chelating by Hdo3ap ligand units, four nitrogen atoms and four oxygen atoms, three from acetates and one from phosphonate. The impact of the exterior counter ions of lithium(I) or proton on the crystal packing is variable. The often detected formation

of infinite chains through Li(I) ions, linking the coordination polyhedrons was established in the complexes Li[Tb(Hdo3ap)(H_2O)•0.5HCl•5H_2O and Li[Nd(Hdo3ap)(H_2O)]•11.5H_2O. In contrast, in the isostructural Li[Ln(Hdo3ap)]•5H_2O (Ln = Dy, Y, Lu) complexes, the lithium(I) ion is bonded only to one carboxylate group without forming any chain. When the Li(I) ion is replaced by a proton, adjacent [Ln(Hdo3ap)] units are interconnected only via hydrogen bonds among uncoordinated carboxylate and phosphonate oxygen atoms along with lattice water molecules.

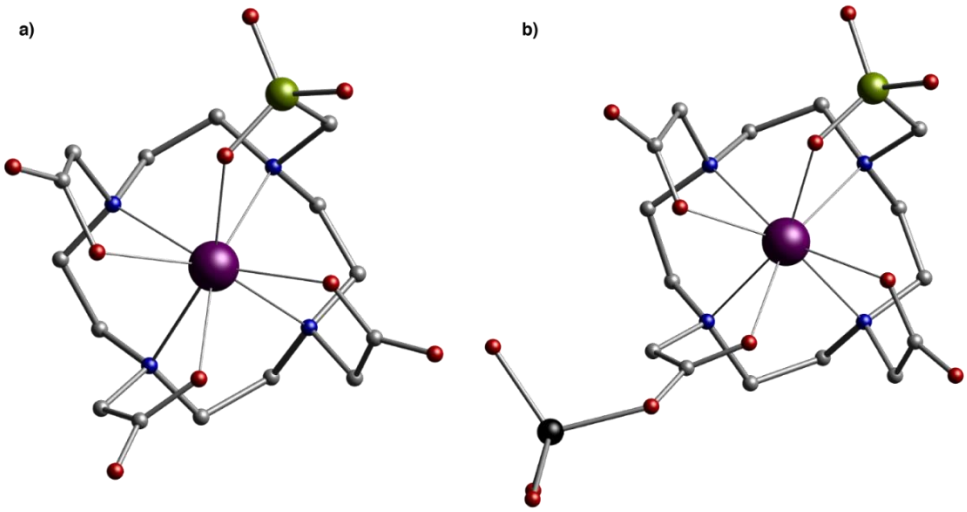

Figure 3.3: The molecular structure of M[Ln(Hdo3ap)]•$x$$H_2O$ [M= H (a) or Li (b)]. Colour code: O, red; C, grey; Ln, purple; P, lime; N, blue. Hydrogens omitted for clarity.

Comby *et al.* also reported a C_2-cymmetrical lanthanide complex with 5'-methyl-2,2'-bipyridyl-6-phosphonic acid (H_2L^4), [$Na_6Eu_9(L^4)_{16}$](OH)•51H_2O (Figure 3.4a).[10] The crystallisation procedure is severely controlled because any change in the Ln-H_2L^4 ratio, in the nature of the base, or in the crystallisation pH leads to a failure to isolate the polymetallic cage. The crystal is monoclinic and crystallises in *C*2/*c* space group,

there are eight eight-coordinate outer Eu(III) ions arranged on the vertices of two parallel parallelepipeds, (Eu1, Eu4, Eu1', and Eu4') and (Eu2, Eu3, Eu2', and Eu3') (Figure 3.4b). The ninth Eu(III) metal ion is disordered and located around the baricenter of the outer Eu(III) atoms, the centroid of these locations lies in the centre of the plane defined by the six sodium ions, but faintly below (–0.101 Å). Each outer Eu(III) is three-coordinated by two ligand elements, and its coordination sphere is finished by two O atoms from the phosphonate groups of two other ligand elements, the central Eu(III) ion is connected to four water molecules, and four O atoms from four diverse phosphonate groups.

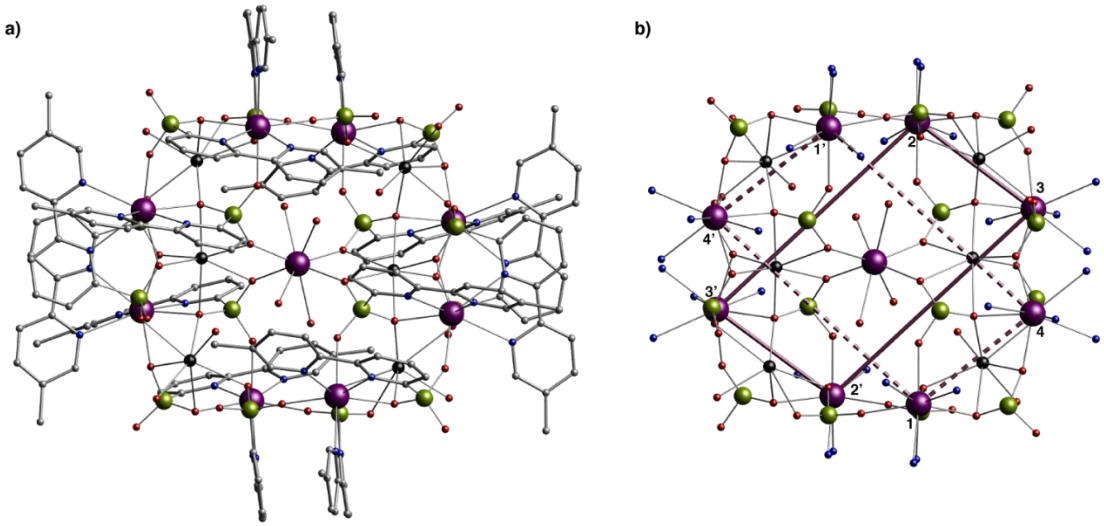

Figure 3.4: (a) Molecular structure of the $Na_6Eu_9L^4_{16}$ cluster; (b) View of the metal ion cluster, along with the numbering scheme of the Eu(III) metal ions. Colour code: O, red; C, grey; Er, purple; P, lime; N, blue. Hydrogens omitted for clarity.

The solvothermal reaction of Ce(III) nitrate with tritylphosphonic acid ($Ph_3CPO_3H_2$) in water-ethanol mixture, gave a molecular dimetallic Ce(III) phosphonate, $[Ce_2\{Ph_3CPO_2(OEt)\}_4(NO_3)_2(H_2O)_4]$ (Figure 3.5a).[11] The compound crystallises in

the triclinic space group $P\bar{1}$ space group, the molecular structure of the compound contains two cerium(III) atoms that are linked to each other by a two $[Ph_3CPO_2(OEt)]^-$ ligands, both phosphonate ligands present 2.011 binding mode, each cerium(III) atom is further coordinated to a 1.001 $[Ph_3CPO_2(OEt)]^-$ ligand and two water molecules. The two cerium(III) atoms are bridged by two nitrate ligands, the nitrate ligands in addition to bridging coordination also act as a chelating ligand. Hence, two oxygen atoms of each nitrate ligand are involved in binding two cerium(III) atoms. The total coordination environment around each cerium(III) is consequently made up of eight oxygen atoms, showing a distorted dodecahedron geometry (Figure 3.5b and c).

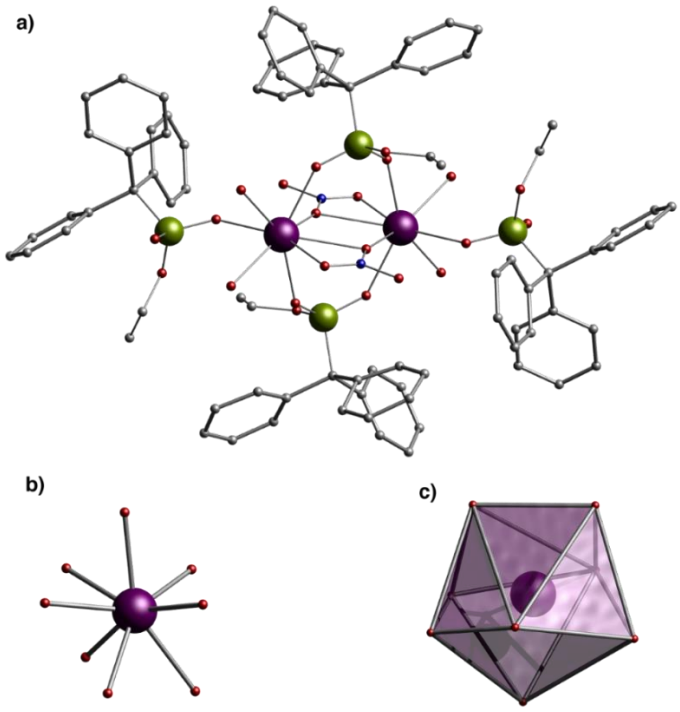

Figure 3.5: (a) Molecular structure of $[Ce_2\{Ph_3CPO_2(OEt)\}_4(NO_3)_2(H_2O)_4]$; (b) Coordination environment around Ce(III) ion; (c) The distorted dodecahedral coordination geometry around cerium. Colour code: O, red; C, grey; Ce, purple; P, lime; N, blue. Hydrogens omitted for clarity.

Two discrete nonametallic Ln(III) phosphonate clusters, formulated as, $[Ln_9(OH)(Hpmp)_{12}(ClO_4)(H_2O)_{26}](ClO_4)_{13}\bullet 18H_2O$ (Ln = Nd and Pr), (H_2pmp = N-piperidinomethane-1-phosphonic acid), were synthesised and structurally determined.[12] The crystal X-ray diffraction and powder XRD patterns shown that they are isostructural and crystallise in a chiral $P2_12_12_1$ space group (Figure 3.6a). The asymmetric unit of each compound contains nine Ln(III) ions, twelve $Hpmp^-$ ligands, one coordinated ClO_4^-, one μ-OH^-, twenty-six coordinated water molecules, thirteen perchlorate counter ions and several lattice water molecules. The Ln(III) ions and $Hpmp^-$ ligands form a cationic $[Ln_9(OH)(RPO_3)_{12}]^{14+}$ cluster along with a bridged μ–OH group. The compound is low symmetry, the organisation of the nine Ln(III) ions can be best described as a lotus-leaf-shape. Nd(5) is located in the bottom of the leaf forming an equilateral triangle with Nd(4) and Nd(7), which is crudely perpendicular to the six member ring formed by the rest six Nd(III) ions, the six Nd(III) ions are non-coplanar, furthermore, the four neighbouring metal ions (Nd(1), Nd(2), Nd(3) and Nd(4)) form a butterfly-shaped conformation (Figure 3.6b). The comparable conformation are also detected for Nd(6), Nd(7), Nd(8) and Nd(9) ions. All the coordination sites of Nd ions are occupied by O atoms from phosphonates, μ–OH, H_2O and ClO_4^-, the Nd–O distances are in the range of 2.323–2.758 Å. Nd(1), Nd(2), Nd(8) and Nd(9) are eight-coordinated, the coordination polyhedra of which can be represented as distorted square antiprisms. The other five Nd(III) ions are nine-coordinated, and their coordination polyhedra can be defined

as distorted monocapped square antiprisms. The $Hpmp^-$ ligands show 2.111, 3.111, 3.220, 4.221, and 5.222 coordination modes in the crystal structure.

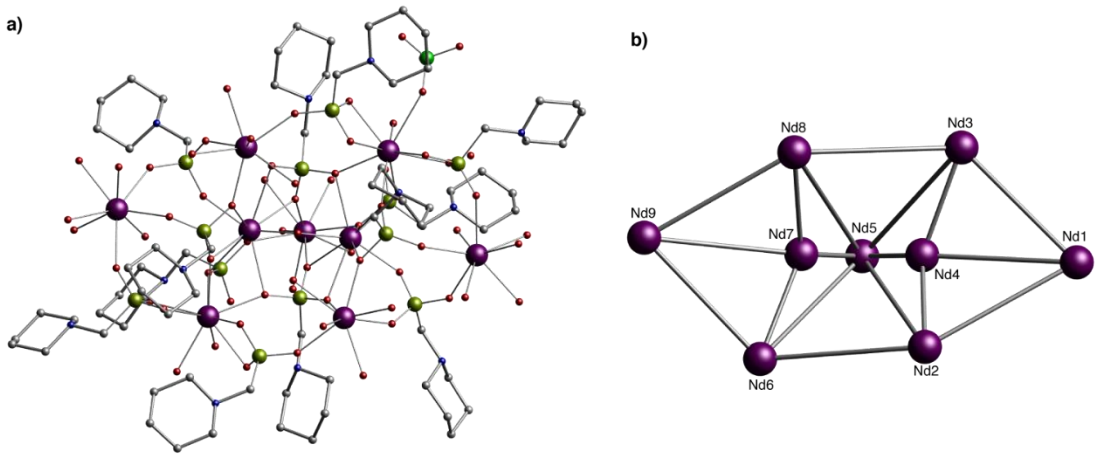

Figure 3.6: (a) Molecular structure of $[Nd_9(OH)(Hpmp)_{12}(ClO_4)(H_2O)_{26}](ClO_4)_{13}\bullet 18H_2O$; (b) View of the arrangement of the nine Nd(III) ions within the complex. Colour code: O, red; C, grey; Nd, purple; P, lime; N, blue. Hydrogens omitted for clarity.

By employing the 4'-[2-(1-oxyl-3-4,4,5,5-tetramethylimidazoline)-phenyl]diethoxylphosphine oxide) ($NITPhPO(OEt)_2$) ligand, a series of lanthanide complexes were isolated by Sessoli and co-workers,[13] namely, $[Ln(hfac)_3(NITPhPO(OEt)_2)]_2$, $[Ln(hfac)_3(NITPhPO(OEt)_2)]_2$, $[Ln(hfac)_3(NITPhPO(OEt)_2)]_2\bullet 2CH_2Cl_2$, and $[Ln(hfac)_3(NITPhPO(OEt)_2)]_2$; (where hfac = hexafluoroacetylacetonate and Ln = Gd, Tb and Dy). The asymmetric unit of $[Tb(hfac)_3(NITPhPO(OEt)_2)]_2\bullet 2CH_2Cl_2$ is built of a $Tb(hfac)_3$ moiety, a $NITPhPO(OEt)_2$ ligand, and a dichloromethane molecule of crystallisation (Figure 3.7a). Each Tb(III) ion is surrounded by eight oxygen atoms belong to three $hfac^-$ ligands, one N–O group and one phosphine oxide group. The oxygen atoms of the P═O and N–O groups are coordinated in a cis orientation on the Tb(III) ion. The

coordination polyhedron of the Tb(III) can be described as a slightly distorted dodecahedron. In the case of crystal packing concerning nitronyl nitroxide derivatives, focusing on the NO groups. There are no substantial intermolecular contacts between the magnetic rectangles. The shortest intermolecular Tb···Tb distance is 9.240(9) Å, each dimer is fairly isolated from the others because of the pierced moieties that are localised in the border of the molecule.

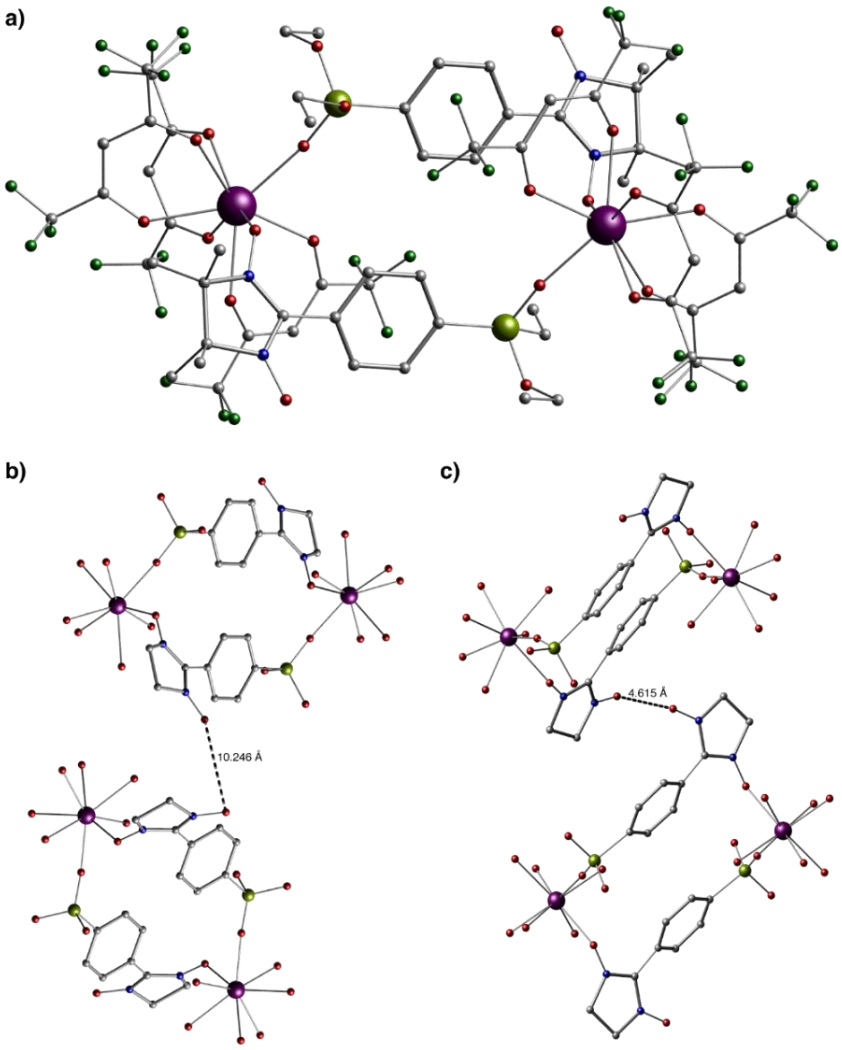

Figure 3.7: (a) Molecular structure of $[Tb(hfac)_3(NITPhPO(OEt)_2)]_2$; (b) and (c) Shortest intermolecular distances between two N–O radicals of neighboring molecules for $[Tb(hfac)_3(NITPhPO(OEt)_2)]_2 \bullet 2CH_2Cl_2$ and $[Tb(hfac)_3(NITPhPO(OEt)_2)]_2$, respectively. Colour code: O, red; C, grey; Tb, purple; P, lime; N, blue. Hydrogens omitted for clarity.

From a molecular point of view, $[Tb(hfac)_3(NITPhPO(OEt)_2)]_2$ is very similar to $[Tb(hfac)_3(NITPhPO(OEt)_2)]_2 \bullet 2CH_2Cl_2$, but the crystal packing is completely different. In $[Tb(hfac)_3(NITPhPO(OEt)_2)]_2$, short intermolecular contacts between the O–N–C–N–O systems takes place with distances of about 4 Å that can be compared with the distance of 10.246(25) Å detected in $[Tb(hfac)_3(NITPhPO(OEt)_2)]_2 \bullet 2CH_2Cl_2$ (Figure 3.7b and c). The shortest intermolecular Tb···Tb distances is 10.317(30) Å. The complex $[Gd(hfac)_3(NITPhPO(OEt)_2)]_2$ is identical to $[Tb(hfac)_3(NITPhPO(OEt)_2)]_2 \bullet 2CH_2Cl_2$. The minor changes of the crystallographic parameters are caused by the dichloromethane molecules of crystallisation in $[Tb(hfac)_3(NITPhPO(OEt)_2)]_2 \bullet 2CH_2Cl_2$ which are not in $[Gd(hfac)_3(NITPhPO(OEt)_2)]_2$. The compound $[Dy(hfac)_3(NITPhPO(OEt)_2)]_2$ is isostructural to $[Tb(hfac)_3(NITPhPO(OEt)_2)]_2$.

Four monometallic lanthanide complexes, $[Ln(hfac)_3(depma)(H_2O)]$ (Ln(III) = Gd and Dy), $[Dy(hfac)_3(depma)_2]_2 \bullet H_2O$ and $[Gd(hfac)_3(depma)_2] \bullet 2H_2O$ were prepared by using a phosphonic acid derived from 9-chloromethylanthracene, (depma = 9-diethylphosphonomethyl anthracene, hfac = hexafluoroacetylacetonate).[15] The complexes were synthesised by partial or complete substitution of the coordination water molecules of $Ln(hfac)_3(H_2O)_2$ [Ln(III) = Dy, Gd] by the depma ligand, using the depma : $Ln(hfac)_3(H_2O)_2$ ratio of 1 : 1 for $[Ln(hfac)_3(depma)(H_2O)]$ (Ln = Dy, Gd), and 2 : 1 for $[Dy(hfac)_3(depma)_2]_2 \bullet H_2O$ and $[Gd(hfac)_3(depma)_2]$. The reactions

were achieved in ethyl acetate, and then crystallisation of products was performed in a mixture of (v/v = 1/1) ethyl acetate and *n*-heptane. The compounds $[Ln(hfac)_3(depma)(H_2O)]$ (Ln(III) = Gd and Dy) are isostructural, and crystallise in the monoclinic space group *C*2/*c*. As presented in (Figure 3.8a), the molecular structure of each compounds contains one Ln(III) ion, three non-equivalent hfac ligands, one depma ligand, and one coordination water molecule. The Ln(III) metal ion is eight-coordinated, surrounded by six oxygen atoms of hfac ligands, one water molecule, and one phosphoryl oxygen atom forming distorted bicapped triangular prism geometry. While, the compounds $[Dy(hfac)_3(depma)_2]_2{\cdot}H_2O$ and $[Gd(hfac)_3(depma)_2]{\cdot}2H_2O$ crystallise in space groups $P2_1/c$ and *C*2/*c*, respectively (Figure 3.8b). The asymmetric unit of $[Dy(hfac)_3(depma)_2]_2{\cdot}H_2O$ contains two types of neutral $[Dy(hfac)_3(depma)_2]$ monometallic moieties and one lattice water molecule. Each Dy(III) ion is surrounded by six oxygen atoms from three nonequivalent hfac ligands, and two phosphoryl oxygen atoms from two nonequivalent depma ligands, forming a distorted square-antiprismatic geometry. The asymmetric unit of $[Gd(hfac)_3(depma)_2]{\cdot}2H_2O$ contains one symmetric $[Gd(hfac)_3(depma)_2]$ moiety and two lattice water molecules. The Gd(III) ion surrounded by six oxygen atoms from three hfac ligands, and two phosphoryl oxygen atoms from two depma ligands showing a distorted square-antiprismatic geometry.

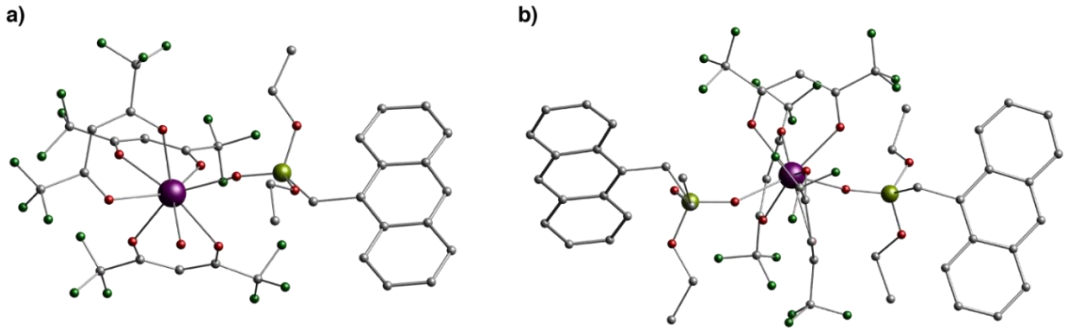

Figure 3.8: (a) Molecular structure of $[Gd(hfac)_3(depma)(H_2O)]$; (b) Molecular structure of $[Gd(hfac)_3(depma)_2]\bullet 2H_2O$. Colour code: O, red; C, grey; Gd, purple; P, lime; N, blue. Hydrogens and lattice water molecules were omitted for clarity.

3.1.2 Lanthanide complexes with bis- phosphonates

Paine and co-workers[16] reported the crystal structure of $Er(NO_3)_3L^5$, the complex was synthesised by reaction of a trifunctional phosphonate ligand of $[(^iPrO)_2P(O)][C(O)NEt_2]C(H)[(CH_2)_2C(O)OMe]$ (L^5) with lanthanide precursor $Er(NO_3)_3\bullet 5H_2O$ in ethanol. The compound crystallises in the monoclinic space group $P2_1/c$ (Figure 3.9a), X-ray crystallographic studies show that the Er(III) ion is nine-coordinate, with a tri-capped trigonal prismatic coordination geometry (Figure 3.9b). Each Er(III) ion is bonded to three bidentate nitrate ions, the phosphoryl and amide oxygen atoms from one bidentate phosphonate ligand, and one phosphoryl oxygen atom from a second phosphonate ligand, the ester carbonyl group in the bidentate ligand remains uncoordinated as do the amide and ester carbonyl groups on the second ligand.

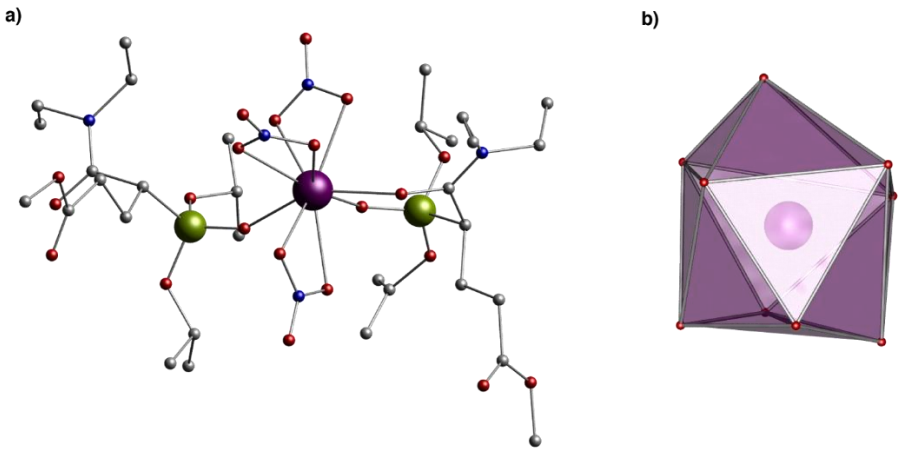

Figure 3.9: (a) Molecular structure of $Er(NO_3)_3L^5$; (b) The tri-capped trigonal prismatic coordination geometry around erbium in the complex. Colour code: O, red; C, grey; Er, purple; P, lime; N, blue. Hydrogens omitted for clarity.

Platt *et al.* prepared two distinct structural types of lanthanide(III) nitrate complexes of $Ln(NO_3)_3(L^6)_2$, and $Ln(NO_3)_3(L^7)_2$; where Ln = La–Lu except Pm, Tb and Tm, L^6 = $[(MeO)_2P(O)]_2C(OH)Ph$, and L^7 = $(MeO)_2P(O)OCHPhP(O)(OMe)_2$.[17] The reaction was performed by stirring $Ln(NO_3)_6 \bullet nH_2O$ in acetonitrile followed by addition of a slurry of corresponding ligand at 0 °C, the resulting solution was evaporated under reduced pressure and the resulting crude product recrystallised from dichloromethane/diethyl ether to give the product. As examples, the structures of $[Pr(NO_3)_3(L^6)_2]$ (Figure 3.10a), and $[Pr(NO_3)_6(L^7)_2]$ (Figure 3.10b) are described. Each complex crystallises in the monoclinic space group *C2/c* and, the lanthanide metal centre is ten coordinate with three bidentate nitrate ligands and four phosphoryl oxygen atoms from two discrete bidentate phosphonate ligands. The $[Pr(NO_3)_3(L^6)_2]$ complex has inexact C_2 symmetry, the terminal methylene ends of the ligands are arranged away from nitrate apex. The mean Pr–O distance is 2.544(1) Å, whereas the mean N–O is 1.254 (3) Å. The $[Pr(NO_3)_6(L^7)_2]$ is with Pr–O mean distances of

2.361(1) Å, while the N–O distances mean is of 1.263(7) Å. In both complexes the bonding of the nitrate groups to the Pr(III) ion is basically planar, the geometry around each Pr(III) ion can be imagined as a distorted tricapped trigonal prism. The ten-coordinate lanthanide site in each of the $Pr(NO_3)_6(L^6)_2$, and $Pr(NO_3)_6(L^7)_2$ complexes has a bicapped square antiprism (D_{4d}) geometry with a Continuous Shape Measure value (CShM) of 3.189 and 19.814, respectively.[18]

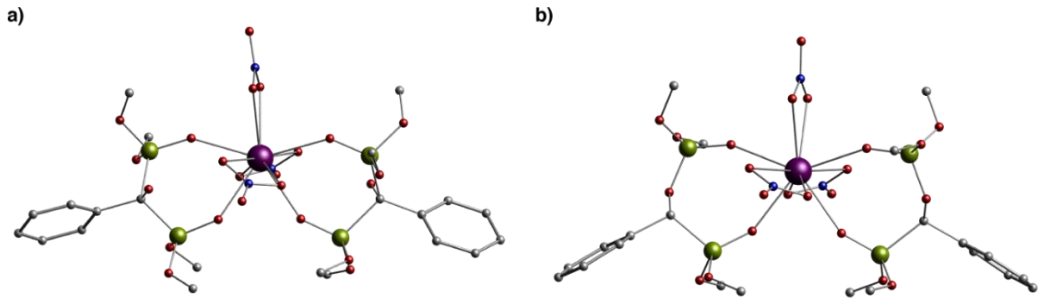

Figure 3.10: (a) and (b) Structures of complexes $Pr(NO_3)_3(L^6)_2$ and $Pr(NO_3)_3(L^7)_2$, respectively. Colour code: O, red; C, grey; Ln, purple; P, lime; N, blue. Hydrogens omitted for clarity.

Platt and co-workers[19] also synthesised complexes of $Ln(NO_3)_3(L^8)_2$ (Ln = La-Er) and $Ln(NO_3)_3(L^9)_2$ (Ln = La-Lu) (where; L^8 = $(MeO)_2P(O)]_2C(OH)Ph$, L^9 = $(MeO)_2P(O)OCHPhP(O)(OMe)_2$. The reaction of a slurry of ligands in acetonitrile with $Ln(NO_3)_6 \bullet nH_2O$ (La–Eu) gave clear solutions from which the products crystallised spontaneously. For gadolinium and subsequent lanthanides the product was more soluble and the product was isolated by evaporation of the solvent under reduced pressure followed by precipitation with diethyl ether from chloroform solution. The $La(NO_3)_3(L^8)_2$ complex crystallises in the monoclinic space group *C*2/*c*, having a C_2 axis of symmetry passing through one of the nitrate ligands and relating

the two remaining pairs of ligands by symmetry (Figure 3.11a). The ranges of La-O (nitrate) distances is about 2.531(2)-2.659(1) Å, the La(III) ion within the complex is ten-coordinated, and chelated by three nitrate anions and by the oxygen atoms of the phosphonate ligand. The $La(NO_3)_3(L^8)_2$ complex is a bicapped square antiprism (D_{4d}) geometry with a Continuous Shape Measure value (CShM) of 3.375 (Figure 3.11b).

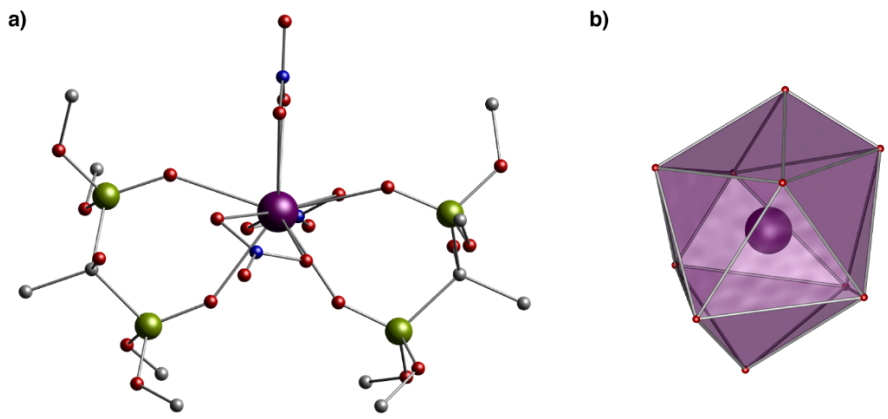

Figure 3.11: (a) Molecular structure of $La(NO_3)_3(L^8)_2$; (b) The bicapped square antiprism (D_{4d}) geometry around lanthanum atom in $La(NO_3)_3(L^8)_2$ complex. Colour code: O, red; C, grey; La, purple; P, lime; N, blue. Hydrogens omitted for clarity.

Three years later, Platt *et al.*[20] reported the crystal structures of complexes $Ln(NO_3)_3L^{10}_2$ (where; L^{10} = $(EtO)_2P(O)CH_2P(O)(EtO)_2$, and Ln = La–Er), employing the procedure outlined above, under similar reaction conditions. The single-crystal X-ray analyses of the complexes show that the compounds are isostructural and crystallise in the monoclinic space group *C*2/*c* (Figure 3.12a), the lanthanide(III) ions within the complexes are ten-coordinate. The coordination geometry about the lanthanide(III) ions can be described as a distorted bicapped square antiprism

(Figure 3.12b), with the nitrate and the diphosphonate ligands each chelating through two oxygen atoms, two nitrates are axial and one equatorial with the PO oxygen atoms forming the other four positions in the equatorial plane. All the complexes have a C_2 axis of symmetry passing through one of the nitrate ligands and relating the two remaining pairs of ligands by symmetry. For all complexes, the Ln–O coordination distances decrease with increasing atomic number of the lanthanide, average values collapsing from 2.591(1) Å, (La) to 2.459(3) Å, (Dy).

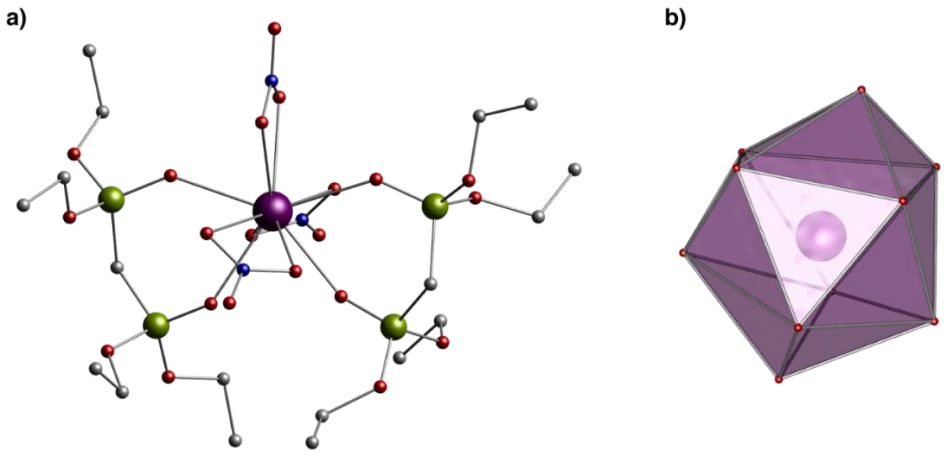

Figure 3.12: (a) The structure of $La(NO_3)_3L^{10}_2$; (b) Coordination polyhedron around La atom in $La(NO_3)_3L^{10}_2$ complex. Colour code: O, red; C, grey; La, purple; P, lime; N, blue. Hydrogens omitted for clarity.

Nief and co-workers studied the complexation behaviour of the bidentate ligand $(^iPrO)_2P(O)CH_2P(O)(O^iPr)_2)$ (L^{11}), the reaction of lanthanide nitrates $Ln(NO_3)_6 \bullet nH_2O$ or triflates ($Ln(OTf)_3$) such as a sources of the Ln(III) cations, and the ligand L^{11} in acetonitrile lead to the isolation of two types of complex; $[Ln(OTf)_3(L^{11})_2(OH_2)_2]$ (Ln = La, Pr, Nd) and $[Ln(NO_3)_3(L^{11})_2](CH_3CN)_2$, (Ln = Ce, Pr, Nd).[21] The compounds $[Ln(NO_3)_3(L^{11})_2](CH_3CN)_2$ are isostructural and

crystallise in the monoclinic *C*2/*c* space group (Figure 3.13a), the complexes adopt structures which are very similar to the $Ln(NO_3)_3L^{10}_2$ complexes, reported by Platt *et al.*[19] The structure of the cerium containing complex is described as a representative, the structure consists of discrete molecules without any apparent intermolecular contacts, similarly, there are no obvious short contacts involving the nitrogen atom belonging to the acetonitrile solvent. The Ce(III) ion is ten coordinate and chelated by three nitrate anions and by the phosphoryl groups of the phosphonate ligands. Two opposite six member rings are formed as a result of the phosphonate ligand coordination to the Ce(III) ion, the mean Ce–O distance within the complex is 2.570(3) Å. The structures of Pr(III) and (Nd) containing complexes do not differ from that of Ce(III) except for the overall shortening of the Ln–O bonds from Ce(III) to Nd(III) as a result of the lanthanide contraction. The isostructural complexes of $[Ln(OTf)_3(L^{11})_2(OH_2)_2]$ crystallise in monoclinic space group $P2_1/c$ (Figure 3.13b), the structure of the Nd(III) containing compound is discussed as an example. The original structure of the complex consists of discrete ion pairs $[Nd(L^{11})_2(OTf)_2(OH_2)_2](OTf)$ without any apparent intermolecular contacts. The eight coordinate Nd(III) ion is coordinated by the phosphoryl groups of the phosphonate ligands, two water molecules and to two monodentate triflate ligands, however, there is one triflate ligand which is not coordinated to Nd(III) ion. The mean Nd–O distance within the complex is 2.438(2) Å, the distance between nearest oxygen atom of uncoordinated triflate ligand and Nd(III) ion within the complex is 4.586(2) Å.

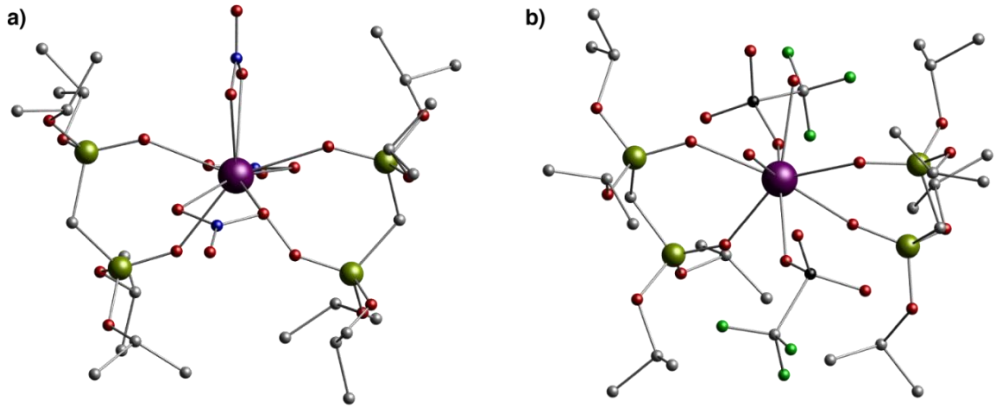

Figure 3.13: (a) Molecular structure of $[Ce(NO_3)_3(L^{11})_2](CH_3CN)_2$; (b) Molecular structure of $[Nd(L^{11})_2(OTf)_2(OH_2)_2](OTf)$. Colour code: O, red; C, grey; Ce, purple; P, lime; N, blue; S, black; F, green. Hydrogens omitted for clarity.

Majoral *et al.* reported the structure of $Gd_2L^{12}{}_2(hfa)_2(tfa)_2(Ac)_2$ (hfa = hexafluoroacetylacetonate, tfa = Trifluoroacetic acid, Ac = acetate and L^{12} = ((isopropoxy(isopropyl)phosphoryl)(4-phenylpiperazin-1-yl)methyl)(isopropyl)-phosphinic acid), the reaction is performed by addition of $Gd(hfa)_3{\bullet}2H_2O$ and $Gd(OOCCH_3)_3{\bullet}nH_2O$ to a stirred solution of the phosphonate ligand of (L^{12}) in diethyl ether.[22] the molecule is bimetallic and crystallises in the triclinic space group $P\bar{1}$, the complex contains four trifluoroacetato anions acting as bridging ligands through their carboxylato groups, hfa and bisphosphonate ligands chelated to Gd(III) ions through oxygen donors (Figure 3.14). The bridging acetates are a mixture of acetate anions and trifluoroacetate in the 0.25 : 0.75 mole ratio, trifluoroacetate derive from hexafluoroacetylacetone decomposition. The Gd(III) ions are nine-coordinate, two six-membered Gd-bisphosphonate cycles are formed by the phosphonate ligand coordination to the Gd(III) ion, both cycles are in a boat

conformation in one unit and in a skew boat conformation in the second unit, with very similar bond lengths, the Gd···Gd distance within the molecule is 3.9816(3) Å.

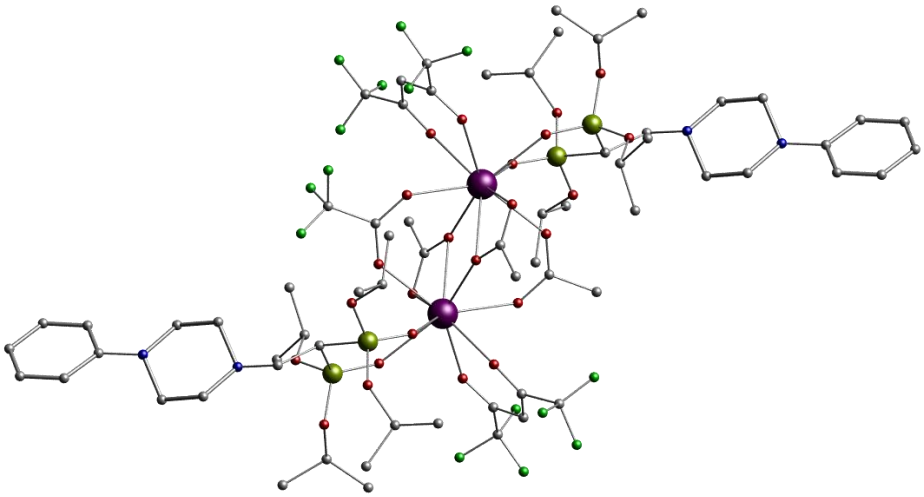

Figure 3.14: (a) Molecular structure of complex $Gd_2L^{12}{}_2(hfa)_2(tfa)_2(Ac)_2$. Colour code: O, red; C, grey; Gd, purple; P, lime; F, green; N, blue. Hydrogens omitted for clarity.

An Er(III) complex of {ethane-1,2-diylbis[imino(pyridin-2-ylmethanediyl)]}-bis(phosphonic acid) (L^{13}), $[C(NH_2)]_6[Eu_2(L^{13})_2(CO_3)_2]\cdot 8H_2O$ was reported by Gałęzowska and co-workers.[23] The compound crystallises in the triclinic space group $P\bar{1}$. The crystal contains dimeric $[Eu_2(L^{14})_2(CO_3)_2]^{6-}$ complex anions, guanidinium cations and water molecules (Figure 3.15a). The phosphonate ligand links to the Eu(III) metal ion by three oxygen atoms from the phosphonate groups, two nitrogen atoms from the imino groups and one nitrogen atom from a pyridine group, carbonate anion occupied the residual two coordination sites in the inner sphere of the Eu(III) ion. Two EuL^{13} units are bonded together to generate a dimeric complex containing an eight-coordinate Eu(III) ion with biaugmented trigonal prism (C_{2v}) geometry (Figure 3.15b), since one oxygen atom from a bidentate phosphonate

group linking to the Eu(III) ion and the other oxygen atom to the europium cation produced by an inversion centre. The Eu–O bond lengths within the complex are in the ranges of 2.369(3) -2.435(1) Å, while the Ce–N bond lengths are in the ranges of 2.586(1) -2.651(3) Å.

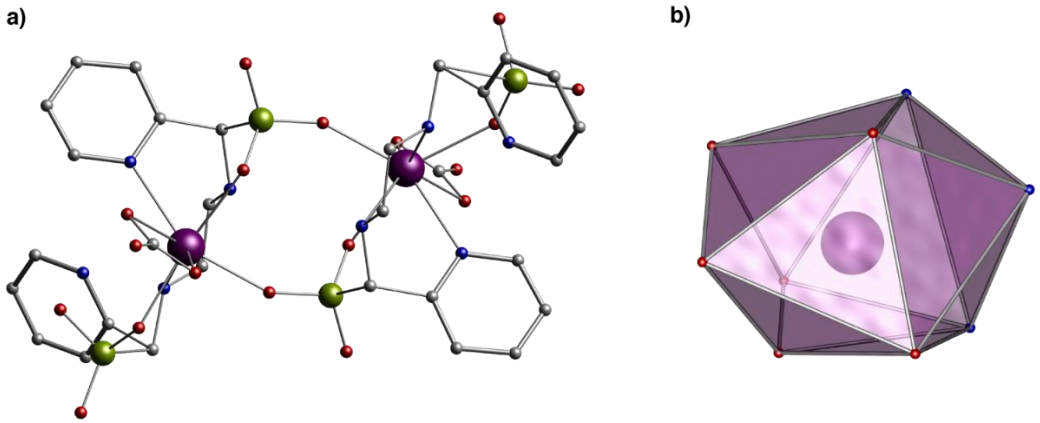

Figure 3.15: (a) A view of the dimeric $[Eu_2(L^{14})_2(CO_3)_2]^{6-}$ complex; (b) The biaugmented trigonal prism C_2v geometry around erbium atom in the complex. Colour code: O, red; C, grey; Eu, purple; P, lime; N, blue. Hydrogens omitted for clarity.

Liu and co-workers isolated the complex of $[Er(NO_3)_3]_2(L^{14})_3H_2O\bullet(H_2O)_2$ (L^{14} = tetraethyl-(2,3,5,6-tetramethyl-1,4-phenylene) bis(methylene)diphosphonate), the complex was prepared by reaction of $Ln(NO_3)_3\bullet nH_2O$ in methanol with a solution of the phosphonate ligand in ethyl acetate, the mixture was stirred, filtered and then sealed in a glass vial for crystallisation at room temperature.[24] The X-ray analysis indicated that the compound crystallises in the triclinic space group $P\bar{1}$ (Figure 3.16a), it consists of a short chain which contains six nitrates, two Er(III) ions and three phosphonate ligands. One phosphonate ligand acts as a bridging group and links two Er(III) ions, though another two phosphonate ligands localise at both ends

of the short chain. The complex is a centrosymmetric molecule, the complex has one end ligand in a general position and an additional ligand lying about the inversion centre. Both Er(III) ions in the complex are nine coordinated (Figure 3.16b), the mean Er–O distance is 2.407(5) Å, the Er–Er distance is in the complex is 14.788(5) Å, the distances between the two phosphonates located at both ends of the short chain is 32.969(1) Å.

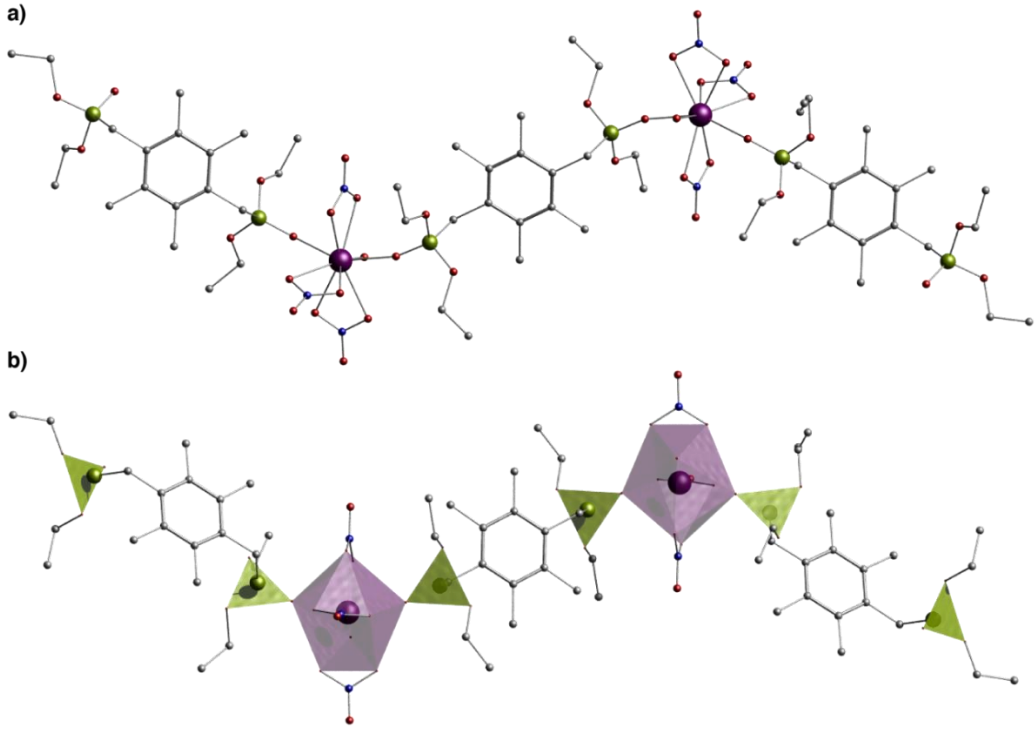

Figure 3.16: (a) Structure of $[Er(NO_3)_3]_2(L^{14})_3H_2O\bullet(H_2O)_2$; (b) The molecular structure of the complex, the lanthanide polyhedra are shaded in purple, and the phosphonate tetrahedra are shaded in green. Colour code: O, red; C, grey; Eu, purple; P, lime; N, blue. Hydrogens and free solvent molecules are omitted for clarity.

By using 1,2-phenylenediphosphonate (H_4L^{15}) ligand, Schmitt *et al.* synthesised two hexametallic anionic clusters of Ce(IV).[25] The Ce(IV) metal ion in both complexes of $(NH_4)_6Ce_6(NO_3)_{12}(H_3L^{15})_6\bullet 9H_2O$ (Ce6-A) and $(NH_4)_6Ce_6(NO_3)_{12}(H_3L^{15})_6\bullet 3H_2O$

(Ce6-B) form a distorted octahedron (Figure 3.17a), the complex Ce6-A has C_3 symmetry, while Ce6-B is more distorted and is in the C_i point group (Figures 3.17b and c). For both complexes Ce6-A and Ce6-B the ligand acts in a similar style in that one PO_3 moiety is bonded to three metal centres, though the other PO_3 group is bonded to only two metal centres and has one protonated O atom. Four PO_3 groups from two phosphonate ligands chelate six metal centres in the complexes, both clusters are anionic, and a single cation is captured in the cage. Further cations, which are required for complete charge balance, are found between the clusters in the crystal structure.

Ce6-A has the higher symmetry and crystallises in the rhombohedral space group $R\bar{3}$, the six Ce(IV) sites in the complex have same coordination environments, the metal ions centres are nine-coordinate with four oxygen atoms from two nitrate anions and five oxygen atoms provided by five PO_3 moieties from three phosphonate ligand units. The Ce–O bond lengths are in the range of 2.228(8) -2.602(8) Å. Ce6-B has lower symmetry and crystallises in the triclinic space group $P\bar{1}$, the inversion centre of the compound is located in the centre of the complex, the six metal ions have similar coordination environment as found in Ce6-A. The Ce–O bond lengths are in the ranges of 2.219(5) -2.594 (5) Å.

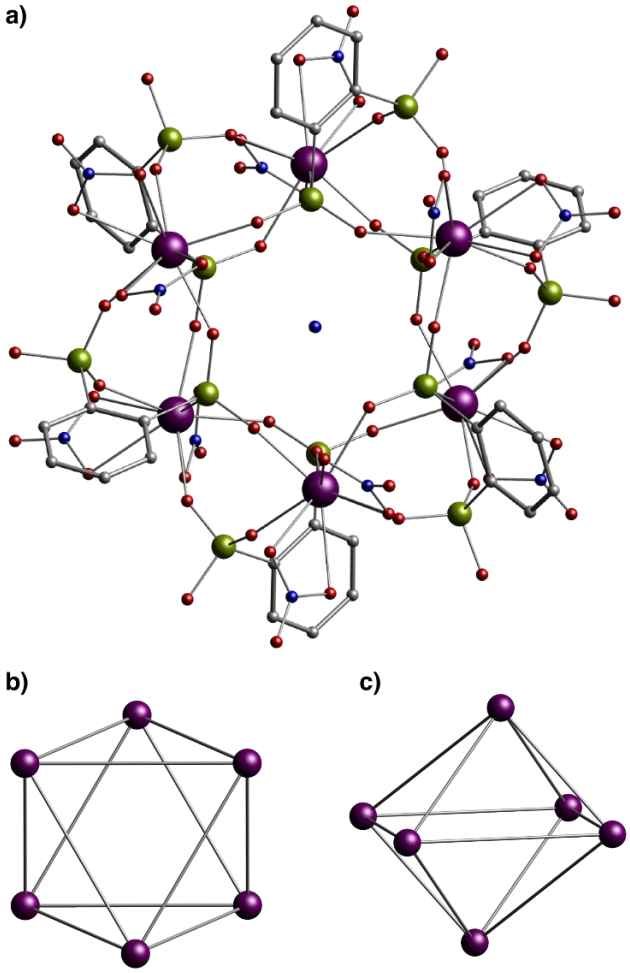

Figure 3.17: (a) Views of the anionic hexametallic Ce(IV) diphosphonate clusters: $(NH_4)_6Ce_6(NO_3)_{12}(H_3L^{15})_6 \bullet 9H_2O$ (Ce6-A) and $(NH_4)_6Ce_6(NO_3)_{12}(H_3L^{15})_6 \bullet 3H_2O$ (Ce6-B) ; (b) and (c) Views of the C_3 (Ce6-A) and C_i (Ce6-B) symmetries of the clusters. Colour code: O, red; C, grey; Ce, purple; P, lime; N, blue. Hydrogens and lattice water molecules were omitted for clarity.

The reactions of $Ln(NO_3)_6 \bullet nH_2O$ with phosphonate ligand $(MeO)_2P(O)CH_2P(O)(OMe)_2$ (L^{16}) were carried out in trimethyl orthoformate solution and led to isolation of two types of complex.[26] Monomeric $Ln(L^{16})_2(NO_3)_3$ are formed for the lighter lanthanides (La–Gd), whilst the smaller ions form dimeric complexes, $Ln_2(NO_3)_6L^{16}{}_3$. Single crystal X-ray diffraction studies were carried out on an example of each type, $Pr(L^{16})_2(NO_3)_3$ possesses approximate C_2 symmetry and

contains a ten-coordinate Pr(III) metal ion centre with three nitrates and two diphosphonate ligands, each chelating by two oxygen atoms (Figure 3.18a). The coordination polyhedron around the metal in each complex shows bicapped square antiprism (D_{4d}) geometry with a Continuous Shape Measure value (CShM) of 3.041 (Figure 3.18c). The phosphonate ligands are arranged so as to have their terminal methylene ends further away from the nitrate apex. The mean Pr–O distance is 2.544(1) Å. $Yb_2(NO_3)_6L^{16}{}_3$ complex contains two nine-coordinate Yb(III) metal centres each bound to three bidentate nitrate groups, one bidentate diphosphonate, and opposite ends of a bridging diphosphonate ligand (Figure 3.18b). The Yb–O mean distances is of 2.361(1) Å, all six nitrate groups show a slight skewing of their coordination with one Yb–O bond about 2.38 Å and the other about 2.46 Å. This must be associated to steric or crystal packing effects, the geometry about each ytterbium atom can be described as a tricapped trigonal prism (D_{3h}) (Figure 3.18d).

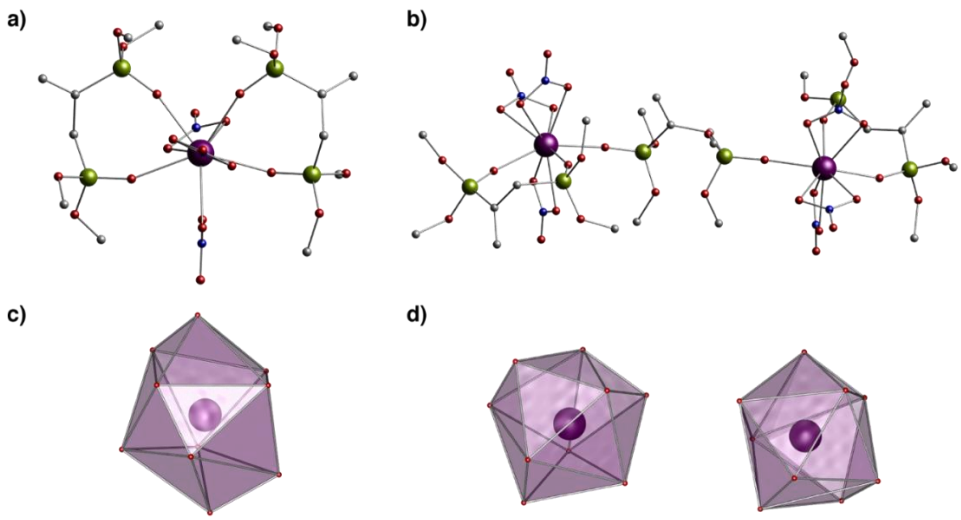

Figure 3.18: (a) Molecular structure of $Pr(L^{16})_2(NO_3)_3$; (b) Molecular structure of $Yb_2(NO_3)_6L^{16}{}_3$; (c) and (d) Coordination geometries around Pr and Yb metal ions. Colour code: O, red; C, grey; Ln, purple; P, lime; N, blue. Hydrogens omitted for clarity.

The L^{16} bridges between the two lanthanides in a series of complexes of general formula $Ln(L^{16})_2(NO_3)_3L^{16}_2$ (Ln = La – Eu), and the yield is seen to decrease significantly with the increasing atomic mass of the lanthanide, then Ln = Gd–Lu solid compounds could not be isolated. The complexes of the La(III) and Sm(III) were selected for structural analysis, since they symbolise the full span of the series for which crystalline compounds could be obtained and, thus, their structures may designate fundamental reasons for the changes in properties along the lanthanide series. Both complexes have similar overall molecular geometries, the Sm(III) complex has a C_2 axis, this symmetry is not obvious in the La(III) complex, the metal ions in both complexes are ten-coordinate with three nitrates and two diphosphonate ligands each chelating by two oxygen atoms. The coordination polyhedron around the metal in each complex can be described as distorted bi-capped square antiprism, the La(III) and Sm(III) complexes can also be describe as pseudo-pentagonal bipyramids, defined by the N-atoms of the nitrate ligands and the phosphoryl oxygens. The Sm–O distances are in the range of 2.430(6)–2.708(3) Å, and La–O distances for the lanthanum complex in the range of 2.464(2)–2.683(3) Å.

Lately, Avarvari and co-workers synthesised a series of ten lanthanide(III) complexes by the direct reaction of an equal mole ratio of $Ln(NO_3)_3 \bullet nH_2O$ (Ln = La, Pr, Nd, Sm, Eu, Gd, Tb, Dy, Ho, and Er) precursors, and the phosphonate ligand of cyanomethylene-bis(5,5-dimethyl-2-oxo-1,3,2λ5-dioxa-phosphorinane) (L^{17}) in ethanol.[27] The reported complexes all are discrete and their structures confirmed by

single-crystal X-ray diffraction. The cell determination investigation designate two structural types; type I for the complexes ($[Ln(L^{17})_3(H_2O)_2]\bullet H_2O$; Ln = La, Pr and Nd) and type II for the complexes ($[Ln(L^{17})_3(H_2O)]\bullet 8H_2O$; Ln = Sm, Eu, Gd, Tb, Dy, Ho and Er). $Ln(L^{18})_3(H_2O)_2]\bullet H_2O$ crystallise in the chiral $P2_12_12_1$ orthorhombic space group. As a representative example, the structure of the Pr(III) containing complex is described in detail, the asymmetric unit consists of one eight-coordinated Pr(III) metal ion centre, chelated by three nonequivalent ligands L^{17} , two water molecules and one crystallisation water molecule (Figure 3.19a). The geometry about the metal is a biaugmented trigonal prism (C_{2v}) with a Continuous Shape Measure value (CShM) of 0.988 (Figure 3.19a), the Pr–O bond lengths range from 2.356(2) - 2.575(2) Å.

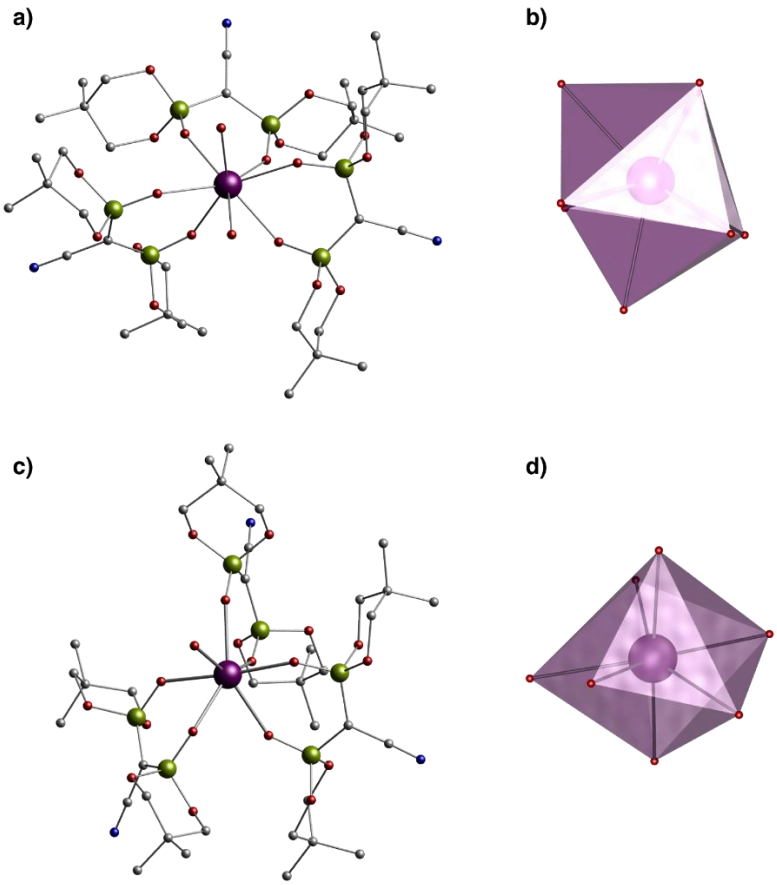

Figure 3.19: (a) and (c) Molecular structure of $[Pr(L^{17})_3(H_2O)_2]\bullet H_2O$ and $[Tb(L^{17})_3(H_2O)]\bullet 8H_2O$, respectively; (b) and (d) Coordination geometries around Pr and Tb ions within structures. Colour code: O, red; C, grey; Ln, purple; P, lime; N, blue. Hydrogens and lattice water molecules were omitted for clarity.

$[Ln(L^{17})_3(H_2O)]\bullet 8H_2O$ are isostructural and crystallise in the noncentrosymmetric monoclinic space group *Pn*, the crystal structure of the Tb(III) analogue is described as an example (Figure 3.19c). The asymmetric unit contains a monometallic complex and eight non coordinated water molecules in general locations. The Tb(III) ion is seven-coordinated, with a capped trigonal prism geometry (C_{2v}), the Continuous Shape Measure value (CShM) is 1.663 (Figure 3.19d), The Tb–O bond lengths range from 2.270(4) -2.330(4) Å.

3.1.3 Lanthanide complexes with tris- phosphonates

Fawcett *et al.* synthesised a dimeric complex of $Ce(NO_3)_3(L^{18})_2Ce(NO_3)_3$, L^{18} = $[(EtO)_2P(O)CH_2]_3Me_3$, the complex was prepared by reaction of hydrated lanthanide nitrates with an excess of the ligand in boiling acetonitrile.[28] The complex crystallises in the monoclinic space group $C2_1/c$. Two phosphonate ligands are bridging between two $Ce(NO_3)_3$ moieties, two phosphoryl oxygens from the phosphonate ligand chelate to one metal whereas the third bonds to the second metal giving a symmetrically bridged dimeric structure (Figure 3.20). The Ce-O distances are slightly shorter (by about 0.05 Å) than might be estimated from an analysis of the Ln–O distances in lanthanide nitrate bis-phosphonate complexes.[18.19] The Ce(III) ion is nine-coordinate, and the geometry around it can be considered as a distorted octahedron, the ligands are organised in an arrangement with N-Ce-N angles being a little broader than 90° with an average of 96.48° whereas the O(P)-Ce-O(P) show a tighter angle of 85.28°, this due to electrostatic repulsions from two negatively charged oxygens per nitrate ligand directing the increased steric repulsions from the bulky phosphonate groups.

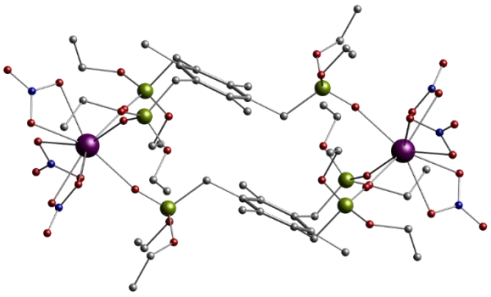

Figure 3.20: (a) Molecular structure of $Ce(NO_3)_3(L^{18})_2Ce(NO_3)_3$. Colour code: O, red; C, grey; Ce, purple; P, lime; N, blue. Hydrogens omitted for clarity.

Schröder and co-workers[29] employed a polyamino ligand, 1,4,7-tris(2-aminoethyl)-1,4,7-triazacyclononane (**1**) to prepare two ligands by Schiff-base condensation, with methyl sodium acetyl phosphonate to give ligand L and methyl sodium 4-methoxybenzoyl phosphonate to give ligand L' in the presence of lanthanide ion as templating agent, they synthesise a series of Ln(III) complexes of Ln(L)•MeOH (Ln = Y, La, Gd, Yb), and Ln(L')•MeOH (Ln = Y, Gd) (Scheme 3.1).

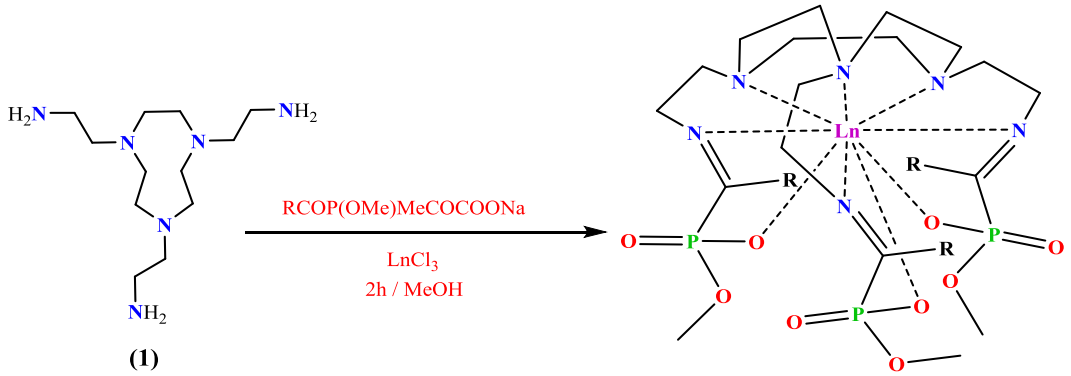

Scheme 3.1: Synthetic scheme for the preparation of complexes Ln(L)•MeOH and Ln(L')•MeOH.

Both Ln(L) and Ln(L') complexes are very similar and compounds crystallise in the monoclinic $C2_1/c$ space group (Figures 3.21a and b). In all complexes, the lanthanide metal ion is nine-coordinate, using all nine donor atoms of the ligands, namely the three amino N-donors of the macrocycle, the three imino N-donors and the three phosphonate O-donors. The coordination geometry about the Ln(III) ion is a distorted tricapped trigonal prismatic, the bond lengths between the Ln(III) ion and the macrocyclic N-donors are in the ranges 2.659(3)–2.698(5) Å, the bond lengths between the metal and N-donors of the imine moieties are in the ranges 2.591(3)–

2.684(5) Å, while the bond lengths between the metal and the phosphonate O-donors are 2.289(3)–2.357(4) Å.

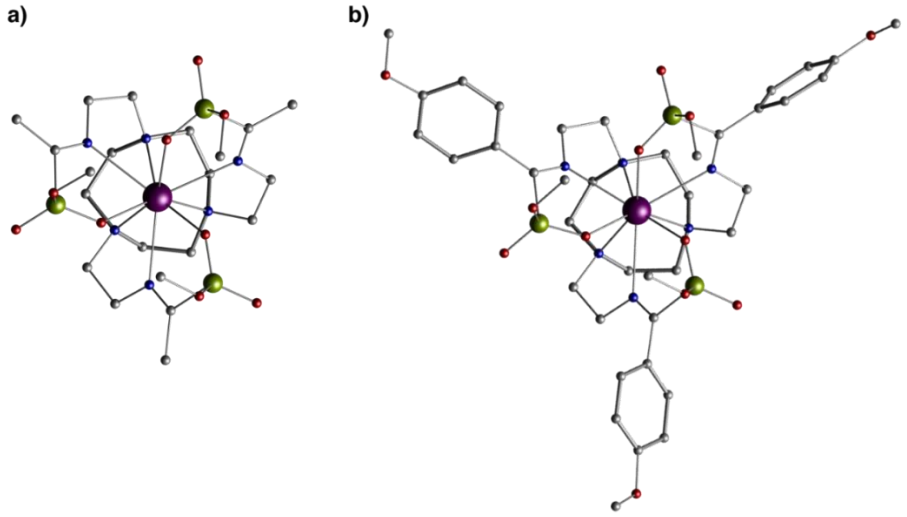

Figure 3.21: (a) and (b); View of the crystal structure of Gd(L)•MeOH and Gd(L')•MeOH, respectively, along the non-crystallographic three-fold axis. Colour code: O, red; C, grey; Gd, purple; P, lime; N, blue. Hydrogen atoms and CH_3OH molecules have been omitted for clarity.

$Ln_2(notpH_4)_2(NO_3)_2(H_2O)_2$ (Ln = Eu , Gd and Tb) were isolated when phosphonate ligand 1,4,7-triazacyclononane-1,4,7-triyl-tris(methylenephosphonic acid) ($notpH_6$) reacted with lanthanide salts $Ln(NO_3)_3 \bullet nH_2O$) (Ln = Eu, Gd and Tb).[30] The complexes are isostructural and compounds crystallise in the monoclinic space group $P2_1/c$, the asymmetric unit contains one Gd(III) ion, one phosphonate ligand ($notpH_4^{2-}$), one nitrate ion, and four lattice water molecules. The gadolinium containing complex is discussed as an example, the complex has a dimetallic molecular structure, two crystallographically equivalent Gd(III) ions are linked by two pairs of O–P–O and one pair of μ–O bonds (Figure 3.22). Each Gd(III) ion is nine-coordinate with four positions occupied by four oxygen donors from the same

phosphonate ligand, two position from equivalent phosphonate ligands, two positions by oxygen atoms from the NO_3^- ligand, and a water molecule filling the remaining site, the Gd···Gd distance is 4.028(2) Å.

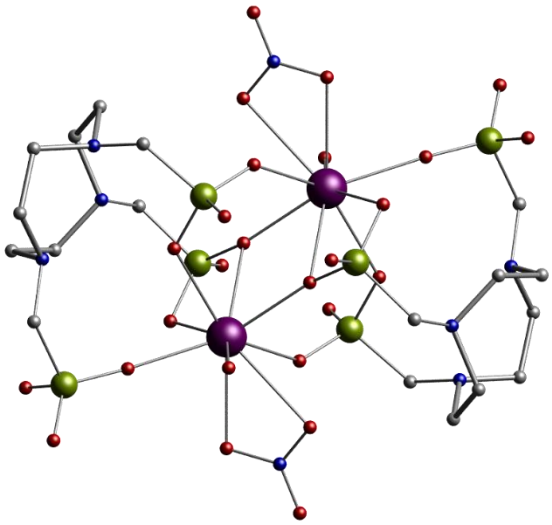

Figure 3.22: (a) Structure of $Gd_2(notpH_4)_2(NO_3)_2(H_2O)_2$. Colour code: O, red; C, grey; Gd, purple; P, lime; N, blue. Hydrogens omitted for clarity.

Kiefer and Woods reported the X-ray crystal structures of $(LnPCTMB)_2$•9.25 H_2O (where; Ln(III) = Eu and Tb; H_3PCTMB = 3,6,9-tris(methylenebutyl phosphonic acid)-3,6,9-15-tetraazabicyclo [9.3.1]pentadeca-1(15),11,13-triene).[31] X-ray diffraction of single crystals of both compounds showed that both crystallised in the triclinic $P\bar{1}$ space group (Figure 3.23). The two complexes are isostructural, with two chelate ligand molecules and water of crystallisation in the unit cell, the asymmetric unit contains one Ln(III) ion and one phosphonate ligand (PCTMB). The compounds have a dimetallic molecular structure, each contains two crystallographically equivalent Ln(III) ions, which are linked through two O–P–O bonds from two discrete phosphonate groups. Each lanthanide metal ion centre

within the structure is eight-coordinated through four oxygen and four nitrogen donor atoms from the phosphonate ligand.

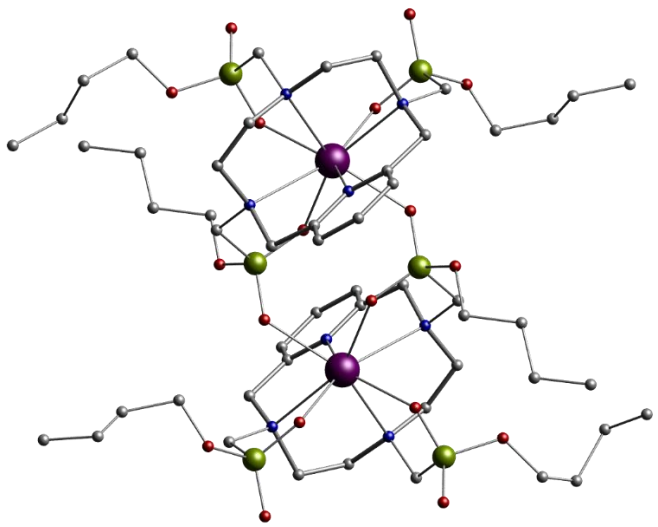

Figure 3.23: (a) Dimeric structure of $(EuPCTMB)_2 \bullet 9.25\ H_2O$. Colour code: O, red; C, grey; Eu, purple; P, lime; N, blue. Hydrogens and lattice water molecules were omitted for clarity.

More recently, the complex of $\{Dy(notpH_4)(NO_3)(H_2O)\}_2 \bullet 8H_2O$ ($notpH_6$ = 1,4,7-tri-azacyclononane-1,4,7-triyl-tris(methylenephosphonic acid)) was synthesised by Zheng and co-workers.[32] The complex is similar to those reported earlier by the same authors, of general formula $Ln_2(notpH_4)_2(NO_3)_2(H_2O)_2$ (Ln = Eu , Gd and Tb).[30] The compound crystallises in monoclinic space group $P2_1/c$, the asymmetric unit contains one nine-coordinated Dy(III) ion, one phosphonate ligand ($notpH_4^{2-}$), one nitrate ligand, one coordinated and four lattice water molecules (Figure 3.24a). Each Dy(III) ion is coordinated by four phosphonate oxygen atoms from the same $notpH_4^{2-}$ ligand, two phosphonate oxygen atoms from the equivalent $notpH_4^{2-}$ ligand, two oxygen atoms from the nitrate anion, and the remaining site is occupied by a water molecule. The $\{DyO_9\}$ core can be considered as a tri-capped trigonal prism,

the coordination geometry of the Dy(III) ion has approximately D_{3h} symmetry (Figure 3.24b). The Dy–O bond lengths are in the range of 2.326(2)–2.814(3) Å, the Dy···Dy distance is 4.055(1) Å, the Dy–O–Dy angle is 109.5(1)°.

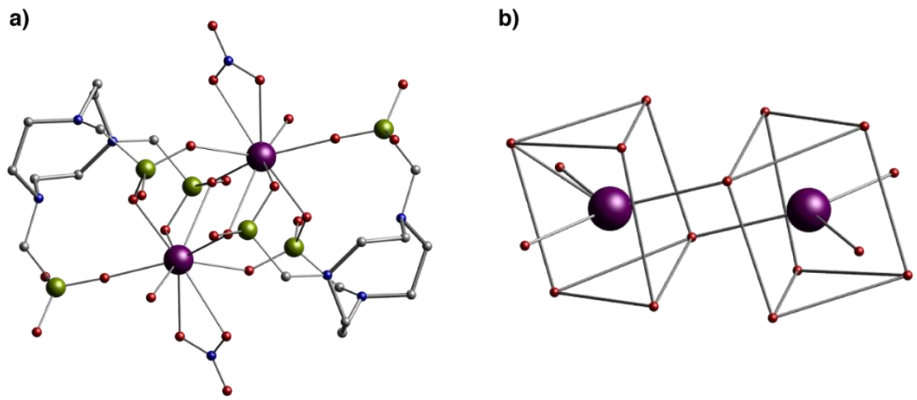

Figure 3.24: (a) Structure of $\{Dy(notpH_4)(NO_3)(H_2O)\}_2 \bullet 8H_2O$; (b) The three capped trigonal prism polyhedron of the $[DyO_9]$ cores. Colour code: O, red; C, grey; Dy, purple; P, lime; N, blue. Hydrogens and lattice water molecules were omitted for clarity.

3.1.4 Lanthanide complexes with tetrakis- phosphonates

Crystals of $[C(NH_2)_3]_6[Ln(CDTP)(OH)(H_2O)_{1/2}] \bullet 16H_2O$ (where: Ln(III) = Eu, Tb; CDTP = *trans*-cyclohexane-1,2-diamine-*N*,*N*,*N*',*N*'-tetrakis(methylenephosphonic acid)) were synthesised,[33] the reaction carried out by neutralisation of a phosphonate solution with $[C(NH_3)_3]_2CO_3$ to pH around 7 and adding it to an aqueous solutions of $Ln(ClO_4)_3$ (L = Tb, Eu). Both complexes are isostructural and compounds crystallise in the triclinic space group $P\bar{1}$. The phosphonate ligand is coordinated to the Ln(III) ion through two nitrogen atoms, and four oxygen atoms from four discrete phosphonic groups, each phosphonate group is linked to the Ln(III) ion through one oxygen atom. The coordination sphere of the metal ion is

partly disordered, *i.e.* three oxygen atoms (OH1, OH2, OW) with occupancy factors of 0.5, the existence of OH1 in the first coordination sphere of the Ln(III) rejects the existence of OH2 and OW in the same sphere (Figure 3.25). In this fashion two adjacent anions form a dimer in which one of the lanthanide ions is eight-coordinate (four O atoms, two N atoms, one hydroxy ion and one water molecule), and the other seven-coordinate (four O atoms, two N atoms and one hydroxy ion). The investigation of bond distances and angles between the Ln(III) ion and the coordinated atoms (O and N) shows that for the eight-coordinate complex the expected local symmetry of the lanthanide ion is C_2, while for the seven-coordinate complex it is C_{2v}.

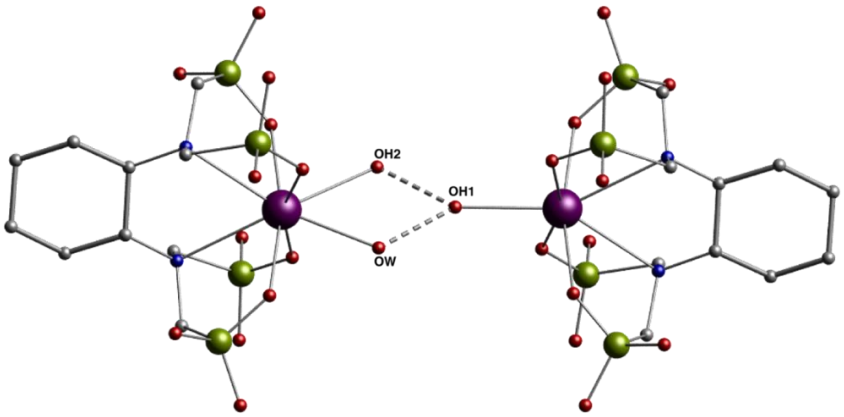

Figure 3.25: (a) Molecular structure of the $[Eu(CDTP)(OH)(H_2O)_{1/2}]^{6-}$ complex. Colour code: O, red; C, grey; Eu, purple; P, lime; N, blue. Hydrogens and lattice water molecules were omitted for clarity.

Crystals of Eu(III) with H_8EDTMP ligand, $[C(NH_2)_3]_7[Eu(EDTMP)(CO_3)]\bullet 10H_2O$ [H_8EDTMP = ((ethane-1,2-diylbis(azanetriyl))tetrakis(methylene))tetrakis-(phosphonic acid)] were synthesised by Janicki and Mondry.[34] The reaction was

achieved with neutralising the ligand solution by $[C(NH_2)_3]_2CO_3$ to pH ~7 and added to an aqueous solution of $Eu(ClO_4)_3$, the resulting solutions were basified with guanidinium carbonate to pH 10.7. The compound crystallises in the monoclinic space group $P2_1/c$, the asymmetric unit consists of one Eu(III) ion, one EDTMP ligand, one CO_3^{2-} ligand, seven $C(NH_2)_3$ and ten lattice water molecules (Figure 3.26a). The lanthanide site in the structure is eight-coordinated (Figure 3.26b), the Eu(III) ion displays a triangular dodecahedron geometry (D_{2d}), and a Continuous Shape Measure value (CShM) of 3.675. The Eu–O and Eu–N bond lengths are in the domain of 2.343(2)–2.445(2) Å and 2.703(3)–2.734(2), respectively. The O–Eu–O angles, formed by the oxygen donor atoms of phosphonate ligands with the Eu(III) ion are in the range of 101.30(7)–102.22(7)°, the O–Eu–O angle which is formed by the two oxygen donor atoms of the nitrate ligand with the metal ion is 53.83(7)°, while the N–Eu–N angle is 66.75(7)°.

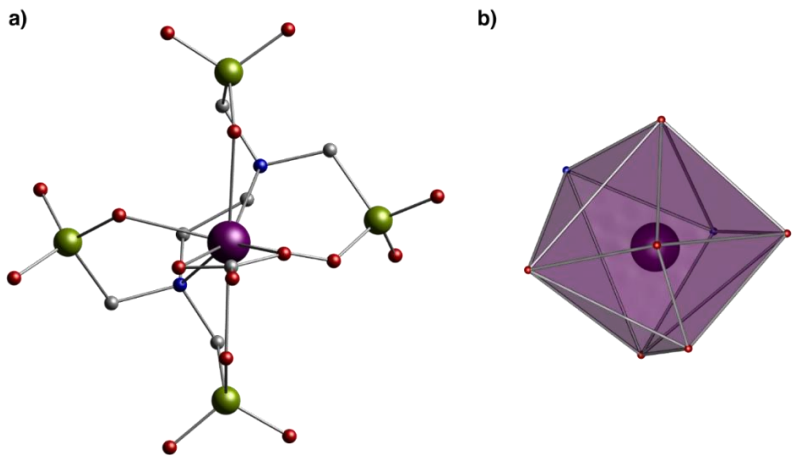

Figure 3.26: (a) Molecular structure of $[Eu(EDTMP)(CO_3)]^{7-}$; (b) View of a triangular dodecahedron geometry (D_{2d}) around europium atom within the complex. Colour code: O, red; C, grey; Eu, purple; P, lime; N, blue. Hydrogens and lattice water molecules were omitted for clarity.

Mondry and Janicki also reported the crystal structure of an anionic octacoordinate Eu(III) complex of the formula $K_{12}H_8[Eu_4(EDTMP)_4]\bullet 45H_2O$ (H_8EDTMP = ((ethane-1,2-diylbis(azanetriyl))tetrakis(methylene))tetrakis(phosphonic acid)), they neutralised H_8EDTMP acid with KOH to a pH value of around 7.5 and added to an aqueous solution of $EuCl_3$.[35] The compound crystallises in the tetragonal space group $I\bar{4}c2$, the compound contains two Eu(III) ions, both are eight-coordinate. Each metal ion is surrounded by six oxygen atoms from phosphonic groups and two nitrogen atoms (Figure 3.27). The EDTMP anion is engaged in bonds with two adjacent lanthanide cations, three phosphonic groups of the ligand are monodentate, while the fourth one is three-coordinate, because one oxygen atom links to Eu1 and the two others links to a Eu(III) cation created by symmetry from Eu1. Thus, Eu(EDTMP) units are linked together to generate a cyclic tetramer with S_4 symmetry.

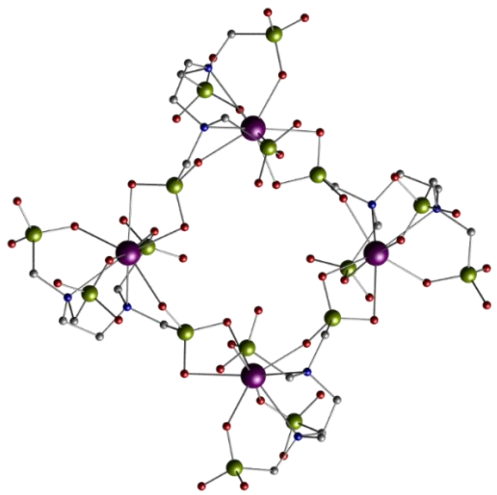

Figure 3.27: A view of the tetrameric complex anions in $K_{12}H_8[Eu_4(EDTMP)_4]\bullet 45H_2O$. Colour code: O, red; C, grey; Eu, purple; P, lime; N, blue. Hydrogens and lattice water molecules were omitted for clarity.

Peters and co-workers synthesised the complex of Li[Gd(DOTP)]•0.5Me_2CO·8H_2O (H_4DOTP = tetraethyl ((1,4,7,10-tetraazacyclododecane-1,4,7,10-tetrayl)tetrakis(methylene))tetrakis(hydrogen phosphonate)).[36] The complex crystallises in the orthorhombic space group $P2_12_12_1$, the Gd(III) ion in the complex is coordinated by four nitrogen atoms of the macrocycle and four oxygen atoms from four different phosphonic groups (Figure 3.28a). The lanthanide site in the compound is eight-coordinated, the Gd(III) ion shows a square antiprism geometry (D_{4d}) with a Continuous Shape Measure value (CShM) of 2.094 (Figure 3.28b). The Gd–O bond lengths are in the range of 2.308(1)–2.321(4), while the Gd–N bond lengths are located in the range of 2.696(2)–2.693(1). The O–Gd–O angles, created by the oxygen donor atoms of phosphonate ligands with the metal ion are in the range of 77.02(6)–80.01(5) °, whereas the N–Gd–N angles are in the range of 66.75(6) – 68.57(4) °.

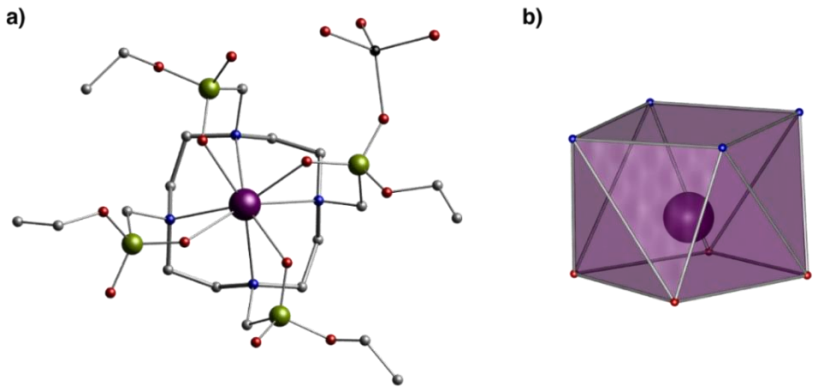

Figure 3.28: (a) Molecular structure of the $[Gd(DOTP)]^-$ species found in the crystal structure of Li[Gd(DOTP)]•0.5Me_2CO·8H_2O; (b) View showing a square antiprism geometry (D_{4d}) about gadolinium atom in the complex. Colour code: O, red; C, grey; Eu, purple; P, lime; N, blue; Li, black. Hydrogens, solvent and lattice water molecules were omitted for clarity.

Recently, Mondry and Janicki reported the crystal structures of a neodymium compound $[C(NH_2)_3]_7[Nd(EDTMP)(CO_3)]\bullet 10H_2O$.[37] The complex was prepared by heating a mixture of Nd_2O_3 and H_8EDTMP at 90 °C for three days, followed by alkalising the mixture with $[C(NH_2)_3]_2CO_3$ to adjust the pH of the solutions to 7.5, the violet crystals of product were collected after slow evaporation of these aqueous solutions. The compound crystallises in the monoclinic space group $P2_1/c$, the asymmetric unit involves of one Nd(III) ion, one EDTMP ligand, one CO_3^{2-} ligand, seven $C(NH_2)_3$ and ten lattice water molecules, the complex is an analogue of $[C(NH_2)_3]_7[Eu(EDTMP)(CO_3)]\bullet 10H_2O$ reported earlier by the same authors (Figure 3.27).[35] The eight-coordinated lanthanide site in the structure has a triangular dodecahedron geometry (D_{2d}) and a Continuous Shape Measure value (CShM) of 2.451. The Nd–O and Nd–N bond lengths are located in the range of 2.466(3)–2.385(2) Å and 2.768(3)–2.715(3), correspondingly.

3.2 References

1. L. M. P. Lima, R. Delgado, F. Marques, L. Gano, I. Santos, *Eur. J. Med. Chem.*, 2010, **45**, 5621.
2. Z. Hnatejko, S. Lis, G. Pawlicki, G. Meinrath, *J. Alloys Compd.*,2008, **451**, 395.
3. S. Lis, G. Pawlicki, *J. Lumin.*, 2010, **130**, 832.
4. M. Atanassova, V. Lachkova, N. Vassilev, S. Varbanov, I. Dukov, *Polyhedron*, 2010, **29**, 655.
5. P. Caravan, J. J. Ellison, T. J. McMurry, R. B. Lauffer, *Chem. Rev.*, 1999, **99**, 2293.
6. L. Pan, K. M. Adams, H. E. Hernandez, X. T. Wang, C. Zheng, Y. Hattori and K. Kaneko, *J. Am. Chem. Soc.*, 2003, **125**, 3062.
7. S. W. A. Bligh, N. Choi, C. M. McGrath, M. McPartlin and T. M. Woodroffe, *J. Chem. Soc., Dalton Trans.*, 2000, **10**, 2587.
8. X.-M. Gan, I. Binyamin, B. M. Rapko, J. Fox, E. N. Duesler and R. T. Paine, *Inorg. Chem.*, 2004, **43**, 2443.
9. P. Vojtíšek, P. Cígler, J. Kotek, J. Rudovský, P. Hermann, and I. Lukeš, *Inorg. Chem.*, 2005, **44**, 5591.
10. S. Comby, R. Scopelliti, D. Imbert, L. Charbonnière, R. Ziessel and J.-C. Bunzli, *Inorg. Chem.*, 2006, **45**, 3158.
11. V. Chandrasekhar and P. Sasikumar, *Dalton Trans.*, 2008, **45**, 6475.
12. X. Li, Q. Liu, J. Lin, Y. Li and R. Cao, *Inorg. Chem. Comm.*, 2009, **12**, 502.

13. F. Pointillart, K. Bernot, G. Poneti and R. Sessoli, *Inorg. Chem.*, 2012, **51**, 12218.

14. K. Bernot, F. Pointillart, P. Rosa, M. Etienne, R. Sessoli and D. Gatteschi, *Chem. Commun.*, 2010, **35**, 6458.

15. D.-K. Cao, Y-W. Gu, J.-Q. Feng, Z.-S. Caia and M. D. Ward, *Dalton Trans.*, 2013, **42**, 11436.

16. G. S. Canary, R. L. Meline, R. Schaeffer, E. N. Duesler and R. T. Paine, *Inorg.Chem. Acta*, 1992, **201**, 165.

17. A. W. G. Platt, D. Simpson, J. Fawcett and D. R. Russell, *Inorg.Chem. Acta*, 1994, **223**, 43.

18. (a) S. Alvarez, *Dalton Trans.*, 2005, **13**, 2209; (b) S. Alvarez, P. Alemany, D. Casanova, J. Cirera, M. Llunell and D. Avnir, *Coord. Chem. Rev.*, 2005, **249**, 1693.

19. A. M. J. Lees, J. M. Charnock, R. A. Kresinski and A. W. G. Platt, *Inorganica Chimica Acta*, 2001, **312**, 170.

20. A. M. J. Lees, R. A. Kresinski and A. W. G. Platt, *New J. Chem.*, 2004, **28**, 1457.

21. Q. H. Jin, L. Ricard and F. Nief, *Polyhedron*, 2005, **24**, 549.

22. G. Franc, C.-O. Turrin, E. Cavero, J.-P. Costes, C. Duhayon, A.-M. Caminade and J.-P. Majoral, *Eur. J. Org. Chem.*, 2009, **25**, 4290.

23. J. Gałęzowska, R. Janicki, H. Kozłowski, A. Mondry, P. Młynarz and Ł. Szyrwiel, *Eur. J. Inorg. Chem.*, 2010, **11**, 1696.

24. X. Hu, W. Dou, C. Xu, X. Tang, J. Zheng and W. Liu, *Dalton Trans.*, 2011, **40**, 3412.

25. J. Diwu, J. J. Good, V. H. DiStefano and T.-A. Schmitt, *Eur. J. Inorg. Chem.*, 2011, **9**, 1374.

26. R. A. Kresinski, A. M. J. Lees and A. W. G. Platt, *Polyhedron*, 2012, **33**, 341.

27. C. Maxim, D. G. Branzea, C. Tiseanu, M. Rouzières, R. Clérac, M. Andruh, and N. Avarvari, *Inorg. Chem.*, 2014, **53**, 2708.

28. J. Fawcett, A. W. G. Platt and S. Vickers, *Polyhedron*, 2003, **22**, 1431.

29. L. Tei, A. J. Blake, C. Wilson and M. Schröder, *Dalton Trans.*, 2004, **13**, 1945.

30. S.-S. Bao, L.-F. Ma, Y. Wang, L. Fang, C.-J. Zhu, Y-Z. Li, and L-M. Zheng, *Chem. Eur. J.*, 2007, **13**, 2333.

31. G. E. Kiefer and M. Woods, *Inorg. Chem.*, 2009, **48**, 11767.

32. M. Ren, S.-S. Bao, N. Hoshino,T. Akutagawa, B. Wang, Y.-C. Ding, S. Wei and L.-M. Zheng, *Chem. Eur. J.*, 2013, **19**, 9619.

33. J. Gałęzowska, R. Janicki, A. Mondry, R. Burgada, T. Bailly, M. Lecouvey and H. Kozłowski, *Dalton Trans.*, 2006, **36**, 4384.

34. A. Mondry and R. Janicki, *Dalton Trans.*, 2006, **39**, 4702.

35. R. Janicki, A. Mondry, *Polyhedron*, 2008, **27**, 1942.

36. Z. Kotková, G. A. Pereira, K. Djanashvili, J. Kotek, J. Rudovský, P. Hermann, L. Vander Elst, R. N. Muller, C. Geraldes, I. Lukeš and J. A. Peters, *Eur. J. Inorg. Chem.*, 2009, **1**, 119.

37. R. Janicki, A. Mondry, *Eur. J. Inorg. Chem.*, 2013, **19**, 3429.

Chapter 4: Paper 1

Octametallic 4f–phosphonate horseshoes

Karzan H. Zangana, Eufemio Moreno Pineda, Jürgen Schnack and Richard E. P. Winpenny, *Dalton Trans.*, 2013, **42**, 14045.

Dalton Transactions

RSC Publishing

COMMUNICATION

View Article Online
View Journal | View Issue

Octametallic 4f-phosphonate horseshoes†

Cite this: *Dalton Trans.*, 2013, **42**, 14045

Received 1st August 2013,
Accepted 16th August 2013

DOI: 10.1039/c3dt52086b

www.rsc.org/dalton

Karzan H. Zangana,[a] Eufemio Moreno Pineda,[a] Jürgen Schnack[b] and Richard E. P. Winpenny*[a]

Three octanuclear phosphonate clusters, formulated as $[Ln_8(O_3P^tBu)_6(\mu_3\text{-}OH)_2(H_2O)_2(HO^iBu)(O_2C^tBu)_{12}](NH_3{}^iPr)_2$ (Ln = Gd, Dy and Tb), were synthesised by refluxing a mixture of pivalic acid (HO_2C^tBu), $Ln(NO_3)_3{\cdot}6H_2O$, *tert*-Butyl phosphonic acid ($H_2O_3P^tBu$) and isopropylamine ($^iPrNH_2$) in isobutyl alcohol ^iBuOH.

There has been considerable recent interest in the synthesis of molecular complexes of phosphonates.[1] This work has been driven by the optimistic opinion that the tendency of phosphonates to generate 2D-lattices[2] could be used to produce molecular cage complexes with anisotropic structures. In turn, this might produce compounds with highly anisotropic magnetic properties and hence produce new "single molecule magnets",[3] *i.e.* paramagnets that show slow relaxation of magnetisation. Some interesting compounds have appeared as a result,[4] and a wide range of metal cage compounds has been reported, covering 3d-metal ions from vanadium(III)[5] to copper(II).[6] More recently, 3d–4f phosphonates have appeared,[7] and have been studied as potential molecular magnetic refrigerants using the magnetocaloric effect (MCE).

Reports on homometallic 4f-phosphonates are more limited, as lanthanide phosphonates have poor solubility in most solvents, therefore it is difficult to obtain single crystals appropriate for X-ray structural analysis. The first reported lanthanide phosphonates where prepared by Mallouk and co-workers,[8] who prepared a series of layered lanthanide alkylphosphonates.

Several routes are used to produce molecular 3d-metal phosphonates;[1] all involve increasing solubility. Some routes involve a co-ligand that binds competitively with the phosphonate. For the co-ligand approach to work with lanthanides, we reasoned a simple oxygen donor would be ideal. Here we report synthesis of three lanthanide phosphonates using *t*-butylphosphonate combined with an excess of pivalic acid (HO_2C^tBu), choosing both ligands to enhance solubility. The new compounds have been characterised by single-crystal X-ray diffraction and SQUID magnetometry.

A simple lanthanide salt, $Ln^{III}(NO_3)_3{\cdot}6H_2O$ (Ln = Gd, Tb, and Dy) was mixed with HO_2C^tBu, $H_2O_3P^tBu$ and a mild base $^iPrNH_2$ in ^iBuOH in the mole ratios 1 : 14 : 0.8 : 1 and the solution refluxed for three hours, *i.e.* the pivalate is in excess over the phosphonate. After cooling to room temperature, crystals formed from the reaction after four days in yields of 50–60%. X-ray structure determination shows the formation of compounds with the formula $(NH_3{}^iPr)_2[Ln_8(O_3P^tBu)_6(\mu_3\text{-}OH)_2(O_2C^tBu)_{12}(H_2O)_2(HO^iBu)]$, where Ln = Gd **1**, Tb **2**, and Dy **3** (Fig. 1).

Compounds **1**–**3**‡ are isomorphous and crystallize in the triclinic space group $P\bar{1}$; we describe the structure of **3** as representative. The molecule contains eight lanthanides, six phosphonates and twelve pivalates. The metal ion and phosphonate core can best be described as consisting of a central distorted octahedron sharing two vertexes with two different distorted pyramids (Fig. 1c). The four Dy^{III} atoms (Dy1, Dy2, Dy3, and Dy4) and the two phosphorous atoms (P1, P2) are in the asymmetric unit and form the central octahedron. The two distorted pyramids are linked to the central octahedron by two vertexes (Dy3, Dy4). One of the pyramids that connected to the central octahedron contains Dy4, Dy5, Dy6, P3 and P4, while the other pyramid is constructed from Dy3, Dy7, Dy8, P5 and P6. There are two μ_3-hydroxide centred dysprosium triangles formed by (Dy2, Dy4, Dy6) and (Dy1, Dy3, Dy7); each triangle is sharing an edge with the distorted central octahedron and another edge with the distorted pyramid.

The Dy···Dy distance in the edges of the triangles is *ca.* 3.8 Å and the two μ_3-OH groups are displaced about 0.82 Å out of the plane of the metal ions. The Dy···Dy distances within the central octahedron $\{Dy_4P_2\}$ are in the range 3.6–4.9 Å, whereas the distances between dysprosium ions inside the two

[a]*School of Chemistry and Photon Science Institute, The University of Manchester, Oxford Road, Manchester M13 9PL, UK.*
E-mail: richard.winpenny@manchester.ac.uk; Fax: +44-(0)161-275-1001
[b]*Faculty of Physics, University of Bielefeld, Universitätsstr. 25, D-33615 Bielefeld, Germany*

†Electronic supplementary information (ESI) available: Synthetic method, crystallographic details and magnetic information. CCDC 953479–953481. For ESI and crystallographic data in CIF or other electronic format see DOI: 10.1039/c3dt52086b

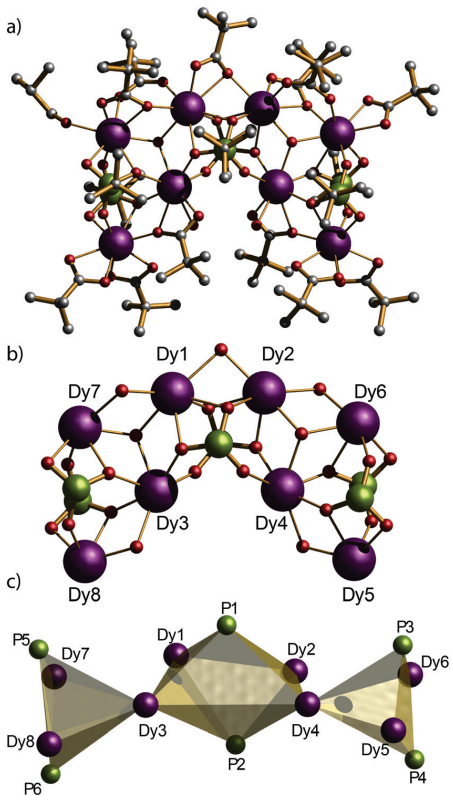

Fig. 1 (a) The structure of compound **3** in the crystal (H-atoms omitted for clarity); (b) the core of **3** showing the phosphonate binding modes; (c) the linked polyhedral representation of **3**. Colours: Dy, purple; P, green; O, orange; C, grey.

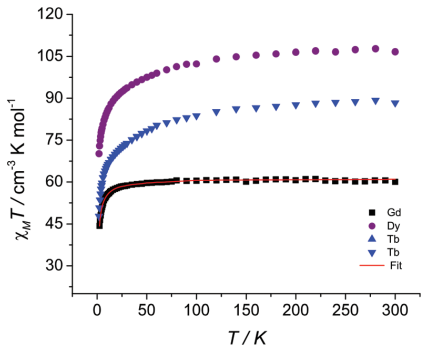

Fig. 2 The product χT *vs.* T for **1–3** under 1 kG DC field. The red line is the fit using parameters given in the text.

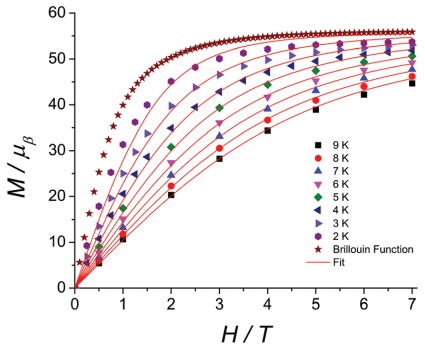

Fig. 3 *M vs. H* of **1** at the temperatures indication. Measured data are given as symbols, with the fit as solid lines. The Brillouin function for eight Gd^{III} ions is shown by the five-pointed stars.

distorted pyramids $\{Dy_3P_2\}$ are in the range 3.9–5.3 Å. All Dy^{III} are eight-coordinate with a dodecahedral geometry.

The phosphonates present two different coordination modes, P1 and P2 binds four Dy with a 4.221 coordination mode, whilst P3, P4, P5 and P6 adopt the 3.211 mode.[9] There are twelve pivalates with 2.21, 2.11 and 1.11 binding modes, and they bridge the edges of the distorted pyramids and central octahedron. Two terminal water and one ^{i}BuOH molecules complete the coordination spheres for Dy3, Dy4 and Dy7 respectively.

The magnetic behaviour of **1** to **3** has been studied on polycrystalline samples (Fig. 2 and 3, and Fig. S1†). At room temperature in each case, the $\chi_M T$ (where χ_M is the molar magnetic susceptibility) value is smaller than the calculated value: for **1**, observed 61.9 emu K mol^{-1} (*calc*. 63 emu K mol^{-1} for eight S = 7/2, g = 2); for **2**, observed 89.3 emu K mol^{-1} (*calc*. 94.5 emu K mol^{-1} for eight J = 6, g_J = 3/2); for **3**, observed 107.7 emu K mol^{-1} (*calc*. 113 emu K mol^{-1} for eight J = 15/2, g_J = 4/3 centres). Upon cooling, for **2** and **3** the product $\chi_M T$ plot decreases with decreasing temperature until approximately 25 K. Below 25 K the product falls more rapidly; this indicates depopulation of the Ln^{III} excited Stark sub-levels, and possibly weak antiferromagnetic interactions between the Ln sites. For **1**, $\chi_M T$ remains constant to around 20 K (Fig. 2) before falling rapidly to 42.2 emu K mol^{-1} at 2 K, indicating a paramagnetic state. A.c. susceptibility studies on the three compounds showed no significant frequency dependence of the out-of-phase susceptibility, χ_M''; therefore none of these compounds are single molecule magnets.[3]

Magnetization (M) against field (H) measurements on **1** at low temperatures (2 to 9 K) were also performed (Fig. 3). The magnetization (M) reaches 53.7μ_B at 7 T at 2 K, this value approaches a saturation value for eight S = 7/2, g = 2 centres. This value is close to the saturation value for eight non-interacting Gd^{III} ions, calculated from the Brillouin function (Fig. 3). For **2**, there is a gradual increase in M *vs.* H curve with increasing field, which reaches 35.7 emu K mol^{-1} at 7 T at 2 K without reaching saturation (Fig. S2a†). For **3**, the M *vs.* T plot rises progressively with rising H reaching 42.2 μ_B at 7 T at 2 K without reaching saturation (Fig. S2b†).

Due to the high magnetisation value obtained in **1** and as Gd^{III} is an isotropic $^8S_{7/2}$ ion, the magnetic entropy change was studied to examine whether **1** could be used for magnetic cooling.[10] The magnetic entropy changes of **1** for changing applied field are calculated indirectly from the magnetization behaviour as a function of applied field and temperatures (Fig. S2†) by using the Maxwell relationship $\Delta S = \int[\partial M(T,H)/\partial T]_H \, dH$. This equation gives the magnetic entropy change for **1** at 3 K and for field changes ΔH = 0–7 T which corresponds to 32.3 J kg^{-1} K^{-1}. To date, no magnetic entropy studies have been reported for 4f-phosphonate clusters. However, higher ΔS_m values have been reported previously for other lanthanide clusters.[11]

The maximum entropy value per mole can be calculated using equation $nR \ln(2S + 1)$ [n = 8 Gd^{III} spins S = 7/2], by replacing n, S and R (gas constant) values in the equation the ΔS_m value, equivalent to 16.64R which corresponds to 45.9 J kg^{-1} K^{-1}. This value is much higher that the observed through magnetic measurements. The difference between the theoretical and the experimental value could be attributed to antiferromagnetic interactions.

As $Gd^{(III)}$ is an isotropic ion we can simulate the magnetic data. The Hilbert space for the problem has a challenging dimension of $(2S + 1)^n$ where n = 8 is the number of Gd centres; this yields 16 777 216, but modern quasi exact approximations allow us to examine the problem. We employ the Finite-Temperature Lanczos Method, which is a Krylov-space method and has proven to be very accurate.[12]

In principle there are multiple exchange paths, but given the likelihood that all exchange interactions are small we have set all nearest neighbour interactions as equivalent (Fig. 4) and fit the data with the Hamiltonian:

$$\hat{H} = -2\sum_{i<j} J_{ij}\hat{S}_i \cdot \hat{S}_j + g\mu_\beta B\hat{S}_z,$$

where $\hat{S}_i$ denote individual spin operators at site i and $\hat{S}_z$ denotes the z-component of the total spin operator.

A very good overall representation of the data, compare Fig. 2 and 3, is achieved when an exchange interaction of J = −0.03 cm^{-1} is assumed. This small value is typical of Gd···Gd exchange interactions.[7f,13] The exchange interaction and the topology of the cage means that the ground state is S = 0 albeit with a large number of paramagnetic excited states close in energy.

In conclusion, by using phosphonate as ligands three horseshoe-shaped isostructural octametallic clusters have been synthesised. The magnetic studies of the Gd_8 cluster show that even small values for anti-ferromagnetic exchange can have a large adverse effect on the MCE if the topology of the compound avoids spin frustration. Further work is in progress to investigate new lanthanide-phosphonate cages using different phosphonates, including functionalised phosphonate ligands.

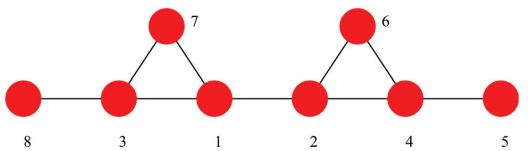

Fig. 4 Schematic sketch of the magnetic core of **1**, lines denote exchange interactions, which for simplicity are assumed to be identical; the numbers correspond to the spin centres numbers as in Fig. 1.

Acknowledgements

KZ thanks the KRG-Scholarship program in "Human Capacity Development (HCDP)". EMP thanks the Panamanian agency SENACYT-IFARHU. JS thanks the Deutsche Forschungsgemeinschaft (SCHN/615-15) for continuous support. Supercomputing time at the LRZ Garching is gratefully acknowledged. REPW thanks the Royal Society for a Wolfson Merit Award.

Notes and references

‡Crystal data for **1** [$C_{94}H_{195}Gd_8N_2O_{47}P_6$]: M_r = 3549.33, triclinic, space group $P\bar{1}$, T = 150.01 K, a = 14.0956(4), b = 24.0968(7), c = 26.5567(8) Å, α = 76.758(2), β = 74.883(2), γ = 82.741(2)°, V = 8455.2(4) Å^3, Z = 2, ρ = 1.393 g cm^{-3}, total data = 47 337, independent reflections 34 034 [$R_{(int)}$ = 0.0380], μ = 3.208 mm^{-1}, 1284 parameters, R_1 = 0.0640 for $I \geq 2\sigma(I)$ and wR_2 = 0.1717. Crystal data for **2** [$C_{94}H_{195}Tb_8N_2O_{47}P_6$]: M_r = 3562.79, triclinic, space group $P\bar{1}$, T = 150.05 K, a = 14.0342(7), b = 24.0928(11), c = 26.4594(12) Å, α = 76.727(4), β = 75.084(4), γ = 82.955(4)°, V = 8394.9(7) Å^3, Z = 2, ρ = 1.409 g cm^{-3}, total data = 46 176, independent reflections 33 802 [$R_{(int)}$ = 0.0899], μ = 3.441 mm^{-1}, 1206 parameters, R_1 = 0.0782 for $I \geq 2\sigma(I)$ and wR_2 = 0.2034. Crystal data for **3** [$C_{94}H_{196}Dy_8N_2O_{47}P_6$]: M_r = 3592.34, triclinic, space group $P\bar{1}$, T = 128.35 K, a = 14.0658(3), b = 24.0994(6), c = 26.4957(6) Å, α = 76.637(2), β = 75.300(2), γ = 83.1827(19)°, V = 8435.1(4) Å^3, Z = 2, ρ = 1.414 g cm^{-3}, total data = 67 875, independent reflections 34 418 [$R_{(int)}$ = 0.0407), μ = 3.614 mm^{-1}, 1253 parameters, R_1 = 0.0499 for $I \geq 2\sigma(I)$ and wR_2 = 0.1293. All three compounds crystallise with large solvent voids and the electron density in these voids has been handled using SQUEEZE.[14]

The magnetic properties in the temperature range 1.8 K–300 K were performed on polycrystalline samples either constrained in eicosane or powdered, using a Quantum Design MPMS-XL7 SQUID magnetometer armed with a 7 T magnet (see ESI† for more details).

1 K. Gopal, S. Ali and R. E. P. Winpenny, in *Metal Phosphonate Chemistry: From Synthesis to Applications*, ed. A. Clearfield and K. Demadis, Royal Society of Chemistry, Cambridge, 2012, pp. 364–419.
2 A. Clearfield and K. D. Karlin, *Prog. Inorg. Chem.*, 1998, **47**, 371.
3 G. Christou, D. Gatteschi, D. N. Hendrickson and R. Sessoli, *MRS Bull.*, 2000, **25**, 66.
4 (*a*) J. Wang, L.-P. Zhang, L. Huang and J. Chen, *J. Coord. Chem.*, 2012, **65**, 3274; (*b*) X. H. Bu, M. L. Tong, H. C. Chang, S. Kitagawa and S. R. Batten, *Angew. Chem., Int. Ed.*, 2004, **43**, 192; (*c*) H. J. Park, D. W. Lim, W. S. Yang, T. R. Oh and M. P. Suh, *Chem.–Eur. J.*, 2011, **17**, 7251; (*d*) Y. F. Zeng, X. Hu, F. C. Liu and X. H. Bu, *Chem. Soc. Rev.*, 2009, **38**, 469; (*e*) M. G. O'Brien, A. M. Beale and B. M. Weckhuysen, *Chem. Soc. Rev.*, 2010, **39**, 4767; (*f*) J. J. Perry, J. A. Perman and M. J. Zaworotko, *Chem. Soc. Rev.*, 2009, **38**, 1400; (*g*) X. L. Wang, C. Qin, S. X. Wu,

K. Z. Shao, Y. Q. Lan, S. Wang, D. X. Zhu, Z. M. Su and E. B. Wang, *Angew. Chem., Int. Ed.*, 2009, **48**, 5291; (*h*) X. L. Tong, T. L. Hu, J. P. Zhao, Y. K. Wang, H. Zhang and X. H. Bu, *Chem. Commun.*, 2010, **46**, 8543.

5 S. Khanra, M. Kloth, H. Mansaray, C. A. Muryn, F. Tuna, E. C. Sañudo, M. Helliwell, E. J. L. McInnes and R. E. P. Winpenny, *Angew. Chem., Int. Ed.*, 2007, **46**, 5568.

6 (*a*) V. Chandrasekhar and S. Kingsley, *Angew. Chem., Int. Ed.*, 2000, **39**, 2320; (*b*) V. Chandrasekhar, D. Sahoo, R. S. Narayanan, R. J. Butcher, F. Lloret and E. Pardo, *Dalton Trans.*, 2013, **42**, 8192; (*c*) V. Baskar, M. Shanmugam, E. C. Sanudo, M. Shanmugam, D. Collison, E. J. L. McInnes, Q. Wei and R. E. P. Winpenny, *Chem. Commun.*, 2007, 37.

7 (*a*) V. Baskar, K. Gopal, M. Helliwell, F. Tuna, W. Wernsdorfer and R. E. P. Winpenny, *Dalton Trans.*, 2010, **39**, 4747; (*b*) Y.-Z. Zheng, M. Evangelisti and R. E. P. Winpenny, *Angew. Chem., Int. Ed.*, 2011, **50**, 3692; (*c*) Y.-Z. Zheng, E. Moreno Pineda, M. Helliwell and R. E. P. Winpenny, *Chem.–Eur. J.*, 2012, **18**, 4161; (*d*) Y.-Z. Zheng, M. Evangelisti, F. Tuna and R. E. P. Winpenny, *J. Am. Chem. Soc.*, 2012, **134**, 1057; (*e*) E. M. Pineda, F. Tuna, R. G. Pritchard, A. C. Regan, Y.-Z. Zheng, R. E. P. Winpenny and E. J. L. Mclnnes, *Chem. Commun.*, 2013, **49**, 3522; (*f*) T. N. Hooper, J. Schnack, S. Piligkos, M. Evangelisti and E. K. Brechin, *Angew. Chem., Int. Ed.*, 2012, **51**, 4633.

8 G. Cao, V. M. Lynch, J. S. Swinnea and T. E. Mallouk, *Inorg. Chem.*, 1990, **29**, 2112.

9 Harris notation describes the binding mode as [*XY*1*Y*2...*Yn*] where *X* is the overall number of metal bound to the whole ligand, and each value of *Y* refers to the number of metal atoms attached to the different donor atoms. See: R. A. Coxall, S. G. Harris, D. K. Henderson, S. Parsons, P. A. Tasker and R. E. P. Winpenny, *Dalton Trans.*, 2000, 2349.

10 M. Evangelisti, F. Luis, L. J. Jongh and M. Affronte, *J. Mater. Chem.*, 2006, **16**, 2534.

11 (*a*) J. W. Sharples, Y.-Z. Zheng, F. Tuna, E. J. L. McInnes and D. Collison, *Chem. Commun.*, 2011, **47**, 7650; (*b*) R. J. Blagg, F. Tuna, E. J. McInnes and R. E. P. Winpenny, *Chem. Commun.*, 2011, **50**, 3692; (*c*) M. Evangelisti, O. Roubeau, E. Palacios, A. Camon, T. N. Hooper, E. K. Brechin and J. J. Alonso, *Angew. Chem., Int. Ed.*, 2011, **50**, 6606; (*d*) F.-S. Guo, J.-D. Leng, J.-L. Liu, Z.-S. Meng and M.-L. Tong, *Inorg. Chem.*, 2012, **51**, 405.

12 (*a*) J. Jaklič and P. Prelovšek, *Phys. Rev. B: Condens. Matter*, 1994, **49**, 5065; (*b*) J. Schnack and O. Wendland, *Eur. Phys. J. B*, 2010, **78**, 535.

13 Y. Zheng, Q.-C. Zhang, L.-S. Long, R.-B. Huang, A. Müller, J. Schnack, L.-S. Zheng and Z. Zheng, *Chem. Commun.*, 2013, **49**, 36.

14 P. van der Sluis and A. L. Spek, *Acta Crystallogr., Sect. A: Fundam. Crystallogr.*, 1990, **46**, 194.

Supporting Information

Octametallic 4f-phosphonate horseshoes

Karzan H. Zangana,[a] Eufemio Moreno Pineda,[a] Jürgen Schnack[b] and Richard E. P. Winpenny[a]*

a. School of Chemistry and Photon Science Institute, The University of Manchester, Oxford Road, Manchester M13 9PL, UK.

b. Faculty of Physics, University of Bielefeld, Universitätsstr. 25, D-33615 Bielefeld, Germany

Experimental Details

All reagents, metal salts and ligands were used as obtained from Aldrich. Analytical data were obtained by the microanalytical service of the University of Manchester.

Preparation of compounds 1 to 3

Compound **1** was synthesised by refluxing a mixture of pivalic acid (HO_2C^tBu) (0.8 g, 7.83 mmol), $Gd(NO_3)_3$•$6H_2O$ (0.25 g, 0.55 mmol), *tert*-butyl phosphonic acid ($H_2O_3P^tBu$) (0.07 g, 0.51 mmol) and isopropylamine ($^iPrNH_2$) (0.1 mL, 1.16 mmol) in *iso*-butyl alcohol (^iBuOH) (15 ml) for 3 hrs to form a clear solution. The solution was filtered and then allowed to stand undisturbed at room temperature for four days. Colourless crystals of **1** suitable for X-ray were collected. Yield 150 mg (50 %), based on $Gd(NO_3)_3$•$6H_2O$. Elemental analysis for $C_{94}H_{197}Gd_8N_2O_{47}P_6$, found (calc); C 31.68 (31.79); H 5.41 (5.59); N 0.81 (0.79); Gd 35.38 (35.42); P 5.21 (5.23).

A similar procedure was used to synthesise **2** except that $Tb(NO_3)_3$•$6H_2O$ was used in place of $Gd(NO_3)_3$•$6H_2O$. Yield 165 mg (55%), based on $H_2O_3P^tBu$. Elemental analysis for $C_{94}H_{197}Tb_8N_2O_{47}P_6$, found (calc); C 31.77 (31.67); H 5.48 (5.57); N 0.83 (0.79); Gd 35.59 (35.67); P 4.16 (5.21).

A similar procedure was used to synthesise **3** except that $Dy(NO_3)_3$•$5H_2O$ was used instead of $Gd(NO_3)_3$•$6H_2O$. Yield 180 mg (59 %), based on $H_2O_3P^tBu$. Elemental analysis for, $C_{94}H_{197}Dy_8N_2O_{47}P_6$, found (calc); C 31.47 (31.41); H 5.49 (5.52); N 0.80 (0.78); Dy 36.25 (36.17); P 5.21 (5.17).

Crystallography

The data of **1** to **3** were collected on Agilent SuperNova CCD diffractometer with MoKα radiation (λ = 0.71073 Å). The structures were solved by direct methods and refined on *F2* using SHELXTL. CCDC 953479-953481 contain the supplementary crystallographic data for this paper. These data can be obtained free of charge via www.ccdc.cam.ac.uk/conts/retrieving.html (or from Cambridge Crystallographic Data Centre, 12 Union Road, Cambridge CB21EZ, UK; fax: (+44)1223-336-033; or deposit@ccdc.cam.ac.uk).

Crystal data for **1** [$C_{94}H_{195}Gd_8N_2O_{47}P_6$]: *M*r = 3549.33, triclinic, space group *P-1*, *T* = 150.01 K, *a* = 14.0956(4), *b* = 24.0968(7), *c* = 26.5567(8) Å, *α* = 76.758(2), *β* = 74.883(2), *γ* = 82.741(2) °, *V* = 8455.2(4) Å^3, *Z* = 2, ρ = 1.393 g cm^{-3}, total data = 47337, independent reflections 34034[$R_{(int)}$ = 0.0380], μ = 3.208 mm^{-1}, 1284 parameters, R_1 = 0.0640 for $I \geq 2\sigma$ (I) and wR_2 = 0.1717.

Crystal data for **2** [$C_{94}H_{195}Tb_8N_2O_{47}P_6$]: *M*r = 3562.79, triclinic, space group *P-1*, *T* = 150.05 K, *a* = 14.0342(7), *b* = 24.0928(11), *c* = 26.4594(12) Å, *α* = 76.727(4), *β* = 75.084(4), *γ* = 82.955(4) °, *V* = 8394.9(7) Å^3, *Z* = 2, ρ = 1.409 g cm^{-3}, total data = 46176, independent reflections 33802 [$R_{(int)}$ = 0.0899), μ = 3.441 mm^{-1}, 1206 parameters, R_1 = 0.0782 for $I \geq 2\sigma$ (I) and wR_2 = 0.2034.

Crystal data for **3** [$C_{94}H_{196}Dy_8N_2O_{47}P_6$]: *M*r = 3592.34, triclinic, space group *P-1*, *T* = 128.35 K, *a* = 14.0658(3), *b* = 24.0994(6), *c* = 26.4957(6) Å, *α* = 76.637(2), *β* = 75.300(2), *γ* = 83.1827(19) °, *V* = 8435.1(4) Å^3, *Z* = 2, ρ = 1.414 g cm^{-3}, total data = 67875, independent reflections 34418 [$R_{(int)}$ = 0.0407), μ = 3.614 mm^{-1}, 1253 parameters, R_1 = 0.0499 for $I \geq 2\sigma$ (I) and wR_2 = 0.1293. All three compounds crystallise with large solvent voids and the electron density in these voids has been handled using SQUEEZE.

Magnetic measurements

The magnetic properties in the temperature range 1.8K-300K were performed on polycrystalline samples either constrained in eicosane or lastly powdered, using a Quantum Design MPMS-XL7 SQUID magnetometer armed with a 7 T magnet. Data were corrected for the diamagnetism of the compounds (Pascal constants) and for diamagnetic contribution of eicosane and the sample holder by measurement.

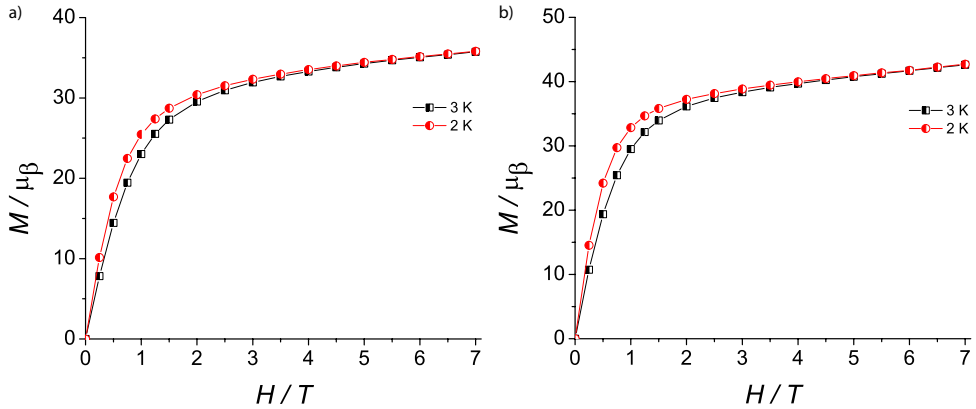

Figure S1. a) $M/N_{\mu\beta}$ magnetization of **2** at different temperatures; b) $M/N_{\mu\beta}$ magnetization of **3** at different temperatures.

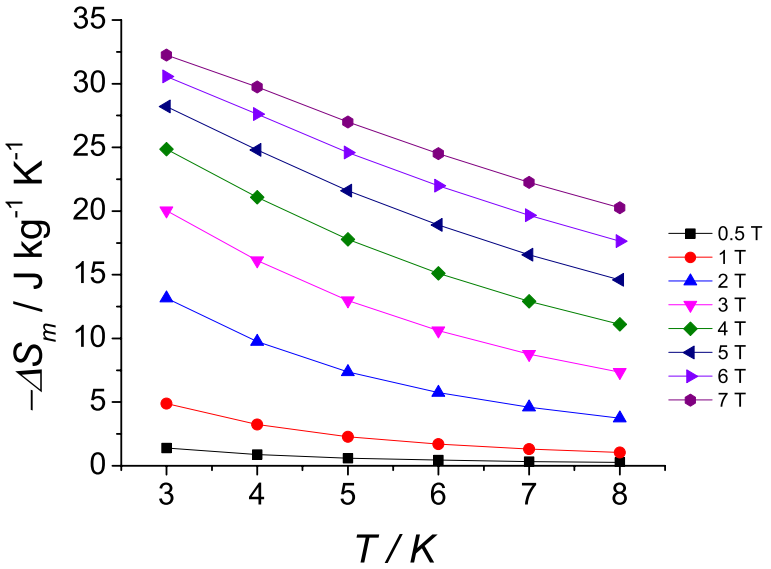

Figure S2. Magnetic entropy change of **1.**

Chapter 5: Paper 2

Centred nine-metal rings of lanthanides

Karzan H. Zangana, Eufemio Moreno Pineda, Eric J. L. McInnes, Jürgen Schnack and Richard E. P. Winpenny, *Chem.Commun.*, 2014, **50**, 1438.

ChemComm

COMMUNICATION

View Article Online
View Journal | View Issue

Centred nine-metal rings of lanthanides†

Cite this: *Chem. Commun.*, 2014, **50**, 1438

Received 14th November 2013,
Accepted 12th December 2013

DOI: 10.1039/c3cc48708c

www.rsc.org/chemcomm

Karzan H. Zangana,[a] Eufemio Moreno Pineda,[a] Eric J. L. McInnes,[a] Jürgen Schnack[b] and Richard E. P. Winpenny*[a]

Two {Ln_{10}} cages are reported (Ln = Dy or Gd) which feature a nine-metal ring surrounding a central metal site. Magnetic studies show weak anti-ferromagnetic exchange around the nine-metal ring, which should create spin frustration.

Cyclic metal cages fall into two broad families. In one family the metal sites are confined to the rim of the cage forming a metal ring, where the metals can be single metal sites[1] or metal cages.[2] In the second family there is a metal at the centre of the cage, and these are called either metallocrowns[3] or metallocoronands.[4] Both classes have been studied, the former largely because of they can act as model compounds for studying physical phenomena, especially in magnetic molecules.[1] For metallocrowns studies extend to selective ion binding, as well as studies of interesting magnetic behaviour.[5] For both families most examples involve 3d-metal ions, although there are remarkable polymolybdate[2a] and palladium phosphonate rings.[2c] Several metal rings have been reported for the 4f-metals,[6] and for 3d–4f cages,[7] but many fewer centred cyclic structures.[8] Most rings and metallocrowns contain an even-number of metal sites in the cyclic portion, although metallocrowns are known with three[9] or five[10] metals in the backbone. Few large odd-numbered rings have been reported.[11] Here we report two cyclic {Ln_{10}} cages (Ln = Dy, **1** or Gd, **2**), where there is a nine-metal ring centred by a tenth metal site.

To synthesise 4f-phosphonate cages we have used pivalate as a co-ligand,[12] and we have reported a number of Co-4f cages.[13] We were intending to extend this work by reacting $[Ln_2(O_2C^tBu)_6(HO_2C^tBu)_6]$ (Ln = Dy and Gd) with $[Co_3(\mu_3\text{-}O)(O_2C^tBu)_6(py)_3](O_2C^tBu)$, $H_2O_3P^tBu$ and pyridine; the Co^{III} cage was used to try to control reactivity by using an inert 3d-metal and hence achieve a more predictable cage than using Co^{II} substrates.[13] After heating for seven hours, light-brown crystals form over two weeks at room temperature in yields of 10–20% based on lanthanide pivalate. X-ray studies show formation of $[Co_3(\mu_3\text{-}O)(O_2C^tBu)_6(py)_3][Ln_{10}(O_2C^tBu)_{18}(O_3P^tBu)_6(OH)(H_2O)_4]$ (Ln = Dy **1**, Gd **2**) (Fig. 1).‡ The compounds are isostructural, and contain an anionic {Ln_{10}} cage co-crystallised with a $[Co_3(\mu_3\text{-}O)(O_2C^tBu)_6(py)_3]^+$ cation (Fig. S1, ESI†). We describe compound **1** as crystals of **2** do not diffract sufficiently well to allow a full structure determination.

The anion of **1** contains nine Dy^{III} metal ions in a ring and a tenth Dy^{III} metal ion at the centre of the structure (Fig. 1). Oxygen donors occupy all the coordination sites on these ten metals. The ten metal sites are almost co-planar; the mean deviation from the plane is 0.23 Å, with the maximum deviation of 0.43 Å found for the central metal site. The nine Dy^{III} metal ions in the ring are arranged at the vertices of an approximately regular nonagon (or enneagon). The distances from the central Dy (Dy10) to the rim fall into two groups; there are longer contacts to Dy2, Dy5 and Dy8,

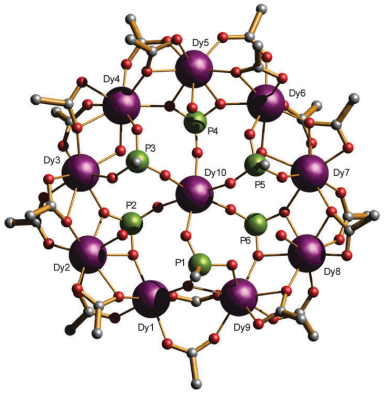

Fig. 1 Crystal structure of **1**. Colours: Dy, purple; P, green; O, red; C, grey. H-atoms and Me groups omitted for clarity.

[a] *School of Chemistry and Photon Science Institute, The University of Manchester, Oxford Road, Manchester M13 9PL, UK. E-mail: richard.winpenny@manchester.ac.uk; Fax: +44 (0)161-275-1001*

[b] *Department of Physics, The University of Bielefeld, Bielefeld, Germany*

† Electronic supplementary information (ESI) available: Synthetic method, crystallographic details, crystallographic figures and magnetic information. CCDC 972030. For ESI and crystallographic data in CIF or other electronic format see DOI: 10.1039/c3cc48708c

averaging 5.92 ± 0.13 Å, while the remaining six contacts average 5.47 ± 0.12 Å. Eight of the distances between neighbouring Dy centres around the ring average 3.83 ± 0.13 Å; the ninth contact (Dy1···Dy9) is longer at 4.1496(2) Å.

Three of the six phosphonates lie below the plane of the $\{Dy_{10}\}$ disc (P2, P4, P6) and adopt the 4.221 binding mode (Harris notation[14]); it is noticeable that these phosphonates chelate to the Dy sites that have the long contacts to the central dysprosium. The remaining three phosphonates are above the plane of metal centres; two (P3 and P5) adopt the 3.111 binding mode, while the third (P1) adopts 3.211 mode. This phosphonate removes the three-fold symmetry of the cage, and it is the Dy1–Dy9 edge bridged by a μ_2-oxygen from this phosphonate that is the long Dy···Dy contact in the ring (see above). Each edge is also bridged by two pivalates, one with a 2.21 mode and the other with the 2.11 mode. The Dy3···Dy4 edge is bridged by a μ-hydroxide (Dy–O distances of 2.308(12) and 2.294(11) Å) while the Dy6···Dy7 is bridged by a μ-water (Dy–O distances 2.537(12) and 2.635(12) Å).

The central Dy10 site is six-coordinate, with a geometry approaching octahedral. The Dy–O distances range from 2.207(10) to 2.338(10) Å, with *cis* O–Dy–O angles between 84.3(4) and 98.4(4)° while *trans* O–Dy–O angles like between 171.6(4) and 178.0(4)°. Dy1 is also six-coordinate, bound to two O-donors from phosphonates and four from carboxylates. Dy2 to Dy8 are eight coordinate, bound to two phosphonate oxygens, five O-atoms from pivalates, and a further oxygen either from a terminal water, a bridging water or a bridging hydroxide. Dy9 is also eight coordinate bound to three phosphonate oxygens and five carboxylate oxygens. The oxo-centred $[Co_3(\mu_3\text{-}O)(O_2C^tBu)_6(py)_3]^+$ cationic triangle features Co^{III} sites around a central μ_3-oxide (Fig. S1, ESI†). Each cobalt is bound to five O-donors, from the central oxide and 2.11 bridging pivalates (av. Co–O distance = 1.89 Å), with a terminal pyridine (av. Co–N distance = 2.24 Å).

Direct-current magnetic susceptibility studies of polycrystalline samples **1** and **2** were carried out in the temperature range 2–300 K (Fig. 2). At room temperature the value of the product $\chi_M T$ (where χ_M is the molar magnetic susceptibility) is 135.0 and 78.5 emu K mol^{-1} for **1** and **2** respectively. The value for **1** is close to that calculated for ten non-interacting ions, while that for **2** is slightly lower than that calculated for ten independent Gd^{III} sites (calc. $\chi_M T$ = 141.2 emu K mol^{-1} for ten Dy^{III} ions, $^6H_{15/2}$, g = 4/3; calc. $\chi_M T$ = 77.9 emu K mol^{-1} for ten Gd^{III} ions, $^8S_{7/2}$, g = 1.99). For **1** the $\chi_M T$ product gradually decreases until around 35 K and then decreases more rapidly. This behaviour is typical of Dy^{III} complexes and is due to depopulation of the Stark sub-levels.[15] **1** does not show slow relaxation of magnetisation. For **2**, $\chi_M T$ remains fairly constant to 20 K before falling. The *M versus H/T* data for **2** at low temperature show a rapid increase of magnetisation, reaching 69.6 μ_B at 7 T at 2 K, which is close to the saturation value for ten S = 7/2 centres with g = 2.00 (69.8 μ_B, inset Fig. 2b). For **1**, the *M versus H/T* curve increases gradually with increasing field, reaching 52.2 μ_B at 7 T at 2 K without reaching saturation (Fig. S3, ESI†).

While it is presently impossible to model data for a $\{Dy_{10}\}$ cage, for the isotropic $\{Gd_{10}\}$ cage modern quasi approximate methods allow us to model the magnetic data, despite the

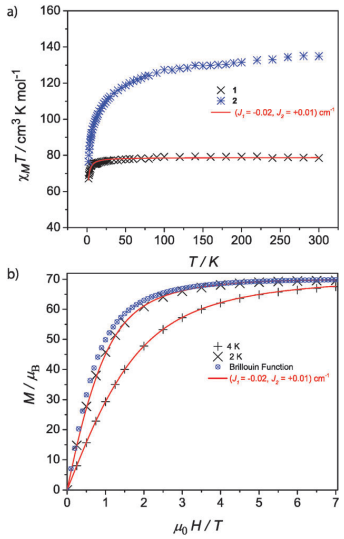

Fig. 2 (a) Variation of $\chi_M T$ with T for **1** and **2** in a magnetic field of 1000 Oe in the temperature range 2 to 300 K; (b) magnetisation against field for **2** from 0–7 T at 2 and 4 K, simulation and *Brillouin* function for 10 non-interacting Gd^{III} ions.

enormous Hilbert space of $(2S+1)^n$ where n = 10 is the number of Gd centres; this yields 576650390625. We employ the Finite-Temperature Lanczos Method, which is a Krylov-space method and has proven to be very accurate.[16] We have chosen a Hamiltonian with one exchange interaction around the ring (J_1), and a second between the central Gd ion and those in the ring (J_2), *i.e.* assuming an approximate C_9 symmetry:

$$\hat{H} = -2J_1\left(\sum_{i=1}^{8}\hat{s}_i\cdot\hat{s}_{i+1} + \hat{s}_1\cdot\hat{s}_9\right) - 2J_2\sum_{i=1}^{9}\hat{s}_i\cdot\hat{s}_{10} + g\mu_B B\hat{S}_z,$$

where $\hat{s}_i$ denote individual spin operators at site i and $\hat{S}_z$ denotes the z-component of the total spin operator. An excellent fit of the $\chi_M T$ *vs.* T and M *vs.* H data could be obtained with several parameter sets, all with both J_1 and J_2 very small (see Fig. S2, ESI,† for further simulations). The best parameters are J_1 = −0.02, J_2 = +0.01 cm^{-1}. These numbers are barely distinguishable from zero, however they would generate a highly frustrated magnetic system, with the nine Gd^{III} ions around the ring unable to align mutually anti-parallel with their nearest neighbours. Unfortunately the extremely small exchange interactions mean that any interesting physics arising from frustration[17] could only be seen at temperatures below 100 mK.

The large magnetisation value obtained for **2** and negligible anisotropy of Gd^{III} ($^8S_{7/2}$) makes this cluster a good candidate for MCE applications (Fig. S3, ESI†). The magnetic entropy changes of **2** for changing applied field can be calculated by the Maxwell equation for magnetic entropy $(\partial S_m/dH)_T = (\partial M(T,M)/\partial T)H$ where the integration for an isothermal process yields $\Delta S = \int[\partial M(T,H)/\partial T]_H\, dH$.[18] This equation gives magnetic entropy

change for **2** at 3 K and for a field changes ΔH = 0.5–7 T which corresponds to 28.5 J kg^{-1} K^{-1}. Much higher values have been reported for pure Gd-cages, for example 46.1 J kg^{-1} K^{-1} for a $\{Gd_{24}\}$ cage,[19] and for 3D Gd-frameworks, *e.g.* 59 J kg^{-1} K^{-1} for $[Gd(O_2CH)_3]_n$.[20] The smaller value observed here must be due to the weak antiferromagnetic interactions between the paramagnetic centres.

KZ thanks the KRG-Scholarship program in "Human Capacity Development (HCDP)". EMP thanks the Panamanian agency SENACYT-IFARHU. J.S. thanks the Deutsche Forschungsgemeinschaft (SCHN/615-15) for continuous support. Supercomputing time at the LRZ Garching is gratefully acknowledged. REPW thanks the Royal Society for a Wolfson Merit Award.

Notes and references

‡ Crystal data for **1** $[C_{159}H_{291}Dy_{10}Co_3O_{72}P_6N_3]$: M_r = 5384.52, triclinic, space group $P\bar{1}$, T = 150.1(8) K, a = 20.7198(8) Å, b = 23.4541(9) Å, c = 26.0799(15) Å, α = 105.194(4)°, β = 93.035(4)°, γ = 103.129(3)°, V = 11825.6(10) Å^3, Z = 2, ρ = 1.512 g cm^{-3}, total data = 65 089, independent reflections 41 489 (R_{int} = 0.0429), μ = 3.432 mm^{-1}, 2169 parameters, R_1 = 0.0903 for $I \geq 2\sigma(I)$ and wR_2 = 0.2570. Unit cell parameters for **2** $[C_{159}H_{291}Gd_{10}Co_3O_{72}P_6N_3]$: triclinic, a = 20.6870(4) Å, b = 23.3983(6) Å, c = 25.9194(7) Å, α = 104.844(2)°, β = 93.166(18)°, γ = 103.3427(18)°, V = 11716.4(5) Å^3. The data were recorded on an Agilent SuperNova CCD diffractometer with $Mo_{K\alpha}$ radiation (λ = 0.71073 Å) The structure of **1** was solved by direct methods and refined on F^2 using SHELXTL.

1 (*a*) K. L. Taft, C. D. Delfs, S. Foner, D. Gatteschi and S. J. Lippard, *J. Am. Chem. Soc.*, 1994, **116**, 823; (*b*) A. J. Blake, C. M. Grant, S. Parsons, J. M. Parsons, J. M. Rawson and R. E. P. Winpenny, *J. Chem. Soc., Chem. Commun.*, 1994, 2363; (*c*) A. Caneschi, A. Cornia, A. Fabretti and D. Gatteschi, *Angew. Chem.*, 1999, **111**, 1372; (*d*) J. Ummethum, J. Nehrkorn, S. Mukherjee, N. B. Ivanov, S. Stuiber, T. Strassle, P. L. W. Tregenna-Piggott, H. Mutka, G. Christou, O. Waldmann and J. Schnack, *Phys. Rev. B*, 2012, **86**, 104403; (*e*) M. L. Baker, T. Guidi, S. Carretta, H. Mutka, G. Timco, E. J. L. McInnes, G. Amoretti, R. E. P. Winpenny and P. Santini, *Nat. Phys.*, 2012, **8**, 906; (*f*) G. A. Timco, E. J. L. McInnes and R. E. P. Winpenny, *Chem. Soc. Rev.*, 2013, **42**, 1796.

2 (*a*) A. Müller, E. Krickemeyer, J. Meyer, H. Bögge, F. Peters, W. Plass, E. Diemann, S. Dillinger, F. Nonnebruch, M. Randerath and C. Menke, *Angew. Chem., Int. Ed. Engl.*, 1995, **34**, 2122; (*b*) A. J. Tasiopoulos, A. Vinslava, W. Wernsdorfer, K. A. Abboud and G. Christou, *Angew. Chem., Int. Ed.*, 2004, **43**, 2117; (*c*) F. Xu, H. N. Miras, R. A. Scullion, D. L. Long, J. Thiel and L. Cronin, *Proc. Natl. Acad. Sci. U. S. A.*, 2012, **109**, 11609; (*d*) T. Nakajima, K. Seto, F. Horikawa, I. Shimizu, A. Scheurer, B. Kure, T. Kajiwara, T. Tanase and M. Mikuriya, *Inorg. Chem.*, 2012, **51**, 12503; (*e*) J. Li, J. Tao, R.-B. Huang and L.-S. Zheng, *Inorg. Chem.*, 2012, **51**, 5988; (*f*) C.-M. Liu, D.-Q. Zhang and D.-B. Zhu, *Chem.–Asian J.*, 2011, **6**, 74.

3 G. Mezei, C. M. Zaleski and V. L. Pecoraro, *Chem. Rev.*, 2007, **107**, 4933–5003, and references therein.

4 R. W. Saalfrank and A. Scheurer, *Top. Curr. Chem.*, 2012, **319**, 125, and references therein.

5 (*a*) C. M. Zaleski, S. Tricard, E. C. Depperman, W. Wernsdorfer, T. Mallah, M. L. Kirk and V. L. Pecoraro, *Inorg. Chem.*, 2011, **50**, 11348; (*b*) T. T. Boron, J. W. Kampf and V. L. Pecoraro, *Inorg. Chem.*, 2010, **49**, 9104.

6 (*a*) L. G. Westin, M. Kriticos and A. Caneschi, *Chem. Commun.*, 2003, 1012; (*b*) S. K. Langley, B. Moubaraki, C. M. Forsyth, I. A. Gass and K. S. Murray, *Dalton Trans.*, 2010, **39**, 1705; (*c*) T. Kajiwara, H. Wu, T. Ito, N. Iki and S. Miyano, *Angew. Chem., Int. Ed.*, 2004, **43**, 1832; (*d*) T. Kajiwara, K. Katagiri, S. Takaishi, M. Yamashita and N. Iki, *Chem.–Asian J.*, 2006, **1**, 349; (*e*) X. Li, Y. Hung and R. Cao, *CrystEngComm*, 2012, **14**, 6045.

7 (*a*) J. B. Peng, Q. C. Zhang, X. J. Kong, Y. P. Ren, L. S. Long, R. B. Huang, L. S. Zheng and Z. Zheng, *Angew. Chem., Int. Ed.*, 2011, **50**, 10649; (*b*) J.-D. Leng, J.-L. Liu and M.-L. Tong, *Chem. Commun.*, 2012, **48**, 5286; (*c*) S. Schmidt, D. Prodius, G. Novitchi, V. Mereacre, G. E. Kostakis and A. K. Powell, *Chem. Commun.*, 2012, **48**, 9825; (*d*) L.-F. Zou, L. Zhao, Y.-N. Guo, G.-M. Yu, Y. Guo, J. Tang and Y.-H. Li, *Chem. Commun.*, 2011, **47**, 8659; (*e*) M. Li, Y. Lan, A. M. Ako, W. Wernsdorfer, C. E. Anson, G. Buth, A. K. Powell, Z. Wang and S. Gao, *Inorg. Chem.*, 2010, **49**, 11587.

8 (*a*) J. W. Sharples, Y.-Z. Zheng, F. Tuna, E. J. L. McInnes and D. Collison, *Chem. Commun.*, 2011, **47**, 7650; (*b*) Z.-M. Zhang, L.-Y. Pan, W.-Q. Lin, J.-D. Leng, F.-S. Guo, Y.-C. Chen, J.-L. Liu and M.-L. Tong, *Chem. Commun.*, 2013, **49**, 8081.

9 For example, H. L. C. Feltham, R. Clérac, A. K. Powell and S. Brooker, *Inorg. Chem.*, 2011, **50**, 4232.

10 (*a*) A. J. Stemmler, J. W. Kampf, M. L. Kirk, B. H. Atasi and V. L. Pecoraro, *Inorg. Chem.*, 1999, **38**, 2807; (*b*) C.-S. Lim, J. Jankolovist, P. Zhao, J. W. Kampf and V. L. Pecoraro, *Inorg. Chem.*, 2009, **48**, 5224.

11 (*a*) O. Cador, D. Gatteschi, R. Sessoli, F. K. Larsen, J. Overgaard, A.-L. Barra, S. J. Teat, G. A. Timco and R. E. P. Winpenny, *Angew. Chem., Int. Ed.*, 2004, **43**, 5196; (*b*) M. N. N. Hoshino, H. Nojiri, W. Wernsdorfer and H. Oshio, *J. Am. Chem. Soc.*, 2009, **131**, 15100; (*c*) H.-C. Yao, H.-J. Wang, Y.-S. Ma, O. Waldmann, W.-X. Du, Y. Song, Y.-Z. Li, L.-M. Zheng, S. Decurtins and X.-Q. Xin, *Chem. Commun.*, 2006, 1745; (*d*) M. L. Baker, G. A. Timco, S. Piligkos, J. Mathieson, H. Mutka, F. Tuna, P. Kozłowski, M. Antkowiak, T. Guidi, T. Gupta, H. Rath, R. J. Woolfson, G. Kamieniarz, R. G. Pritchard, H. Weihe, L. Cronin, G. Rajaraman, D. Collison, E. J. L. McInnes and R. E. P. Winpenny, *Proc. Natl. Acad. Sci. U. S. A.*, 2012, **109**, 19113.

12 K. H. Zangana, E. M. Pineda, J. Schnack and R. E. P. Winpenny, *Dalton Trans.*, 2013, **42**, 14045.

13 Y. Zheng, M. Evangelisti, F. Tuna and R. E. P. Winpenny, *J. Am. Chem. Soc.*, 2012, **134**, 1057.

14 Harris notation describes the binding mode as $[X{\cdot}Y_1Y_2Y_3\ldots Y_n]$, where X is the overall number of metals bound by the whole ligand, and each value of Y refers to the number of metal atoms attached to the different donor atoms. See ESI† and R. A. Coxall, S. G. Harris, D. K. Henderson, S. Parsons, P. A. Tasker and R. E. P. Winpenny, *J. Chem. Soc., Dalton Trans.*, 2000, 2349.

15 L. Sorace, C. Benelli and D. Gatteschi, *Chem. Soc. Rev.*, 2011, **40**, 3092.

16 (*a*) J. Jaklic and P. Prelovsek, *Phys. Rev. B*, 1994, **49**, 5065; (*b*) J. Schnack and O. Wendland, *Eur. Phys. J. B*, 2010, **78**, 535; (*c*) J. Schnack, P. Hage and H.-J. Schmidt, *J. Comput. Phys.*, 2008, **227**, 4512.

17 (*a*) K. Bärwinkel, P. Hage, H.-J. Schmidt and J. Schnack, *Phys. Rev. B*, 2003, **68**, 054422; (*b*) J. Schnack, *Dalton Trans.*, 2010, **39**, 4677.

18 M. Evangelisti, F. Luis, L. J. de Jongh and M. Affronte, *J. Mater. Chem.*, 2006, **16**, 2534.

19 L.-X. Chang, G. Xiong, L. Wang, P. Cheng and B. Zhao, *Chem. Commun.*, 2013, **49**, 1055.

20 G. Lorusso, J. W. Sharples, E. Palacios, O. Roubeau, E. K. Brechin, R. Sessoli, A. Rossin, F. Tuna, E. J. L. McInnes, D. Collison and M. Evangelisti, *Adv. Mater.*, 2013, **25**, 4653.

Supporting Information

Centred nine-metal rings of lanthanides

Karzan H. Zangana,[a] Eufemio Moreno Pineda,[a] Eric J. L. McInnes,[a] Jürgen Schnack[b] and Richard E. P. Winpenny[a]

[a] *School of Chemistry and Photon Science Institute, The University of Manchester, Oxford Road, Manchester M13 9PL, UK. Fax: 44-161-275-1001; E-mail:richard.winpenny@manchester.ac.uk*
[b] *Department of Physics, The University of Bielefeld, Bielefeld, Germany*

Experimental Details

All reagents, metal salts and ligands were used as obtained from Aldrich. Analytical data were obtained by the microanalytical service of the University of Manchester.

Preparation of starting materials

$[Gd_2(O_2C^tBu)_6(HO_2C^tBu)_6]$, $[Dy_2(O_2C^tBu)_6(HO_2C^tBu)_6]$ and $[Co_3(\mu_3\text{-}O)(O_2C^tBu)_6(py)_3]\cdot O_2C^tBu$ were prepared as reported.[a,b]

Preparation of compounds 1 and 2

Compound **1** was synthesised by reacting a mixture of dysprosium pivalate $[Dy_2(O_2C^tBu)_6(HO_2C^tBu)_6]$ (0.46 g, 0.30 mmol), $[Co_3(\mu_3\text{-}O)(O_2C^tBu)_6(py)_3]\cdot O_2C^tBu$ (1 g, 0.88 mmol), *tert*-butyl phosphonic acid ($H_2O_3P^tBu$) (0.07 g, 0.507 mmol) and pyridine (C_5H_5N) (0.5 mL, 6.20 mmol) in acetonitrile (CH_3CN) (15 ml) for 7 hrs to form a dark brown solution. The solution was filtered and then allowed to stand undisturbed at room temperature for ten days. Light brown colour crystals of **1** suitable for X-ray were collected. Yield 30 mg (10.56%), based on $[Dy_2(O_2C^tBu)_6(HO_2C^tBu)_6]$ EA for $C_{159}H_{291}Dy_{10}Co_3N_3O_{72}P_6$, found (calc); C 35.57 (35. 46); H 5.48 (5.45); N 0.79 (0.78); Dy 30.21 (30.18); P 3.49 (3.45); Co 3.33 (3.29).

A similar procedure to that used for **1** was used for **2** using $[Gd_2(O_2C^tBu)_6(HO_2C^tBu)_6]$ (0.30 mmol) in place of $[Dy_2(O_2C^tBu)_6(HO_2C^tBu)_6]$. Yield 55 mg (19.24 %), based on $[Gd_2(O_2C^tBu)_6(HO_2C^tBu)_6]$ EA for $C_{159}H_{291}Dy_{10}Co_3N_3O_{72}P_6$, found (calc); C 35.86 (35.81); H 5.54 (5.50); N 0.80 (0.79); Gd. 29.52 (29.49); P 3.51 (3.49); Co 3.35 (3.31).

a. Y. Zheng, M. Evangelisti, F. Tuna and R. E. P. Winpenny, *J. Amer. Chem. Soc.*, 2012, **134**, 1057.
b. G. Aromi, A. S. Batsanov, P. Christian, M. Helliwell, A. Parkin, S. Parsons, A. A. Smith, G. A. Timco, R. E. P. Winpenny, *Chem. Eur. J.* **2003**, *9*, 5142-5161.

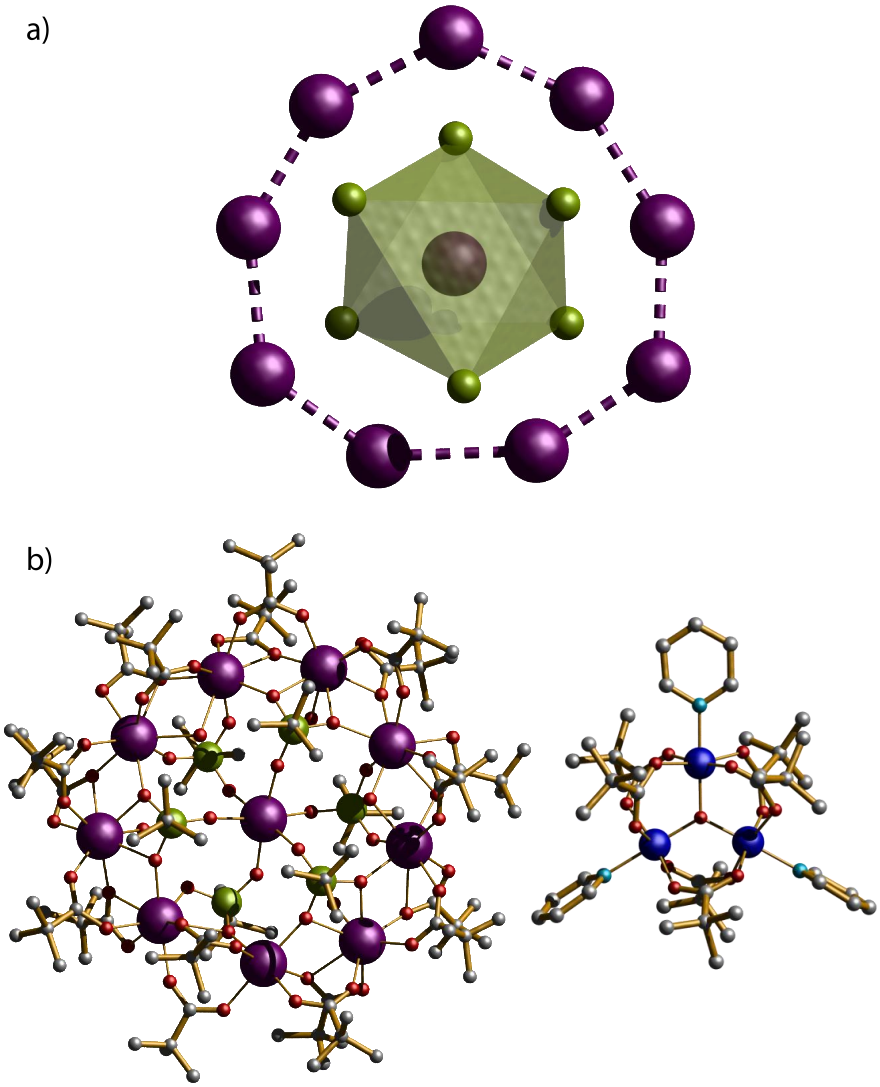

Figure S1. a) Polyhedral representation of central Dy with octahedral environment in $\{Dy_{10}\}$; b) Crystal structure of anion $\{Dy_{10}\}$ and $\{Co_3\}$ cation. Scheme: Dy, purple; P, green; Co, cyan:O, red.

Magnetic measurements

Magnetic measurements were performed on polycrystalline samples, using a Quantum Design MPMS-XL7 SQUID magnetometer armed with a 7 T magnet. Data were corrected for the diamagnetism of the compounds (Pascal constants) and for diamagnetic contribution of eicosane and the sample holder by measurement.

Fits of data for compound **2**

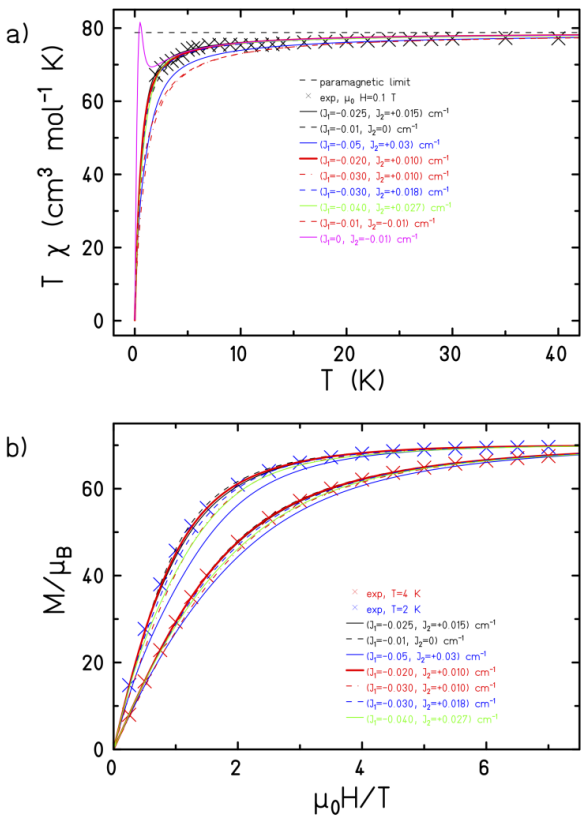

Figure S2. Alternative fits of (a) χT vs T and (b) M vs H for compound **2**. The various exchange value parameter sets used are given in the key.

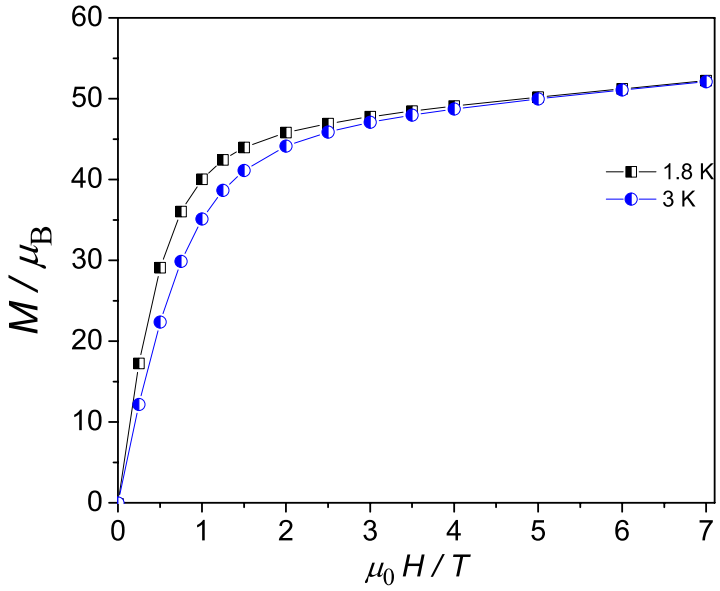

Figure S3. Magnetisation as a function of applied field at different temperatures for **1**.

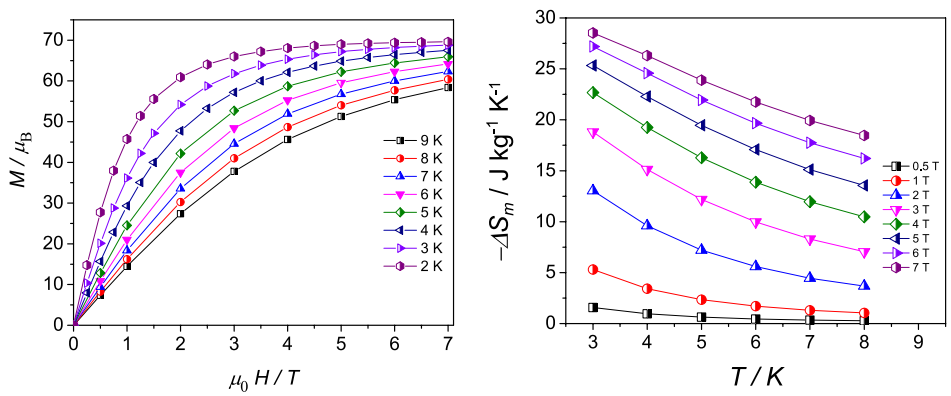

Figure S4. Magnetisation as a function of applied field (*M* vs *H/T*) at different temperatures (left) for **2** and magnetic entropy change (ΔS_m) of **2** at various field and temperatures (right).

Chapter 6: Paper 3

Tetrametallic lanthanide(III) phosphonate cages: synthetic, structural and magnetic studies

Karzan H. Zangana, Eufemio Moreno Pineda and Richard E. P. Winpenny, *Dalton Trans.*, 2014, **43**, 1710.

Dalton Transactions

PAPER

View Article Online
View Journal | View Issue

Cite this: *Dalton Trans.*, 2014, **43**, 17101

Tetrametallic lanthanide(III) phosphonate cages: synthetic, structural and magnetic studies†

Karzan H. Zangana, Eufemio Moreno Pineda and Richard E. P. Winpenny*

Received 28th August 2014,
Accepted 25th September 2014

DOI: 10.1039/c4dt02630f

www.rsc.org/dalton

The synthesis, structures and magnetic properties of a family of lanthanide complexes containing phosphonate ligands are reported. Reaction of hydrated lanthanide nitrate and ^{t}butylphosphonic acid under reflux conditions in iso-butanol, in the presence of pivalic acid as a co-ligand produced five new lanthanide complexes; pyridine (py) was present as a base. The compounds formed are tetrametallic, with the general formula $[pyH]_4[Ln_4(\mu_3\text{-}OH)(O_3P^tBu)_3(HO_3P^tBu)(O_2C^tBu)_2(NO_3)_6]$ where Ln = Gd^{III}, **1**; Tb^{III}, **2**; Dy^{III}, **3**; Ho^{III}, **4** and Er^{III}, **5**. The metal sites within the complexes lie on the vertices of a triangle-based pyramid, with phosphonate ligands on the triangular faces linking the apical Ln site to the Ln sites in the base. Each lanthanide(III) site is eight-coordinate. Magnetic studies of the compounds show a decline in the product $\chi_M T$ with T; modelling the behaviour of **1** shows anti-ferromagnetic exchange between Gd^{III} centres within the triangle with a negligible interaction to the fourth Gd^{III} centre at the apex of the trigonal pyramid.

Introduction

During the past two decades, the synthesis and characterisation of metal phosphonate cages has been an attractive field of synthetic chemistry and molecular magnetism for their aesthetically pleasant structures with interesting magnetic properties,[1] including some examples of single molecule magnets (SMMs).[2] Other metal phosphonate cages have been studied as possible magnetic refrigerants.[3] Phosphonate moieties are interesting functional groups for the construction of molecular cages, as the three tetrahedral oxygen atoms mimic well the zeolite building blocks, providing suitable anchoring sites for a large variety of metal ion centres (including both transition metals and lanthanides).[4] It is also possible to influence the reactivity of compounds using the steric bulk of the phosphonate ligands.[5]

Many research groups, notably those of Clearfield and Zubieta have used phosphonate ligands to synthesise a large number of metal phosphonates that possess mainly extended structures 1D-coordination polymer, 2D-layered structured and 3D-pillared structures.[6] As a result of these studies a wide range of 3d-phosphonate and 3d–4f phosphonate cages have been synthesised.[7] In contrast to transition metal phosphonates, reported molecular assemblies of purely 4f-phosphonates are rare. The first reported lanthanide phosphonates where prepared in 1990 by Mallouk and coworkers;[7] cerium and lanthanum phenylphosphonates with composition $[Ln(O_3PC_6H_5)(HO_3PC_6H_5)]$ and a series of alkylphosphonates such as $[Ln(O_3PMe)(HO_3PMe)]$ were reported. Recently, we have been synthesising molecular cages of lanthanide metal ions with phosphonate ligands with the aim of preparing new cages, optimistically with interesting physical properties.[8]

Lanthanide phosphonate complexes normally have low solubility and poor crystallinity in water and organic solvents, hence it is generally difficult to obtain single crystals suitable for X-ray structural analysis.[9] One of the major reasons for this is that the multisite coordination ability of the phosphonate ligands leads to the formation of insoluble compounds. We and others have proved that synthetically, this problem can be overcome for 3d-metal ions by different strategies, the first example arises from an initial report by Chandrasekhar and Kingsley,[10] where a second ligand is added alongside the phosphonate. The co-ligand occupies certain number of coordination sites on the metal ion as a result of which the number of coordination sites that are accessible for the phosphonate ligands decrease and soluble products can be isolated in the form of single crystals. This methodology has been used with a co-ligand to synthesise molecular cages containing manganese,[11] iron,[12] cobalt,[13] nickel,[14] copper,[15] vanadium.[16] A second method for introducing a phosphonate or ligand without causing an immediate precipitate is to react the ligand with a preformed metal carboxylate cage, which was originally

School of Chemistry and Photon Science Institute, The University of Manchester, Oxford Road, Manchester M13 9PL, UK.
E-mail: richard.winpenny@manchester.ac.uk

†Electronic supplementary information (ESI) available: Cif files, further synthetic details, structural and magnetic plots. CCDC 1021470–1021474. For ESI and crystallographic data in CIF or other electronic format see DOI: 10.1039/c4dt02630f

reported for iron and manganese and has since been extended by our group and others.[17,18]

In this work, we extend the co-ligand approach to 4f-ions, reacting simple lanthanide salts $Ln^{III}(NO_3)_3{\cdot}nH_2O$ (Ln^{III} = Gd, Tb, Dy, Ho and Er) with *t*-butylphosphonic acid ($H_2O_3P^tBu$) in the presence of pivalic acid (HO_2C^tBu) as a co-ligand, giving tetrametallic lanthanide phosphonate cages.

Experimental section

Starting material

All reagents, metal salts, solvents and ligands were used as purchased without any further purification. Analytical data were obtained by the microanalytical service of the University of Manchester, the data and yields are given in Table 1.

Synthetic method

Pivalic acid (0.8 g, 7.83 mmol), $Gd(NO_3)_3{\cdot}6H_2O$ (0.55 mmol), *t*-butyl phosphonic acid (0.07 g, 0.50 mmol) and pyridine (py) (0.5 mL, 6.15 mmol) were dissolved in ^{i}butanol (HO^iBu) (15 mL) and the solution was refluxed at 120 °C for 3 hours. The solution was filtered and then allowed to stand undisturbed at room temperature for nine days. Colourless plate-like crystals suitable for single crystal X-ray diffraction of $[pyH]_4[Gd_4^{III}(\mu_3\text{-}OH)(O_3P^tBu)_3(HO_3P^tBu)(O_2C^tBu)_2(NO_3)_6]$ **1** were formed. Similar reactions with $Ln^{III}(NO_3)_3{\cdot}nH_2O$, (where Ln^{III} = Tb, Dy, Er and Ho) gave analogous metal cages (Table 1).

X-ray data collection and structure solution

X-ray crystallographic measurements for compounds **1–5** were collected on an Agilent SUPERNOVA diffractometer with MoK_α radiation (λ = 0.71073 Å). In all cases the selected single crystals were mounted on a tip of a glass pin using Paraton-N oil and placed in a cold nitrogen flow. Structure solution and refinement was performed with the SHELXS-97 package,[19a] the structures were solved by direct method and completed by iterative cycles of ΔF synthesis and full-matrix least-squares refinement against F^2 using program Olex2.[19b] Crystal data and refinement parameters are given in Table 2. Complete hemispheres data were collected using ϕ and ω scans chosen to give a complete asymmetric unit. All atoms excluding hydrogen were refined anisotropically. Hydrogen atoms were located on the basis of geometrical consideration and treated according to the riding model during refinement with isotropic displacement corresponding to the heavy atom they are linked to. Full crystallographic details can be found in CIF format: CCDC for **1–5**, 1021470–1021474.

Magnetic measurements

Magnetic measurements were performed in temperature ranges 2–300 K, using a Quantum Design MPMS-XL7 SQUID magnetometer equipped with a 7 T magnet. The samples were grounded and placed in a gel capsule. A small amount of eicosane was used to avoid movement of the sample during the measurement. Diamagnetic corrections for the compounds were estimated using Pascal's constants, and the magnetic data were corrected for diamagnetic contribution of the gel capsule, the eicosane and the sample holder. Magnetic data were fitted using the program PHI.[20]

Results and discussion

Synthetic description

To date, just a few examples of lanthanide phosphonates cages have been reported due to the tendency of these systems to form polymeric materials.[9] However we, and others, have recently proved that introducing of co-ligands along with aliphatic R groups on the phosphonate can render better solubility allowing their characterisation. This has led to families of $\{Ln_8P_6\}$[8a] cages and $\{Ln_{10}P_6\}$[8b] centred-rings. To illustrate how variation of other reaction conditions influence the product formed, herein we report the synthesis of five new lanthanide phosphonate clusters $\{Ln_4P_4\}$, using the same general procedure as used for synthesising $\{Ln_8P_6\}$, but replacing the base $^iPrNH_2$ with pyridine. Using an aromatic base produces a compound of lower nuclearity, containing four Ln(III) metal ions and four phosphonates. Three of the Ln(III) metal ions in the cluster form a μ_3-OH centred triangle with the fourth Ln site capping this triangle.

Crystal structures

Compounds **1–5** crystallise in the monoclinic space group *C*2/*c* and have the same molecular structures (Fig. 1); we describe

Table 1 Elemental analysis and yield (%) for compounds **1–5**

	Formula	Yield[a]	Elemental analysis: calculated (found)				
			C	H	Ln	P	N
1	$[pyH]_4[Gd_4(\mu_3\text{-}OH)(O_3P^tBu)_3(HO_3P^tBu)(O_2C^tBu)_2(NO_3)_6]$	45%	26.48 (26.22)	3.86 (3.55)	30.15 (30.10)	5.93 (5.89)	6.71 (6.66)
2	$[pyH]_4[Tb_4(\mu_3\text{-}OH)(O_3P^tBu)_3(HO_3P^tBu)(O_2C^tBu)_2(NO_3)_6]$	39%	26.40 (26.18)	3.85 (3.71)	30.37 (30.25)	5.92 (5.88)	6.69 (6.63)
3	$[pyH]_4[Dy_4(\mu_3\text{-}OH)(O_3P^tBu)_3(HO_3P^tBu)(O_2C^tBu)_2(NO_3)_6]$	30%	26.22 (26.11)	3.82 (3.79)	30.84 (30.77)	5.88 (5.73)	6.67 (6.61)
4	$[pyH]_4[Ho_4(\mu_3\text{-}OH)(O_3P^tBu)_3(HO_3P^tBu)(O_2C^tBu)_2(NO_3)_6]$	35%	26.10 (25.98)	3.80 (3.75)	31.11 (30.97)	5.85 (5.80)	6.61 (6.59)
5	$[pyH]_4[Er_4(\mu_3\text{-}OH)(O_3P^tBu)_3(HO_3P^tBu)(O_2C^tBu)_2(NO_3)_6]$	44%	25.98 (25.66)	3.79 (3.71)	31.46 (31.33)	5.82 (5.78)	6.58 (6.51)

[a] Calculated based on the lanthanide pivalate starting material.

Table 2 Crystallographic information for clusters **1**–**5**

	1	**2**	**3**	**4**	**5**
Chem formula	$C_{51}H_{85}O_{35}N_{11}Gd_4P_4$	$C_{51}H_{85}O_{35}N_{11}Tb_4P_4$	$C_{46}H_{80}O_{35}N_{10}Dy_4P_4$	$C_{46}H_{80}O_{35}N_{10}Ho_4P_4$	$C_{46}H_{80}O_{35}N_{10}Er_4P_4$
fw	2123.10	2129.79	2065.01	2074.73	2084.05
Temp. (K)	150.01(11)	150.04(13)	150.01(10)	150.02(19)	150.03(18)
Cryst system	Monoclinic	Monoclinic	Monoclinic	Monoclinic	Monoclinic
space group	*C*2/*c*	*C*2/*c*	*C*2/*c*	*C*2/*c*	*C*2/*c*
a/Å	44.8769(7)	44.8792(6)	44.8591(11)	44.7075(5)	44.7348(10)
b/Å	19.0562(4)	19.1254(3)	19.1273(5)	19.0970(2)	19.1138(4)
c/Å	24.0257(4)	24.0145(3)	23.9486(5)	23.9771(2)	23.8851(4)
α/°	90	90	90	90	90
β/°	91.0776(16)	91.0749(14)	91.090(2)	91.2548(9)	91.3155(18)
γ/°	90	90	90	90	90
V/Å^3	20542.7(7)	20608.8(5)	20545.1(8)	20466.1(4)	20417.6(7)
Z	8	8	8	8	8
ρ calcd/g cm^{-3}	1.373	1.373	1.335	1.347	1.356
μ (Mo K$_\alpha$)/mm^{-1}	2.679	2.841	3.003	3.186	3.382
R_1 ($I > 2\sigma$)(I)^a	0.0319	0.0389	0.0430	0.0361	0.0370
wR_2 ^{a}	0.0745	0.0846	0.0841	0.0816	0.0854

^{a} $R_1 = ||F_o| - |F_c||/|F_o|$, $wR_2 = [w(|F_o| - |F_c|)^2/w|F_o|^2]^{1/2}$.

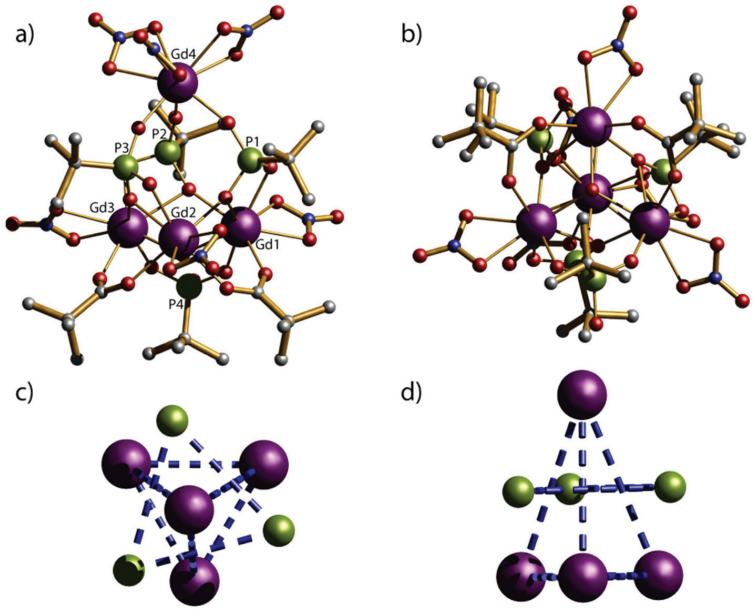

Fig. 1 (a) and (b) side and top view of Crystal structure of the {Gd_4P_4} cluster. Scheme: Ln, purple; P, green; O, red; C, grey; N, cyan; (H omitted for clarity); (c) and (d) top and side view of metal and phosphonate core of the crystal structure of {Gd_4P_4} cluster.

the structure of $[pyH]_4[Gd_4^{III}(\mu_3\text{-OH})(O_3P^tBu)_3(HO_3P^tBu)(O_2C^tBu)_2(NO_3)_6]$ **1** as representative. Overall the molecular cage contains four lanthanide metal ions, four phosphonates, six nitrates, one μ_3-OH and two pivalates. The metallic core of **1** can be described as a triangular pyramid; the four Gd(III) ions (Gd1, Gd2, Gd3, and Gd4) lie on the vertexes of a triangular pyramid. The three phosphonate ligands sit above the triangular faces linking the base to the apex, and adopt the 3.111 bonding mode (Harris notation).[21] The fourth phosphonate is located below the base of a triangular pyramid and bridges the (Gd1···Gd3) edge using the 2.11 bonding mode. There are six chelating nitrate ligands in the structure; one nitrate coordinates to each of the vertices in the triangular base and there are three nitrate ligands coordinated to the apex of the triangular pyramid (Gd4). Two of the Gd···Gd edges within the triangular base are bridged by 2.11 pivalates.

The distances between Gd1···Gd2, Gd2···Gd3 and Gd1···Gd3 that are forming the edges of the base of the triangular pyramid are 3.8104(6), 3.8151(8) and 3.8642(6) Å respectively. The μ_3-OH group is displaced about 0.8230(1) Å out of the plane of the gadolinium metal ions. The Gd–O–Gd angles range from 108.34(11) to 109.19(10)°; these angles are consistent with a μ_3-hydroxide and not with a bridging oxide. The distances between the plane of base (Gd1, Gd2 and Gd3) and the apex (Gd4) within the triangular pyramid are exactly 5.1150(1) Å.

Two different geometries are adopted by the Gd^{III} ions in the cluster: whilst Gd2, Gd3 and Gd4 exhibit a biaugmented trigonal prism geometry (C_{2v}) and a Continuous Shape Measure value (CShM) of 2.494, 2.573 and 2.434 respectively; Gd4 adopts a less regular coordination (muffin, Cs, with a CShM value of 2.345).[22] There are no significant intermolecular interactions between clusters within the lattice.

Magnetic description

The magnetic properties of **1–5** were investigated by solid-state magnetic susceptibility (where χ_M stands for molar magnetic susceptibility) measurements in the 2–300 K range in a 0.1 Tesla (T) DC field. The resulting data for complexes **1–5** are shown as $\chi_M T$ *versus* T plot in Fig. 2 and 3, respectively. In each case the room temperature value for $\chi_M T$ is equivalent to that for four non-interacting metal ions of the appropriate type. For compounds **2–5** $\chi_M T$ decreases steadily upon cooling down to *ca.* 90 K (Fig. 2), below which they drop at 2 K, respectively. Such behaviour is typical for the individual metal ions concerned, and is probably due to depopulation of Stark levels within the individual metal sites. While magnetic exchange between the Ln sites in these compounds cannot be ruled out, there is certainly no evidence for such exchange from these measurements. Magnetisation (M) *versus* applied magnetic field were performed at temperatures of 2 and 3 K in the field range of 0–7 T. For **1** M saturates at 27.7 emu K mol^{-1} at 7 T at 2 K, as expected for four non-interacting Gd^{III} metal ions with $S = 7/2$ and $g_{Gd} = 1.99$ (Fig. 3). For compounds **2–5**, there is a gradual increase in M *vs.* H curve with increasing field, which reach 20.8, 22.7, 23.7, 21.5 μ_B at 7 T at 2 K without reaching saturation.

As Gd^{III} is an isotropic metal ion this allowed us to simulate the magnetic data of complex **1**. Structurally there is little difference between the Gd···Gd edges of the triangles (see above); however the Gd···Gd contacts between the apical Gd and those in the base are between 5.544(1)–5.604(1) Å. Furthermore, any intermolecular interaction between would be rather small since the closest Gd···Gd intercluster distance is 9.8665(6) Å. Based on this structure, we have fitted simultaneously $\chi_M T(T)$ and $M(H)$, using the program *PHI*,[20] using as a model

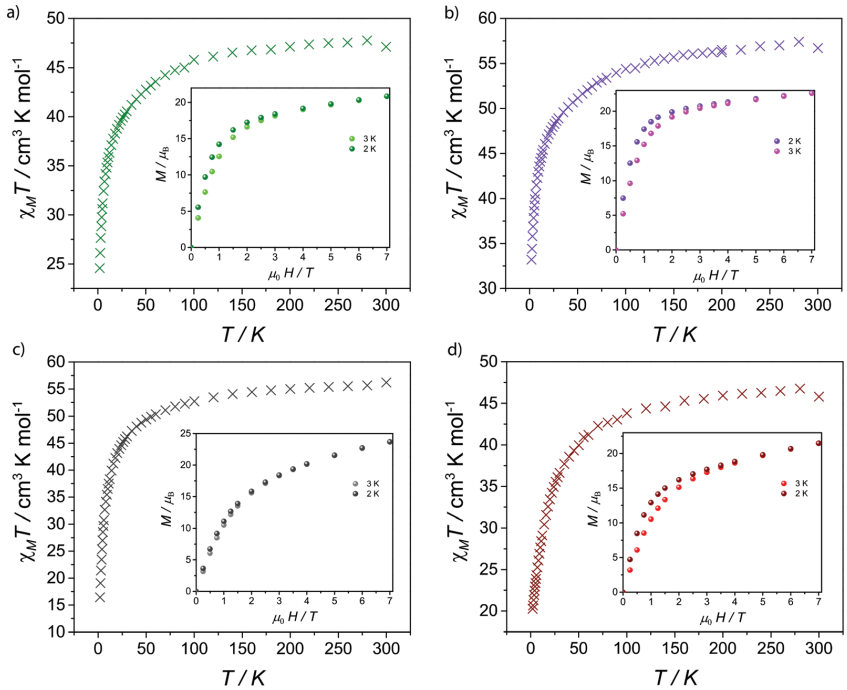

Fig. 2 Molar magnetic susceptibility ($\chi_M T$) *vs.* T plot for **2–5** under 1 kG dc field and molar magnetization (M) as a function of applied magnetic field (H) at 2 and 3 K (inset) for (a) **2**, (b) **3**, (c) **4** and (d) **5**.

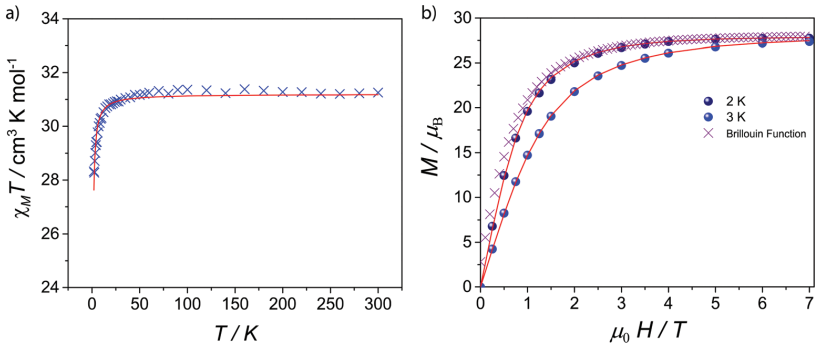

Fig. 3 (a) Molar magnetic susceptibility ($\chi_M T$) *vs.* T and simulation plots for **1** under 1 kG dc field; (b) Molar magnetization (M) as a function of applied magnetic field (H) at 2 and 3 K for **1**.

an equilateral Gd_3, with no exchange interaction to the fourth Gd, using the Hamiltonian (1).

$$H = -2J\left(\hat{S}_1\hat{S}_2 + \hat{S}_2\hat{S}_3 + \hat{S}_1\hat{S}_3\right) + g\mu_B H\sum_{i=1}^{4}\hat{S}_i \qquad (1)$$

where the first term is the isotropic exchange interaction between Gd(1)···Gd(2), Gd(2)···Gd(3) and Gd(1)···Gd(3) and the second term is the Zeeman term of each Gd centre. This gives an antiferromagnetic exchange interaction $J = -0.01$ cm^{-1} between the Gd ions, where $g = 1.99$ (Fig. 3). Clearly with such a small interaction other models would also fit; we prefer this model as it has the minimum number of parameters and fits the crystallography (see above).

AC magnetic susceptibility measurements are a suitable method to judge whether a molecule exhibits a slow magnetisation relaxation rate, which is an essential property of a molecules that might be a single-molecule magnet (SMM). Such measurements were carried out between 10 and 1.8 K with and without applied DC field, however no out-of-phase component was obtained for any of the clusters.

Discussion

The core of compounds **1**–**5** is related to those found in 3d-metal phosphonate cages (Fig. 4).[12a,b] An Fe(III) phosphonate

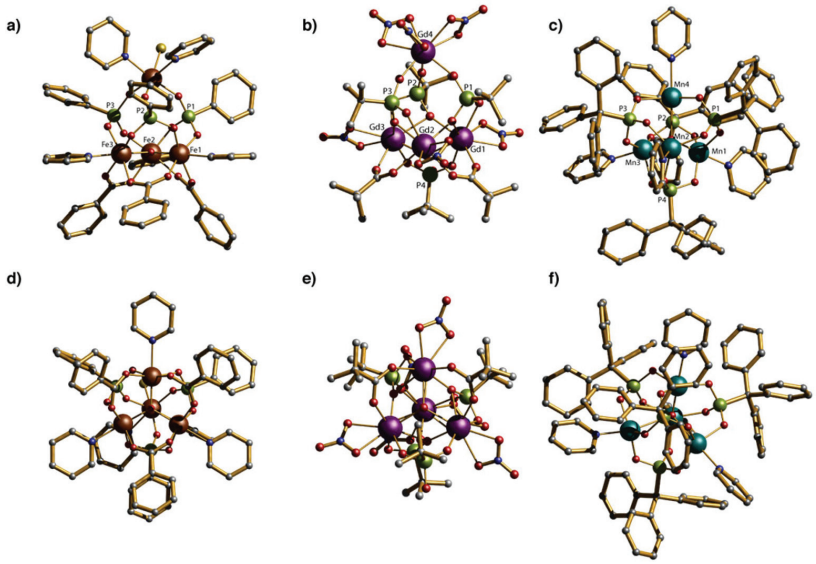

Fig. 4 (a) and (d) side and top view of crystal structure of the $\{Fe_4P_4\}$ cluster; (b) and (e) side and top view of Crystal structure of the $\{Ln_4P_4\}$ cluster; (c) and (f) side and top view of Crystal structure of the $\{Mn_4P_4\}$ cluster; Scheme: Ln, purple; Fe, brown; Mn, cyan; P, green; O, red; C, grey; N, cyan; (H omitted for clarity).

cage $\{Fe_4P_4\}$ has been reported which contains a μ_3-O centred triangle of Fe(III) sites capped by a fourth Fe^{III} ion. The μ_3-O Fe(III) triangle is clearly related to the oxo-centred $\{Fe_3\}$ carboxylate triangle precursor. As in **1–5** three phosphonate units sit on the faces of the trigonal pyramid that link the base to the apex. All Fe(III) metal ion centres are six coordinated. The distance between the plane of base (Fe1, Fe2 and Fe3) and the apex (Fe4) is 4.25(1) Å while the Fe···Fe distances within the triangular base of the tetrahedron are between 3.34 and 3.37 Å. A similar manganese phosphonate cage $\{Mn_4P_4\}$ involves the bulky tritylphosphonic acid (TPA) as ligand; this manganese cage is a mixed valent with two Mn^{II} and two Mn^{III} sites. In this compound all four faces of the triangle pyramid are occupied by TPA ligands and the oxo-centred Mn triangle is much more distorted with Mn···Mn distances within of 3.19 and 3.61 Å; the Mn···Mn distances to the apical Mn site remain longer at 3.88(1) Å. In these 3d-cages, the phosphonates present 3.111 coordination mode and each metal ion centre is coordinated to a pyridine molecule to complete its coordination sphere. In the 4f-phosphonate compounds **1–5** reported here there is a μ_3-OH centred triangle, not oxide centred, and the phosphonates show two diverse binding modes. There is no pyridine binding to 4f metals, with the coordination of the 4f-centres completed by chelating nitrates.

Conclusions

A new group of 4f-phosphonate tetranuclear clusters have been synthesised from the reactions of a simple Ln(III) salt with *t*-butyl phosphonic acid. These products represent new additions to what is still a very small family of such molecular 4f-phosphonate species. We have previously reported that reaction of lanthanide nitrates with phosphonates in the presence of aliphatic base like isopropylamine produce a series of $\{Ln_8\}$ clusters.[20] Herein, our original goal of synthetic program was to explore whether same strategy with aromatic base could be used to assemble Ln(III) ions into large combinations with new structures and magnetic properties. It was observed that the reaction progress well in the presence of aromatic base, as the base promotes the reaction by deprotonation of the phosphonic acid ligand. So, in the present reaction system the identity of the cluster isolated is controlled by the nature of the base used, each single component of the reaction matrix has a strong effect on the final product, and hence on the magnetic behaviour. The magnetic susceptibility data for all complexes display dominant antiferromagnetic interactions. Hopefully further efforts in this area will lead to more magnetically interesting compounds.

Acknowledgements

KZ thanks the KRG-Scholarship program in "Human Capacity Development (HCDP)". EMP thanks the Panamanian agency SENACYT-IFARHU. REPW thanks the Royal Society for a Wolfson Merit Award. We thank the EPSRC (UK) for funding for an X-ray diffractometer (grant number EP/K039547/1).

References

1 (*a*) S. K. Langley, M. Helliwell, R. Sessoli, P. Rosa, W. Wernsdorfer and R. E. P. Winpenny, *Chem. Commun.*, 2005, 5029; (*b*) E. I. Tolis, L. P. Engelhardt, P. V. Mason, G. Rajaraman, K. Kindo, M. Luban, A. Matsuo, H. Nojiri, J. Raftery, C. Schroder, G. A. Timco, F. Tuna, W. Wernsdorfer and R. E. P. Winpenny, *Chem. – Eur. J.*, 2006, **12**, 8961; (*c*) S. K. Langley, M. Helliwell, R. Sessoli, S. J. Teat and R. E. P. Winpenny, *Inorg. Chem.*, 2008, **47**, 497; (*d*) J.-T. Li, Y.-S. Ma, S.-G. Li, D.-K. Cao, Y.-Z. Li, Y. Song and L.-M. Zheng, *Dalton Trans.*, 2009, 5029; (*e*) M. Wang, C. Ma, H. Wen and C. Chen, *Dalton Trans.*, 2009, 994.

2 (*a*) Y.-Z. Zheng, M. Evangelisti, F. Tuna and R. E. P. Winpenny, *J. Am. Chem. Soc.*, 2012, **134**, 1057; (*b*) V. Baskar, K. Gopal, M. Helliwell, F. Tuna, W. Wernsdorfer and R. E. P. Winpenny, *Dalton Trans.*, 2010, **39**, 4747.

3 (*a*) G. K. H. Shimizu, R. Vaidhyanathan and J. M. Taylor, *Chem. Soc. Rev.*, 2009, **38**, 1430; (*b*) A. Clearfeld, *Curr. Opin. Solid State Mater. Sci.*, 1996, **1**, 268.

4 (*a*) A. Clearfield, *Curr. Opin. Solid State Mater. Sci.*, 2002, **6**, 495; (*b*) E. M. Pineda, F. Tuna, R. G. Pritchard and A. C. Regan, *Chem. Commun.*, 2013, **49**, 3522; (*c*) M. Thompson, *Chem. Mater.*, 1994, **6**, 1168; (*d*) A. Subbiah, D. Pyle, A. Rowland, J. Huang, R. A. Narayanan, P. Thiyagarajan, J. Zon and A. Clearfield, *J. Am. Chem. Soc.*, 2005, **127**, 10826.

5 (*a*) V. Baskar, K. Gopal, M. Helliwell, F. Tuna, W. Wernsdorfer and R. E. P. Winpenny, *Dalton Trans.*, 2010, **39**, 4747; (*b*) Y.-Z. Zheng, M. Evangelisti and R. E. P. Winpenny, *Angew. Chem., Int. Ed.*, 2011, **50**, 3692; (*c*) Y.-Z. Zheng, E. M. Pineda, M. Helliwell, M. Evangelisti and R. E. P. Winpenny, *Chem. – Eur. J.*, 2012, **18**, 4161; (*d*) E. M. Pineda, F. Tuna, Y.-Z. Zheng, S. J. Teat, R. E. P. Winpenny, J. Schnack and E. J. L. McInnes, *Inorg. Chem.*, 2014, **53**, 3032; (*e*) M. I. Khan and J. Zubieta, *Prog. Inorg. Chem.*, 1995, **43**, 1; (*f*) V. Chandrasekhar and S. Kingsley, *Angew. Chem., Int. Ed.*, 2000, **39**, 2320.

6 (*a*) J.-G. Mao, *Chem. Rev.*, 2007, **251**, 1493; (*b*) S.-M. Ying and J.-G. Mao, *Cryst. Growth Des.*, 2006, **6**, 964; (*c*) S.-F. Tang, J.-L. Song, X.-L. Li and J.-G. Mao, *Cryst. Growth Des.*, 2007, **7**, 360; (*d*) Y.-Q. Guo, S.-F. Tang, B.-P. Yang and J.-G. Mao, *J. Solid State Chem.*, 2008, **181**, 2713.

7 G. Cao, V. M. Lynch, J. S. Swinnea and T. E. Mallouk, *Inorg. Chem.*, 1990, **29**, 2112.

8 (*a*) K. H. Zangana, E. M. Pineda, J. Schnack and R. E. P. Winpenny, *Dalton Trans.*, 2013, **42**, 14045; (*b*) K. H. Zangana, E. M. Pineda, E. J. L. McInnes,

J. Schnack and R. E. P. Winpenny, *Chem. Commun.*, 2014, **50**, 1438.

9 (*a*) J.-G. Mao, *Coord. Chem. Rev.*, 2007, **251**, 1493; (*b*) S.-M. Ying and J.-G. Mao, *Cryst. Growth Des.*, 2006, **6**, 964; (*c*) S.-F. Tang, J.-L. Song, X.-L. Li and J.-G. Mao, *Cryst. Growth Des.*, 2007, **7**, 360; (*d*) Y.-Q. Guo, S.-F. Tang, B.-P. Yang and J.-G. Mao, *J. Solid State Chem.*, 2008, **181**, 2713.

10 V. Chandrasekhar and S. Kingsley, *Angew. Chem., Int. Ed.*, 2000, **39**, 2320.

11 (*a*) S. Maheswaran, G. Chastanet, S. J. Teat, T. Mallah, R. Sessoli, W. Wernsdorfer and R. E. P. Winpenny, *Angew. Chem., Int. Ed.*, 2005, **44**, 5044; (*b*) M. Shanmugam, G. Chastanet, T. Mallah, R. Sessoli, S. J. Teat, G. A. Timco and R. E. P. Winpenny, *Chem. – Eur. J.*, 2006, **12**, 8777.

12 (*a*) E. I. Tolis, M. Helliwell, S. Langley, J. Raftery and R. E. P. Winpenny, *Angew. Chem., Int. Ed.*, 2003, **42**, 3804; (*b*) S. Konar and A. Clearfield, *Inorg. Chem.*, 2008, **47**, 3492.

13 (*a*) S. Langley, M. Helliwell, R. Sessoli, S. J. Teat and R. E. P. Winpenny, *Inorg. Chem.*, 2008, **47**, 497; (*b*) S. Langley, M. Helliwell, R. Sessoli, S. J. Teat and R. E. P. Winpenny, *Dalton Trans.*, 2009, 3102; (*c*) S. K. Langley, M. Helliwell, S. J. Teat and R. E. P. Winpenny, *Dalton Trans.*, 2012, **41**, 12807.

14 (*a*) B. A. Breeze, M. Shanmugam, F. Tuna and R. E. P. Winpenny, *Chem. Commun.*, 2007, 5185; (*b*) S. K. Langley, M. Helliwell, S. J. Teat and R. E. P. Winpenny, *Inorg. Chem.*, 2014, **53**, 1128.

15 (*a*) V. Chandrasekhar and S. Kingsley, *Angew. Chem., Int. Ed.*, 2000, **39**, 6175; (*b*) V. Chandrasekhar, L. Nagarajan, K. Gopal, V. Baskar and P. Kögerler, *Dalton Trans.*, 2005, 3143; (*c*) V. Chandrasekhar, L. Nagarajan, R. Clérac, S. Ghosh, T. Senapati and S. Verma, *Inorg. Chem.*, 2008, **47**, 5347.

16 (*a*) S. Khanra, M. Kloth, H. Mansaray, C. A. Muryn, F. Tuna, E. C. Sañudo, M. Helliwell, E. J. L. McInnes and R. E. P. Winpenny, *Angew. Chem., Int. Ed.*, 2007, **46**, 5568; (*b*) S. Khanra, L. Batchelor, M. Helliwell, F. Tuna, E. J. L. McInnes and R. E. P. Winpenny, *J. Mol. Struct.*, 2008, **890**, 157; (*c*) S. Khanra, R. Shaw, M. Helliwell, F. Tuna, C. A. Muryn, E. J. L. McInnes and R. E. P. Winpenny, *Materials*, 2010, **3**, 232.

17 (*a*) K. Brechin, R. A. Coxall, A. Parkin, S. Parsons, P. A. Tasker and R. E. P. Winpenny, *Angew. Chem., Int. Ed.*, 2001, **40**, 2700; (*b*) E. I. Tolis, M. Helliwell, S. Langley, J. Raftery and R. E. P. Winpenny, *Angew. Chem., Int. Ed.*, 2003, **42**, 3804; (*c*) E. I. Tolis, L. P. Engelhardt, P. V. Mason, G. Rajaraman, K. Kindo, M. Luban, A. Matsuo, H. Nojiri, J. Raftery, C. Schroder, G. A. Timco, F. Tuna, W. Wernsdorfer and R. E. P. Winpenny, *Chem. – Eur. J.*, 2006, **12**, 8961; (*d*) M. Maheswaran, G. Chastanet, S. J. Teat, T. Mallah, R. Sessoli, W. Wernsdorfer and R. E. P. Winpenny, *Angew. Chem., Int. Ed.*, 2005, **44**, 5044; (*e*) M. Shanmugam, G. Chastanet, T. Mallah, R. Sessoli, S. J. Teat, G. A. Timco and R. E. P. Winpenny, *Chem. – Eur. J.*, 2006, **12**, 8777.

18 (*a*) I. G. Fomina, M. A. Kiskin, A. G. Martynov, G. G. Aleksandrov, Z. V. Dobrokhotova, Y. G. Gorbunova, Y. G. Shvedenkov, A. Y. Tsivadze and V. M. Novotortsev, *Zh. Neorg. Khim.*, 2004, **49**, 1463; (*b*) T. A. Zoan, N. P. Kuzmina, S. N. Frolovskaya, A. N. Rykov, N. D. Mitrofanova, S. I. Troyanov, S. I. Pisarevsky, A. P. Martynenko and L. I. Korenev, *J. Alloys Compd.*, 1995, **225**, 396.

19 (*a*) G. M. Sheldrick, *Acta Crystallogr.*, 2008, **A64**, 112; (*b*) O. V. Dolomanov, L. J. Bourthis, R. L. Gildea, J. A. K. Howard and H. Puschmann, *J. Appl. Crystallogr.*, 2009, **42**, 339.

20 N. F. Chilton, R. P. Anderson, L. D. Turner, A. Soncini and K. S. Murray, *J. Comput. Chem.*, 2013, **34**, 1164.

21 Harris notation describes the binding mode as [*X.Y*1*Y*2... Yn] where *X* is the overall number of metal bond by the whole ligand, and each value of *Y* refers to the number of metal atoms attached to the different donor atoms. See ESI† and R. A. Coxall, S. G. Harris, D. K. Henderson, S. Parsons, P. A. Tasker and R. E. P. Winpenny, *Dalton Trans.*, 2000, **14**, 2349.

22 (*a*) S. Alvarez, *Dalton Trans.*, 2005, 2209; (*b*) S. Alvarez, P. Alemany, D. Casanova, J. Cirera, M. Llunell and D. Avnir, *Coord. Chem. Rev.*, 2005, **249**, 1693.

Tetrametallic lanthanide(III) phosphonate cages: synthetic, structural and magnetic studies

Karzan H. Zangana, Eufemio Moreno Pineda and Richard E. P. Winpenny*

School of Chemistry and Photon Science Institute, The University of Manchester, Oxford Road, Manchester M13 9PL, UK.

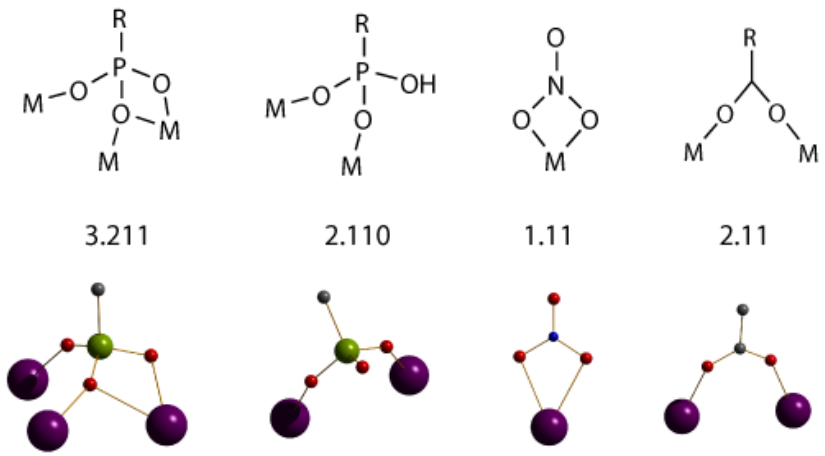

Figure S1. Scheme for binding modes by Harris notation of the phosphonates, nitrates and acetates in the clusters **1**−**5**. Scheme: La, purple; P, light green; O, red; C, grey; N, cyan; H omitted for clarity.

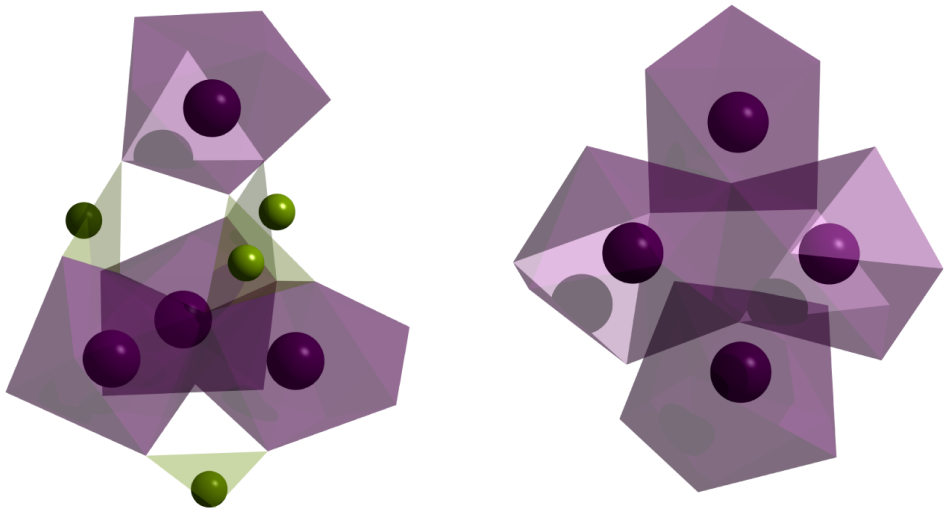

Figure S2. Left**;** Polyhedral view of $\{Ln_4P_4\}$ core. Right; Polyhedral view of metal core of the clusters **1**−**5**.

Table S3. Selected bond distances and angles of **1**−**5**.

	1	**2**	**3**	**4**	**5**
Ln1…Ln2	3.8642(6)	3.86034(6)	3.83996(9)	3.81835(2)	3.79389(5)
Ln2…Ln3	3.8104(6)	3.81040(5)	3.78803(8)	3.77887(3)	3.74962(5)
Ln1…Ln3	3.8151(8)	3.81543(7)	3.79302(10)	3.77498(4)	3.75378(7)
Ln1…O1…Ln2/°	109.1(2)	108.9690(1)	109.1750(15)	109.0140(3)	109.4290(1)
Ln2…O1…Ln3/°	108.8(3)	108.3313(5)	107.9582(8)	108.6251(2)	108.6518(6)
Ln1…O1…Ln3/°	108.9(2)	108.8080(1)	108.700(2)	108.1132(4)	108.9010(13)

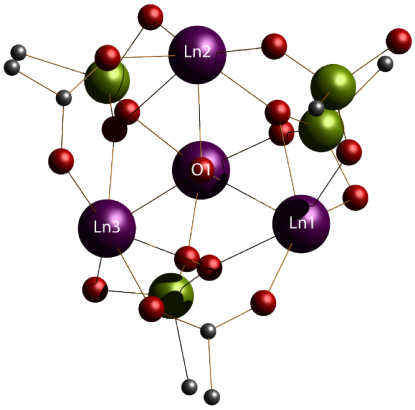

Figure S3. {Ln_3} moiety for Ln_4P_4 clusters. Scheme: La, purple; P, light green; O, red; C, grey; H omitted for clarity.

Chapter 7: Paper 4

Single Molecule Magnet behaviour in a Lanthanide-Phosphonate Octahedron

Karzan H. Zangana, Eufemio Moreno Pineda and Richard E. P. Winpenny, *Dalton Trans.*, 2015, **44**, 12522.

Dalton Transactions

COMMUNICATION

View Article Online
View Journal

Single molecule magnet behaviour in a $\{Dy_4P_2\}$ octahedron†

Karzan H. Zangana, Eufemio Moreno Pineda‡ and Richard E. P. Winpenny*

Cite this: DOI: 10.1039/c5dt01786f

Received 12th May 2015,
Accepted 10th June 2015

DOI: 10.1039/c5dt01786f

www.rsc.org/dalton

Two new tetrametallic lanthanide-phosphonate complexes have been structurally and magnetically characterised. The $\{Dy_4\}$ complex is a single molecule magnet.

Organophosphonates $[RP(O)_2OH]^-$ and $[RPO_3]^{2-}$, obtained from the deprotonation of $[RP(O)(OH)_2]$, are ideal for assembly of cage compounds.[1–3] We have been studying these ligands as routes to cages involving lanthanides, including mixed-metal 3d–4f cages.[4,5] The possible applications of such cages are dependent on the 4f-ions; where the isotropic ion Gd(III) is involved most studies target magnetic cooling through the magnetocaloric effect (MCE).[6] When the anisotropic ion Dy(III) is employed, the blockage of the relaxation of the magnetisation is often observed, leading to single molecule magnets (SMMs),[7] which have been proposed for application in information storage and processing.[8]

In principle, a single phosphonate ligand can bind to as many as nine metal centres; this can create problems especially for metal ions with high coordination numbers. Lanthanide phosphonates often have poor solubility due to a propensity to form coordination polymers, and this can make them difficult to characterise.[9] We have circumvented this problem with a variety of strategies, and demonstrated that discrete molecules containing lanthanides and phosphonates, such as $\{Ln_4P_4\}$,[5a] $\{Ln_8P_6\}$[5b] and $\{Ln_{10}P_6\}$[5c] can be obtained. These cages besides having aesthetically pleasant structures also show some potential for magnetocaloric applications when Ln = Gd(III).[5,6]

Homometallic lanthanide phosphonate cages remain rare. Here we report the synthesis and magnetic properties of two further Ln-phosphonate cages (Ln = Gd(III), **1** and Dy(III), **2**) formed using *t*-butylphosphonate, The compounds have the general formula $[Ln_4(O_3P^tBu)_2(O_2C^tBu)_4(NO_3)_6(H_2O)_2]^{2-}$ (Fig. 1 and S1†). Compound **2** shows slow relaxation of magnetisation.

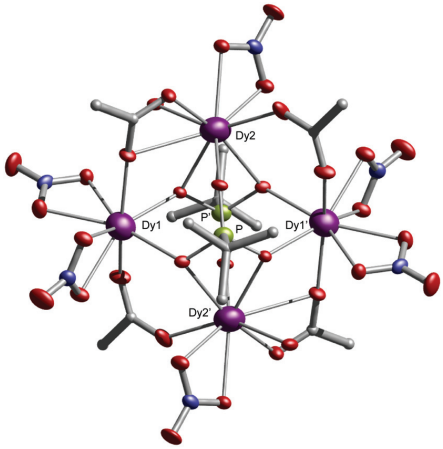

Fig. 1 Crystal structure of $[Dy_4(O_3P^tBu)_2(O_2C^tBu)_4(NO_3)_6(H_2O)_2]^{2-}$. Colour code: Dy, purple; P, green; N, blue; O, red; C, grey; H omitted for clarity.

We have previously studied the reaction of $[Ln_2(O_2C^tBu)_6(HO_2C^tBu)_6]$ with oxo-centred metal triangles $[M_3(\mu_3\text{-}O)(O_2C^tBu)_6(py)_3](O_2C^tBu)$ in the presence of $H_2O_3P^tBu$ and pyridine.[5c,10] When M = Cr(III) we find formation of $\{Cr_6Ln_2\}$ cages,[10] but with M = Co(III) we find the triangle is inert, and merely acts as cation with the phosphonate reacting with the lanthanide to form anionic $\{Ln_{10}P_6\}$ centred-rings.[5c]

The reaction depends on the lanthanide precursor. Here, the same general procedure was followed that produces the $\{Ln_{10}P_6\}$ rings,[5c] but hydrated lanthanide nitrates were used as the precursor, thus significantly reducing the availability of pivalate as a ligand. After heating for 7 h light-brown crystals

School of Chemistry, The University of Manchester, Oxford Road, Manchester M13 9PL, UK. E-mail: richard.winpenny@manchester.ac.uk; Fax: +44-(0)161-275-1001

†Electronic supplementary information (ESI) available: Synthetic method, crystallographic details and figures and magnetic information. CCDC 1051263 and 1051264. For ESI and crystallographic data in CIF or other electronic format see DOI: 10.1039/c5dt01786f

‡Current address: Institute of Nanotechnology, Karlsruhe Institute of Technology, D-76344, Eggenstein-Leopoldshafen, Germany.

formed over three weeks at room temperature in yields of 20–25%. X-ray studies show a salt of formula $[Co_3(\mu_3\text{-}O)(O_2C^tBu)_6(py)_3]_2[Ln_4(O_3P^tBu)_2(O_2C^tBu)_4(NO_3)_6(H_2O)_2]$ (Ln = Gd(III), **1** and Dy(III), **2**) (Fig. 1 and S1†) has formed.

The compounds **1** and **2** are isostructural§, and crystallise in the monoclinic space group $P2_1/n$. They contain an anionic $\{Ln_4\}^{2-}$ cage with two $[Co_3(\mu_3\text{-}O)(O_2C^tBu)_6(py)_3]^+$ cations (Fig. S1†). We describe the dysprosium-containing compound **2** as representative. The anion is on an inversion centre and contains four Dy(III) metal ions, two phosphonates, six nitrates, four pivalates and two terminal water molecules. The metal ions along with the phosphorous centres can be described as a tetragonally distorted octahedron (Fig. 1). The four Dy(III) atoms (Dy(1), Dy(2), Dy(1′) and Dy(2′)) lie in a single plane and form a distorted rectangle (Dy(1)···Dy(2) = 3.965(5), Dy(1)···Dy(2′) = 4.203(8) Å, Dy(2′)–Dy(1)–Dy(2) = 85.91(4), Dy(1′)–Dy(2)–Dy(1) = 94.09(5)°). The two phosphorous atoms P and P′ from the phosphonates are in *trans*-sites of an octahedron; the phosphonates bind using the 4.221 coordination mode (Harris notation)[11] (Fig. 1). The P···P′ distance within the distorted octahedron is 3.717(3) Å.

The metal centre Dy(1) is bound to two 2.110-nitrates while Dy(2) is bound to one such nitrate ligand and one terminal water molecule. The Dy···Dy edges within the parallelogram are bridged by four pivalates, two of them adopting 2.11 coordination mode and the other two adopting 2.21 coordination mode. The Dy(1) site is eight coordinate with a triangular dodecahedral geometry (D_{2d}) (with a Continuous Shape Measure value (CShM) of 2.745).[12] The Dy(2) site is nine coordinate with a less regular geometry, described as a muffin (*Cs*, with a CShM value of 3.265)[12] (Table S1 and Fig. S2†).

The magnetic properties of both systems have been studied in the temperature range of 2–300 K under an applied DC field of 1 kOe. For **1** the product $\chi_M T$ (being χ_M the molar magnetic susceptibility) shows an expected room temperature value of 31.3 cm^3 mol^{-1} (calcd 31.2 cm^3 K mol^{-1}, for four Gd(III); g = 1.99, S = 7/2). Upon cooling $\chi_M T$ stays practically constant down to *ca.* 15 K where it decreases to 26.5 cm^3 K mol^{-1} (at 2 K) (Fig. 2a) indicating weak antiferromagnetic interactions. The molar magnetisation (M_β) at 1.8 and 3 K saturates at 28μ_B above *ca.* 5 T (Fig. 2b). The exchange interaction in **1** can easily be obtained through simultaneous fitting of $\chi_M T(T)$ and $M_\beta(H)$ to a Hamiltonian of the form: $H = -2J(\hat{S}_1\hat{S}_2 + \hat{S}_2\hat{S}_3 + \hat{S}_3\hat{S}_4 + \hat{S}_1\hat{S}_4) + g\mu_B H\sum_{i=1}^{4}\hat{S}_i$ (see inset Fig. 2a) using the program PHI.[13] This gives a single exchange interaction, J = −0.01 cm^{-1}. This very small interaction is of the order of the zero-field splitting of Gd(III) ions, and we cannot exclude the possibility that this fall is a purely single ion effect.

The room temperature $\chi_M T$ for **2** similarly is in good agreement with the expected value for four non-interacting Dy(III) ions 55.2 cm^3 K mol^{-1} (calcd 56.6 cm^3 K mol^{-1}, for four Dy(III), ground state $^6H_{15/2}$ g_J = 4/3, J = 15/2). Upon cooling $\chi_M T$ slowly decreases to a minimum of 46.2 cm^3 K mol^{-1} at about 5 K due

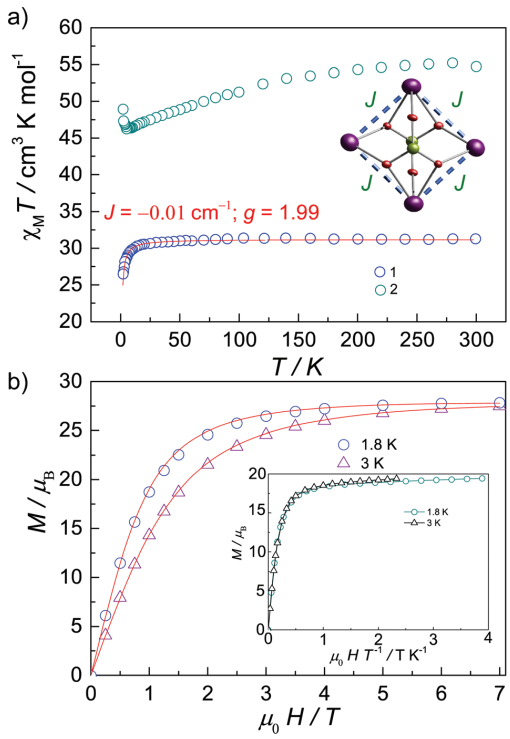

Fig. 2 (a) Variation of $\chi_M T$ *vs.* T for **1** and **2** at 1 kOe from 2–300 K; (b) M_β *vs.* H for **1** and simulations (solid red lines) and reduced magnetisation for compound **2** (inset) from 0–7 T at 2 and 4 K and (solid lines in inset are guides to the eye).

to depopulation of the Stark levels[14] before increasing again at lower temperatures to a maximum of 48.9 cm^3 K mol^{-1}. This suggests a weak ferromagnetic interaction between the Dy centres (Fig. 2a). Interestingly, the $M_\beta(H)$ for **2** rapidly increases upon application of the magnetic field leading to as saturation value of 19μ_B at *ca.* 5 T (see inset Fig. 2b).

The dynamic magnetic behaviour of **2** was investigated by alternating current (ac) susceptibility measurements as a function of temperature (2–16 K) and frequency (ν = 0.1–1400 Hz) (Fig. 3). Ac measurements of **2** show a frequency dependent behaviour, which is further improved by the application of a small-applied dc field, which reduces fast quantum tunnelling. Under an optimal field of 0.6 kG both the in-phase (χ'_M) and out-of-phase (χ''_M) susceptibility shows frequency dependence below 16 K, characteristic of SMMs (Fig. 3a,b and S3†).

A single frequency dependent peak is observed in the $\chi'_M(T)$ and $\chi''_M(T)$, which becomes broader at lower temperatures. The $\chi''_M(T)$ shows a maximum at 15 K for the highest measurement frequency (ν) of 1.4 kHz. The peaks in $\chi''_M(\nu)$ show a linear dependence on temperature above 11 K, and can be described using the Arrhenius law (Fig. 3d), giving a thermal energy

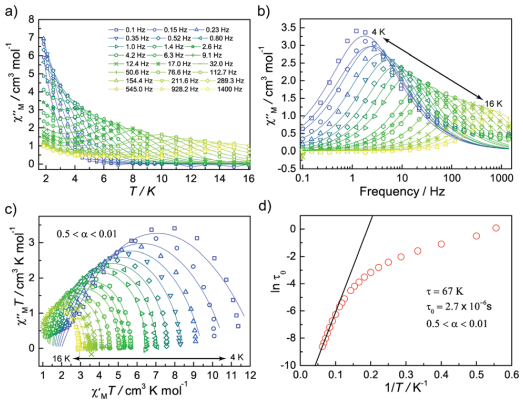

Fig. 3 (a) $\chi''_M(T)$, (b) $\chi''_M(\nu)$, (c) Cole–Cole plot and simulations (solid lines) and (d) Arrhenius analysis for **2** at 0.6 kOe.

barrier to magnetisation relaxation U_{eff} = 67 K with $\tau_0 = 2.7 \times 10^{-6}$ s (Fig. 3d). Cole–Cole plots (χ'_M *vs.* χ''_M) for the temperature range 4–9.5 K give temperature-dependent α parameters: at high temperatures $\alpha = 0.05$, characteristic of a single relaxation time. Below 11 K the peaks show a non-linear dependence on temperature, indicating non-Orbach relaxation processes are becoming important; the α value increases to 0.50, also suggesting multiple relaxation processes are operative (Fig. 3c).

The slow relaxation of the magnetisation observed in Dy(III) complexes is due to a well-defined $m_J = \pm 15/2$ ground state doublet and highly axial *g*-tensors (ideally $g_x = g_y = 0$; $g_z = 20$) of the $^6H_{15/2}$ manifold. Taking into account the ligand set surrounding the two Dy(III) sites in **2**, and employing an electrostatic method[15] based upon electrostatic minimisation of $\rho^{(\alpha,\beta)}_{\pm 15/2}$ Sievers electron density[16] and a minimal valence bond model we have been able to predict the directionality of the magnetic axes in **2**, resulting in an almost collinear arrangement with a deviation between magnetic axes of 21° (Fig. 4). The almost parallel arrangement of the axes is in good agreement with the dynamic magnetic behaviour, since non-collinear magnetic arrangement and small exchange interactions tend to accelerate the quantum tunnelling through further relaxation pathways.[17]

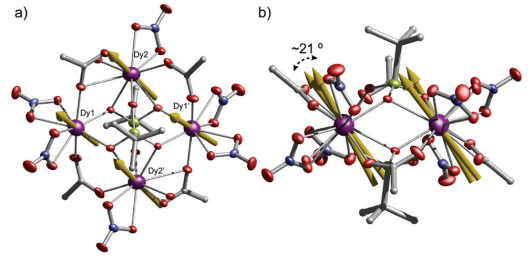

Fig. 4 Magnetic axes obtained through electrostatic method (yellow arrows) (a) top and (b) side view for compound **2**. Colour code: same than in Fig. 1.

In summary, by using phosphonates, we have successfully synthesised two isostructural molecular cages, the metal core consists of four Ln(III) ions which are arranged at the vertices of a parallelogram. While there has been a great deal of recent work to make paramagnetic phosphonate cages,[1] compound **2** appears to be the first homometallic 4f-phosphonate cages with SMM behaviour.

KZ thanks the KRG-Scholarship program in "Human Capacity Development (HCDP)". EMP thanks the Panamanian agency SENACYT-IFARHU. REPW thanks the Royal Society for a Wolfson Merit Award. We also thank EPSRC (UK) for funding an X-ray diffractometer (grant number EP/K039547/1).

References

§ Crystal data for **1** [$C_{122}H_{202}Co_6Gd_4N_{14}O_{60}P_2$]: M_r = 3869.48, monoclinic, space group $P2_1/n$, T = 128.1(4) K, a = 11.7554(2), b = 19.4689(4), c = 36.4118(7) Å, β = 97.9131(17)°, V = 8254.0(3) Å^3, Z = 2, ρ = 1.557 g cm^{-3}, total data = 64 303, R_1 = 0.0479 for $I \geq 2\sigma(I)$ and wR_2 = 0.0670; Crystal data for **2** [$C_{122}H_{202}Co_6Dy_4N_{14}O_{60}P_2$]: M_r = 3890.48, monoclinic, space group $P2_1/n$, T = 150.0(1) K, a = 11.7542(2), b = 19.4585(19), c = 36.4590(7) Å, β = 97.9842(19)°, V = 8258.0(3) Å^3, Z = 2, ρ = 1.565 g cm^{-3}, total data = 41 706, R_1 = 0.0448 for $I \geq 2\sigma(I)$ and wR_2 = 0.0900. These data were collected on an Agilent SuperNova CCD diffractometer with MoK$_\alpha$ radiation (λ = 0.71073 Å), solved using SUPERFLIP,[18a] and refined on F^2 using SHELX-14[18b] in Olex2.[18c]

1 K. Gopal, S. Ali and R. E. P. Winpenny, *"Structural Studies of Paramagnetic Metal Phosphonates", Metal Phosphonate Chemistry: From Synthesis to Applications*, ed. A. Clearfield and K. Demadis, Royal Society of Chemistry, Cambridge, 2012, pp. 364–419.
2 M. G. Walawalkar, H. W. Roesky and R. Murugavel, *Acc. Chem. Res.*, 1999, **32**, 117–126.
3 R. Murugavel, M. G. Walawalkar, M. Dan, H. W. Roesky and C. N. R. Rao, *Acc. Chem. Res.*, 2004, **37**, 763–774.
4 (*a*) Y.-Z. Zheng, M. Evangelisti, F. Tuna and R. E. P. Winpenny, *J. Am. Chem. Soc.*, 2012, **134**, 1057; (*b*) E. M. Pineda, F. Tuna, Y.-Z. Zheng, S. J. Teat, R. E. P. Winpenny, J. Schnack and E. J. L. McInnes, *Inorg. Chem.*, 2014, **53**, 3032; (*c*) E. M. Pineda, F. Tuna, Y.-Z. Zheng, S. J. Teat, R. E. P. Winpenny and E. J. L. McInnes, *Inorg. Chem.*, 2013, **52**, 13702; (*d*) Y.-Z. Zheng, E. M. Pineda, M. Helliwell and R. E. P. Winpenny, *Chem. – Eur. J.*, 2012, **18**, 4161; (*e*) Y.-Z. Zheng, M. Evangelisti and R. E. P. Winpenny, *Chem. Sci.*, 2011, **2**, 99; (*f*) Y.-Z. Zheng and R. E. P. Winpenny, *Sci. China: Chem.*, 2012, **55**, 910; (*g*) V. Baskar, K. Gopal, M. Helliwell, F. Tuna, W. Wernsdorfer and R. E. P. Winpenny, *Dalton Trans.*, 2010, **39**, 4747.
5 (*a*) K. H. Zangana, E. M. Pineda and R. E. P. Winpenny, *Dalton Trans.*, 2014, **43**, 17101; (*b*) K. H. Zangana, E. M. Pineda, J. Schnack and R. E. P. Winpenny, *Dalton Trans.*, 2013, **42**, 14045; (*c*) K. H. Zangana, E. M. Pineda,

E. J. L. McInnes, J. Schnack and R. E. P. Winpenny, *Chem. Commun.*, 2014, **50**, 1438.
6 Y.-Z. Zheng, G.-J. Zhou, Z. Zheng and R. E. P. Winpenny, *Chem. Soc. Rev.*, 2014, **43**, 1462–1475.
7 See for example: (*a*) D. N. Woodruff, R. E. P. Winpenny and R. A. Layfield, *Chem. Rev.*, 2013, **113**, 5110; (*b*) J. D. Rinehart, M. Fang, W. J. Evans and J. R. Long, *Nat. Chem.*, 2011, **3**, 538; (*c*) R. J. Blagg, L. Ungur, F. Tuna, J. Speak, P. Comar, D. Collison, W. Wernsdorfer, E. J. L. McInnes, L. F. Chibotaru and R. E. P. Winpenny, *Nat. Chem.*, 2013, **5**, 673; (*d*) K. S. Pedersen, L. Ungur, M. Sigrist, A. Sundt, M. Schau-Magnussen, V. Vieru, H. Mutka, S. Rols, H. Weihe, O. Waldmann, L. F. Chibotaru, J. Bendix and J. Dreiser, *Chem. Sci.*, 2014, **5**, 3287; (*e*) M. Perfetti, E. Lucaccini, L. Sorace, J. P. Costes and R. Sessoli, *Inorg. Chem.*, 2015, **54**, 3090; (*f*) W. L. Huang, J. J. LeRoy, S. I. Khan, L. Ungur, M. Murugesu and P. L. Diacnescu, *Inorg. Chem.*, 2015, **54**, 2374; (*g*) T. Pugh, F. Tuna, L. Ungur, D. Collison, E. J. L. McInnes, L. F. Chibotaru and R. A. Layfield, *Nat. Commun.*, 2015, **6**, 7492.
8 (*a*) R. Vincent, S. Klyatskaya, M. Ruben, W. Wernsdorefer and F. Balestro, *Nature*, 2010, **488**, 357; (*b*) S. Thiele, F. Balestro, R. Ballou, S. Klyatskaya, M. Ruben and W. Wernsdorfer, *Science*, 2014, **344**, 113; (*c*) K. Katoh, H. Isshiki, T. Komeda and M. Yamashita, *Chem. – Asian J.*, 2012, **7**, 1154.
9 J.-G. Mao, *Coord. Chem. Rev.*, 2007, **251**, 1493.
10 K. H. Zangana, E. M. Pineda, I. J. Vitorica-Yrezabal, E. J. L. McInnes and R. E. P. Winpenny, *Dalton Trans.*, 2014, **35**, 13242–13249.
11 Harris notation describes the binding mode as [*X.Y1Y2...Yn*] where *X* is the overall number of metal bond by the whole ligand, and each value of *Y* refers to the number of metal atoms attached to the different donor atoms. See ESI† and R. A. Coxall, S. G. Harris, D. K. Henderson, S. Parsons, P. A. Tasker and R. E. P. Winpenny, *Dalton Trans.*, 2000, **14**, 2349.
12 (*a*) H. Zabrodsky, S. Peleg and D. Avnir, *J. Am. Chem. Soc.*, 1993, **115**, 8278; (*b*) S. Alvarez, *Dalton Trans.*, 2005, 2209; (*c*) S. Alvarez, P. Alemany, D. Casanova, J. Cirera, M. Llunell and D. Avnir, *Coord. Chem. Rev.*, 2005, **249**, 1693.
13 N. F. Chilton, R. P. Anderson, L. D. Turner, A. Soncini and K. S. Murray, *J. Comput. Chem.*, 2013, **34**, 1164–1175.
14 L. Sorace, C. Benelli and D. Gatteschi, *Chem. Soc. Rev.*, 2011, **40**, 3092.
15 N. F. Chilton, D. Collison, E. J. L. McInnes, R. E. P. Winpenny and A. Soncini, *Nat. Commun.*, 2013, **4**, 2551.
16 J. Sievers, *Z. Phys. B: Condens. Matter*, 1982, **45**, 289.
17 E. M. Pineda, N. F. Chilton, R. Marx, M. Dörfel, D. O. Sells, P. Neugebauer, S.-D. Jiang, D. Collison, J. v. Slageren, E. J. L. McInnes and R. E. P. Winpenny, *Nat. Commun.*, 2014, **5**, 5243.
18 (*a*) G. Oszlanyi and A. Suto, *Acta Crystallogr., Sect. A: Fundam. Crystallogr.*, 2006, **63**, 156; (*b*) G. M. Sheldrick, *Acta Crystallogr., Sect. A: Fundam. Crystallogr.*, 2008, **64**, 112; (*c*) O. V. Dolomanov, L. J. Bourthis, R. L. Gildea, J. A. K. Howard and H. Puschmann, *J. Appl. Crystallogr.*, 2009, **42**, 339.

Supporting Information

Single Molecule Magnet behaviour in a Lanthanide-Phosphonate Octahedron

Karzan H. Zangana, Eufemio Moreno Pineda and Richard E. P. Winpenny*

School of Chemistry and Photon Science Institute, The University of Manchester, Oxford road, Manchester M13 9PL, UK. Fax: 44 – 161 – 275 – 4606; E-mail: richard.winpenny@manchester.ac.uk

Experimental Details

All reagents, metal salts and ligands were used as obtained from Aldrich. Analytical data were obtained by the microanalytical service of the University of Manchester, $[Co_3(\mu_3\text{-}O)(O_2C^tBu)_6(py)3]\bullet O_2C^tBu$ was prepared as reported.[1]

Preparation of compounds 1 and 2

Compound **1** was synthesised by reacting a mixture of gadolinium nitrate $Gd(NO_3)_6\bullet 6H_2O$ (0.13 g, 0.30 mmol), $[Co_3(\mu_3\text{-}O)(O_2C^tBu)_6(py)_3]\bullet O_2C^tBu$ (1g, 0.88mmol), *tert*-butyl phosphonic acid ($H_2O_3P^tBu$) (0.07g, 0.507 mmol) and pyridine (C_5H_5N) (0.5mL, 6.20mmol) in acetonitrile (CH_3CN) (15 ml) for 7 hrs to form a brown solution. The solution was filtered and then allowed to stand untouched at room temperature for two weeks. Light brown colour crystals of the compound **1** suitable for X-ray were collected. Yield 65 mg (25%), based on $Gd(NO_3)_6\bullet 6H_2O$. EA for $C_{122}H_{202}Co_6Gd_4N_{14}O_{60}P_2$, found (calc); C 37.85 (37.87); H 5.20 (5.26); N 5.04 (5.07); Gd. 16.22 (16.25); P 1.55 (1.60); Co 9.10 (9.14).

A parallel procedure to that used for synthesis of compound **1** was used for compound **2**, using $Dy(NO_3)_6\bullet 5H_2O$ (0.30 mmol) in place of $Gd(NO_3)_6\bullet 6H_2O$. Yield 50 mg (20%), based on $Dy(NO_3)_6\bullet 5H_2O$. EA for $C_{122}H_{202}Co_6Dy_4N_{14}O_{60}P_2$, found (calc); C 37.70 (37.66); H 5.20 (5.23); N 5.01 (5.04); Dy 16.65 (16.71); P 1.57 (1.59); Co 9.06 (9.09).

Crystallography

The data were collected on Agilent SuperNova CCD diffractometer with MoK_α radiation (λ = 0.71073 Å). The structures were solved by direct methods and refined on *F2* using SHELXTL.

CCDC 1051263 and 1051264 contain the supplementary crystallographic data for this paper. These data can be obtained free of charge via www.ccdc.cam.ac.uk/conts/retrieving.html (or

[1] G. Aromi, A. S. Batsanov, P. Christian, M. Helliwell, A. Parkin, S. Parsons, A. A. Smith, G. A. Timco, R. E. P. Winpenny, *Chem. Eur. J.*, 2003, **9**, 5142.

from Cambridge Crystallographic Data Centre, 12 Union Road, Cambridge CB21EZ, UK; fax: (+44)1223-336-033; or deposit@ccdc.cam.ac.uk).

Crystal data for **1** [$C_{122}H_{202}Co_6Gd_4N_{14}O_{60}P_2$]: *Mr* = 3869.48, monoclinic, $P2_1/n$, *T* = 128(4) K, *a* = 11.7554(2), *b* = 19.4689(4), *c* = 36.4118(7) Å, α /° = 90, *β*/° = 97.9131(17), *γ*/° = 90, *V* = 8254.0(3) Å^3, *Z* = 2, *ρ* = 1.557 g cm^{-3}, total data = 64303, independent reflections 16879 (R_{int} = 0.0631), *μ* = 2.274 mm^{-1}, 1053 parameters, R_1 = 0.0479 for *I* ≥2σ (*I*) and wR_2 = 0.0687 CCDC 1051264.

Crystal data for **2** [$C_{106}H_{196}Co_6Gd_4N_{12}O_{60}P_2$]: *Mr* = 3890.48, monoclinic, $P2_1/n$, *T* = 150.02(10) K, *a* = 11.7542(2), *b* = 19.4585(4), *c* = 36.4590(7) Å, α /° = 90, *β*/° = 97.9842(19), *γ*/° = 90, *V* = 8258.0(3) Å^3, *Z* = 2, *ρ* = 1.565 g cm^{-3}, total data = 41706, independent reflections 18920 (R_{int} = 0.0750), *μ* = 2.476 mm^{-1}, 1059 parameters, R_1 = 0.0448 for *I* ≥2σ (*I*) and wR_2 = 0.0900 CCDC 1051263.

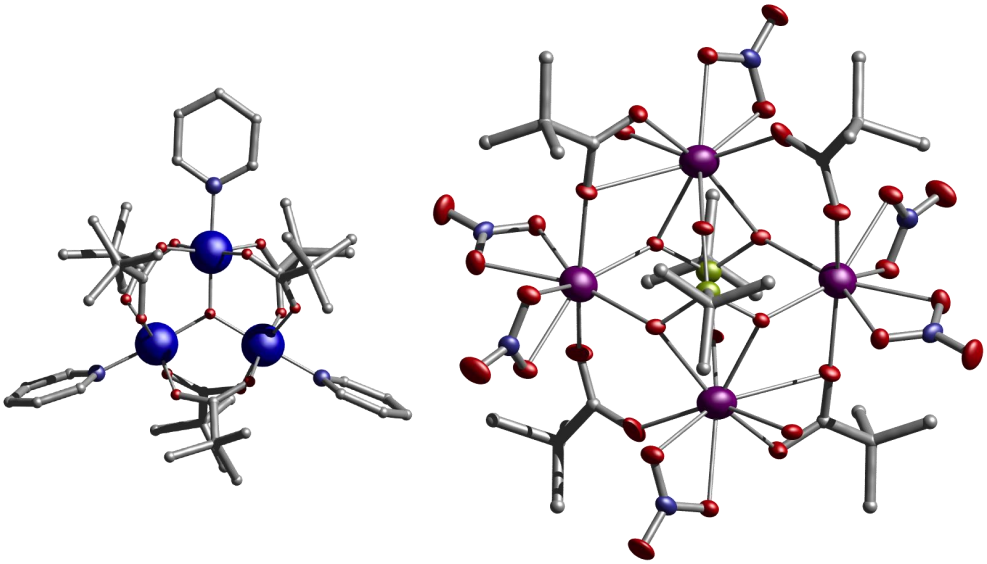

Figure S1. Crystal structure of **2**. Colour codes: Dy, purple; P, green; Co, blue; N, cyan; O, red; C, grey. H-atoms are omitted for clarity.

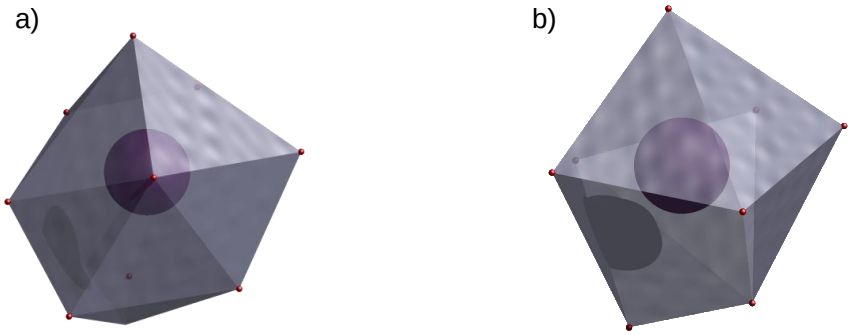

Figure S2. (a) and (b) are the polyhedral view of Dy1 and Dy2, respectively.

Table S1. CShM values for the Dy metal ion centres of **2**.

Dy1		**Dy2**	
Geometry	CShM	Geometry	CShM
OP	31.623	**EP**	30.136
HPY	23.144	**OPY**	22.402
HBPY	13.442	**HBPY**	15.576
CU	12.503	**JTC**	14.218
SAPR	4.705	**JCCU**	8.029
TDD	2.745	**CCU**	6.926
JGBF	11.410	**JCSAPR**	5.858
JETBPY	26.724	**CSAPR**	4.840
JBTPR	4.333	**JTCTRP**	4.777
BTPR	3.905	**TCTPR**	5.830
JSD	3.575	**JTDIC**	10.421
TT	13.256	**HH**	5.955
ETBPY	24.075	**MFF**	3.265

Magnetic measurements

The magnetic properties in the temperature range 1.8 K–300 K were performed on polycrystalline samples either constrained in eicosane or powdered, using a Quantum Design MPMS-XL7 SQUID magnetometer armed with a 7 T magnet. Data were corrected for the diamagnetism of the compounds (Pascal constants) and for diamagnetic contribution of eicosane and the sample holder by measurement.

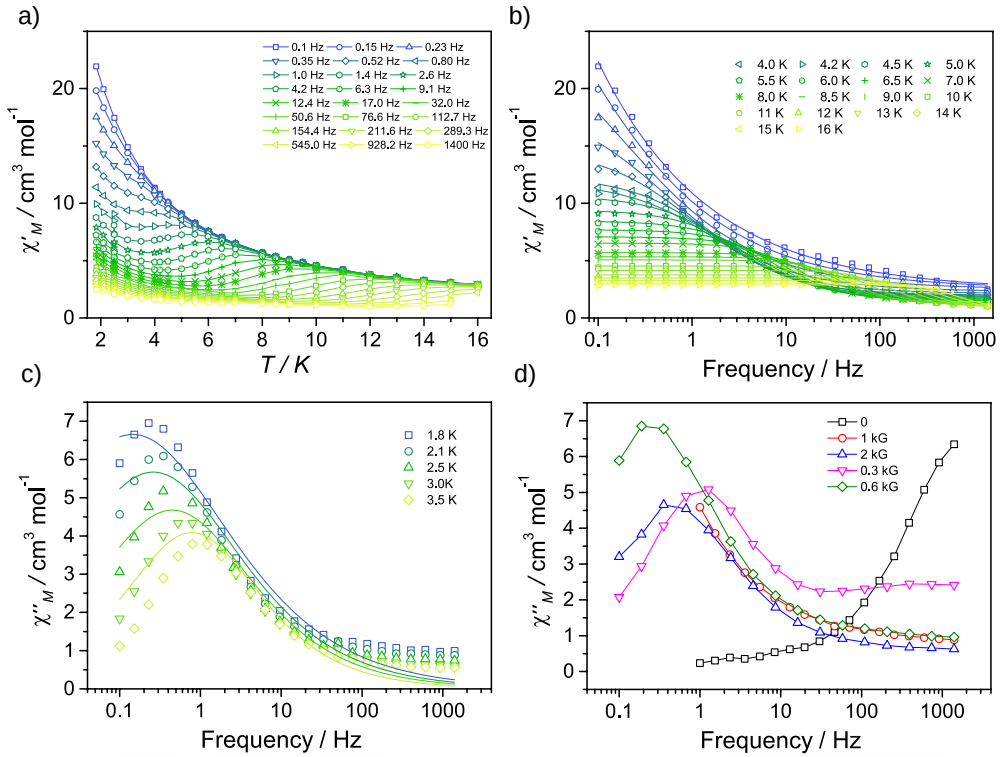

Figure S3. $\chi_M'(T)$ (a); $\chi_M'(\nu)$ (b); $\chi_M''(\nu)$ (c); and (d) field dependence of the $\chi_M''(\nu)$ for compound **2**.

Chapter 8

8.1 A review of discrete 3d–4f phosphonate cages

As far as we are aware, there are ten reports on discrete Ln–TM cages based on phosphonate ligands. Out of these, nine have been reported by Winpenny and co-workers.[1-10] This section analyses the structural chemistry of discrete 3d–4f phosphonate cages, all reported 3d–4f phosphonate cages in the following section, only mono-phosphonate ligands were employed as metal linkers.

Reaction of $Ln(NO_3)_3 \bullet nH_2O$ (Ln = Dy, Gd, Y) and $Cu(OAc)_2 \bullet H_2O$ with tritylphosphonic acid (TPA) in the presence of base give rise to the formation of cages, $[H_3O]$ $[Cu_{24}Dy_8(Ph_3C\text{-}PO_3)_6(Ph_3C\text{-}PO_3H)_6(MeCO_2)_{12}(MeCO_2H)_6(OH)_{42}(NO_3)(OH_2)_6]$, $[(Me_4N)_2K_2]$ $[Cu_{24}Gd_8(Ph_3C\text{-}PO_3)_6(Ph_3C\text{-}PO_3H)_6(MeCO_2)_{12}(MeCO_2H)_{12}(OH)_{42}(NO_3)][(OH)_3]$ and $[Cu_{16}Y_{12}(Ph_3C\text{-}PO_3)_{12}(MeCO_2)_{22}(OH)_{24}(NO_3)_2(OH_2)_6][Me_4N]_3[OH]$.[1] The structures of $[Cu_{24}Dy_8(Ph_3C\text{-}PO_3)_6(Ph_3C\text{-}PO_3H)_6(MeCO_2)_{12}(MeCO_2H)_6(OH)_{42}(NO_3)(OH_2)_6][H_3O]$ and $[(Me_4N)_2K_2][Cu_{24}Gd_8(Ph_3C\text{-}PO_3)_6(Ph_3C\text{-}PO_3H)_6(MeCO_2)_{12}(MeCO_2H)_{12}(OH)_{42}(NO_3)][(OH)_3]$ are similar in the organisation of the metal ions, nevertheless the coordination modes of the carboxylates and phosphonates ligands are slightly different. $[H_3O]$ $[Cu_{24}Dy_8(Ph_3C\text{-}PO_3)_6(Ph_3C\text{-}PO_3H)_6(MeCO_2)_{12}(MeCO_2H)_6(OH)_{42}(NO_3)(OH_2)_6]$ crystallises in triclinic space group $P\bar{1}$, and contains eight Dy(III) ions at the vertices of a cube, there are twelve Cu(II) ions inside and twelve Cu(II) ions outside the cube

(Figure 2.8a). The twelve internal coppers are organised in the form of a cuboctahedron which are connected by one nitrate and twenty four hydroxide bonds. Each triangular face of the copper cuboctahedron is capped by Dy(III) ion to form a $DyCu_3$ tetrahedron with each Cu(II) ion being part of two such tetrahedra, a copper dimer is capping each square face of the Dy(III) ion, internally. Six of the Dy(III) ions are eight-coordinate and two are nine-coordinate, the Cu(II) ions of the cuboctahedron have almost tetragonally elongated octahedral geometry. Twelve phosphonates and eighteen acetate groups are surrounding the metal core of the cage, six phosphonates are dianionic, whereas the other six are monoanionic, the phosphonate ligands show [3.111] and [2.110] coordination modes. Twelve of the eighteen acetate units are anionic and the other six are neutral acids.

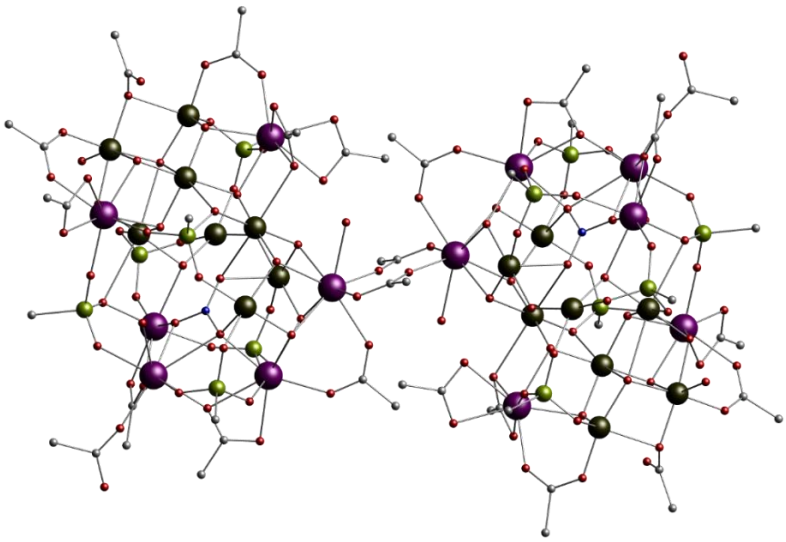

Figure 8.1: (a) View of the molecular structure of $[Cu_{16}Y_{12}(Ph_3C\text{-}PO_3)_{12}(MeCO_2)_{22}(OH)_{24}(NO_3)_2(OH_2)_6][Me_4N]_3[OH]$. Colour code: O, red; C, grey; Y, purple; Cu, olive green; P, lime; N, blue. All hydrogens and phenyl groups on phosphonates were omitted for clarity.

The cluster of $[Cu_{16}Y_{12}(Ph_3C\text{-}PO_3)_{12}(MeCO_2)_{22}(OH)_{24}(NO_3)_2(OH_2)_6][Me_4N]_3[OH]$ crystallises in monoclinic space group *C*2/*c*, the asymmetric unit involves eight Cu(II) and six Y(III) ions linked together by hydroxide and nitrate bridges (Figure 8.1). The Cu(II) atoms have square planar geometry, the Cu–O distances are in the range of 1.910(7) to 2.142(8) Å. One of the Y(III) ions is seven coordinate, whereas the others are eight coordinate, having square antiprismatic geometry, the Y-O bond distances are in the range of 2.227(7)-2.534(7) Å.

The complex of $[Ce_2Mn_6O_6(OH)_5(^tBuPO_3)_6(O_2CMe)_3]\bullet 53H_2O$, was produced by a reaction of $(NH_4)_2[Ce(NO_3)_6]$ with a stirred solution of $Mn(O_2CMe)_2\bullet 4H_2O$ and MeCOOH in MeOH, in the presence of ^{t}butylphosphonic acid.[2] The complex crystallises in a hexagonal space group $P6_3/m$, having an octametallic core of $[Ce(IV)_2Mn(IV)_6(\mu_3\text{-}O)_6(\mu_4\text{-}OH)_3(OH)_2]^{15+}$ with a C_{3h} point group symmetry, hence one sixth of the complex is in the asymmetric unit (Figure 8.2a). The Ce(IV) ion is ten coordinated by three μ_3-O, three phosphonate oxygen atoms, one OH and three μ_4–OH groups. The six Mn(IV) ions have same coordination environment, each of which is bonded to two μ_3-O, two phosphonate oxygen atoms, one acetate oxygen atom, and one μ_4–OH, creating an octahedral coordination geometry around each metal centre. The core of the complex can be described as including three symmetry-related distorted cubanes $\{Ce_2Mn_2O_2(OH)_2\}$ with a trigonal-bipyramidal unit $\{Ce_2(OH)_3\}$ in the centre, producing a triangular framework (Figures 8.2b and c). There are five hydroxide, three acetate and six $^tBuPO_3^{2-}$ ligands within the complex,

the three μ_2-bridging acetate groups are linking two Mn(IV) in a distorted cubane, whereas the three $^tBuPO_3^{2-}$ each bridging two Mn(IV) and one Ce(IV) showing 3.111 binding mode. The Ce–O bond lengths are in the range of 2.2784(17)–2.6400(17) Å.

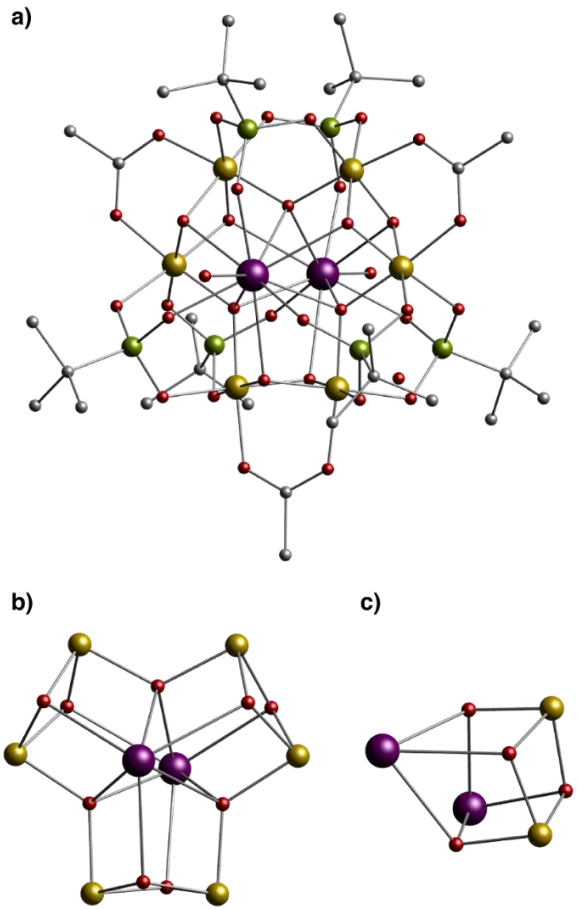

Figure 8.2: (a) The molecular structure of $[Ce_2Mn_6O_6(OH)_5(^tBuPO_3)_6(O_2CMe)_3]\cdot 53H_2O$; (b) polyhedron view of the metal core; (c) One of the three distorted cubanes in the complex. Colour code: O, red; C, grey; Ce, purple; Mn, gold; P, lime; N, blue. Hydrogens omitted for clarity.

Winpenny and co-workers used a solvothermal method to synthesise a series of molecular cages of $[Ni(II)_6Ln(III)_6(OH)_2(O_3PCH_2Ph)_6(O_2C^tBu)_{16}(MeCO_2H)_2]$-$(MeCN)_4$ (Ln=Gd , Dy, and Y).[3] The reaction was performed by mixing $[Ni_2(\mu$-$OH_2)(O_2C^tBu)_4]\bullet(HO_2C^tBu)_4$, $[Ln_2(O_2C^tBu)_6(HO_2C^tBu)_6]$ and $H_2O_3PCH_2Ph$ in

MeCN, the resulting slurry was stirred and transferred into a Teflon-lined autoclave, which was heated at 150 °C for 12 h and then cooled to room temperature at a rate of 0.05 °C min^{-1}. The compounds are isomorphous and crystallise in the monoclinic space group $P2_1/n$ (Figure 8.3a), Each structure features a centrosymmetric rugby-ball core (Figure 8.3b), the two ends of the rugby-ball are capped by a $\{Ni_3(\mu_3–OH)\}$ triangle, one acetate and two pivalate ligands bridging the edges of these triangles using 2.20 and 2.11 coordination modes, respectively. The existence of the acetate in the molecular structure is probably from the hydrolysis of the acetonitrile during solvothermal reaction. The oxygen atoms from three pivalates and three phosphonates are coordinated to the inner side of the Ni_3 triangles, the phosphonates show either 5.221 or 5.222 coordination modes, linking three neighbouring Gd(III) and two Ni(II) ions, whereas the pivalates linking one neighbouring Gd(III) and one Ni(II) ion adopt either 2.21 or 2.11 coordination modes. A Gd_3P_3 six-membered ring is produced by the alternating arrangement of the P and the Gd atoms, the Gd···Gd distances between the Gd_3P_3 six-membered ring are in the range of 3.9–4.9 Å, while those inside the Gd_3P_3 six-membered ring are around 6.2 Å.

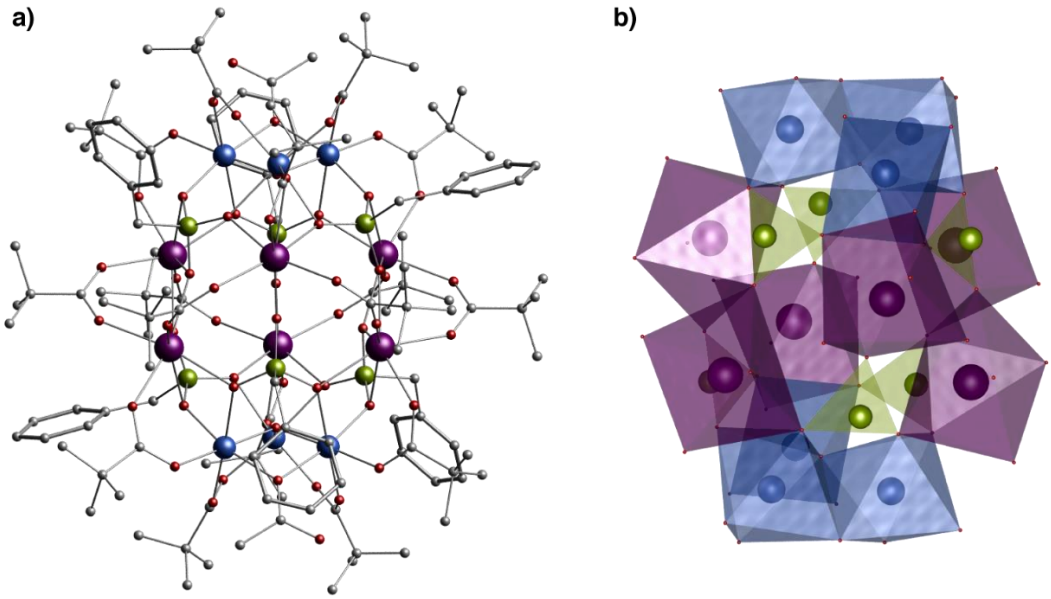

Figure 8.3: (a) The structure of $[Ni_6Gd_6(OH)_2(O_3PCH_2Ph)_6(O_2C^tBu)_{16}(MeCO_2H)_2](MeCN)_4$ in the crystal; (b) polyhedral view of the metal core. Colour code: O, red; C, grey; Gd, purple; Ni, light blue; P, lime. Hydrogens and solvent molecules were omitted for clarity.

Complexes $Co(II)_8Gd(III)_8(\mu_3{-}OH)_4(NO_3)_4(O_3P^tBu)_8(O_2C^tBu)_{16}$, $Co(II)_8$-$Gd(III)_4(O_3P^tBu)_6(O_2C^tBu)_{16}$ and $Co(II)_4Gd(III)_6(O_3PCH_2Ph)_6(O_2C^tBu)_{14}(MeCN)_2$, have been solvothermally synthesised from two precursors, $[Co(II)_2(\mu{-}OH_2)(O_2C^tBu)_4(HO_2C^tBu)_4]$ and $[Gd_2(O_2C^tBu)_6(HO_2C^tBu)_6]$.[4] All compounds crystallise in the monoclinic space group $C2_1/c$, the molecular structure of the compound $Co(II)_8Gd(III)_8(\mu_3{-}OH)_4(NO_3)_4(O_3P^tBu)_8(O_2C^tBu)_{16}$ possesses a C_2 axis and the structure is based on a square (Figure 8.4). There are four hexa-coordinate cobalt(II) ions (Co_4 square grid) in the centre of the molecule, which are bridged by four 2.210 nitrate ligands, the Co···Co distances within the Co_4 square grid are in the range of 4.26–4.33 Å. The phosphonate ligands that bridge between the inner Co_4 square grid and an external (Gd_8Co_4) frame display a 4.221 coordination mode, the four cobalt(II) ions of the external Gd_8Co_4 square are four-coordinate with

two oxygen atoms from two phosphonates, and the other two oxygen atoms from two pivalates. The Co···Gd distances in the outer Gd_8Co_4 square are in the range of 3.646–3.920 Å. A [$CoGd_2(\mu_3$–OH)] triangle is formed by bridging of four μ_3–OH groups with each vertex of the Co_4 square and two neighbouring Gd(III). The Gd···Gd distances are in the range of 3.58–3.81Å and the Co···Gd distances in this triangle are in the range of 3.48-3.53 Å.

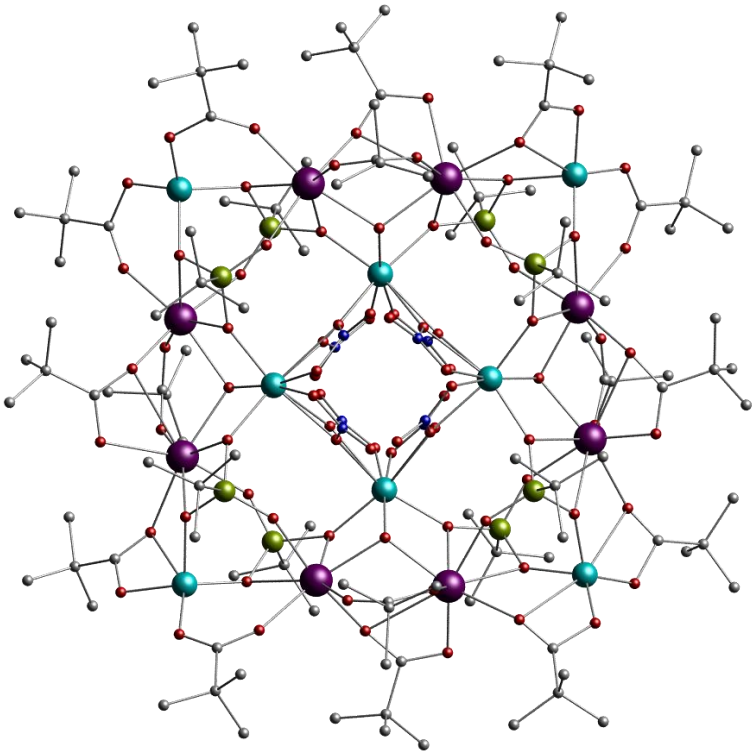

Figure 8.4: The structure of $Co_8Gd_8(\mu_3\text{–}OH)_4(NO_3)_4(O_3P^tBu)_8(O_2C^tBu)_{16}$. Colour code: O, red; C, grey; Gd, purple; Co, cyan; P, lime; N; blue. Hydrogens omitted for clarity.

The four lanthanide metal outer rows within the compound [$Co(II)_8Gd(III)_4(O_3P^tBu)_6(O_2C^tBu)_{16}$] are symmetry equivalent, and each contains two penta-coordinate terminal Co(II) ions which are linked to the two central Gd(III) ions by one oxygen from a 4.221 phosphonate, two 2.21 carboxylate and one

2.11 carboxylate, the two central Gd(III) ions are also liked by two 2.11 pivalates and an oxygen from a 4.222 phosphonate (Figure 8.5a). The central row of the grid comprises four tetra-coordinate Co(II) ions, and they are linked by phosphonates with coordination modes of 4.221 and 4.222. The three Co···Co distances within the central row are in the range of 4.322– 4.782 Å.

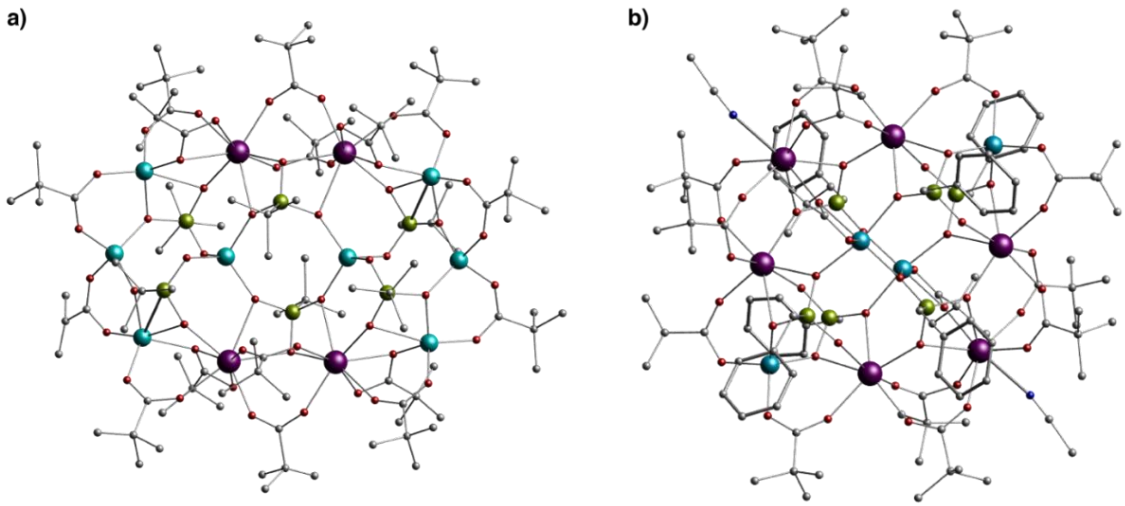

Figure 8.5: (a) and (b); The crystal structures of $Co_8Gd_4(O_3P^tBu)_6(O_2C^tBu)_{16}$ and $Co_4Gd_6(O_3PCH_2Ph)_6(O_2C^tBu)_{14}(MeCN)_2$, respectively. Colour code: O, red; C, grey; Gd, purple; Co, cyan; P, lime. Hydrogens omitted for clarity.

The compound $[Co(II)_4Gd(III)_6(O_3PCH_2Ph)_6(O_2C^tBu)_{14}(MeCN)_2]$ has a couple of octahedral Co(II) ions at the centre, surrounded by two tetrahedal Co(II) ions and six Gd(III) ions (Figure 8.5b). There is a central Co(II) dimer which is a part of a Co_2O_2 ring, with the oxygen atoms belonging to two 5.222 phosphonates, the Co···Co distance is 3.190(2) Å. Each Gd···Gd edge is linked by an oxygen from a 4.221 phosphonate and two 2.11 pivalates, with Gd···Gd distances of either 4.051 or 4.076 Å, the corner tetrahedral Co(II) ions are linked to the neighbouring Gd(III) ions by

one oxygen atom from a 4.221 phosphonate and one 2.11 pivalate, the Co···Gd distances of about 3.68 Å.

Solvothermal reaction of two precursors, namely $[Mn(II)(O_2C^tBu)4(EtOH)]_n$ and $[Ln_2(O_2C^tBu)_6(HO_2C^tBu)_6]$ (Ln = Gd and Dy) with phosphonic acid ligands resulted in formation of molecular cages $Mn(II)_9Gd(III)_9(O_3PMe)_{12}(O_2C^tBu)_{18}(\mu_3\text{-}OH)_{1.5}(O_2C^tBu)_{1.5}$, $[Mn(II)_4Gd(III)_6(O_3PCH_2Ph)_6(HO_2C^tBu)_{13}(O_2CMe)(HO_2C^tBu)(OH_2)_2(MeCN)_2]\bullet(MeCN)_3$ and $[Mn(II)_6Dy(III)_6(\mu_3\text{–}OH)_2(O_3PCH_2Ph)_6(O_2C^tBu)_{16}]\bullet(MeCN)_5$.[5] The complex of $Mn(II)_9Gd(III)_9(O_3PMe)_{12}(O_2C^tBu)_{18}(O_2C^tBu)_{18}(\mu_3\text{-}OH)_{1.5}(O_2C^tBu)_{1.5}$ involves the smallest organophosphonate (methylphosphonic acid). The complex crystallises in the hexagonal space group $R\bar{3}c$, and it has D_{3h} symmetry (Figure 8.6). Three Mn(II) sites lie in the trigonal plane of a trigonal bipyramid, with the remaining six Mn(II) ions forming two triangles close the apical locations, the nine sites produce a trigonal bipyramid that is truncated on the trigonal axis (Figures 8.6b and c). Three Gd(III) ions form a triangle that lies between the two Mn(II) triangles, whereas the rest of the Gd(III) ions lie on the nonequatorial edges of the trigonal bipyramid. Six 5.222 phosphonate ligands coordinate to two Mn(II) ions from a triangle, two Gd(III) ions from the central triangle, and one Gd(III) ion, on an edge. The remaining six phosphonates display the 4.221 mode, coordinating to a Gd(III) ion from the central triangle, a Mn(II) ion within the trigonal plane, and two Gd(III)

ions on the edges of the polyhedron. The Mn(II) ions in the structure are five-coordinate, and the Gd(III) ions are eight-coordinate.

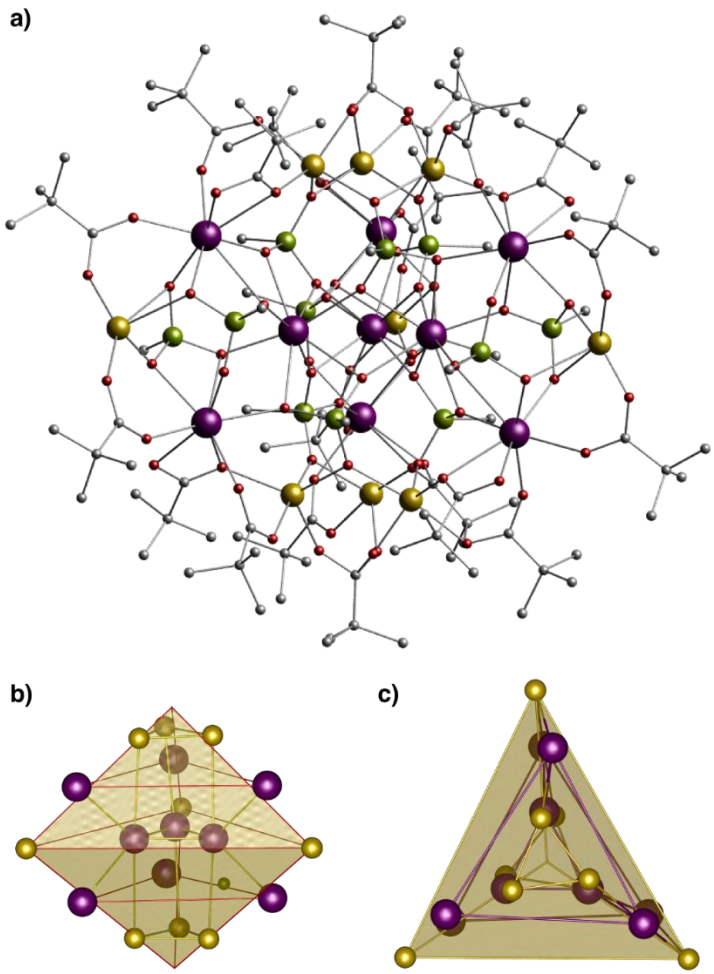

Figure 8.6: (a) The molecular structure of $Mn_9Gd_9(O_3PMe)_{12}(O_2C^tBu)_{18}(O_2C^tBu)_{18}(\mu_3\text{-}OH)_{1.5}(O_2C^tBu)_{1.5}$; (b) and (c) Side and top view of the trigonal bipyramid $\{Mn_9Gd_9\}$ core along the C_3 axis. Two-fold disordered central Gd and peripheral Mn are shown in just one position. Colour code: O, red; C, grey; Gd, purple; Mn, gold; P, lime. Hydrogens omitted for clarity.

Methylphosphonic acid was replaced with benzylphosphonic acid to synthesise the cage $[Mn(II)_4Gd(III)_6(O_3PCH_2Ph)_6(HO_2C^tBu)_{13}(O_2CMe)(HO_2C^tBu)(OH_2)_2\text{-}(MeCN)_2]\bullet(MeCN)_3$ (Figure 8.7a). The crystal structure features a distorted [3 × 3] $\{Mn_4Gd_6\}$ grid as its core, if a pair of manganese ions is considered as one node

(Figure 8.7b). The structure contains four Mn(II) and six Gd(III) metal ions, there are six phosphonate ligands, which coordinate in three diverse ways to the neighbouring metal ions. The first type of phosphonate ligand has the 5.322 coordination mode, sitting on the top part of the core binds three gadolinium and two manganese metals. Under this, three outward-facing 4.221 phosphonate ligands coordinate to the residual gadolinium and manganese metals, the other two 3.211 phosphonate ligands bind to two gadolinium and one manganese atoms and lie below the plane. The two isolated corner Mn(II) ions within the cage are five-coordinate with a geometry close to square pyramidal, while the two connected manganese dimers are six-coordinate with a Mn···Mn distance of 3.59 Å.

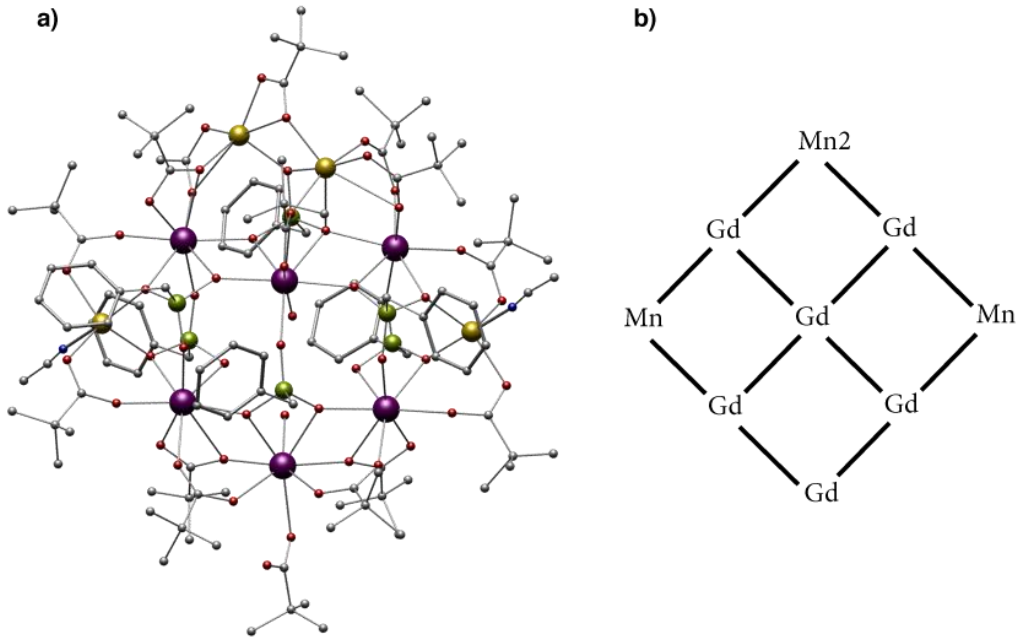

Figure 8.7: (a) The structure of $\{Mn_4Gd_6P_6\}$ cage; (b) The [3 × 3] $\{Mn_4Gd_6\}$ grid by taking the manganese dimer as a node. Colour code: O, red; C, grey; Gd, purple; Mn, gold; P, lime; N, blye. Hydrogens and solvent molecules were omitted for clarity.

Gadolinium is replaced by dysprosium to synthesise the cage of $[Mn(II)_6Dy(III)_6(\mu_3{-}OH)_2(O_3PCH_2Ph)_6(O_2C^tBu)_{16}]\bullet(MeCN)_5$ (Figure 8.8a). The compound crystallises in the monoclinic space group $C2_1/c$, the molecular structure contains, six phosphorus, six manganese, and six dysprosium atoms forming a hexagonal bipyramid, with a cap on each of the square faces of the polyhedron. The top hexagon consists of P-Mn-Dy-P-Mn-Dy, with each edge bridged by an oxygen. The bottom hexagon has the same composition, having a Mn under each Dy from the top hexagon, and a Dy under each Mn from the top (Figure 8.8b). There are two kinds of phosphonate ligands within the structure, the four phosphonates that form part of the hexagonal prism display the 4.211 coordination mode, whereas the two that form caps display the 6.222 coordination mode. All the Dy(III) ions are seven-coordinate, the two manganese ions of the upper hexagon are four-coordinate with oxygen atoms from either pivalates or phosphonates, though the remaining Mn(II) ions are six-coordinate, the nearest Dy···Mn distances are in the range of 3.47 to 3.93 Å.

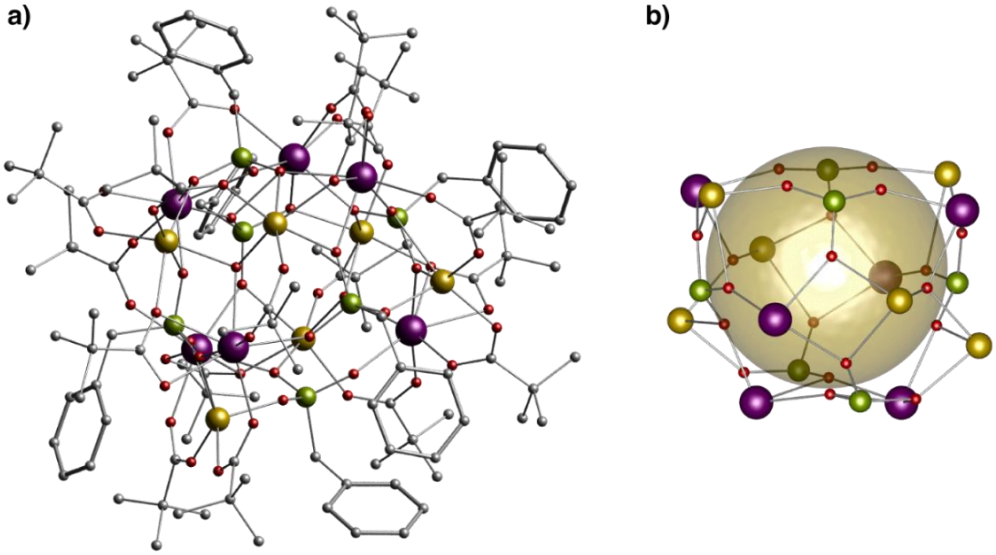

Figure 8.8: (a) The structure of $[Mn_6Dy_6(\mu_3{-}OH)_2(O_3PCH_2Ph)_6(O_2C^tBu)_{16}]\bullet(MeCN)_5$ within the crystal; (b) Side view of the truncated ball-shaped $\{Mn_6Dy_6\}$ metal core. The gold sphere is to show the space in the core. Colour code: O, red; C, grey; Dy, purple; Mn, gold; P, lime Hydrogens and solvent molecules were omitted for clarity.

By solvothermal reaction of dimetallic cobalt(II) pivalate $[Co(II)_2(\mu{-}OH_2)(O_2C^tBu)_4]\bullet(HO_2C^tBu)_4$ with a range of different lanthanide starting materials (either hydrated lanthanide nitrate salts or dimetallic pivalate complexes $Ln_2(O_2C^tBu)_6(HO_2C^tBu)_6$), Winpenny and co-workers synthesised a range of 3d–4f mixed metal complexes with six type of cores: $\{Co_8Ln_8\}$, $\{Co_8Ln_4\}$, $\{Co_4Ln_6\}$, $\{Co_6Ln_8\}$, $\{Co_6Ln_8\}$, $\{Co_4Ln_2\}$, and $\{Co_8Ln_2\}$.[6] The reactions were carried out with and without additional base, and with variation of the phosphonic acid used, through these variations, formed seven diverse structural types (See Figure 8.9). In the absence of base, the reaction of cobalt(II) pivalate with a lanthanide nitrate and ^{t}butylphosphonic acid gives the first family, $[Co(II)_8Ln(III)_8{-}(\mu_3{-}OH)_4(NO_3)_4(O_3P^tBu)_8(O_2C^tBu)_{16}]$ (Ln = Gd, Tb, Dy, Ho, Er, Yb, and Y) (Figure 8.9a). The complex of $[Co(II)_4Gd(III)_2(O_3P^tBu)_2(O_2C^tBu)_{10}(MeCN)_2](MeCN)_2$ was

isolated by allowing the clear solution obtained from the autoclave to stand at room temperature. If a base (such as, KOH, NaOMe, NaOEt, and Et_3N) is added to the reaction, a second family of complexes produces: $[Co(II)_6Ln(III)_8(\mu_3{-}OH)_8(O_3P^tBu)_6(O_2C^tBu)_{16}(H_2O)_2(MeCN)_x](MeCN)_y$ (for x = 0 and y = 2, Ln = Gd, Tb, Dy, and Ho; for x = 2 and y = 1, Ln = Er, Yb, and Y). This reaction take place in a range of bases and in acetonitrile, dimethylformamide, and toluene. Crystalline material from this reaction when using lighter lanthanides were not isolated, which suggests the size of the lanthanide ions is important in affecting the reaction pathway. If $Gd_2(O_2C^tBu)_6(HO_2C^tBu)_6$ is used instead of the $Gd(NO_3)_3{\bullet}nH_2O$ salts in the same reaction that gives first family of complexes, $[Co(II)_8Gd(III)_4(O_3P^tBu)_6(O_2C^tBu)_{16}]$ can be synthesised. However, this reaction does not work for heavier lanthanides. Under the same conditions, if benzylphosphonic acid is used instead of ^{t}butylphosphonic acid, a third family of complexes can be synthesised: $[Co(II)_4Ln(III)_6(O_3PCH_2Ph)_6(O_2C^tBu)_{14}(HO_2C^tBu)_x(MeCN)_y(H_2O)_z]$ (for x = z = 0 and y = 2, Ln = Gd and Tb; for x = 1, y = 1, and z = 2, Ln = Dy and Y) (Figure 8.9c). If $Nd_2(O_2C^tBu)_6(HO_2C^tBu)_6$ is used, crystals were not isolated directly from the autoclave, but crystals grow in the solutions formed in the autoclave after a few weeks. The complexes $[Co(II)_8Nd(III)_2(\mu_3{-}OH)_2(O_3PCH_2Ph)_4(O_2C^tBu)_{12}$-$(HO_2CMe)_2](MeCN)_6$, and the gadolinium analogue of $[Co(II)_8Gd(III)_2(\mu_3{-}OH)_2(O_3PCH_2Ph)_4(O_2C^tBu)_{12}(HO_2CMe)_2](MeCN)_6$ can also be synthesised by this method.

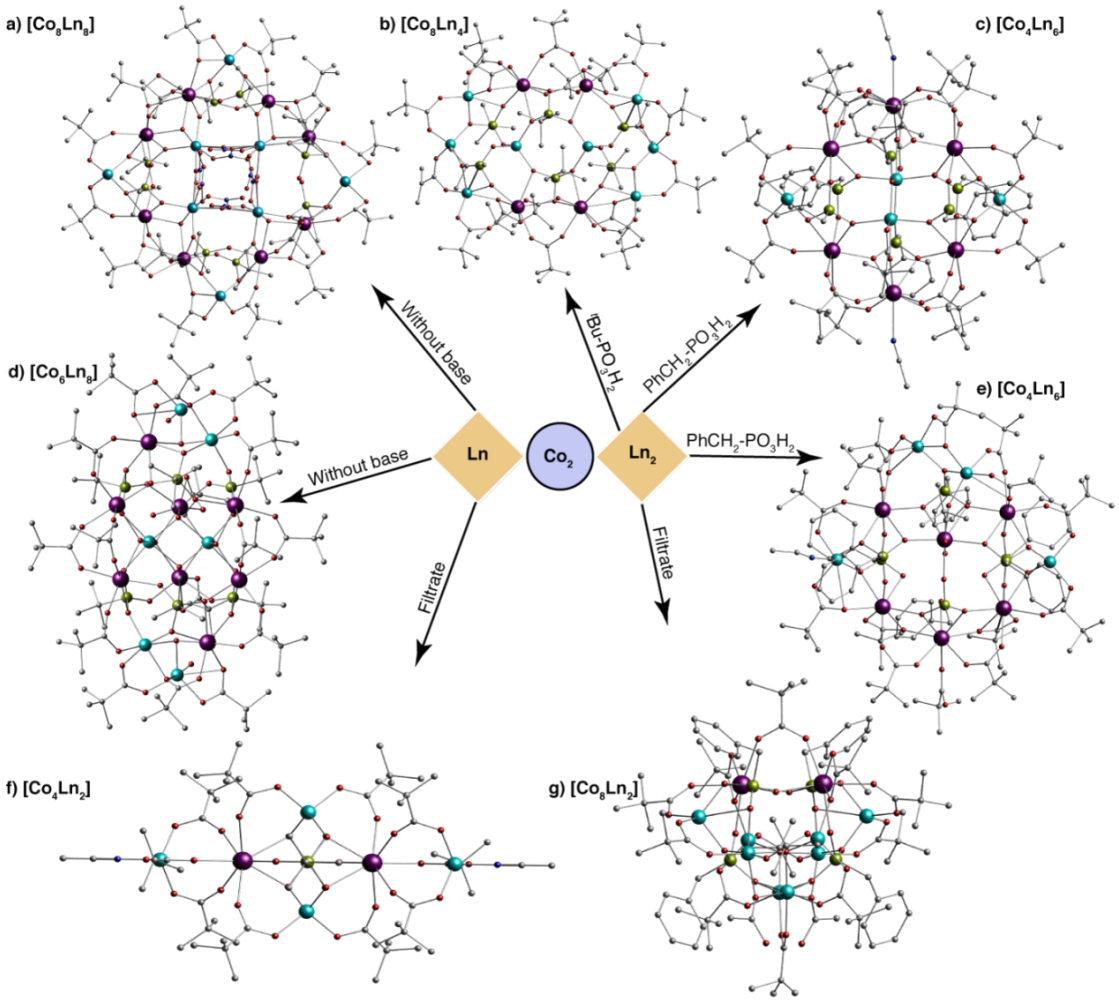

Figure 8.9: Synthetic procedures and produced structures. Colour code: O, red; C, grey; Ln, purple; Co, cyan; P, lime; N, blue. Hydrogens omitted for clarity. Co_2 = $[Co(II)_2(\mu\text{-}OH_2)(O_2C^tBu)_4]\bullet(HO_2C^tBu)_4$; Ln = $Ln(NO_3)_3\bullet nH_2O$; Ln_2 = $[Ln_2(O_2C^tBu)_6(HO_2C^tBu)_6$. Based on reference [6].

The core of family $\{Co_8Ln_8\}$ contains a central nitrate-bridged $[Co_4]$ square (Figure 8.9a), which is linked to an outer $[Ln_8]$ ring by oxygen atoms from either hydroxide or phosphonate ligands. There are also four tetrahedral cobalt(II) metal ions at the corners of the outer square. The $\{Co_8Ln_4\}$ family contains four tetra-coordinate cobalt(II) ions with tetrahedral coordination geometries, while the four Co(II) ions in the outer rows of the grid are five-coordinate with a geometry near to trigonal-bipyramidal (Figure 8.9b), the Co···Gd distances is (4.0 Å) greater than the Co···Co

distance (3.3 Å). The core structure of family {Co_4Ln_6} displays the effect of the phosphonate ligands (Figure 8.9b); as compared to the ^{t}butyl substitute used in families {Co_8Ln_8} and {Co_8Ln_4}, the less bulky benzyl group permits the phosphonate ligand to coordinate to more metal ions, when the lanthanides are Gd(III) or Tb(III), the core consists of a central cobalt(II) dimer that is surrounded by other metal centres due to the bridging phosphonate. Complex {Co_4Dy_6} (Figure 8.9e) is less symmetrical than {Co_4Tb_6}, there is also a change of space group from $P2_1/n$ to $P\bar{1}$, the coordination geometries of the cobalt(II) ions vary between the two structures. In {Co_4Tb_6}, two Co sites have tetrahedral geometries and two octahedral, while in {Co_4Dy_6} only one cobalt site is tetrahedral and the other three are five-coordinate with square-pyramidal geometries. The metal–metal distances differ between the structures, for example, in the complex of {Co_4Tb_6}, average distances are Tb···Tb 4.09 Å, Co···Tb 3.85 Å, with the Co···Co distance in the dimetallic unit 3.18 Å, while in {Co_4Dy_6}, average contacts are Dy···Dy 3.92 Å, Co···Dy 3.72 Å, and the short Co···Co distance 3.34 Å. In each of {Co_4Gd_6} and {Co_4Tb_6} the phosphonates display the 4.221 and 5.222 coordination mode, while in {Co_4Dy_6} a single example of the 3.211 mode is also found. The core of the {Co_4Ln_2} family has two cobalt and lanthanide ions at alternate corners of a rhombus (Figure 8.9f), the Co···Ln edges of the rhombus are 3.74 Å. The metal ions are bridged by two 4.221 phosphonates at the centre and four 2.11 pivalates on the edges, an additional outer cobalt site is bound to each lanthanide ion by three 2.11 bridging pivalates, with a Co···Ln contact of 3.92 Å, the four cobalt(II) ions within the complex with a tetrahedral geometry.

If base is added to the synthesis that yields the first family $\{Co_8Ln_8\}$, a new family of cages $\{Co_6Ln_8\}$ can be synthesised (Figure 8.9d). The structure of this family contains eight μ_3–OH that bridge between the six Co(II) and eight Ln(III) ions at the core of the complexes. At the centre is a $[Co(II)_2Ln(III)_2(\mu_3\text{–}OH)_4]^{6+}$ cubane, this cubane is linked to one side of a $\{Co_2Ln_6O_8\}$ ring, via four 4.221 phosphonates and two μ_3–OH. There are two auxiliary 4.221 phosphonates coordinated to the under-side of this ring, furthermore, there are two Co(II) ions coordinated to the $\{Co_2Ln_6O_8\}$ ring through μ_3–OH. All of the Co(II) ions are five-coordinate with a geometry close to trigonal bipyramidal with the fifth coordination site occupied by a solvent molecule. The average nearest Ln···Ln, Co···Ln and Co···Co distances within the structure are about 3.90, 3.50, and 3.20 Å, correspondingly.

The core of the $\{Co_8Ln_2\}$ complexes contains eight Co(II) and two Ln(III) ions that are bridged by four 4.221 phosphonate ligands (Figure 8.9g). At the centre is a Ln_2O_2 rhombus formed by two lanthanide ions that are bridged by a μ–oxygen from a phosphonate ligand. The two phosphonates involved each bridge to two Co(II) ions, in each case, one of these Co(II) ions produces part of a $[Co_3(\mu_3\text{–}OH)]$ triangle, with these two triangles within the structure linked through two μ–oxygens from an auxiliary phosphonate. In each triangle, two of the Co(II) ions have an octahedral geometry, whereas the third is tetrahedral. In each case, the second Co(II) ion coordinated to the central phosphonates has a tetrahedral coordination geometry.

The average nearest Ln···Ln, Co···Ln, and Co···Co distances are about 3.99, 3.72, and 3.23 Å, correspondingly.

In Chapter 3 it was shown many functionalised phosphonates have been involved in 4f–phosphonate complexes. To the best of our knowledge, there are only two reports on mixed 3d–4f cages utilising an amino-functionalised phosphonate. Cages of $[Co_4Ln_{10}(O_2C^tBu)_{12}(O_3PC_6H_{10}NH_2)_8(PO_4)_2(O_2CMe)_2(O_3PC_6H_{10}NH_3)_2]$ (Ln = Gd and Dy) were synthesised by the reaction of $(1\text{-}NH_2\text{-}1\text{-}C_6H_{10})PO_3H_2$ with $[Co_2(\mu\text{-}OH_2)(O_2C^tBu)_4(HO_2C^tBu)_4]$ and $[Ln_2(O_2C^tBu)_6(HO_2C^tBu)_6]$, (Ln = Gd or Dy) with Et_3N such as base, in MeCN under solvothermal conditions.[7] Both cages have the same molecular structures, and crystallise in the triclinic space group $P\bar{1}$. The $\{Ln_{10}P_{12}\}$ (Figure 8.10a) core can be best described as based on two centred 12-vertex polyhedra sharing a face, the polyhedra are distorted, but can be derived from an icosahedron, with the distortion increasing towards the shared face (Figure 8.10b).

There are four Co(II) ions capping the $\{Ln_{10}P_{12}\}$ core, eight aminophosphonates coordinated to three Ln(III) ions, each O-arm coordinating a single Dy(III) ion, with the amino-group coordinating to a Co(II) ion using a 4.2111 binding mode. Therefore, each cobalt ion is N,O-chelated by two aminophosphonates, with a last coordination site being taken by a carboxylate giving a distorted *cis*-N_2O_3 geometry at Co(II) ion. All Ln(III) ions are exclusively O-bound, with either capped octahedral or dodecahedral geometry. Thus, the N-donor is only found bound to Co(II) not

Ln(III). The remaining two aminophosphonates, which form part of the shared face of the $\{Ln_{10}P_{12}\}$ core. Obviously, neither the phosphate nor the acetates in the structures were present in the reaction starting materials, therefore probably they result from hydrolysis of phosphonate and acetonitrile under the solvothermal reaction conditions.

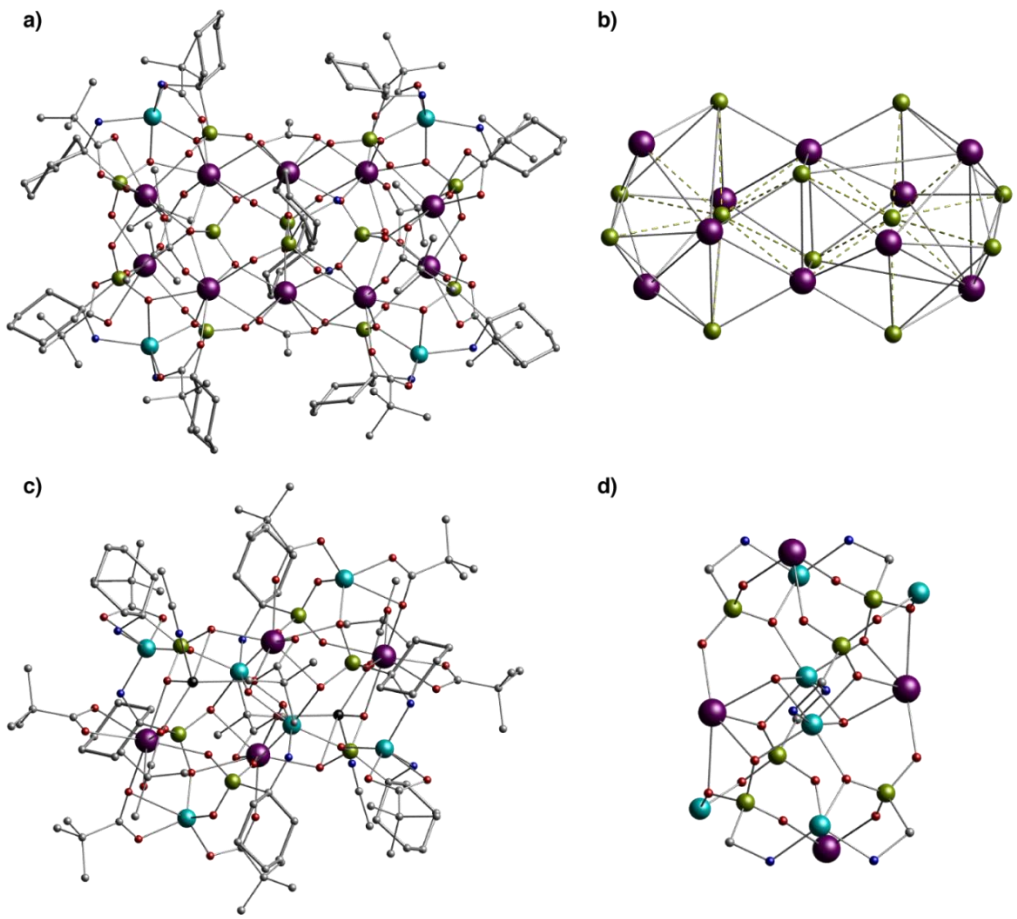

Figure 8.10: (a) Crystal structure of $\{Co_4Dy_{10}P_{12}\}$ cluster; (b) 12-Vertex polyhedral sharing a face $\{Dy_{10}P_{12}\}$ core; (c) Crystal structure of $\{Co_6Gd_4P_6\}$ cluster; (d) Phosphonate coordination modes in $\{Co_6Gd_4P_6\}$. Colour codes: O, red; C, grey; Ln, purple; Co, cyan; Na, black; P, lime Hydrogens omitted for clarity.

If Na_3PO_4 is added to the synthesis that yields the previous $\{Co_4Ln_{10}P_{12}\}$ cages, a new molecular cage of $[Na_2Co_6Ln_4(\mu_3\text{-}OH)_2(O_2C^tBu)_{12}(O_3PC_6H_{10}NH_2)_6(MeCN)_2]$ (Ln =

Gd and Dy) (Figure 8.10c) is formed. These complexes do not contain phosphate, but do include Na ions and a less regular structure results. The compounds are isostructural and crystallise in the monoclinic space group $P2_1/n$, these inversion-symmetric $\{Ln_4Co_6P_6Na_2\}$ clusters comprise accordingly more Co(II) ion than the previous $\{Co_4Ln_{10}P_{12}\}$ cages, and with three different geometric environments (tetrahedral, distorted five-coordinate, and octahedral). Two Co(II) ions with octahedral geometry sit at the centre of the cluster, bridged by two μ_3-OH which additionally bridge to a Ln(III) ion. Three amino-phosphonates bridge this butterfly-like core, on either side, to an extra two Co(II) ions, a Ln(III) and a Na ion. One Co(II) ion has a distorted $\{N_2O_3\}$ coordination sphere, comprising one N,O-chelating amino-phosphonate and one N-bound, the remaining Co(II) ions have tetrahedral geometry from two phosphonates and two carboxylates(Figure 8.10d). The amino-phosphonates adopt three diverse coordination modes; 5.2221, 4.2111 and 5.2211.

Five clusters with the general formula $[Ni_6Gd_6(\mu_3{-}OH)_2(\mu_2{-}OAc)_2(O_3PR)_6(O_2C^tBu)_{16}]$, where R = methyl, *n*-hexyl, *n*-octyl, phenyl or benzyl (Figure 8.11 a–e respectively), were prepared by solvothermal reaction of $[Ni_2(\mu_2{-}OH_2)(O_2C^tBu)_4(HO_2C^tBu)_4]$ with $[Gd_2(O_2C^tBu)_6(HO_2C^tBu)_6]$ and RPO_3H_2 (R = methyl, *n*-octyl, *n*-hexyl, phenyl and benzyl) in acetonitrile (MeCN).[8] All of the clusters have a $\{Ni_6Gd_6P_6\}$ core that can be related to the cages reported earlier by Winpenny *et al.*[3] The cages crystallise in either the triclinic $P\bar{1}$ or monoclinic $P2_1/n$ space group. However, there is little difference between the

molecular structures, the cage can be described as a rugby ball (Figure 8.11). An isosceles $\{Ni_3(\mu_3–OH)\}$ triangle caps the two ends of the rugby ball, the μ_3–OH group is displaced about 0.47(2)–0.49(2) Å out of the $\{Ni_3\}$ plane. Two of triangle edges are coordinated by a 2.11 pivalate and one arm of a 5.222 phosphonate ligand, additionally, coordinating to three Ln(III) ions. While, the third edge is coordinated by a 2.20 acetate and a 5.221 phosphonate. The acetates in the structures did not exist in the reaction starting materials, most probably, acetate was produced from hydrolysis of MeCN under solvothermal conditions. The bridging between the Ni(II) and Ln(III) ions is completed by three pivalates using either the 2.11 or the 2.21 binding modes. A $\{Ln_3P_3\}$ six-membered ring forms by the alternating arrangement of the Ln and P atoms, the Ln···Ln distances within the $\{Ln_3P_3\}$ six-membered rings in fall the range 5.90(2)-6.57(3) Å.

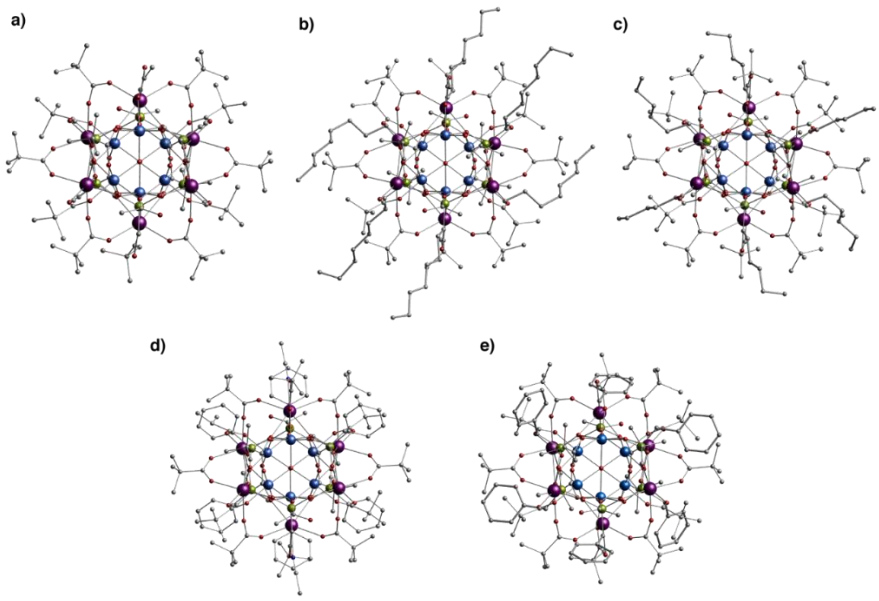

Figure 8.11: (a–e) Crystal structures of $[Ni_6Gd_6(\mu_3–OH)_2(\mu_2–OAc)_2(O_3PR)_6(O_2C^tBu)_{16}]$; where R = methyl, *n*-octyl, *n*-hexyl, phenyl or benzyl, respectively. Colour codes: O, red; C, grey; Gd, purple; Ni, light blue; P, lime. Hydrogens omitted for clarity.

Solvothermal reaction of $[Fe_3(\mu_3{-}O)(O_2C^tBu)_6(HO_2C^tBu)_3](O_2C^tBu)$ and $[Ln_2(O_2C^tBu)_6(HO_2C^tBu)_6]$ with phosphonic acids yielded a family of $\{Fe_6Ln_6P_6\}$ clusters with general formula $[Fe_6Gd_6(\mu_3{-}O)_2(CO_3)(O_3PR)_6(O_2C^tBu)_{18}]$, where R = methyl, phenyl, or *n*-hexyl.[9] All the clusters have an analogous metal frame to the previously discussed $\{Ni_6Ln_6P_6\}$ cages, and they have similar structures, the cages crystallise in either the trigonal $R\bar{3}c$ or monoclinic $P2_1/n$ space group.

The clusters core consists of six Fe(III) and six Ln(III) ions, bound by six phosphonates, eighteen pivalates, and two oxides, the structure is layered, with two $\{Fe_3\}$ triangles capping two central Ln(III) layers, the total giving a rugby ball-like shape (See Figure 8.12). The six Ln(III) ions can be described as forming a ring in a chair conformation, the two equilateral $\{Fe_3(\mu_3{-}O)\}$ triangles are oxo-centred with the $\mu_3{-}O^{2-}$ in the $\{Fe_3\}$ plane. The $\{Fe_3\}$ triangles sit eclipsed over the adjacent $\{Ln_3\}$ triangle. Each Fe···Fe is bridged by one 2.11 pivalate and by two arms of a phosphonate. The 5.222 phosphonates further coordinating to two Ln(III) ions in the neighbouring $\{Ln_3\}$ layer and one in the other $\{Ln_3\}$ layer. The Gd(III) and Fe(III) ions are further bridged by 2.11 pivalates, as are the two $\{Gd_3\}$ layers. A 6.222 carbonate ion is found in the middle of the cage, coordinating to all the Ln(III) ions, this may arise from atmospheric CO_2 fixation.

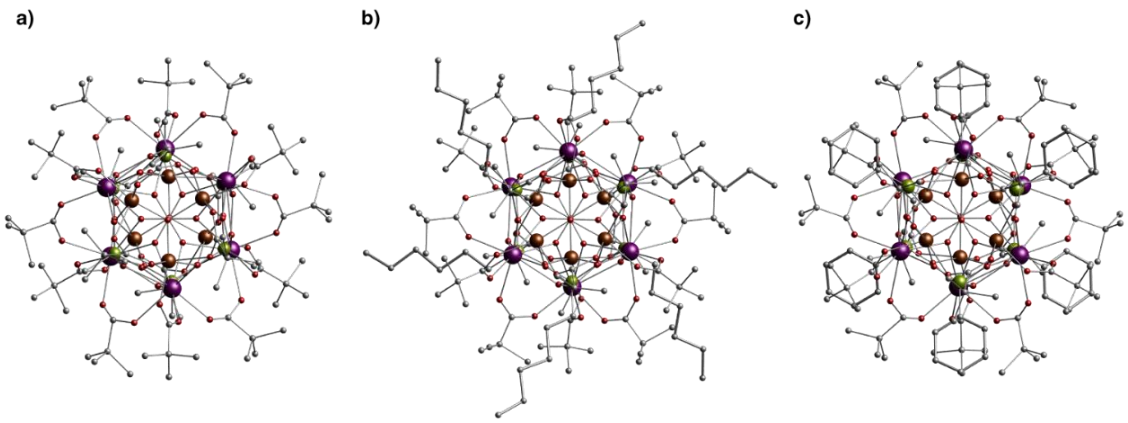

Figure 8.12: (a–c) Crystal structures of $[Fe_6Gd_6(\mu_3\text{–}O)_2(CO_3)(O_3PR)_6(O_2C^tBu)_{18}]$; where R = methyl, *n*-hexyl or phenyl, respectively. $\{Fe_6Gd_6P_6\}$ viewed down the C_3 axis. Colour codes: O, red; C, grey; Gd, purple; Fe, brown; P, lime. Hydrogens omitted for clarity.

The $\{Fe_3\}$ triangles in $\{Fe_6Ln_6P_6\}$ include μ_3–O rather than μ_3–OH as in the equivalent $\{Ni_3\}$ triangles, most likely carrying through from the $\{Fe_3O\}$ starting material. As a result, the $\{Fe_3O\}$ moieties are planar, while in $\{Ni_3(OH)\}$ the hydroxide is displaced about 0.5 Å from the $\{Ni_3\}$ plane toward the centre of the cage (Figure 8.13a and b). The $\{Ni_3\}$ triangles within the $\{Ni_6Ln_6P_6\}$ core have two edges with 2.11 carboxylate bridges, the third edge has instead a 2.20 bridging carboxylic acid, this makes the $\{Ni_3\}$ triangle isosceles, with the single edge shorter than the other two (Ni···Ni) distances. In the $\{Fe_6Ln_6P_6\}$ all the carboxylates are with 2.11 coordination mode, and the $\{Fe_3\}$ triangle is equilateral. The Ln(III) sites in the $\{Ni_6Ln_6P_6\}$ cages are seven-coordinate, with a capped octahedral geometry, whereas in $\{Fe_6Ln_6P_6\}$ the Ln(III) sites are eight-coordinate with a dodecahedral coordination geometry.

The phosphonate ligands in the compounds $\{Fe_6Ln_6P_6\}$ have the 5.222 coordination mode, while the phosphonate ligands in the compounds $\{Ni_6Ln_6P_6\}$ have either 5.222

or 5.221 coordination modes. Gd···Gd distances in the $\{Fe_6Gd_6P_6\}$ compound are 3.931(2) Å, in the $\{Ni_6Gd_6P_6\}$ compound the Gd···Gd edges of 3.889(1) Å. The nearest adjacent Fe···Ln distances are a little longer than Ni···Ln, for example; 3.677(3) Å in $\{Fe_6Gd_6P_6\}$ and 3.360(2)–3.509(2) Å in the equivalent $\{Ni_6Gd_6P_6\}$ compound.

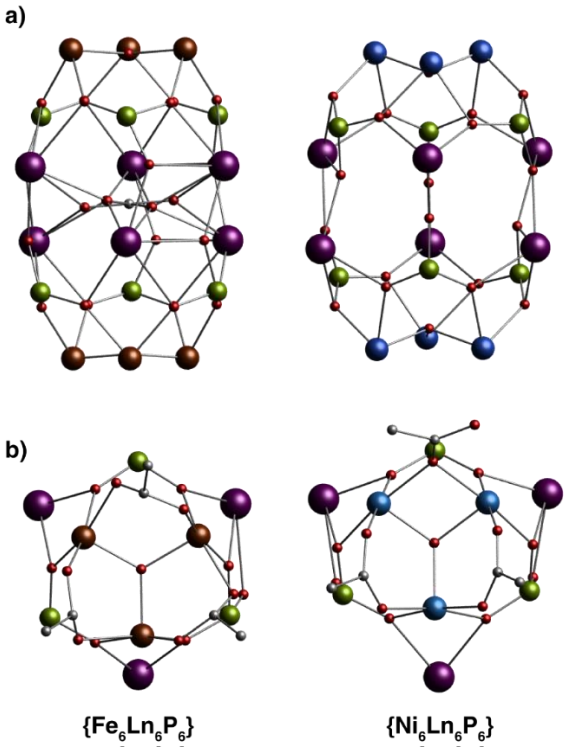

Figure 8.13: Viewing comparison of $\{Ni_6Ln_6P_6\}$ and $\{Fe_6Ln_6P_6\}$. (a) Metal and phosphonate core of $\{Fe_6Ln_6P_6\}$ (left) and $\{Ni_6Ln_6P_6\}$ (right), showing $\{Fe_3(\mu_3–O)\}$ and $\{Ni_3(\mu_3–O)\}$ fragments; (c) View of environment of the iron and nickel triangles in the clusters, $\{Fe_6Ln_6P_6\}$ and $\{Ni_6Ln_6P_6\}$. Colour code: O, red; C, grey; Ln, purple; Fe, brown; Ni, light blue; P, lime. Hydrogens omitted for clarity.

Recently, Winpenny and co-workers reported the clusters, with general formula $[Cu(MeCN)_4][Cu_3Ln_9(\mu_3\text{-}OH)_7(O_3P^tBu)_6(O_2C^tBu)_{15}]$ and $[Cu_6Ln_6(\mu_3–OH)_6\text{-}(O_3PC(NH_2)Me_2)_6(O_2C^tBu)_{12}]$ (Ln = Gd(III), Tb(III), Dy(III) or Ho(III)).[10] They have used two phosphonate sources, which led to high nuclearity discrete cages. First,

reaction of *tert*–butylphosphonic acid with a preformed copper pivalate dimer and $Ln(NO_3)_3{\cdot}nH_2O$ produced $\{Cu_3Ln_9P_6\}$ compounds. Second, a functionalised phosphonate, (1-amino-1-methylethyl)phosphonic acid was reacted with a preformed copper pivalate dimer and $[Ln_2(O_2C^tBu)_6(HO_2C^tBu)_6]$ giving $\{Cu_6Ln_6P_6\}$ cages.

Single crystal X-ray diffraction of $[Cu(MeCN)_4]$-$[Cu_3Ln_9(\mu_3{-}OH)_7(O_3P^tBu)_6(O_2C^tBu)_{15}]$ show that the clusters crystallise as anions with $[Cu(MeCN)_4]^+$ cations in the space group *R*3 and have an overall C_3v symmetry (Figure 8.14a). The presence of $[Cu(MeCN)_4]^+$ must be the reduction product of $[Cu_2(O_2C^tBu)_4(HO_2C^tBu)_2]$ in the precence of free carboxylic acid.[11] Three Ln atoms form a triangle inside a $\{Cu_3Ln_6\}$ ring, a Cu(II) is found between each two Ln(III) ions, the nine Ln(III) sites have dodecahedral geometries, while three Cu(II) sites have five coordinate square pyramidal geometries. The metal ions in the anionic cage are sandwiched between two phosphonate triangles. One of the triangles is composed of phosphonates with a bridging mode 4.221 while the other has a 4.222 mode (Figure 8.14b), each copper metal ion is bridged by two hydroxides to two neighbouring Ln(III) and one Ln(III) of the inner triangle.

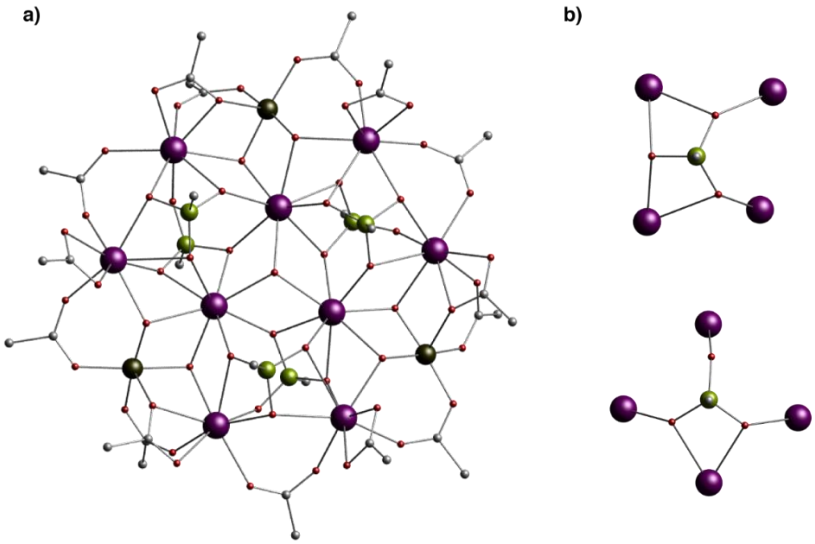

Figure 8.14: (a) Structure of $[Cu(MeCN)_4][Cu_3Ln_9(\mu_3\text{-}OH)_7(O_3P^tBu)_6(O_2C^tBu)_{15}]$ along the C_3 axis; (b) binding modes of phosphonates. Colour code: O, red; C, grey; Ln, purple; Cu, olive green; P, lime. ^{t}Bu groups on phosphonates and carboxylates and hydrogens were omitted for clarity.

$[Cu_6Ln_6(\mu_3\text{–}OH)_6(O_3PC(NH_2)Me_2)_6(O_2C^tBu)_{12}]$ clusters crystallise in the space group *Fddd* and have an overall D_{3h} symmetry (Figure 8.15a). The $\{Ln_6P_6\}$ core resembles the double-six-ring building block unit found in zeolites,[12] the structure featuring a cylindrical drum with a hexagonal prism form, whose bottom and top faces are made up of 12-membered $\{Ln_3O_6P_3\}$ rings. The central hexagonal prism of Ln_6P_6 centres are linked by phosphonate oxygens; The Ln_3P_3 faces are staggered so that the Ln site of one face sits above the P site of the other (Figure 8.15b). The amino group is terminally bound to Cu(II), whereas one O–donor bridges between a Ln(III) and a Cu(II) ions. Two μ_3–OH link the top and bottom face of the cluster with two Cu(II) ions and a Ln(III) ion. All aminophosphonates within the clusters display a 4.2111 binding mode (Figure 8.15c).

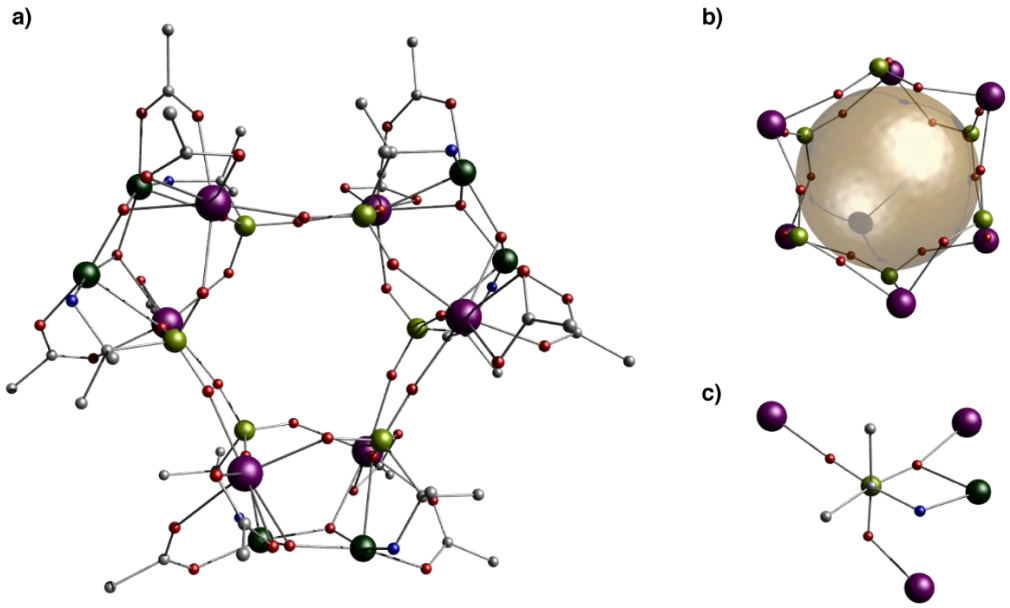

Figure 8.15: (a) Structure of $[Cu_6Ln_6(\mu_3\text{–}OH)_6(O_3PC(NH_2)Me_2)_6(O_2C^tBu)_{12}]$ along the C_3 axis; (b) 4f-phosphonate metal core of the structure, the brown dummy atom in the middle is to fill space; (c) phosphonate binding mode within the cage. Colour code: O, red; C, grey; Ln, purple; Cu, olive green; P, lime. ^{t}Bu groups on phosphonates and carboxylates and hydrogens were omitted for clarity.

8.2 Magnetic studies of 3d–4f phosphonate cages

Since initial work by Benelli and Gatteschi it has been known that the coupling of 3d-metal ions with Gd(III) tends to be weakly ferromagnetic.[13] Hence, if lanthanide metal ions can be inserted between transition ions the ideal weak magnetic interactions should be achieved to produce high spin molecules. Karotsis and co-workers, synthesised a $[Mn(III)_4Ln(III)_4(OH)_4(C4)_4(NO_3)_2(DMF)_6(H_2O)_6](OH)_2$ (where C4 = calix[4]arene) cage that shows MCE larger than any previous 3d metal clusters.[14]

Phosphonates are a new family of ligands in constructing 3d–4f mixed-metal complexes, most of molecular 3d–4f phosphonates have been synthesised in order to study their magnetic properties.[15] These works followed from initial studies for example, the zero dimensional cluster $[Ce(IV)_2Mn(IV)_6O_6(OH)_5(O_3P^tBu)_6(O_2CMe)_3]\bullet 53H_2O$, which was studied for their SMM behaviour.[2] Baskar and co-workers also prepared a series of compounds using the bulky trityl-phosphonic acid ligand, the cage $[H_3O][Cu_{24}Dy_8(Ph_3C\text{-}PO_3)_6(Ph_3C\text{-}PO_3H)_6(MeCO_2)_{12}(MeCO_2H)_6(OH)_{42}(NO_3)(OH_2)_6]$ shows SMM behaviour with an effective energy barrier for the reorientation of the magnetisation of $U_{eff} \approx 4.6$ K and $\tau_0 = 2.1 \times 10^{-8}$ s.[3] These are the only reports of 3d–4f phosphonates that show slow relaxation of magnetisation.

Formula	ΔS_{max} (J kg^{-1} K^{-1}) obs.	ΔS_{max} (J kg^{-1} K^{-1}) calcd.	T_{max} (K)	Ref.
$[Ni_6Gd_6(OH)_2(O_3PCH_2Ph)_6(O_2C^tBu)_{16}(MeCO_2H)_2](MeCN)_4$	26.5	37.4	3	3
$[Ni_6Dy_6(OH)_2(O_3PCH_2Ph)_6(O_2C^tBu)_{16}(MeCO_2H)_2](MeCN)_4$	12.2	33.7	3	3
$[Ni_6Y_6(OH)_2(O_3PCH_2Ph)_6(O_2C^tBu)_{16}(MeCO_2H)_2](MeCN)_4$	5.6	14.3	3	3
$Co_8Gd_8(\mu_3{-}OH)_4(NO_3)_4(O_3P^tBu)_8(O_2C^tBu)_{16}$	20.4	48.3	4	4
$Co_8Gd_4(O_3P^tBu)_6(O_2C^tBu)_{16}$	19.9	30.7	4	4
$Co_4Gd_6(O_3PCH_2Ph)_6(O_2C^tBu)_{14}(MeCN)_2$	22.3	40.5	4	4
$Mn_9Gd_9(O_3PMe)_{12}(O_2C^tBu)_{18}(\mu_3{-}OH)_{1.5}(O_2C^tBu)_{1.5}$	28	57.0	3	5
$[Mn_4Gd_6(O_3PCH_2Ph)_6(HO_2C^tBu)_{13}(O_2CMe)(HO_2C^tBu)(OH_2)_2(MeCN)_2](MeCN)_3$	33.7	41.8	3	5
$[Mn_6Dy_6(\mu_3{-}OH)_2(O_3PCH_2Ph)_6(O_2C^tBu)_{16}](MeCN)_5$	13	42.5	3	5
$[Co_6Gd_8(\mu_3{-}OH)_8(O_3P^tBu)_6(O_2C^tBu)_{16}(H_2O)_2](MeCN)_2$	28.6	47.6	3	6
$[Co_8Gd_2(\mu_3{-}OH)_2(O_3PCH_2Ph)_4(O_2CtBu)_{12}(HO_2CMe)_2]$	11.8	40.4	3	6
$[Co_4Gd_2(O_3P^tBu)_2(O_2C^tBu)_{10}(MeCN)_2](MeCN)_2]$	20	40.5	3	6
$[Co_4Gd_{10}(O_2C^tBu)_{12}(O_3PC_6H_{10}NH_2)_8(PO_4)_2(O_2CMe)_2(O_3PC_6H_{10}NH_3)_2]$	32.6	41.9	2	7
$[Na_2Co_6Gd_4(\mu_3{-}OH)_2(O_2C^tBu)_{12}(O_3PC_6H_{10}NH_2)_6(MeCN)_2]$	19.7	39.5	2	7
$[Ni_6Gd_6(\mu_3{-}OH)_2(\mu_2{-}OAc)_2(O_3PCH_3)_6(O_2C^tBu)_{16}]$	32	42.7	3	8
$[Ni_6Gd_6(\mu_3{-}OH)_2(\mu_2{-}OAc)_2(O_3PC_6H_5)_6(O_2C^tBu)_{16}]$	27.9	39.2	3	8
$[Ni_6Gd_6(\mu_3{-}OH)_2(\mu_2{-}OAc)_2(O_3PC_6H_{13})_6(O_2C^tBu)_{16}]$	28.2	39.1	3	8
$[Ni_6Gd_6(\mu_3{-}OH)_2(\mu_2{-}OAc)_2(O_3PC_8H_{17})_6(O_2C^tBu)_{16}]$	26.6	36.2	3	8
$[Fe_6Gd_6(\mu_3{-}O)_2(CO_3)(O_3PCH_3)_6(O_2C^tBu)_{18}]$	25.4	51.4	3	9
$[Fe_6Gd_6(\mu_3{-}O)_2(CO_3)(O_3PC_6H_5)_6(O_2C^tBu)_{18}]$	22	46.8	3	9
$[Fe_6Gd_6(\mu_3{-}O)_2(CO_3)(O_3PC_6H_{13})_6(O_2C^tBu)_{18}]$	22.9	46.3	3	9
$[Cu(MeCN)_4][Cu_3Gd_9(\mu_3{-}OH)_7(O_3P^tBu)_6(O_2C^tBu)_{15}]$	26.9	40.4	3	10
$[Cu_6Gd_6(\mu_3{-}OH)_6(O_3PC(NH_2)Me_2)_6(O_2C^tBu)_{12}]$	27.4	38.7	3	10

Table 8.1: Summary of the reported molecule-based magnetic coolers at 7 T.

Most 3d–4f phosphonates that have been studied, have been studied as molecule-based coolers (See Table 8.1). Most utilised Ln = Gd(III) as isotropic metal ion, the two studies of M–Dy complexes show poor MCE performance because Dy(III) is highly anisotropic. For 3d–metals there are studies of d^5 ions such as Mn(II) and Fe(III), Co(II) which is d^7, Ni(II) which is d^8 and Cu(II) which is d^9.

For Mn(II)–Ln phosphonate cages (Figures 8.6, 8.7 and 8.8), Dy(III), which has a large single-ion anisotropy can intensely hamper a large $-\Delta S_M$,[5]. In spite of its large spin of 5/2 for Mn(II), the large anisotropy of Dy(III) ions will lead to a much lower MCE than any Gd(III) analogues of these cages. From susceptibility data, dominant antiferromagnetic interactions could be minor for the Gd(III) compounds, although these were considerably weaker for $\{Mn_4Gd_6\}$ than $\{Mn_9Gd_9\}$. This reveals a much larger $-\Delta S_M$ of 33.7 J kg^{-1} K^{-1} for the former, which was the highest reported to date and in excess of that seen for all transition metal compounds. Compared to the $-\Delta S_M$ = 28 J kg^{-1} K^{-1} found under the same conditions for $\{Mn_9Gd_9\}$ complex, lower than the theoretical maximum values of about 57 J kg^{-1} K^{-1}. The MCE value are less than experimental values mostly because of the antiferromagnetic interactions between the metal centres in $\{Mn_9Gd_9\}$ and $\{Mn_4Gd_6\}$, and the magnetic anisotropy of Dy(III) in complex $\{Mn_6Dy_6\}$. Besides, the larger MCE in $\{Mn_4Gd_6\}$ compared to that in $\{Mn_9Gd_9\}$ is probably proportional to the density of the gadolinium within the complexes.

The MCE value for Co(II)–Ln phosphonate cages is poor (Figure 8.9), this due to spin orbit coupling for octahedral, high spin d^7 ions, however the behaviour is hugely variable. Cobalt(II) has a large orbital contribution to its magnetic moment, which can give significant zero field splitting, this is quenched in an appropriate crystal field. There is a direct correlation between the percentage of Gd(III) in each cage and its magnetic entropy change, the largest MCE found in this series is for

$[Co_6Gd_8(\mu_3{-}OH)_8(O_3P^tBu)_6(O_2C^tBu)_{16}(H_2O)_2](MeCN)_2$, and from magnetisation data this is 28.6 J kg^{-1} K^{-1}.

The Wells–Dawson type $[Ni_6Ln_6(OH)_2(O_3PCH_2Ph)_6(O_2C^tBu)_{16}(MeCO_2H)_2]$-$(MeCN)_4$ compounds were prepared by Winpenny and co-workers for MCE investigations (Figure 8.3), then Ni(II) in presence with Gd(III) should be an improvement, as the latter is isotropic in an octahedral environments. For $\{Ni_6Gd_6\}$, susceptibility and magnetisation data propose ferromagnetic interactions dominate untill very low temperatures and a saturation corresponding to fully aligned spins, with a comparatively fast magnetisation rate. This results in $-\Delta S_M$ of 26.5 J kg^{-1} K^{-1}, which approaches the theoretical maximum of around 37 J kg^{-1} K^{-1}. For the Dy(III) cage $\{Ni_6Dy_6\}$ no saturation of magnetisation observed, $-\Delta S_M$ is 12.2 J kg^{-1} K^{-1}, a theoretical maximum of 34 J kg^{-1} K^{-1} which confirms the significance of the choice of lanthanide. The cage $\{Ni_6Y_6\}$ supports this view as $-\Delta S_M$ is 5.6 J kg^{-1} K^{-1}, the theoretical maximum being 14 J kg^{-1} K^{-1}. Hence, the lanthanide makes a positive contribution whether Gd(III) or Dy(III), the small anisotropy of the Ni(II) ion is having a major negative impact.

The effect of different R groups in RPO_3^{2-} on the MCE have been studied (Figure 8.11), comparing the molar magnetic entropy change for each case, we can obviously see that the $-\Delta S_M$ is higher for R = Me (32 J kg^{-1} K^{-1}), followed by hexyl (28.2 J kg^{-1} K^{-1}), Ph (27.9 J kg^{-1} K^{-1}), octyl (26.6 J kg^{-1} K^{-1}) and CH_2Ph (26.5 J kg^{-1} K^{-1}). In these

five cages there is evidence for ferromagnetic interactions within $[Ni_6Gd_6(\mu_3{-}OH)_2(\mu_2{-}OAc)_2(O_3PCH_3)_6(O_2C^tBu)_{16}]$ and not in the rest, a weak ferromagnetic interaction between Ni(II) and Gd(III) could explain the increase in magnetic entropy found for the complex with $MePO_3^{2-}$. Maybe the $MePO_3^{2-}$ is slightly different from the other phosphonates, and possibly the electron-releasing nature of the Me group gives rise to larger electron density around the phosphonate and later stronger superexchange.

For $[Fe_6Gd_6(\mu_3{-}O)_2(CO_3)(O_3PR)_6(O_2C^tBu)_{18}]$ (R = Me, Ph or hexyl) compounds (Figure 8.12), the larger MCE value for $[Fe_6Gd_6(\mu_3{-}O)_2(CO_3)(O_3PCH_3)_6(O_2C^tBu)_{18}]$ is because of the lower molecular weight phosphonate substituent (R = Me *vs* Ph, hexyl; $-\Delta S_M$ = 25.4, 22, and 22.9 J kg^{-1} K^{-1}, respectively), it is useful to compare these results to those for $\{Ni_6Gd_6P_6\}$: these are in the range of 32–27.9 J kg^{-1} K^{-1}. Thus, we have larger magnetic entropy changes for $\{Ni_6Gd_6P_6\}$ *cf.* $\{Fe_6Gd_6P_6\}$ in spite of the lower spin and greater magnetic anisotropy of Ni(II) *cf.* Fe(III). This is due to the strength of the exchange interaction within the 3d metal triangles. For $\{Fe_6Gd_6P_6\}$ J_{Fe-Fe} = −30 cm^{-1}, for an isolated equilateral $\{Fe_3\}$ triangle. While, the magnetic data for $\{Ni_6Gd_6P_6\}$ could only be modelled with two J_{Ni-Ni} exchange values, depending on the isosceles $\{Ni_3\}$ symmetry, two interactions of +2 to +5 cm^{-1} and one interaction of −1 to −4 cm^{-1}. Hence, the couplings are weaker for Ni(II), and there are ferromagnetic interactions for Ni(II), these result in greater a proportion of magnetic entropy.

Functionalisation of phosphonate ligands proved to be a very promising route to synthesise 3d–4f with promising MCE properties (Figures 8.14 and 8.15), For example, the cage $[Co_4Gd_{10}(O_2C^tBu)_{12}(O_3PC_6H_{10}NH_2)_8(PO_4)_2(O_2CMe)_2(O_3PC_6H_{10}NH_3)_2]$ ($-\Delta S_M$ = 32.6 J kg^{-1} K^{-1}) has the second highest magnetic entropy change for 3d–4f phosphonate clusters, just exceeded by $\{Mn_4Gd_6P_6\}$. Moreover, the cage $[Cu_6Gd_6(\mu_3\text{–}OH)_6(O_3PC(NH_2)Me_2)_6(O_2C^tBu)_{12}]$ has $-\Delta S_M$ = 27.4 J kg^{-1} K^{-1}. In each case, comparison of the experimental $-\Delta S_M$ with the theoretical value shows that experimental value is lower than the theoretical value, this is probably referable to the antiferromagnetic exchange within the cages.

8.2 References

1. V. Baskar, K. Gopal, M. Helliwell, F. Tuna, W. Wernsdorfer and R. E. P. Winpenny, *Dalton Trans.*, 2010, **39**, 4747.
2. M. Wang, D.-Q. Yuan, C.-B. Ma, M.-J Yuan, M.-Q. Hu, N. Li, H. Chen, C.-N. Chen and Q.-T. Liu, *Dalton Trans.*, 2010, **39**, 7276.
3. Y.-Z. Zheng, M. Evangelisti and R. E. P. Winpenny, *Angew. Chem. Int. Ed.*, 2011, **50**, 3692.
4. Y.-Z. Zheng, M. Evangelisti and R. E. P. Winpenny, *Chem. Sci.*, 2011, **2**, 99.
5. Y.-Z. Zheng, E. M. Pineda, M. Helliwell and R. E. P. Winpenny, *Chem. Eur. J.*, 2012, **18**, 4161.
6. Y.-Z. Zheng, M. Evangelisti, F. Tuna and R. E. P. Winpenny, *J. Am. Chem.Soc.*, 2012, **134**, 1057.
7. E. M. Pineda, F. Tuna, R. G. Pritchard, A. C. Regan, R. E. P. Winpenny and E. J. L. McInnes, *Chem. Commun.,* 2013, **49**, 3522.
8. E. M. Pineda, F. Tuna, Y.-Z. Zheng, R. E. P. Winpenny and E. J. L. McInnes, *Inorg. Chem.*, 2013, **52**, 13702.
9. E. M. Pineda, F. Tuna, Y.-Z. Zheng, S. J. Teat, R. E. P. Winpenny, J. Schnack and E. J. L. McInnes, *Inorg. Chem.*, 2014, **53**, 3032.
10. E. M. Pineda, C. Heesing, F. Tuna, Y.-Z. Zheng, E. J. L. McInnes, J. Schnack, and R. E. P. Winpenny,*Inorg. Chem.*, 2015, ***54***, 6331.

11. T. L. Dellamary, J. A. Sampedro, G. Carlos, M. Fontes, T. Ogura, *Transition Met. Chem.*, 1978, **3**, 342.

12. M. G. Walawalkar, H. W. Roesky, R. Murugavel, *Acc. Chem. Res.*, 1999, **32**, 117.

13. A. Bencini, C. Benelli, A. Caneschi, R. L. Carlin, A. Dei and D. Gatteschi, *J. Am. Chem. Soc.*, 1985, **107**, 8128.

14. G. Karotsis, M. Evangelisti, S. J. Dalgarno and E. K. Brechin, *Angew. Chem., Int. Ed.*, 2009, **48**, 9928.

15. S. Khanra, M. Helliwell, F. Tuna, E. J. L. McInnes and R. E. P. Winpenny, *Dalton Trans.*, 2009, **31**, 6166.

Chapter 9: Paper 5

Linking Cr_3 triangles through phosphonates and lanthanides: synthetic, structural, magnetic and EPR studies

Karzan H. Zangana, Eufemio Moreno Pineda, Iñigo J. Vitorica-Yrezabal, Eric J. L. McInnes and Richard E. P. Winpenny, *Dalton Trans.*, 2014, **43**, 13242.

Dalton Transactions

PAPER

View Article Online
View Journal | View Issue

Cite this: *Dalton Trans.*, 2014, **43**, 13242

Linking Cr_3 triangles through phosphonates and lanthanides: synthetic, structural, magnetic and EPR studies†

Karzan H. Zangana, Eufemio Moreno Pineda, Iñigo J. Vitorica-Yrezabal, Eric J. L. McInnes and Richard E. P. Winpenny*

Received 29th April 2014,
Accepted 18th July 2014

DOI: 10.1039/c4dt01264j

www.rsc.org/dalton

The preparation and structural characterisation of five 3d–4f mixed metal phosphonate cages with general formula $[Cr^{III}_6Ln^{III}_2(\mu_3\text{-}O)_2(H_2O)_2(O_3P^tBu)_4(O_2C^tBu)_{12}(HO^iBu)_2(^iPrNH_2)_2]$ where Ln^{III} = La, **1**; Tb, **3**; Dy, **4**; Ho, **5** and $[Cr^{III}_6Gd^{III}_2(\mu_3\text{-}O)_2(H_2O)_2(O_3P^tBu)_4(O_2C^tBu)_{12}(HO^iBu)_4]$ (**2**) are reported. The structure contains two oxo-centred $\{Cr_3\}$ triangles, bridged by phosphonates and lanthanides. The magnetic behaviour of **1** has been modelled as two non-interacting isosceles triangles, involving two antiferromagnetic interactions (J_1 = −8.8 cm^{-1}) with a smaller ferromagnetic interaction for the unique edge of the triangle (J_2 = +1.3 cm^{-1}) giving an isolated S = 3/2 ground state per triangle. The quartet ground state has been proven through simulation of electron paramagnetic resonance (EPR) spectra obtained at the X- and Q-band. EPR simulations have also resulted in the introduction of small single-ion Zero Field Splitting (ZFS) parameters D = ±0.19 cm^{-1} and rhombic term E = ±0.02 cm^{-1}, which are consistent with strong exchange limit calculations for an isolated S = 3/2 (D = ±0.22 and E = ±0.018 cm^{-1}).

Introduction

The synthesis of paramagnetic polymetallic complexes has been an area of significant interest since the discovery of the single molecule magnet (SMM), $[Mn_{12}O_{12}(O_2CMe)_{16}(H_2O)_4]$.[1] One area of current interest is in making 3d–4f cage compounds, hoping that the combination of strong exchange from the 3d-ions will combine with the large anisotropy of the 4f-ions to produce interesting SMMs. The earliest studies of such 3d–4f heterometallic compounds were by Gatteschi and colleagues, who used designed Schiff-base ligands to bind to both types of metal selectively.[2] There was also considerable work involving use of anions of 2-hydroxypyridine and its derivatives.[3] More recently there has been a huge expansion in this area, with many beautiful new compounds reported.[4,5]

Phosphonates are multidentate ligands that in their mono or dianionic form can adopt many different coordination modes, with a range of structures and nuclearities containing copper,[6] iron,[7] manganese,[8] nickel,[9] cobalt[9c,10] and vanadium.[11] More recently phosphonates have been used for 3d–4f-complexes,[4n,5a,c,e,m] and for 4f-compounds.[12]

One of our first forays into this area involved reactions of oxo-centred tri-iron carboxylates with phosphonates,[7a] where we found that the phosphonate could displace a carboxylate and link triangles together. Frequently we found that additional reactions occurred, with an iron centre extracted from a triangle to bind to the phosphonate separately. This produced compounds containing four (one triangle plus one iron) and seven (two triangles bridged by one iron) metals.[7a] We reasoned that if we used more stable oxo-centred triangles, and deliberately added a source of a second metal we could make similar arrays, but heterometallic. Therefore we have undertaken the reaction of oxo-centred chromium(III) carboxylates with phosphonates in the presence of lanthanide ions.

In this paper we report the synthesis, structural characterisation, and magnetic properties of a series of octanuclear Cr^{III}–Ln^{III} phosphonate cages (Ln^{III} = La, **1**; Gd, **2**; Tb, **3**; Dy, **4**; Ho, **5**) using ^{t}butyl phosphonic acid as ligand. We were able to single out the contribution of Ln^{III} by comparing **2**, **3**, **4** and **5** with the lanthanum analogue **1**; this family of cages provides a good opportunity to systematically study the magnetic exchange between 3d and 4f metal ions.

Experimental section

Material and physical measurements

$[Cr^{III}_3(\mu_3\text{-}O)(O_2C^tBu)_6(H_2O)_3][O_2C^tBu]\cdot 3H_2O$ was synthesised according to reported methods.[13] All reagents, metal salts,

School of Chemistry and Photon Science Institute, The University of Manchester, Oxford Road, Manchester M13 9PL, UK.
E-mail: richard.winpenny@manchester.ac.uk; Fax: +44-161-275-1001

†Electronic supplementary information (ESI) available: Further crystallographic details. CCDC 999505–999509. For ESI and crystallographic data in CIF or other electronic format see DOI: 10.1039/c4dt01264j

Table 1 Elemental analysis and yield (%) for compounds **1–5**

Cage	Yield[a]	Elemental analysis: found (calculated)					
		C	H	Cr	Ln	P	N
1[b]	40%	41.33 (41.06)	7.32 (7.38)	10.58 (10.88)	9.41 (9.69)	4.19 (4.32)	0.94 (0.98)
2[b]	31%	41.15 (40.95)	7.16 (7.28)	10.97 (10.64)	10.80 (10.72)	4.33 (4.21)	— (—)
3[c]	30%	41.09 (40.75)	7.38 (7.26)	10.48 (10.80)	11.21 (11.00)	4.10 (4.27)	0.93 (0.97)
4[c]	29%	40.48 (40.65)	7.43 (7.24)	10.42 (10.77)	11.35 (11.22)	4.11 (4.28)	0.90 (0.97)
5[d]	22%	40.89 (40.84)	6.79 (7.20)	10.53 (10.82)	10.97 (11.44)	4.07 (4.30)	0.93 (0.97)

[a] Based on phosphonate source. Calculated EA and crystallisation solvents. [b] $2(HO^iBu)\cdot2(H_2O)$. [c] $2(HO^iBu)\cdot(H_2O)$. [d] $2(HO^iBu)$.

solvents and ligands were used as purchased without any further purification. Analytical data were obtained by the microanalytical service of the University of Manchester. The data and yields are given in Table 1.

Synthesis

$[Cr^{III}_3(\mu_3\text{-}O)(O_2C^tBu)_6(H_2O)_3][O_2C^tBu]$ (1 g, 1.225 mmol), $Gd(NO_3)_3\cdot6H_2O$ (0.554 mmol), *t*-butyl phosphonic acid (0.07 g, 0.507 mmol) and isopropylamine ($^iPrNH_2$) (0.1 mL, 1.164 mmol) in isobutanol (HO^iBu)(15 mL) were refluxed at 120 °C for 24 hours to form a dark green solution. The solution was filtered and then allowed to stand undisturbed at room temperature. Green plate-like crystals suitable for single crystal X-ray diffraction of $[Cr^{III}_6Gd^{III}(\mu_3\text{-}O)_2(H_2O)_2(O_3P^tBu)_4(O_2C^tBu)_{12}(HO^iBu)_4]$ (**2**) were collected after 10 days. Similar reactions with $Ln^{III}(NO_3)_3\cdot nH_2O$, where Ln^{III} = La(**1**), Tb(**3**), Dy(**4**) and Ho(**5**) gave crystals of $[Cr^{III}_6Ln^{III}_2(\mu_3\text{-}O)_2(H_2O)_2(O_3P^tBu)_4(O_2C^tBu)_{12}(HO^iBu)_2(^iPrNH_2)_2]$ (Table 1).

X-ray data collection and structure solution

Data collection was carried out on Agilent SUPERNOVA diffractometer with MoKα radiation (λ = 0.71073 Å), data reduction and unit cell refinement were performed with CrysAlisPro software. The structures were solved by direct method using SHELXS-97[14a] and were refined by full-matrix least-squares calculations on F^2 using the program Olex2.[14b] Suitable crystals of **1–5** were mounted on a tip using crystallographic oil and placed in a cryostream and used for data collection. Data were collected using ϕ and ω scans chosen to give a complete asymmetric unit. All non-hydrogen atoms were refined anisotropically. Hydrogen atoms were calculated geometrically and were riding on their respective atoms. Hydrogens corresponding to disorder water molecules and hydroxyl groups form solvated isobutanol molecules were omitted but included in the formula. Some degree of disorder was found in all cages. The ^tBu groups of the pivalates, ^tBu groups of the phosphonates, the coordinated and uncoordinated (only compound **2**) isobutanol and isopropylamine are found to be disordered over two sites. These disordered groups were modelled splitting their occupancy into two parts. The isobutanol solvent molecules were found to be disordered over three sites for compound **1**, **3–5**. These disordered molecules were modelled splitting their occupancy into three parts and restraining their value to add to 1 using the SUMP command. The amount of uncoordinated solvent was determined using SQUEEZE. The number of electrons calculated agrees with two isobutanol and two water molecules per unit cell for compounds **1**, **3–5**. For compound **2**, it was found to have four isobutanol and eight water molecules per unit cell. The C–C distances of the ^tBu groups of the pivalates and the phosphonates were restrained to be equal using SADI command. The C–C, C–O and C–N distances for both the isopropylamine and the isobutanol were restrained using DFIX command. The atomic displacement parameters of the disorder moieties were restrained using RIGU command. Full crystallographic details can be found in CIF format: CCDC for **1–5**, 999505–999509. Crystal data and refinement parameters are given in Table 2.

Magnetic measurements

The magnetic properties of polycrystalline samples of **1–5** were measured in the temperature range 1.8 K–300 K with a Quantum Design MPMS-XL7 SQUID magnetometer armed with a 7 T magnet. The samples were ground, placed in a gel capsule, and fixed with a small amount of eicosane to avoid movement during the measurement. The data were corrected for the diamagnetism from the gel capsule and the eicosane with the diamagnetic contribution from the complexes calculated from Pascal constants. Magnetic data were fitted using the program PHI.[15]

Electron paramagnetic resonance

X-band (*ca.* 9.5 GHz) and Q-band (*ca.* 34 GHz) EPR spectra of polycrystalline powders were recorded with a Bruker EMX580 spectrometer. The data was collected in the temperature range 5–30 K using liquid helium. Spectral simulations were performed using the *EasySpin 4.5.5*[16] simulation software.

Results and discussion

Synthetic description

Many synthetic procedures rely on the reaction of oxo-centred metal triangles,[7,8,17] however fewer reactions use chromium oxo-centered triangles $[Cr^{III}_3(\mu_3\text{-}O)(RCO_2)_6(L)_3]X$ (R = Me, Ph, ^tBu; X = Cl, NO_3) and in many of those reactions the triangle is not found in the final product.[18] However here we find that refluxing a mixture of chromium pivalate oxo-centred triangle $[Cr^{III}_3(\mu_3\text{-}O)(O_2C^tBu)_6(H_2O)_3][O_2C^tBu]\cdot3H_2O$, hydrated lantha-

Table 2 Crystallographic information for cages **1**–**5**

	1·2^{i}BuOH·2H_2O	**2**·2^{i}BuOH·4H_2O	**3**·2^{i}BuOH·2H_2O	**4**·2^{i}BuOH·2H_2O	**5**·2^{i}BuOH·2H_2O
Chem formula	$C_{98}H_{210}Cr_6La_2N_2O_{46}P_4$	$C_{100}H_{210}Cr_6Gd_2O_{50}P_4$	$C_{98}H_{210}Cr_6N_2O_{46}P_4Tb_2$	$C_{98}H_{210}Cr_6Dy_2N_2O_{46}P_4$	$C_{98}H_{210}Cr_6Ho_2N_2O_{46}P_4$
fw	2866.37	2957.00	2906.39	2913.55	2916.83
Cryst system	Triclinic	Monoclinic	Triclinic	Triclinic	Triclinic
Space group	$P\bar{1}$	$P2_1/n$	$P\bar{1}$	$P\bar{1}$	$P\bar{1}$
a/Å	13.7609(5)	13.8020(7)	13.918(1)	13.7094(6)	13.7501(4)
b/Å	13.9671(5)	27.527(2)	14.0369(7)	14.0352(5)	14.0220(5)
c/Å	23.3521(8)	19.718(2)	23.346(2)	23.1626(9)	23.1827(8)
α/°	100.081(3)	90	99.776(5)	100.096(3)	100.079(3)
β/°	100.916(3)	95.817(7)	101.128(6)	100.639(3)	100.637(3)
γ/°	107.940(3)	90	108.202(5)	108.186(4)	108.254(3)
V/Å^3	4059.8(3)	7453(1)	4119.7(5)	4029.8(3)	4040.0(2)
Z	1	2	1	1	1
ρ_{calcd}/g cm^{-3}	1.172	1.295	1.171	1.201	1.199
T/K	150(1)	150.0(2)	210.1(2)	150.0(1)	150.0(1)
μ (Mo K$_\alpha$)/mm^{-1}	1.003	1.412	1.328	1.407	1.458
R_1 ($I > 2\sigma(I)$)^a	0.0753	0.0777	0.0664	0.0661	0.0637
wR_2^{a} (all data)	0.2342	0.2048	0.2045	0.2052	0.2055

^{a} $R_1 = ||F_o| - |F_c||/|F_o|$, $wR_2 = [w(|F_o| - |F_c|)^2/w|F_o|^2]^{1/2}$.

nide nitrate, $Ln^{III}(NO_3)_3 \cdot nH_2O$, phosphonic acid, $H_2O_3P^tBu$, and a mild base, $^{i}PrNH_2$, in ^{i}BuOH in the mole ratios 1.2 : 0.50 : 0.50 : 1.2 gives reasonable yields of a family of $\{Cr_6Ln_2\}$ cages Ln = La **1**, Gd **2**, Tb **3**, Dy **4** and Ho **5**.

Crystallography

The cages **1**–**5** crystallise in two different space groups monoclinic $P2_1/n$ (**2**) and triclinic $P\bar{1}$ (**1**, **3**, **4** and **5**) (Fig. 1), however the molecular structures are very similar and we describe the structure of **1** as representative. Overall the structure contains six Cr^{III} and two La^{III} ions, which are held together by two μ_3-oxide and four phosphonates beside ten bridging pivalates. The octanuclear cage consists of two equivalent oxo-centered chromium triangles $\{Cr^{III}_3(\mu_3\text{-O})\}$.

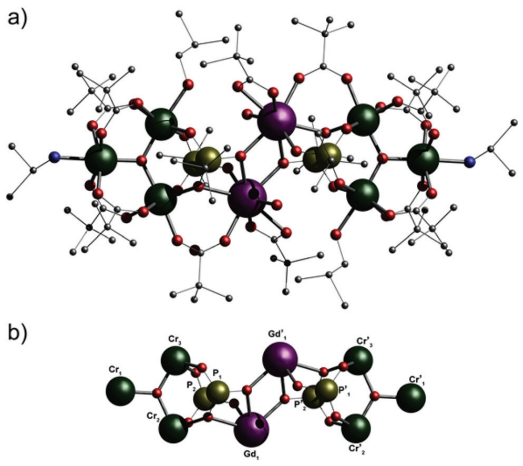

Fig. 1 Crystal structure of the $\{Cr_6Gd_2P_4\}$ cage **1**. (a) Top left: top view of cage. (b) Metal core of cage **1** without carbons. Scheme: La, purple; Cr, dark green; P, light green; O, red; C, grey; N, cyan; H omitted for clarity.

In each triangle two edges are bridged by 2.11 pivalates (Harris notation)[19] (ESI, Fig. S1†), as in the starting material, but on the third edge both pivalates have been displaced by phosphonates. These phosphonates bridge the Cr···Cr edge, but use their third oxygen atom to bind to a La^{III} site; in one phosphonate (and its symmetry equivalent) the oxygen bridges between two La^{III} sites, given it a 4.211 binding mode. In the other pair of symmetry equivalent phosphonates the third O-atom is terminal to a La^{III}, giving it the 3.111 binding mode. A 2.11 bridging pivalate also bridges between one Cr site, occupying the position *trans* to the μ_3-oxide, and a lanthanum. This site is occupied by a terminal ^{i}BuOH for the other four Cr sites (Fig. 1).

The distance between the two μ_3-oxides and the three Cr^{III} ions within triangles fall in the range 1.8924(1)–1.94955(8) Å, the Cr–O–Cr angles are very close to 120° and sum to 360° (ESI, Table S1 and Fig. S4†).

The Cr–Cr distances within the triangles fall in the range 3.2351(2)–3.4275(5) Å, while the La–La′ distance within the cage is 4.192(8) Å. In **2**, all Cr^{III} centres have an O_6 coordination sphere, with octahedral coordination geometry; whilst in the remaining analogues a terminal amine fill the coordination sphere of Cr1 and Cr(1)′, leading to a O_5N set, and a O_6 coordination sphere for Cr(2), Cr(3), Cr(2)′ and Cr(3)′. The Ln^{III} ion centres have an LnO_8 coordination sphere, consisting of four oxygen atoms from the phosphonate bridging groups, three oxygens belonging to two pivalates and one water oxygen atom (ESI, Fig. S2 and S3†).

Magnetic description

We have studied the magnetic behaviour of complexes **1**–**5** using polycrystalline samples in the temperature range 2–300 K under 1000 Oe applied magnetic field. Similarly we

have investigated the magnetisation as function of applied magnetic field (H) at 2 and 4 K in the range of 0–7 T. The temperature dependence of the $\chi_M T(T)$ (where χ_M is the molar magnetic susceptibility) for all polycrystalline samples show values lower than expected for the single ion contribution of six Cr^{III} S = 3/2 and the paramagnetic lanthanide contribution *e.g.* the contribution from Gd^{III}, Tb^{III}, Dy^{III} or Ho^{III} for **2–5** respectively. Complex **1** shows a $\chi_M T$ at room temperature of 9.6 cm^3 K mol^{-1} considerably lower than expected (calcd 11.1 cm^3 K mol^{-1} for six Cr^{III}: g_{Cr} = 1.99, S = 3/2). For complex **1** $\chi_M T(T)$ decreases with lowering temperature reaching a value of 3.6 cm^3 K mol^{-1} at 2 K suggesting, along with the $\chi_M T(T)$ value at room temperature, antiferromagnetic interactions between the Cr sites in the cage. Complexes **2** to **5** exhibit similar behaviour: for **2** the $\chi_M T$ room temperature value is 23.3 cm^3 K mol^{-1} (calcd 26.7 cm^3 K mol^{-1} for six Cr^{III}: g_{Cr} = 1.99, S = 3/2 and two Gd^{III}: g_{Gd} = 1.99; S = 7/2) which gradually decreases to 20 K where it sharply decreases to 15.9 cm^3 K mol^{-1} at 2 K indicating that at this temperature paramagnetic states are still populated; **3** to **5** reveal room temperature $\chi_M T$ values of 33.2 cm^3 K mol^{-1} (calcd 34.8 cm^3 K mol^{-1} for six Cr^{III}: g_{Cr} = 1.99, S = 3/2 and two Tb^{III}: g_J = 3/2; J = 6), 38.1 cm^3 K mol^{-1} (calcd 39.5 cm^3 K mol^{-1} for six Cr^{III}: g_{Cr} = 1.99, S = 3/2 and two Dy^{III}: g_J = 4/3; J = 15/2) and 37.6 cm^3 K mol^{-1} (calcd 39.3 cm^3 K mol^{-1} for six Cr^{III}: g_{Cr} = 1.99, S = 3/2 and two Ho^{III}: g_J = 5/4; J = 8) mol^{-1} respectively (Fig. 2).

The temperature dependent susceptibility gradually decreases upon lowering temperature for all complexes, however at low temperature two different behaviours are observed. For complex **3** a small plateau is observed from *ca.* 13 to 5 K, before dropping to 21.6 cm^3 K mol^{-1} at 2 K. In the case of complex **4** the gradual decrease in $\chi_M T(T)$ upon lowering temperature stops at about 8 K where it starts gradually to increase up to 27.2 cm^3 K mol^{-1} at 2 K. The behaviour exhibited by **3** and **4** suggest some ferromagnetic interactions, probably between the 3d–4f system.[1–4] Complex **5** decreases gradually up to *ca.* 40 K where it drops sharply to 12.9 cm^3 K mol^{-1} indicating antiferromagnetic interactions and/or depopulation of the Stark sublevels (see Fig. 2).

The molar magnetisation (M) as function of applied magnetic field at 2 K in the field range of 0–7 T shows a saturation value at 7 T for compounds **1** and **2** of 5.9 and 20.2 μ_B. Complex **3** to **5** show $M(H)$ values of 14.7 for the **3** and 16.4 μ_B for the other two. No conclusion can be drawn from the field dependence for **3** to **5** due to the high anisotropy presented for these lanthanide-containing cages.

The magnetic behaviour of **1** was modelled using PHI package,[15] fitting $\chi_M T(T)$ and $M(H)$ simultaneously. As **1** contains La^{III}, study of this compound allows the determination of

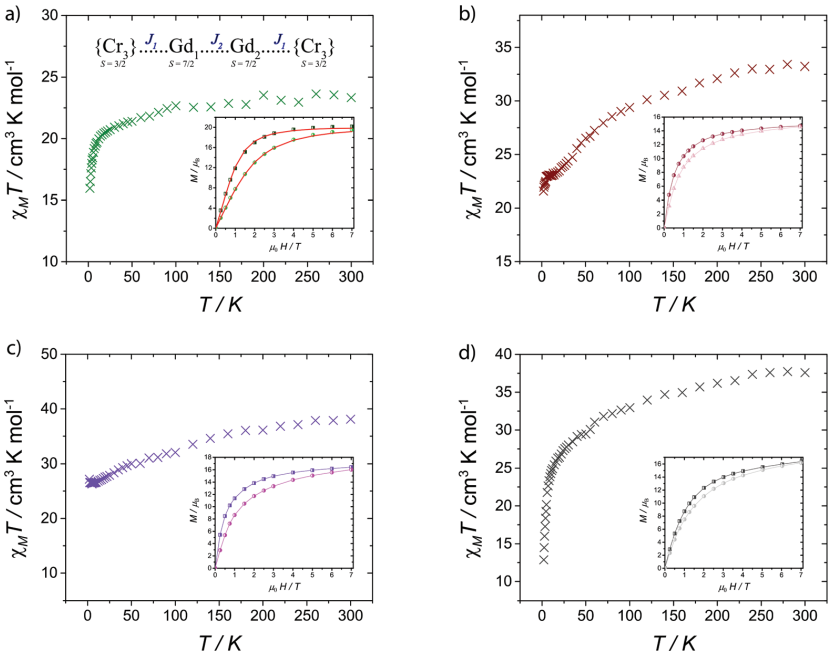

Fig. 2 Molar magnetic susceptibility ($\chi_M T$) *vs.* T plot for **2–5** under 1 kG dc field and molar magnetization (M) as a function of applied magnetic field (H) at 2 and 4 K (inset) for (a) **2**, (b) **3**, (c) **4** and (d) **5**.

the exchange interaction within the two $\{Cr_3\}$ moieties. A simple model has been used based on the sum of two non-interacting $\{Cr_3\}$ triangles (based on the crystallographic data, the nearest $Cr_3\cdots Cr_3$ distance from each triangle is 9.289(1) Å). Each $\{Cr_3\}$ triangle has been modelled using a Hamiltonian of the form (1):

$$H = -2J_1(\hat{S}_1\hat{S}_2 + \hat{S}_1\hat{S}_3) - 2J_2(\hat{S}_2\hat{S}_3) + g\mu_B H\sum_{i=1}^{3}\hat{S}_i \qquad (1)$$

where the first term is the isotropic exchange interaction between Cr(1)···Cr(2) and Cr(2)···Cr(3), and the second term that between Cr(1)···Cr(3), the chemically unique edge (Fig. 3). The fourth term is the Zeeman term of each Cr centre.

Good agreement between experiment and simulation for $\chi_M T$ *vs.* T and M *vs.* H is also obtained including a small ZFS (see below). Simultaneous fitting of $\chi_M T(T)$ and $M(H)$ yield agreement between experimental data and simulation with an antiferromagnetic exchange interaction J_1 = −8.8 cm^{-1}, and a ferromagnetic interaction of J_2 = +1.3 cm^{-1} between the Cr ions in the unique edge of the triangle, giving a total spin ground state for each individual $\{Cr_3\}$ fragment of S = 3/2 (see Fig. 3), with the first excited state, S = 1/2, at 33 cm^{-1} above it. The field dependence of the magnetisation can be reproduced using the Brillouin function for two S = 3/2 states, which

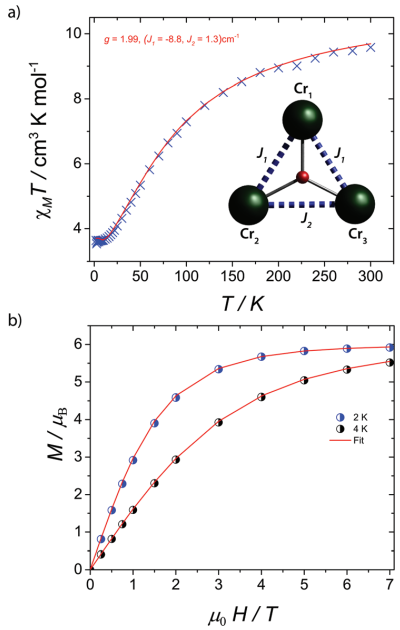

Fig. 3 (a) Molar magnetic susceptibility ($\chi_M T$) *vs.* T and simulation plots for **1** under 1 kG dc field. (b) Molar magnetization (M) as a function of applied magnetic field (H) at 2 and 4 K for **1**.

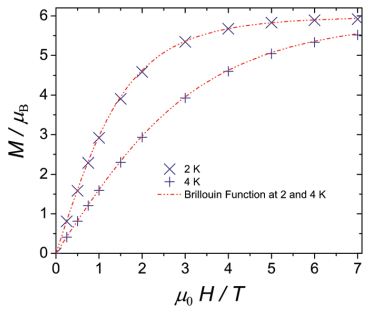

Fig. 4 Magnetisation of complex **1** and Brillouin function (red line) for two S = 3/2 states at 2 and 4 K.

suggests there is very little communication between the two $\{Cr_3\}$ triangles in the $\{Cr_6La_2\}$ cage (Fig. 4).

Attempts to investigate the magnetic behaviour of **2** were made, however due to the huge Hilbert space ($(2S_i + 1)^n \times (2S_j + 1)^n$ = 262 144) for the six Cr^{III} (S = 3/2) and two Gd^{III} (S = 7/2), the system is rendered quite difficult for the evaluation of its Hamiltonian. To overcome this issue the magnetic data of **2** was modelled assuming two $\{Cr_3\}$ with S = 3/2, obtained from the magnetic behaviour of **1** and the EPR data (see below) and two Gd^{III}. We have used a simple Hamiltonian (2) considering a linear combination of Cr···Gd···Gd···Cr (see inset Fig. 2a).

$$H = -2J_1(\hat{S}_1\hat{S}_2 + \hat{S}_3\hat{S}_4) - 2J_2(\hat{S}_2\hat{S}_3) + g\mu_B H\sum_{i=1}^{4}\hat{S}_i \qquad (2)$$

Simultaneous fitting of $M(H)$ at 2 and 4 K resulted in ferromagnetic interactions between each $\{Cr_3\}$ and the neighbour Gd^{III} J_1 = +0.19 cm^{-1}, whilst a small antiferromagnetic interaction was obtained for the Gd···Gd pair J_2 = −0.08 cm^{-1}.

Electron paramagnetic resonance

EPR spectroscopy has generally been an important tool in probing the spin ground states of molecular complexes.[20] The EPR spectroscopy of **1** was studied in the temperature range of 5–30 K using X- and Q-band frequencies, *ca.* 9.5 GHz and 34.5 GHz respectively. Several features are observed in X-band EPR at 5 K (Fig. 5). Broad intense transitions are observed at 60, 160 and 440 mT resonance fields, whilst a less intense signal is observed at about 350 mT ($g \sim 2$). Upon raising the temperature the intense signals decrease while the minor signal at $g \sim 2$ sharply increases, suggesting the population of an excited state, probably S = 1/2 (see below). The Q-band EPR data shows similar behaviour, with several features at 5 K, which broaden upon raising the temperature, whilst the signal at $g \sim 2$ sharply increases.

We have simulated the X- and Q-band EPR data using the parameters obtained from fitting the magnetic data (see

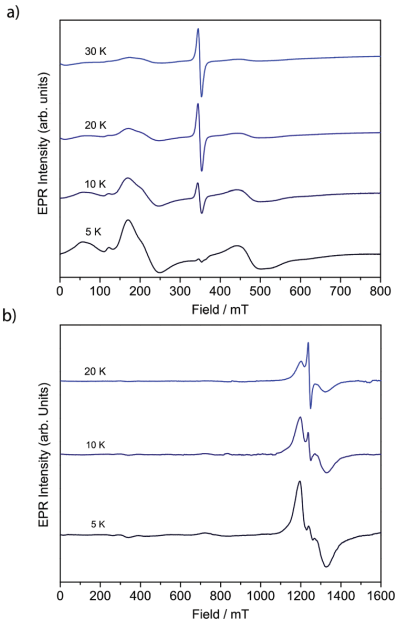

Fig. 5 (a) X-band spectrum for compound **1** in the temperature range of 5–30 K; (b) Q-band spectrum for compound **1** in the temperature range of 5–20 K.

above), with inclusion of axial (D) and rhombic (E) ZFS terms, giving Hamiltonian (3):

$$H = -2J_1\left(\hat{S}_1\hat{S}_2 + \hat{S}_2\hat{S}_3\right) - 2J_2\left(\hat{S}_1\hat{S}_3\right) + D\sum_{i=1}^{3} S_{iz}{}^2 + E\sum_{i=1}^{3}\left(S_{ix}{}^2 - S_{iy}{}^2\right) + g\mu_B H\sum_{i=1}^{3}\hat{S}_i \quad (3)$$

Agreement between experimental data was achieved using the parameters above with D_{Cr} = ±0.19 cm^{-1} and E_{Cr} = ±0.02 cm^{-1} (Fig. 6a and b). Inclusion of these small ZFS terms in the fit of magnetic data makes little difference to the quality of the fit.

The EPR behaviour can also be modelled in the strong exchange limit as an isolated S = 3/2 state with $D_{3/2}$ = ±0.22 cm^{-1} and $E_{3/2}$ = ±0.018 cm^{-1} revealing an isolated quartet state with nearly no contribution from excited states present at 5 K (see Fig. 6c and d). If the strong exchange limit is valid here, the vector coupling method of Bencini and Gatteschi[21] would give $D_{3/2} = 29D_{Cr}/25$. Our two values for the zero-field splitting are entirely consistent with one another, demonstrating that use of the strong exchange limit is reasonable.

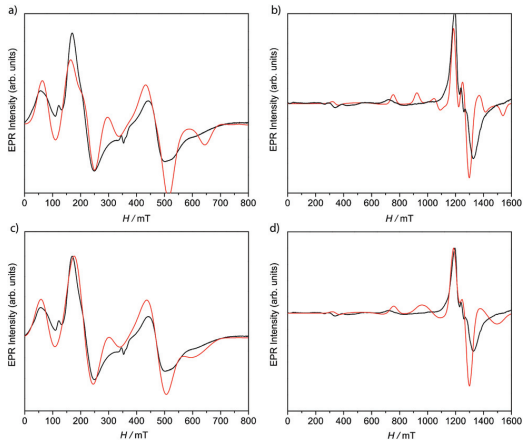

Fig. 6 (a) X-band and (b) Q-band spectra (black trace) and simulation (red trace) for compound **1** modelled as exchange coupled system at 5 K: g_{Cr} = 1.99, D_{Cr} = ±0.19, E_{Cr} = ±0.02, J_1 = +1.8, J_2 = −8.8 cm^{-1}; (c) X-band and (d) Q-band spectra (black trace) and simulation (red trace) for compound **1** at 5 K modelled as S = 3/2, g = 1.99, D = ±0.22, E = ±0.018 cm^{-1}.

Conclusions

To summarise, by using an oxo-centered chromium pivalate triangles complex as a starting material reacted with a range of different lanthanide starting materials and using *t*-butylphosphonate as a ligand we have obtained a range of 3d–4f mixed metal octanuclear complexes. The precursor {Cr_3} triangles can be recognized in all the resulting cages, and there is a relation to the {Fe_7} cages we have reported previously,[7a] where a single Fe^{III} ion bound to the phosphonates, linking triangles. At present we cannot control or predict how the phosphonates assemble the 4f-ions in order to form larger cages, but it appears this is a valuable strategy for synthesizing moderately large polymetallic cages.

Acknowledgements

KZ thanks the KRG-Scholarship program in "Human Capacity Development (HCDP)". EMP thanks the Panamanian agency SENACYT-IFARHU. REPW thanks the Royal Society for a Wolfson Merit Award. We thank the EPSRC(UK) for funding for an X-ray diffractometer (grant number EP/K039547/1) and the National EPR Facility.

References

1 (*a*) R. Sessoli, D. Gatteschi, A. Caneschi and M. A. Novak, *Nature*, 1993, **365**, 141; (*b*) R. Sessoli, H. L. Tsai, A. R. Schake, S. Y. Wang, J. B. Vincent, K. Folting,

D. Gatteschi, G. Christou and D. N. Hendrickson, *J. Am. Chem. Soc.*, 1993, **115**, 1804.

2 (*a*) A. Bencini, C. Benelli, A. Caneschi, R. L. Carlin, A. Dei and D. Gatteschi, *J. Am. Chem. Soc.*, 1985, **107**, 8128; (*b*) A. Bencini, C. Benelli, A. Caneschi, A. Dei and D. Gatteschi, *Inorg. Chem.*, 1986, **25**, 572; (*c*) C. Benelli, A. Caneschi, D. Gatteschi, O. Guillou and L. Pardi, *Inorg. Chem.*, 1990, **29**, 1750.

3 R. E. P. Winpenny, *Chem. Soc. Rev.*, 1998, **27**, 447 and references therein.

4 (*a*) A. Mishra, A. J. Tasiopoulos, W. Wernsdorfer, E. E. Moushi, B. Moulton, M. J. Zaworotko, K. A. Abboud and G. Christou, *Inorg. Chem.*, 2008, **47**, 4832; (*b*) R. Sessoli and A. K. Powell, *Coord. Chem. Rev.*, 2009, **253**, 2241; (*c*) S. K. Langley, L. Ungur, N. F. Chilton, B. Moubaraki, L. F. Chibotaru and K. S. Murray, *Chem. – Eur. J.*, 2011, **17**, 9209; (*d*) T. D. Pasatoiu, M. Etienne, A. M. Madalan, M. Andruh and R. Sessoli, *Dalton Trans.*, 2010, **39**, 4802; (*e*) C. G. Efthymiou, T. C. Stamatatos, C. Papatriantafyllopoulou, A. J. Tasiopoulos, W. Wernsdorfer, S. P. Perlepes and G. Christou, *Inorg. Chem.*, 2010, **49**, 9737; (*f*) G. Rigaux, R. Inglis, S. Morrison, A. Prescimone, C. Cadiou, M. Evangelisti and E. K. Brechin, *Dalton Trans.*, 2011, **40**, 4797; (*g*) Y. Gao, L. Zhao, X. Xu, G.-F. Xu, Y.-N. Guo, J. Tang and Z. Liu, *Inorg. Chem.*, 2011, **50**, 1304; (*h*) C. Papatriantafyllopoulou, W. Wernsdorfer, K. A. Abboud and G. Christou, *Inorg. Chem.*, 2011, **50**, 421; (*i*) A. Saha, M. Thompson, W. Wernsdorfer, K. A. Abboud and G. Christou, *Inorg. Chem.*, 2011, **50**, 10476; (*j*) Y.-F. Zeng, G.-C. Xu, X. Hu, Z. Chen, X.-H. Bu, S. Gao and E. C. Sañudo, *Inorg. Chem.*, 2010, **49**, 9734; (*k*) H. L. C. Feltham, R. Clérac, A. K. Powell and S. Brooker, *Inorg. Chem.*, 2011, **50**, 4232; (*l*) E. Colacio, J. Ruiz-Sanchez, F. J. White and E. K. Brechin, *Inorg. Chem.*, 2011, **50**, 7268; (*m*) M. Hołyńska, D. Premužić, I.-R. Jeon, W. Wernsdorfer, R. Clérac and S. Dehnen, *Chem. – Eur. J.*, 2011, **17**, 9605; (*n*) V. Baskar, K. Gopal, M. Helliwell, F. Tuna, W. Wernsdorfer and R. E. P. Winpenny, *Dalton Trans.*, 2010, **39**, 4747.

5 (*a*) Y.-Z. Zheng, M. Evangelisti and R. E. P. Winpenny, *Angew. Chem., Int. Ed.*, 2011, **50**, 3692; (*b*) R. Sessoli and A. K. Powell, *Coord. Chem. Rev.*, 2009, **253**, 2241; (*c*) Y.-Z. Zheng, E. M. Pineda, M. Helliwell, M. Evangelisti and R. E. P. Winpenny, *Chem. – Eur. J.*, 2012, **18**, 4161; (*d*) M. Wang, D.-Q. Yuan, C.-B. Ma, M.-J. Yuan, M.-Q. Hu, N. Li, H. Chen, C.-N. Chen and Q.-T. Liua, *Dalton Trans.*, 2010, **39**, 7276; (*e*) Y.-Z. Zheng, M. Evangelisti, F. Tuna and R. E. P. Winpenny, *J. Am. Chem. Soc.*, 2012, **134**, 1057; (*f*) T. N. Hooper, J. Schnack, S. Piligkos, M. Evangelisti and E. K. Brechin, *Angew. Chem., Int. Ed.*, 2012, **51**, 4633; (*g*) J.-P. Peng, Q.-C. Zhang, X.-J. Kong, Y.-Z. Zheng, Y.-P. Ren, L.-S. Long, R.-B. Huang, L.-S. Zheng and Z. Zheng, *J. Am. Chem. Soc.*, 2012, **134**, 3314; (*h*) J.-B. Peng, Q.-C. Zhang, X.-J. Kong, Y.-P. Ren, L.-S. Long, R.-B. Huang, L.-S. Zheng and Z. Zheng, *Angew. Chem., Int. Ed.*, 2011, **50**, 10649; (*i*) Y. Zheng, Q.-C. Zhang, L.-S. Long, R.-B. Huang, A. Müller, J. Schnack, L.-S. Zheng and Z. Zheng, *Chem. Commun.*, 2013, **49**, 36; (*j*) K. C. Mondal, A. Sund, Y. Lan, G. E. Kostakis, O. Waldmann, L. Ungur, L. F. Chibotaru, C. E. Anson and A. K. Powell, *Angew. Chem., Int. Ed.*, 2012, **51**, 7550; (*k*) J.-P. Costes, L. Vendiera and W. Wernsdorfer, *Dalton Trans.*, 2011, **40**, 1700; (*l*) K. C. Mondal, G. E. Kostakis, Y. Lan, W. Wernsdorfer, C. E. Anson and A. K. Powell, *Inorg. Chem.*, 2011, **50**, 11604; (*m*) E. M. Pineda, F. Tuna, Y.-Z. Zheng, S. J. Teat, R. E. P. Winpenny, J. Schnack and E. J. L. McInnes, *Inorg. Chem.*, 2014, **53**, 3032.

6 (*a*) V. Chandrasekhar and S. Kingsley, *Angew. Chem., Int. Ed.*, 2000, **39**, 6175; (*b*) V. Chandrasekhar, L. Nagarajan, K. Gopal, V. Baskar and P. Kögerler, *Dalton Trans.*, 2005, 3143; (*c*) V. Chandrasekhar, L. Nagarajan, R. Clérac, S. Ghosh, T. Senapati and S. Verma, *Inorg. Chem.*, 2008, **47**, 5347; (*d*) V. Chandrasekhar, T. Senapati and E. C. Sañudo, *Inorg. Chem.*, 2008, **47**, 9553; (*e*) V. Chandrasekhar and L. Nagarajan, *Dalton Trans.*, 2009, 6712; (*f*) V. Chandrasekhar, D. Sahoo, R. S. Narayanan, R. J. Butcher, F. Lloret and E. Pardo, *Dalton Trans.*, 2013, **42**, 8192; (*g*) V. Baskar, M. Shanmugam, E. C. Sañudo, M. Shanmugam, D. Collison, E. J. L. McInnes, Q. Wei and R. E. P. Winpenny, *Chem. Commun.*, 2007, 37; (*h*) J. A. Sheikh, H. S. Jena, A. Adhikary, S. Khatua and S. Konar, *Inorg. Chem.*, 2013, **52**, 9717.

7 (*a*) E. I. Tolis, M. Helliwell, S. Langley, J. Raftery and R. E. P. Winpenny, *Angew. Chem., Int. Ed.*, 2003, **42**, 3804; (*b*) S. Konar and A. Clearfield, *Inorg. Chem.*, 2008, **47**, 3492; (*c*) S. Khanra, M. Helliwell, F. Tuna, E. J. L. McInnes and R. E. P. Winpenny, *Dalton Trans.*, 2009, 6166.

8 (*a*) S. Maheswaran, G. Chastanet, S. J. Teat, T. Mallah, R. Sessoli, W. Wernsdorfer and R. E. P. Winpenny, *Angew. Chem., Int. Ed.*, 2005, **44**, 5044; (*b*) M. Shanmugam, G. Chastanet, T. Mallah, R. Sessoli, S. J. Teat, G. A. Timco and R. E. P. Winpenny, *Chem. – Eur. J.*, 2006, **12**, 8777; (*c*) M. Shanmugam, M. Shanmugam, G. Chastanet, R. Sessoli, T. Mallah, W. Wernsdorfer and R. E. P. Winpenny, *J. Mater. Chem.*, 2006, **16**, 2576.

9 (*a*) B. A. Breeze, M. Shanmugam, F. Tuna and R. E. P. Winpenny, *Chem. Commun.*, 2007, 5185; (*b*) S. K. Langley, M. Helliwell, S. J. Teat and R. E. P. Winpenny, *Inorg. Chem.*, 2014, **53**, 1128; (*c*) J. A. Sheikh, A. Adhikary, H. S. Jena, S. Biswas and S. Konar, *Inorg. Chem.*, 2014, **53**, 1606.

10 (*a*) S. Langley, M. Helliwell, R. Sessoli, S. J. Teat and R. E. P. Winpenny, *Inorg. Chem.*, 2008, **47**, 497; (*b*) S. Langley, M. Helliwell, R. Sessoli, S. J. Teat and R. E. P. Winpenny, *Dalton Trans.*, 2009, 3102; (*c*) S. K. Langley, M. Helliwell, S. J. Teat and R. E. P. Winpenny, *Dalton Trans.*, 2012, **41**, 12807; (*d*) E. M. Pineda, F. Tuna, Y.-Z. Zheng, R. G. Pritchard, A. C. Regan, R. E. P. Winpenny and E. J. L. McInnes, *Chem. Commun.*, 2013, **49**, 3522; (*e*) J. A. Sheikh, S. Goswami, A. Adhikary and S. Konar, *Inorg. Chem.*, 2013, **52**, 6765.

11 (*a*) S. Khanra, M. Kloth, H. Mansaray, C. A. Muryn, F. Tuna, E. C. Sañudo, M. Helliwell, E. J. L. McInnes and R. E. P. Winpenny, *Angew. Chem., Int. Ed.*, 2007, **46**, 5568; (*b*) S. Khanra, L. Batchelor, M. Helliwell, F. Tuna, E. J. L. McInnes and R. E. P. Winpenny, *J. Mol. Struct.*, 2008, **890**, 157; (*c*) S. Khanra, R. Shaw, M. Helliwell, F. Tuna, C. A. Muryn, E. J. L. McInnes and R. E. P. Winpenny, *Materials*, 2010, **3**, 232.

12 (*a*) K. H. Zangana, E. M. Pineda, J. Schnack and R. E. P. Winpenny, *Dalton Trans.*, 2013, **42**, 14045; (*b*) K. H. Zangana, E. M. Pineda, E. J. L. McInnes, J. Schnack and R. E. P. Winpenny, *Chem. Commun.*, 2014, **50**, 1438.

13 (*a*) Y. Simonov, P. Bourosh, G. Timco, S. Grebenco, M. Mazus, C. Indrichan and N. Gerbeleu, *Chem. Bull.*, 1998, **43**, 128; (*b*) K. Abdulwahab, M. A. Malik, P. O'Brien, K. Govender, C. A. Muryn, G. A. Timco, F. Tuna and R. E. P. Winpenny, *Dalton Trans.*, 2013, **42**, 196.

14 (*a*) G. M. Sheldrick, *Acta Crystallogr., Sect. A: Fundam. Crystallogr.*, 2008, **64**, 112; (*b*) O. V. Dolomanov, L. J. Bourthis, R. L. Gildea, J. A. K. Howard and H. Puschmann, *J. Appl. Crystallogr.*, 2009, **42**, 339.

15 N. F. Chilton, R. P. Anderson, L. D. Turner, A. Soncini and K. S. Murray, *J. Comput. Chem.*, 2013, **34**, 1164.

16 S. Stoll and A. Schweiger, *J. Magn. Reson.*, 2006, **178**, 42.

17 For example, G. Christou, *Acc. Chem. Res.*, 1989, **22**, 328.

18 (*a*) D. M. Low, G. Rajaraman, M. Helliwell, G. Timco, J. van Slageren, R. Sessoli, S. T. Ochsenbein, R. Bircher, C. Dobe, O. Waldmann, H. U. Güdel, M. A. Adams, E. Ruiz, S. Alvarez and E. J. L. McInnes, *Chem. – Eur. J.*, 2006, **12**, 1385; (*b*) R. A. Coxall, A. Parkin, S. Parsons, A. A. Smith, G. A. Timco and R. E. P. Winpenny, *J. Solid State Chem.*, 2001, **159**, 321; (*c*) S. Parsons, A. A. Smith and R. E. P. Winpenny, *Chem. Commun.*, 2000, 579; (*d*) I. M. Atkinson, C. Benelli, M. Murrie, S. Parsons and R. E. P. Winpenny, *Chem. Commun.*, 1999, 285; (*e*) Y.-Z. Zheng, B. A. Breeze, G. A. Timco, F. Tuna and R. E. P. Winpenny, *Dalton Trans.*, 2010, **39**, 6175.

19 Harris notation describes the binding mode as [X·Y1Y2···Yn] where X is the overall number of metal bond by the whole ligand, and each value of Y refers to the number of metal atoms attached to the different donor atoms. See ESI† and R. A. Coxall, S. G. Harris, D. K. Henderson, S. Parsons, P. A. Tasker and R. E. P. Winpenny, *Dalton Trans.*, 2000, **14**, 2349.

20 (*a*) E. J. L. McInnes, *Struct. Bonding*, 2006, **122**, 69; (*b*) J. van Slageren, *Top. Curr. Chem.*, 2012, **321**, 199.

21 A. Bencini and D. Gatteschi, *EPR of Exchange Coupled Systems*, Springer-Verlag, Berlin, 1989, reprinted Dover Publications Inc., 2012.

Linking Cr_3 triangles through phosphonates and lanthanides: synthetic, structural, magnetic and EPR studies

Karzan H. Zangana, Eufemio Moreno Pineda, Iñigo J. Vitorica-Yrezabal, Eric J. L. McInnes and Richard E. P. Winpenny*

School of Chemistry and Photon Science Institute, The University of Manchester, Oxford Road, Manchester M13 9PL, UK.

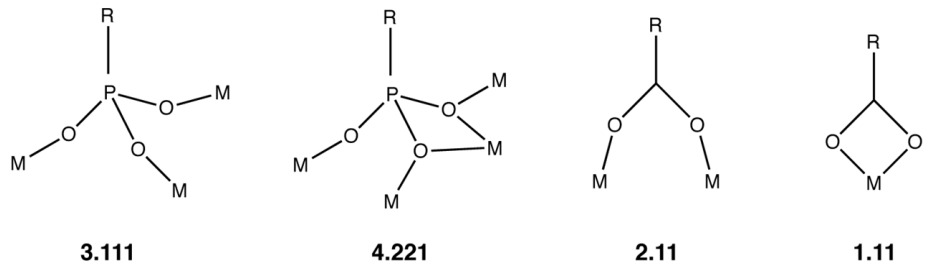

Figure S1. Scheme for binding modes by Harris notation of the phosphonates and carboxylates.

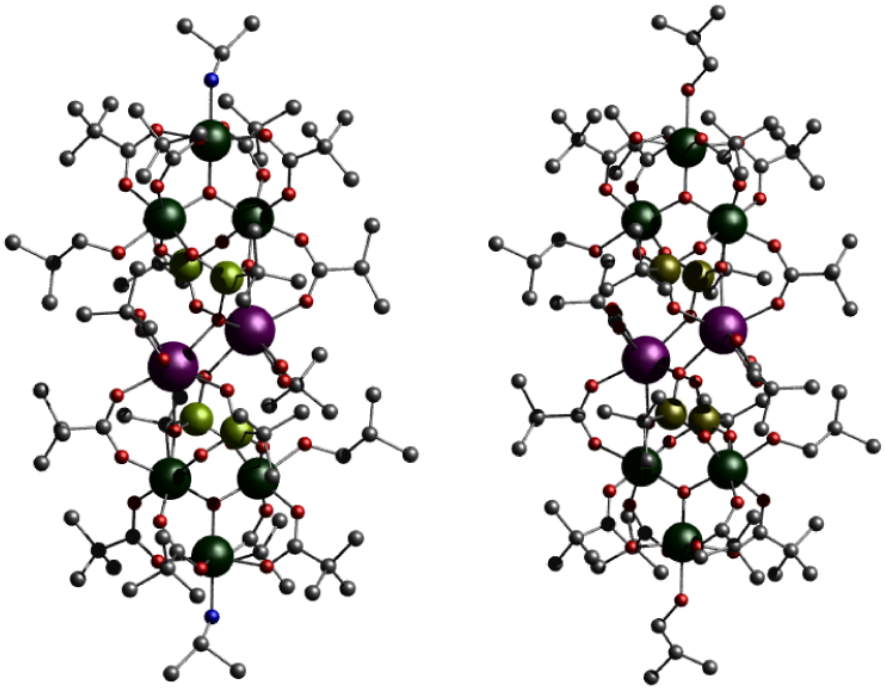

Figure S2. Crystal structure of cluster **2** showing ^{t}BuOH terminals (right); Crystal structure of clusters **1**, **3**, **4** and **5** showing amine terminals (left). Scheme: La, purple; Cr, dark green; P, light green; O, red; C, grey; N, cyan; H omitted for clarity.

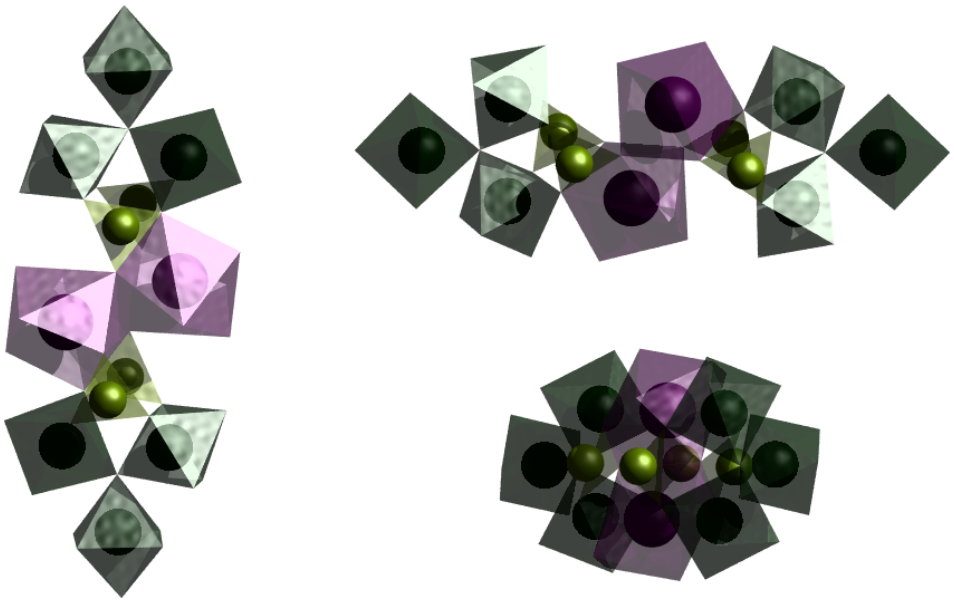

Figure S3. Polyhedral view of $\{Cr_6Ln_2P_4\}$ core.

Table S1. Selected bond distances and angles of **1**−**5**.

	1	**2**	**3**	**4**	**5**
$Cr_1 \ldots Cr_2$ /Å	3.263(1)	3.258(3)	3.271(2)	3.273(2)	3.281(1)
$Cr_2 \ldots Cr_3$/Å	3.427(1)	3.422(2)	3.425(1)	3.426(2)	3.424(1)
$Cr_1 \ldots Cr_3$/Å	3.263(2)	3.268(3)	3.287(1)	3.235(1)	3.271(1)
O_1 ─Ln_1/Å	6.560(4)	6.503(8)	6.492(4)	6.459(4)	6.470(4)

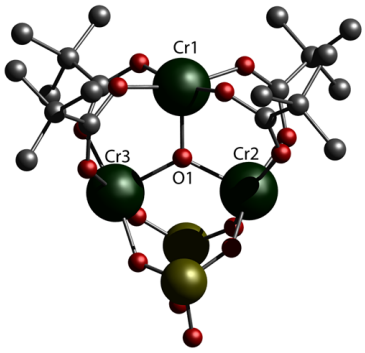

Figure S4. $\{Cr_3\}$ moiety for $Cr_6Ln_2P_4$ clusters. Scheme: La, purple; Cr, dark green; P, light green; O, red; C, grey; N, cyan; H omitted for clarity.

Chapter 10

10.1 Conclusions and Future Work

Phosphonic acids have been shown to be extremely adaptable and flexible ligands that can support polymetallic cages with high metal : ligand ratios and can be employed in combination with many different types of co-ligand. The flexible nature of the ligand permits many diverse coordination modes, allowing different cage nuclearities. This work demonstrates that the combination of lanthanides and phosphonates can yield diverse structural motifs including clusters, similar to transition metal phosphonate species. The solubility and crystallinity of lanthanide phosphonates can be improved by introducing secondary ligands. Employing these synthetic techniques, we have synthesised varied lanthanide phosphonates with different magnetic properties (See Chapters 4–7). The phosphonate ligands in such clusters can adopt a number of different coordination modes depending on many factors the pH of the reaction media, the temperature, the ionic radius of the lanthanide cation and the chosen counteranion.

Herein, we have exported the rich conformational flexibility of our ligands by using the 'serendipitous assembly' technique in order to synthesise molecular cages that could be used in the area of molecular magnetism (Figure 10.1). Using knowledge of the binding properties of phosphonate ligands as well as the co-ligands we have been successful in obtaining a range of 4f and 3d–4f phosphonates complexes which could

potentially be used in MCE and SMM applications. We have employed pivalic acid as a co-ligand to prepare a series of $\{Ln_8P_6\}$ 'horseshoes', where the Gd analogue, $[Gd_8(O_3P^tBu)_6(\mu_3{-}OH)_2(H_2O)_2(HO^iBu)(O_2C^tBu)_{12}](NH_3{}^iPr)_2$, has been investigated for its MCE potential. The structure of this complex comprises a $\{Gd_8P_6\}$ core encapsulated by hydrophobic ^{t}butyl groups, which assist good separation between molecules (See Chapter 4). This represents the first investigation of the MCE properties of any 4f–phosphonate cluster. The interactions among Gd(III) are weak but antiferromagnetic, which were evaluated based on an equivalent adjacent exchange parameter of $J = -0.03\text{cm}^{-1}$. The maximum value of ΔS_m is 32.3 J $kg^{-1}K^{-1}$ at 3 K with ΔH = 70 kOe, which is lower than the predicted value of 45.9 J kg^{-1} K^{-1} for eight uncoupled Gd(III) ions.

To highlight the influence of the source of base in the reaction, we have followed the same general process as used for synthesis the $\{Ln_8P_6\}$ 'horseshoes', but swapped the aliphatic amine base (isopropylamine) for an aromatic base (pyridine) (See Chapter 6). It was detected that the reaction proceed fine in the presence of aromatic base, as the base supports the reaction by deprotonation of the phosphonic acid. As a result of this reaction five new lanthanide phosphonate cages produced, $[pyH]_4[Ln_4(\mu_3\text{-}OH)(O_3P^tBu)_3(HO_3P^tBu)(O_2C^tBu)_2(NO_3)_6]$ (Ln = Gd, Tb, Dy, Ho or Er). Thus, in the current reaction system, the final product is controlled by the nature of the base employed. This suggests that in solution cages are in equilibrium and depending on the *pKa* of the reaction medium we could isolate a certain type of cage, however it is

hard to guess the product of the reaction because of the different coordination modes for phosphonate ligands.

The $[Ln_2(O_2C^tBu)_6(HO_2C^tBu)_6]$ and $[Cr^{III}_3(\mu_3\text{-}O)(O_2C^tBu)_6(H_2O)_3][O_2C^tBu]$ precursors have been shown to be good starting materials for creating large coordination clusters with phosphonic acids (See Chapters 5 and 9). These starting materials were utilised to check the hypothesis that phosphonate-carboxylate ligand substitution will proceed as seen for oxo-centred metal triangles. It has been shown that this is indeed true and that a range of carboxylate and phosphonate containing lanthanide(III) compounds can be synthesised in this way. A series of related cores have been synthesised by varying the reaction conditions and by the addition of various co-ligands (See Chapters 4–7 and 9). The phosphonate ligand is capable of binding both transition metal and lanthanide ions, and therefore we believed that it would be feasible to prepare lanthanide-transition metal phosphonates which may possess novel structural architectures as well as novel magnetic properties. This work shows the versatile bridging and chelating potential of the phosphonate ligands for the assembly of mixed 3d and 4f compound (See Chapters 8 and 9). The precursor $\{Cr_3\}$ triangles remain recognisable in all the resulting cages as a substructure, where two triangles are found bridged to each other via lanthanides and phosphonate ligands.

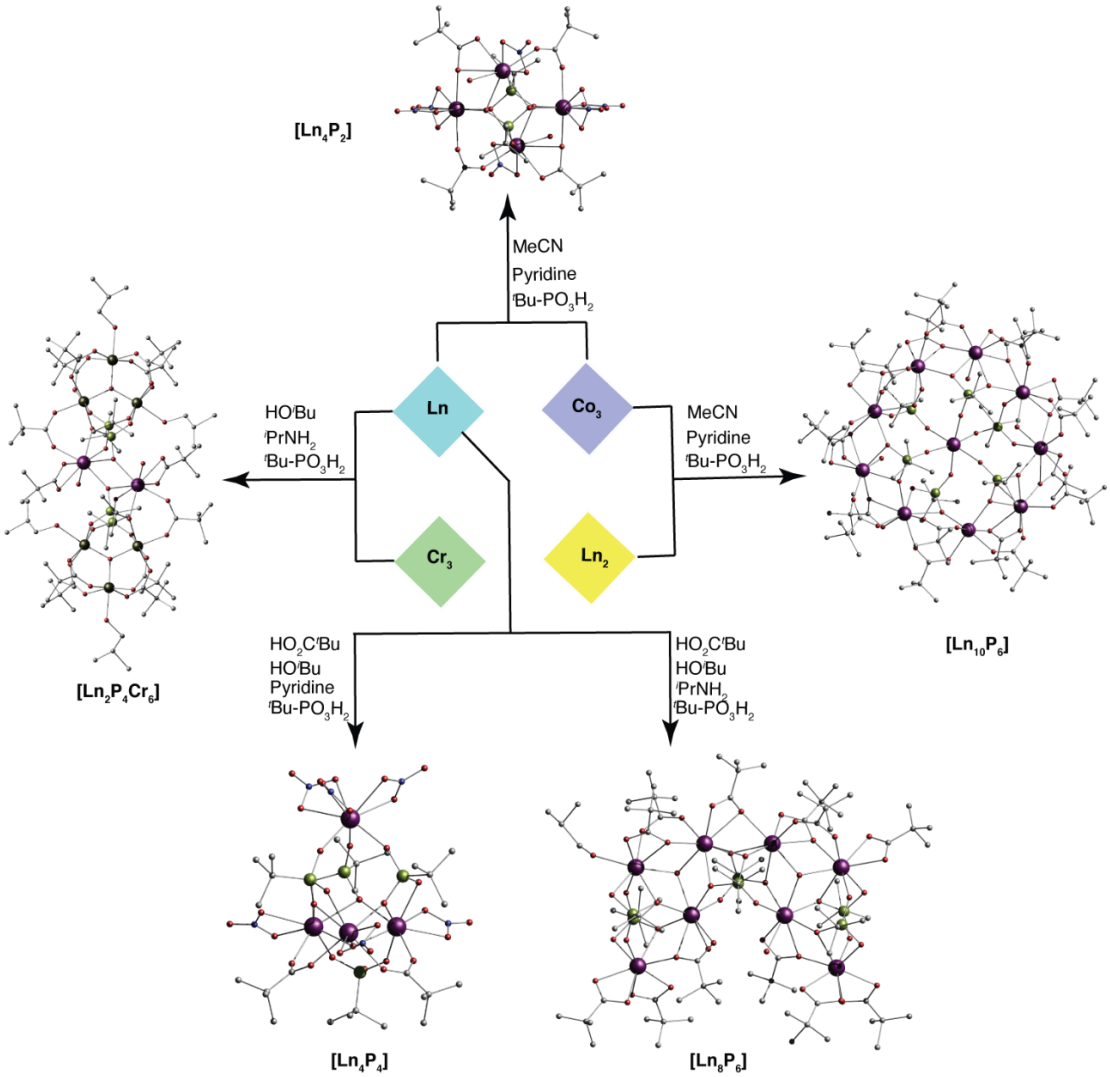

Figure 10.1: Synthetic procedures and produced structures. Colour code: O, red; C, grey; Ln, purple; Co, cyan; P, lime; N, blue. Hydrogens omitted for clarity. Co_3 = $[Co_3(\mu_3\text{-}O)(O_2C^tBu)_6(py)_3]\bullet(O_2C^tBu)$; Cr_3 =$[Cr_3(\mu_3\text{–}O)(O_2C^tBu)_6(H_2O)_3]\bullet(O_2C^tBu)$; Ln = $Ln(NO_3)_3\bullet nH_2O$; Ln_2 = $Ln_2(O_2C^tBu)_6(HO_2C^tBu)_6$.

To extend previous work, the $H_2O_3P^tBu$ ligand was used with $[Ln_2(O_2C^tBu)_6(HO_2C^tBu)_6]$, $[Co_3(\mu_3\text{–}O)(O_2C^tBu)_6(py)_3](O_2C^tBu)$, and pyridine, to synthesise two new lanthanide phosphonate cages $[Co_3(\mu_3\text{-}O)(O_2C^tBu)_6(py)_3]_2[Ln_4(O_3P^tBu)_2(O_2C^tBu)_4(NO_3)_6(H_2O)_2]$ (Ln = Gd or Dy). The Dy(III) analogue displays SMM behaviour, becoming the first example of a 4f–phosphonate SMM. The thermal energy barrier to magnetisation relaxation U_{eff} = 67

K with $\tau_0 = 2.7 \times 10^{-6}$ s. So, each precursor of the reaction medium has a strong influence on the final product, and henceforth on the magnetic behaviour.

To examine the influence of the lanthanide precursors on the formation of the product, we have followed the same general procedure as for synthesis of the $\{Ln_4P_2\}$ cage, but exchanged the precursor $Ln(NO)_3 \bullet nH_2O$ for$[Ln_2(O_2C^tBu)_6(HO_2C^tBu)_6]$ (See Chapter 7), resulting in formation of two centred-ring complexes, $[Co_3O(O_2C^tBu)_6(py)_3][Ln_{10}(O_2C^tBu)_{18}(O_3P^tBu)_6(OH)(H_2O)_4]$ (Ln = Dy or Gd) (See Chapter 5). The hypothesis for using Co(III) was to control the reactivity by using an inert 3d-metal and hence achieve a more targeted outcome than possible if using a Co(II) substrate. This is the first large centred odd-numbered metal ring. Unfortunately, the very small $J_{Gd\text{-}Gd}$ exchange interaction means no interesting physics associated with spin frustration is observed.

However, at present we cannot predict how the phosphonates assemble the pre-formed metal cluster 'precursors' into larger clusters, but this work reveals that this is a convenient strategy for assembly large polymetallic cages. Besides, we could go ahead, we should perhaps simply say that phosphonate ligands are fun for chemists, who perhaps just want to synthesise something with a new structure, but less so for physicists who may know what they want.

10.2 Further Work

10.2.1 Reaction of the Pivalate Dimetallic and Trimetallic Compound

Although the series of compounds presented throughout this body of work display some innovative and intriguing results, it is clear there is still great scope to develop this work even further. For example, the iron analogues of the chromium clusters could be attempted, and the effect or perhaps the use of lanthanide or transition metal dimer salts in place of lanthanide nitrate or μ_3–O chromium triangle may lead to further interesting species. No systematic study of the influence of varying the carboxylate ligand has been made, for example, $[Fe_3O(O_2CMe)_6(H_2O)_3]Cl$ and $[Cr_3O(O_2CMe)_6(H_2O)_3]Cl$, this may extend the accessible topologies.[1] The use of pivalic acid was due to its help with crystallisation of the products, so using more or less bulky carboxylates may have a dramatic effect on the structures of the products.

Attempts toward utilising preformed precursor such as $[Ln_7(OH)_6(thmeH_2)_5(thmeH)(tpa)_6(MeCN)_2](NO_3)_2$ (where Ln = Dy or Gd; $thmeH_3$ = [tris(hydroxymethyl)ethane; tpaH = triphenylacetic acid),[2] $[Cr_{14}(bta)_6O_6(OMe)_{18}Cl_6]$ (btaH = 1,2,3–benzotriazol),[3] $[Mn_9O_7(O_2C^tBu)_{13}(THF)_2]$,[4] $[Co_{14}O_4(OH)_{12}(O_2C^tBu)_{14}(HO_2C^tBu)_2(H_2O)_6(MeCN)_2]$ or polymers such as $[Co(O_2C^tBu)_2]_n$, [5] have not been fully explored. It may be interesting to react these alongside phosphonates and suitable solvent (Figure 10.2).

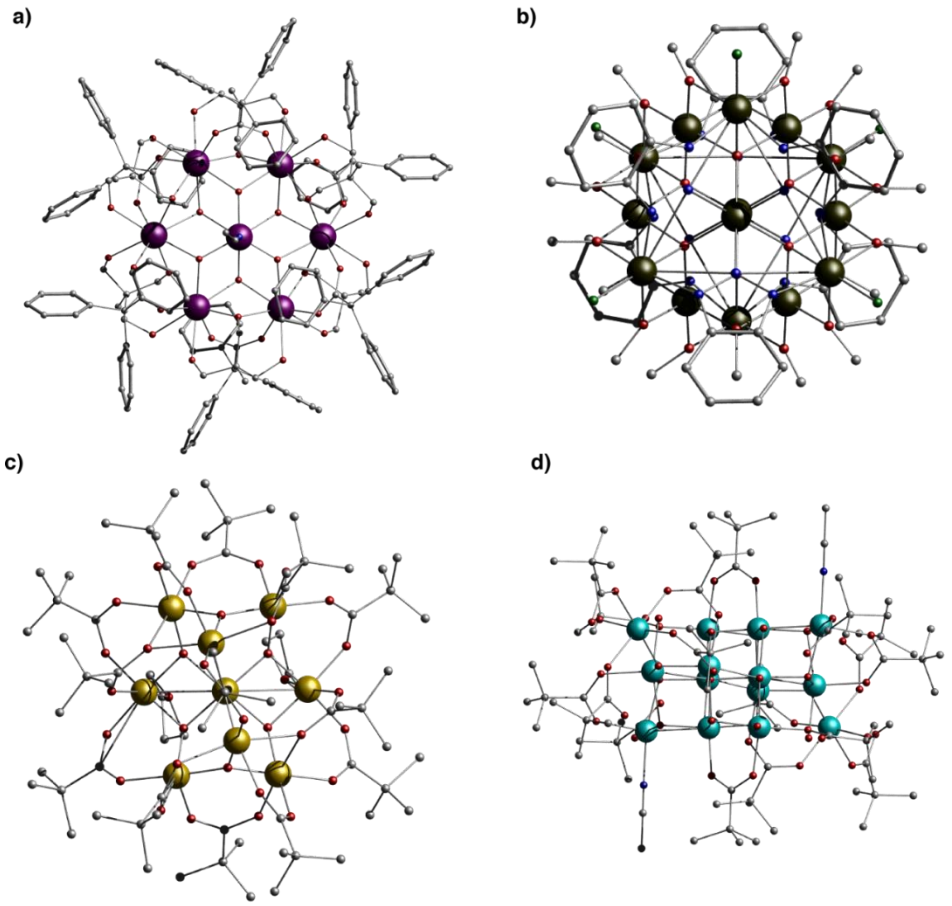

Figure 10.2: The structures of $[Ln_7(OH)_6(thmeH_2)_5(thmeH)(tpa)_6(MeCN)_2](NO_3)_2$ (a); $[Cr_{14}(bta)_6O_6(OMe)_{18}Cl_6]$ (b); $[Mn_9O_7(O_2C^tBu)_{13}(THF)_2]$ (c) and $[Co_{14}O_4(OH)_{12}(O_2C^tBu)_{14}(HO_2C^tBu)_2(H_2O)_6(MeCN)_2]$ (d). Colour code: O, red; C, grey; Cr, olive green; Ln, purple; Mn, gold; Co, cyan. Hydrogens and solvent molecules were omitted for clarity.

Since the choice of co-ligand is highly influential on the structure of the final product,[6] more varied co-ligands could be employed. Pivalate is a bidentate ligand displaying a range of binding modes in this work, hence other co-ligands with a variety of binding modes could be used, for example oxalate, acetate, citrate, lactate or formate. Use of smaller co-ligand may result in higher nuclearity products, while use of an open bridging ligand such as oxalate may result in extended networks.

10.2.2 Solubility Problems

The difficulty with finding an appropriate solvent for the dissolution of the bi- or tri-metallic starting materials and the phosphonic acid has limited the reactions that could be carried out. Solvothermal reaction conditions could be employed to allow less soluble starting materials to be utilised thus yielding novel products directly from mother liquor.[7] Solvothermal techniques have been used to synthesise diverse iron phosphonate cages, for example, $[Fe_9(\mu_3\text{-}O)_5(\mu_3\text{-}OH)(O_2C^tBu)_{12}(HO_2C^tBu)(O_3P^tBu)_2]$, $Fe_4(O_2C^tBu)_5(O_3P^tBu)_3Br$ and $[Fe_{14}(\mu_3\text{-}O)_4(\mu\text{-}OH)_8(O_2C^tBu)_{14}(O_3P^tBu)_6]$.[8] Recently, a series of Cr(III) stars and butterflies have been synthesised by solvothermal reaction, namely, $[CrCl_2(bipy)_2]_2[Cr_2Cl_8(MeCN)_2]$, $[Cr_4\{EtC(CH_2O)_3\}_2(bipy)_3Cl_6]$, $[Cr_4\{(HOCH_2)C(CH_2O)_3\}_2(bipy)_3Cl_6$ and $[Cr_4\{EtC(CH_2O)_3\}_2\{NH(C(Me)NH)_2\}_2Cl_6]$, and the magnetic properties of these clusters was studied intensively (Figure 10.3).[9]

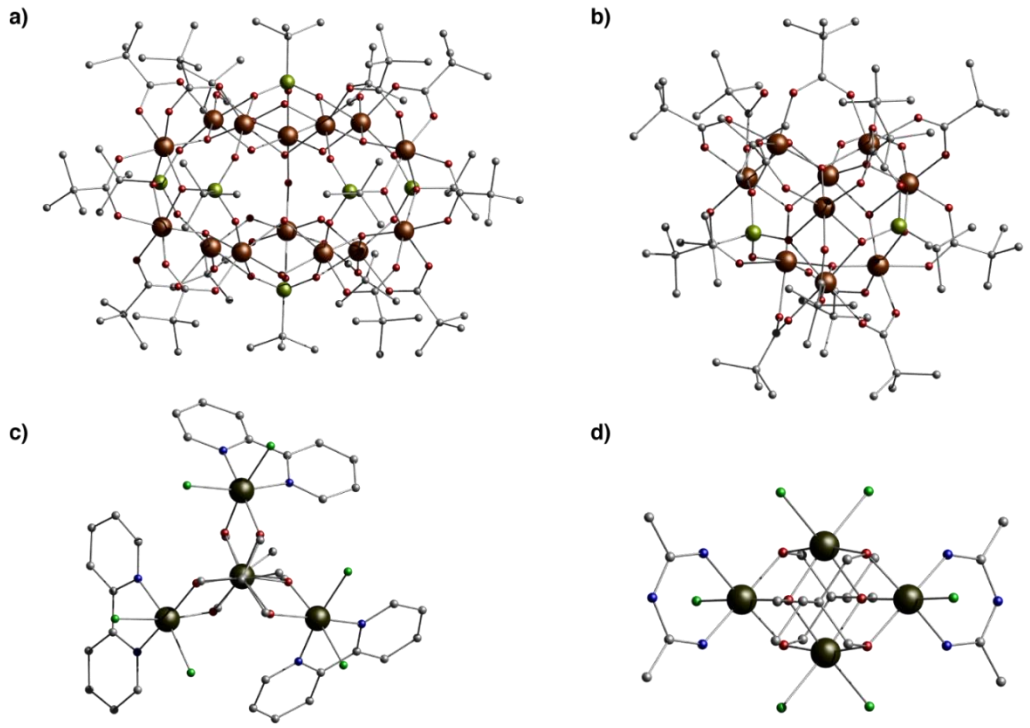

Figure 10.3: (a), (b), (c) and (d) The structure of $[Fe_{14}(\mu_3\text{-}O)_4(\mu\text{-}OH)_8(O_2C^tBu)_{14}(O_3P^tBu)_6]$,$[Fe_9(\mu_3\text{-}O)_5(\mu_3\text{-}OH)(O_2C^tBu)_{12}(HO_2C^tBu)(O_3P^tBu)_2]$, $[Cr_4\{EtC(CH_2O)_3\}_2(bipy)_3Cl_6]$ and $[Cr_4\{EtC(CH_2O)_3\}_2\{NH(C(Me)NH)_2\}_2Cl_6]$, respectively. Colour code: O, red; C, grey; Cr, olive green; iron, brown. Hydrogens and solvent molecules were omitted for clarity.

10.2.3 Functionalisation of Phosphonate Ligands

The final structures are strongly dependent on the phosphonates used,[10,11] and functionalisation of phosphonate ligands is a very promising route to synthesis 3d–4f clusters, with the potential to exploit the differing coordination preferences of d-block and f-block ions.[12-14] (Figures 8.10 and 10.4).

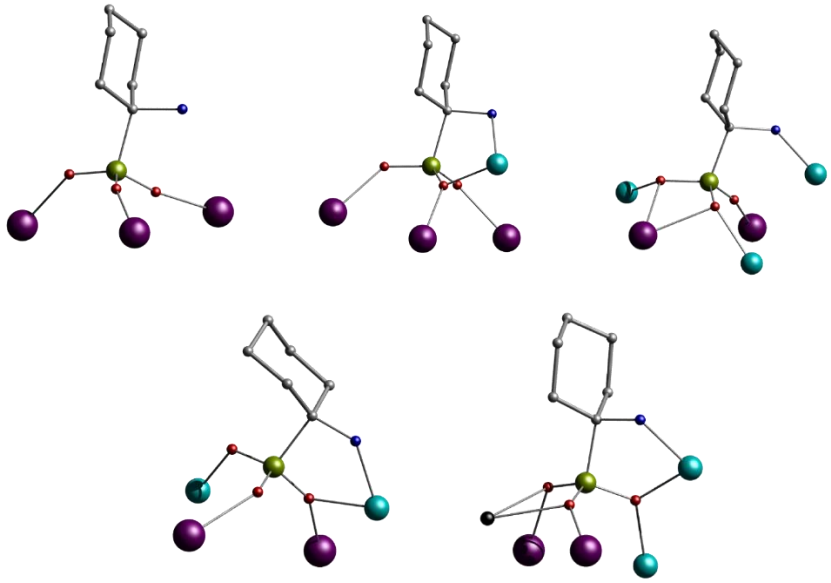

Figure 10.4: Phosphonate binding modes in the cages $[Co_4Ln_{10}(O_2C^tBu)_{12}(O_3PC_6H_{10}NH_2)_8(PO_4)_2(O_2CMe)_2(O_3PC_6H_{10}NH_3)_2]$ and $[Na_2Co_6Ln_4(\mu_3\text{-}OH)_2(O_2C^tBu)_{12}(O_3PC_6H_{10}NH_2)_6(MeCN)_2]$. Colour codes: O, red; C, grey; Ln, purple; Co, cyan; Na, black; P, lime. Hydrogens omitted for clarity. (See Chapter 8, reference 7)

To date, only few 4f-aminophosphonate molecular cages have been reported (See Chapter 3 and the references therein), the first lanthanide aminophosphonate, $[Lu(III)(HO_3PCH_2CH_2NH_3)_3(ClO_4)_3\bullet\ 3D_2O]_n$ was reported by Legendziwicz *et al.* in 1991.[15] Its structure consists of a 1D lutetium(III) phosphonate chain (Figure 10.5). Each Lu(III) ion is octahedrally coordinated with six phosphonate oxygen atoms from six phosphonate ligands. The phosphonate group is bidentate coordinating, the third phosphonate oxygen atom and the amine group are protonated and stay uncoordinated. No intensive effort has been made to use phosphonic acid ligands with an additional binding group, for example, an amino-functionalised phosphonate could be used to synthesise new families of 3d–4f molecular clusters.

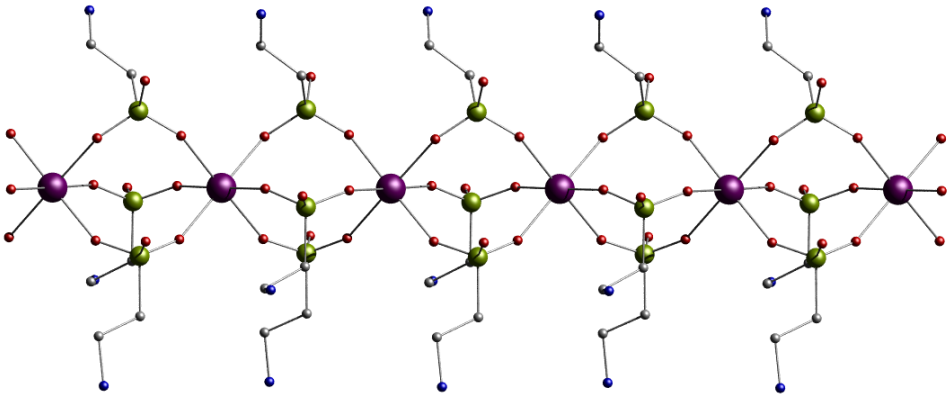

Figure 10.5: The structure of 1D chain in $Lu(HO_3PCH_2CH_2NH_3)_3(ClO_4)_3 \bullet 3D_2O]_n$. Colour codes: O, red; C, grey; N. blue; Ln, purple; P, lime. Hydrogens omitted for clarity.

10.3 References

1. B. Blake, E. Sinn, A. Yavari, K. S. Murray and B. Moubaraki, *Dalton Trans.*, 1998, **1**, 45.
2. J. W. Sharples, Y.-Z. Zheng, F. Tuna, E. J. L. McInnes and D. Collison, *Chem. Commun.*, 2011, **47**, 7650.
3. R. Shaw, R. H. Laye, L. F. Jones, D. M. Low, C. Talbot-Eeckelaers, Q. Wei, C. J. Milios, S. Teat, M. Helliwell, J. Raftery, M. Evangelisti, M. Affronte, D. Collison, E. K. Brechin and E. J. L. McInnes, *Inorg. Chem.*, 2007, **46**, 4968
4. S. Mukherjee, K. A. Abboud, W. Wernsdorfer and G. Christou, *Inorg. Chem.*, 2013, **52**, 873.
5. G. AromÌ, S. Batsanov, P. Christian, M. Helliwell, A. Parkin, S. Parsons, A. A. Smith, G. A. Timco, and R. E. P. Winpenny, *Chem. Eur. J.*, 2003, **9**, 5142.
6. S. Konar, N. Bhuvanesh and A. Clearfield, *J. Am. Chem. Soc.*, 2006, **128** , 9604.
7. R. I. Walton, *Chem. Soc. Rev.*, 2002, **31**, 230, and references therein.
8. Y.-Z. Zheng and R. E. P. Winpenny, *Sci. China Chem.*, 2012, **55**, 910.
9. L. J. Batchelor, M. Sander, F. Tuna, M. Helliwell, F. Moro, J. van Slageren, E. Burzurí, O. Montero, M. Evangelisti, F. Luis and E. J. L. McInnes, *Dalton Trans.*, 2011, 40, 5278.
10. S. Langley, M. Helliwell, R. Sessoli, S. J. Teat and R. E. P. Winpenny, *Inorg. Chem., 2008*, **47**, 497.

11. S. Langley, M. Helliwell, R. Sessoli, S. J. Teat and R. E. P. Winpenny, *Dalton Trans.*, 2009, **16**, 3102.

12. Y.-S. Ma, Y.-Z. Li, Y. Song and L.-M. Zheng, *Inorg. Chem.*, 2008, **47,** 4536.

13. J. Kratochvil, M. Necas, V. Petricek and J. Pinkas, *Inorg. Chem.*, 2006, **45**, 6562.

14. Y.-S. Ma, Y. Song, W.-X. Du, Y.-Z. Li and L.-M. Zheng, *Dalton Trans.*, 2006, **26**, 3228.

15. T. Głowiak, E. Huskowska and J. Legendziewicz, *Polyhedron*, 1991, **10**, 175.